Seismology

Steam and minor ash plume rising above the summit of Augustine Volcano on January 12, 2006. View from the northwest Alaska Volcano Observatory photo by Game McGimsey.

The 2006 Eruption of Augustine Volcano, Alaska
Power, J.A., Coombs, M.L., and Freymueller, J.T., editors
U.S. Geological Survey Professional Paper 1769

Chapter 1

Seismic Observations of Augustine Volcano, 1970–2007

By John A. Power[1] and Douglas J. Lalla[2]

Abstract

Seismicity at Augustine Volcano in south-central Alaska was monitored continuously between 1970 and 2007. Seismic instrumentation on the volcano has varied from one to two short-period instruments in the early 1970s to a complex network comprising 8 to 10 short-period, 6 broadband, and 1 strong-motion instrument in 2006. Since seismic monitoring began, the volcano has erupted four times; a relatively minor eruption in 1971 and three major eruptions in 1976, 1986, and 2006. Each of the major eruptions was preceded by 9 to 10 months of escalating volcano-tectonic (VT) earthquake activity that began near sea level. The major eruptions are characterized seismically by explosive eruptions, rock avalanches, lahars, and periods of small repetitive low-frequency seismic events often called drumbeats that are associated with periods of lava effusion, and they all followed a similar pattern, beginning with an explosive onset that was followed by several months of discontinuous effusive activity.

Earthquake hypocenters were observed to move upward from near sea level toward the volcano's summit over a roughly 9-month period before the 1976 and 1986 eruptions. The 1976 eruption was preceded by a small number of earthquakes that ranged in depth from 2 to 5 km below sea level. Earthquakes in this depth range were also observed following the 2006 eruption. The evolution of earthquake hypocenters associated with the three major eruptions, in conjunction with other supporting geophysical and geological observations, suggests that the Augustine magmatic system consists of a deeper magma source area at about 3.5 to 5 km below sea level and a shallower system of cracks near sea level where volatiles and magma may temporally reside as they ascend to the surface. The strong similarity in seismicity and character of the 1976, 1986, and 2006 eruptions suggests that the processes responsible for magma generation, rise, and eruption at Augustine Volcano have been roughly constant since the early 1970s.

Introduction

Continuous seismic monitoring of Augustine Volcano began in the summer of 1970 and has continued to the present. During this 38-year period Augustine has experienced a minor eruptive event in 1971 and three major eruptions in 1976, 1986, and 2006, as well as long periods of relative seismic quiescence characterized by low-level earthquake activity. The major eruptions were all preceded by roughly 9 months of increased volcano-tectonic (VT) earthquake activity and were characterized by an explosive onset lasting several days to weeks that was followed by several months of episodic effusive activity. The eruptions are characterized by complex sequences of seismic events involving VT and long-period (LP) events, as well as seismic signals from explosions, pyroclastic flows, lahars, rock falls and avalanches, and small shallow repetitive earthquakes (see "Augustine Seismicity" section for definitions). The three major eruptions were remarkably similar in terms of the character of eruptive style, the sequence of eruptive events, and the character of associated seismicity. The similarities in seismic activity and eruptive behavior during these three eruptions suggests that the processes that govern production, ascent, and eruption of magma at Augustine have remained roughly constant or changed only slowly over the 38-year period of instrumental data available for this volcano.

As a result of the volcano's frequent eruptive activity, the associated volcanic hazards, and proximity to communities surrounding Cook Inlet, Augustine has a relatively long history of geologic investigation and seismic monitoring for an Aleutian arc volcano. Augustine's frequent eruptive activity, coupled with magmas recently ranging in composition from high-silica andesite (57 weight percent SiO_2) to dacite (64 weight percent SiO_2), make this volcano an excellent location to study the seismic expression of the processes that govern

[1]Alaska Volcano Observatory, U.S. Geological Survey, 4200 University Drive, Anchorage, AK 99508.

[2]5106 Wesleyan Drive, Anchorage, AK 99508.

and accompany the accumulation, ascent, and eruption of higher viscosity magmas that are typical of explosive volcanism in a convergent margin setting.

In this paper we review the long-term seismic observations of Augustine Volcano between 1970 and 2007 and develop a conceptual model of the subsurface magmatic system. We begin with a review of the seismic instrumentation deployed on and around Augustine Island as a function of time. We then discuss the characteristics of seismicity observed during quiescent, precursory, and eruptive periods. This characterization relies principally on seismic measurements, such as the earthquake locations, magnitudes, waveform character, and durations of seismic signals associated with explosion events and lava effusion. We then develop detailed seismic chronologies of the activity surrounding the 1976, 1986, and 2006 eruptions. We offer a volcanological interpretation of the patterns of observed seismicity in combination with associated observations reported by other workers. We conclude with a discussion of the role that seismic observations played in forecasting the 2006 eruptions and make recommendations for evaluating future episodes of unrest through seismic investigations of Augustine Volcano.

Background

Augustine Volcano is a 1,200-m-high stratovolcano located on a small (8 x 11 km) island roughly 280 km southwest of Anchorage, Alaska (fig. 1). Augustine Volcano consists of a central complex of summit lava domes and flows surrounded by an apron of pyroclastic, lahar, avalanche, and ash deposits. The volcano is frequently active, with major eruptions recorded in 1883, 1935, 1963–64, 1976, 1986, and 2006. Minor eruptive events were reported in 1812, 1885, 1908, 1944, and 1971. The large eruptions are characterized by an explosive onset followed by the quieter effusion of lava. The three most recent eruptions in 1976, 1986, and 2006 had explosive onsets lasting from 4 to 18 days and included numerous individual vulcanian explosions that produced large ash plumes reaching altitudes of 10–15 km. Pyroclastic flows generated during these events swept down the flanks of the volcano, often reaching the surrounding waters of Cook Inlet. The quieter effusion of magma that generally followed the explosive onsets formed summit lava domes and/or short blocky flows that moved down the steep upper portions of the volcanic cone. Effusive activity typically occurred episodically over a period of 2 to 6 months and was often accompanied by block and ash flows produced when portions of the growing lava dome and flows became oversteepened and failed. Estimated eruptive volumes for the 1976, 1986, and 2006 eruptions are 0.39 km^3 (Kienle and Swanson, 1985), 0.10 km^3 (Holasek and Rose, 1991), and 0.12 km^3 (Coombs and others, this volume), respectively.

Geologic deposits on Augustine Island suggest that the present volcanic cone began to form more than 40,000 years ago (Waythomas and Waitt, 1998). Deposits from at least 13 major debris avalanches younger than 2,500 years are exposed on the sea cliffs surrounding Augustine Island, and they indicate that the Augustine cone is subject to frequent Bezymianny-style collapses similar to that of Mount St. Helens in 1980 (Gorshkov, 1959; Siebert and others, 1995). The most recent collapse and debris avalanche occurred during the 1883 eruption and generated a small tsunami in southern Cook Inlet (Waythomas and Waitt, 1998). Augustine's eruptive history during the Holocene is described by Waitt and Begét (2009).

Recent Augustine magmas are compositionally heterogeneous, with whole rock compositions ranging from basaltic andesites to dacites (56–64 weight percent SiO_2) (Johnston, 1978; Daley, 1986; Harris, 1994; Roman and others, 2006; Larsen and others, this volume). Roman and others (2006) suggest that the compositional heterogeneity of magmas erupted in 1986 resulted from the mixing of a cooler dacitic magma (residual from the 1976 eruption) and a newly injected more mafic magma. Progressive homogenization was not observed. Roman and others (2006) proposed that the mixing event took place in a network of dikes extending from roughly 2 to 5 km depth that prevented progressive homogenization throughout the 1986 eruption. Larsen and others (this volume) suggest the 2006 eruption was triggered by a similar mixing event that occurred at 3.5 to 5 km below mean sea level (b.m.s.l.)

In 1975, Augustine Volcano was the target of an extensive geophysical investigation that included temperature and heat flow measurements (Kienle and others, 1979), active and passive seismic investigations (Pearson, 1977), and an aeromagnetic survey (Barrett, 1978). The results of these investigations are summarized by Kienle and others (1979). The active seismic experiment involved the firing of 10 chemical shots that were recorded on 14 temporary, as well as the 5 permanent seismic stations. Data from this field experiment combined with data from exploratory wells drilled in southern Cook Inlet and a short seismic refraction line along Augustine's north shore were used to determine a three-dimensional velocity structure of the volcano (Kienle and others, 1979). The elements of this model are described in detail by Lalla and Power (this volume).

Augustine has also been the focus of a long-term program to monitor ground deformation. Between 1986 and 1989 a trilateration network was established that consisted of 19 benchmarks and 30 slope distances measured with an electronic distance measurement (EDM) device and zenith angles measured at six instrumentation stations (Power and Iwatsubo, 1998). This network was partially remeasured using the global positioning system (GPS) in 1992, 1993, 1994, 1995, and 1996. A complete reoccupation of the network with the inclusion of two benchmarks on the western shore of Cook Inlet was completed in 2000 (Pauk and others, 2001). A network of three telemetered single frequency continuous GPS (CGPS) receivers was established on the island in 1992 (Dzurisin and others, 1994), and a dual frequency receiver was added in 2000. These surveys and instruments indicated

that the Augustine edifice was stable and not deforming above the precision of the measurements between 1986 and 2000. A portion of the 1986 summit lava dome was found to be subsiding at roughly 8 cm per year, however. This movement was attributed to a landslide block that formed the northern portion of the 1986 lava dome (Pauk and others, 2001). Synthetic aperture radar (InSAR) measurements of the volcano between 1992 and 2005 also indicate that the broader edifice has inflated during this period (Lee and others, this volume). In 2004 a network of five CGPS receivers was installed on the island as part of the National Science Foundation funded EarthScope program (Pauk and others, this volume).

Seismic Instrumentation, Recording and Analysis

Seismometers have been in operation on Augustine Island since 1970 (Harlow, 1971), with only minor gaps in data resulting from station and telemetry failures. A summary of seismic stations operated on Augustine Island between 1970 and 2007 is contained in table 1. The first permanent seismometer, AU1, was installed on the north flank of Augustine Volcano in 1970. By 1972 seismic instrumentation on the island had expanded to a five-station network capable of calculating standard earthquake hypocenters and magnitudes (fig. 2*A*). A number of other seismic stations (OPT, CKK, HOM, CDD, MMN) were installed surrounding southern Cook Inlet in the early 1970s to monitor regional earthquake activity (fig. 1) (Kienle and Swanson, 1983). All of these stations were 1-Hz short-period instruments that used standard analog telemetry. Unfortunately, all stations on Augustine Island failed in late December 1975 as a result of heavy winter storms and did not record the final month of the 1976 eruption's precursory seismicity. Three of these stations were repaired in February 1976, and a network of new stations was established in 1978.

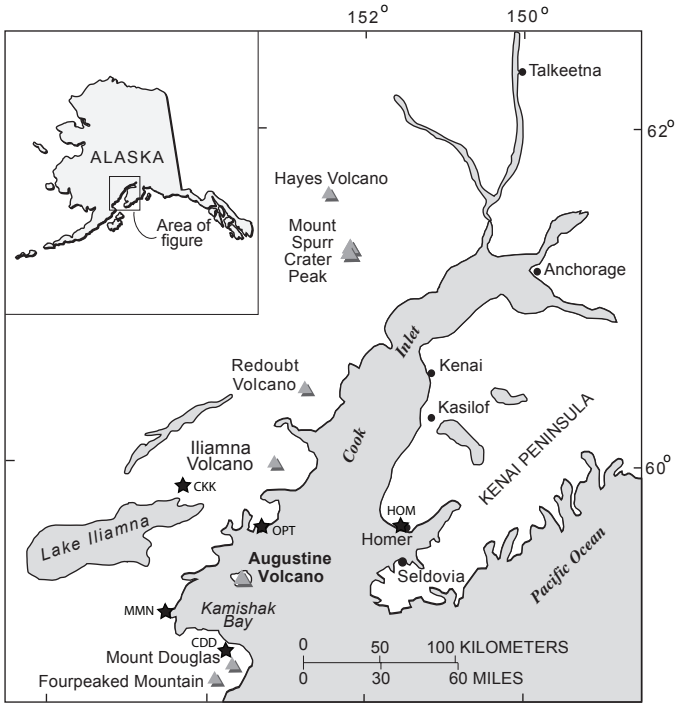

Figure 1. Map showing the location of Augustine Volcano relative to other volcanoes and to population centers in the Cook Inlet region of Alaska. Stars indicate locations of seismic stations CKK, OPT, MMN, CDD, and HOM.

The new four-station network established in 1978 (fig. 2*B*) operated through the 1986 eruption. Station AUT was added to the network on March 22, 1986, just 4 days before the 1986 eruption began (Power, 1988). No seismic stations were destroyed or disabled by volcanic activity in 1986.

Following the 1986 eruption the Augustine seismic network was reconfigured initially with five stations in 1987 and then eventually expanded to nine permanent short-period stations in the early 1990s (table 1). Most of these new stations were placed surrounding the 1986 summit lava dome to track shallow microearthquake activity (fig. 2*C*). A broadband seismometer, AUB, was initially co-located with station AUL in 1995. In 1998 the broadband components were renamed to be part of AUL (table 1).

The 2006 eruption disabled or destroyed stations AUS, AUR, AUP, AUH and AUL (fig. 2*C*). New stations AUSE and AUNW were installed on February 10 and March 30, 2006, respectively, to augment the impaired network, and station AUH was repaired on August 7. AUL and AUP were reestablished on September 4 and 6, 2006, respectively. A strong-motion instrument, AU20, was deployed on the island on January 9, 2006, and replaced by AU22 on September 1, 2006. A six-station temporary network of broadband seismometers, AU10 through AU15, was installed on Augustine Island (fig. 2*C*) in December of 2005 in response to increasing earthquake activity (Power and others, 2006). Three of these instruments operated throughout the 2006 eruption. Station AU12 operated until 0329 Alaska Standard Time (AKST) on January 30, 2006, when it was overrun by a pyroclastic flow, and station AU11 stopped recording data on February 11 as a result of water damage to the seismometer. Station AU10 failed as a result of water damage and did not return any useable data (table 1).

From 1970 through 1985, data from each of the Augustine Island seismic stations was telemetered to Homer, Alaska (fig. 1) and recorded on 16-mm photographic film. Film was read back on a Geotech 6585 film viewer that allows the arrival times from seismograms to be read at a scale of 1 s/cm. The primary limitation of this system is that individual events can be difficult to recognize during intense periods of earthquake or eruptive activity when adjacent traces overlap on the film. Starting in January 1986 the signals were relayed by leased telephone circuits to the Geophysical Institute in Fairbanks and were recorded on photographic film until April 1, 1989. A variety of specialized digital recording systems were used to track the seismic activity during the 1986 Augustine eruption (Power, 1988). Beginning on July 1, 1988, the data

were digitally recorded on a number of computerized acquisition systems at the Geophysical Institute. In October 1989, AVO began to record Augustine data on an RSAM system (Endo and Murray, 1991) and intermittently on an event-detected IASPEI system (Lee and others, 1988). On January 1, 1994, the AVO expanded the number of channels on the IASPEI system and began to consistently record event-detected data at 100 samples per second (Jolly and others, 1996). An Earthworm acquisition system replaced the IASPEI system on March 1, 2002, and AVO began to maintain both an event-detected and a continuous archive of seismic data (Dixon and others, 2004).

From 1972 through December 1975, all earthquakes that had identifiable P-arrivals on four or more stations in the Augustine network were located. A total of 678 earthquakes were located during this period. From July 1985 through March 1986, 421 hypocenters were calculated, which is roughly twelve percent of the total number of events that were estimated to have occurred. The selected subset is thought to be representative of the entire population of earthquakes from this interval (Power, 1988). Since 1993 we have relied on the computerized acquisition systems to identify locatable earthquakes. When the detection algorithm identified several shocks closely spaced in time, hypocenters were calculated for all possible earthquakes based on a manual review of the event detected data. From 1993 through 2007, AVO cataloged 3,866 earthquakes at Augustine Island. The details of these locations can be found in a series of annual reports; the most recent is compiled by Dixon and Stihler (2009). From January 1976 to July 1985 and April 1986 to January 1993, hypocenters were not routinely calculated at Augustine Volcano (fig. 3).

From 1989 to the present, events detected by the various AVO seismic acquisition systems were processed using the interactive analysis program XPICK (Robinson, 1990) and the earthquake location program HYPOELLIPSE (Lahr, 1999) in a manner similar to that described by Lahr and others (1994). All detected earthquakes with more than three P and two S phases and with standard hypocentral errors less than 15 km were processed and saved in the AVO earthquake catalog (Dixon and Stihler, 2009). Located events were classified as VT, LP, shore-ice events, or unknown based on the time-domain appearance of the velocity seismogram as viewed on a computer screen. Of the of 3,866 located shocks, AVO classified 3,795 as VT earthquakes, 28 as LP events, and 43 as shore- or sea-ice events between 1993 and the end of 2007. Earthquakes with a P- and S-wave separation of more than 5 seconds on Augustine Island stations were assumed to come from a source other than the volcano and were not located.

We use two location techniques to calculate earthquake hypocenters for this study. The first uses the program HYPOELLIPSE (Lahr, 1999) in a similar fashion to the standard AVO earthquake catalog (Dixon and others, 2008). In both location techniques, hypocentral depths are referenced to sea level, with negative depths reflecting height above mean sea level (a.m.s.l.). For this study we use a one-dimensional

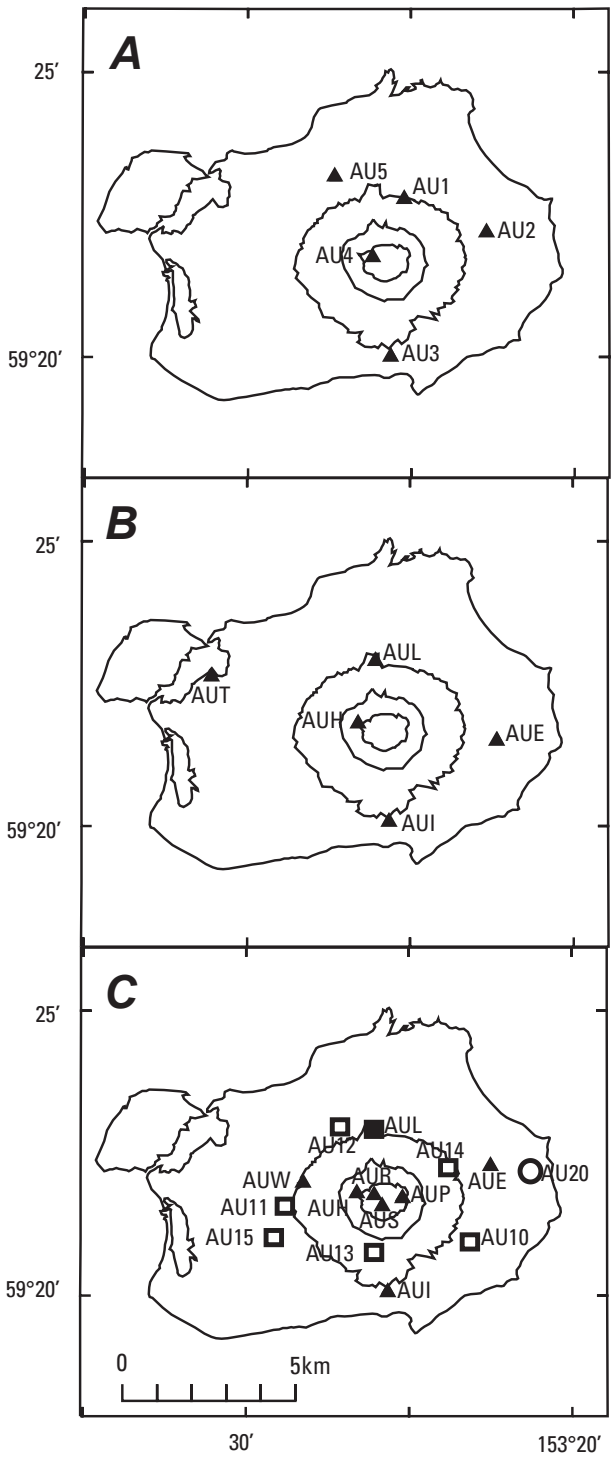

Figure 2. Maps showing the locations of seismic stations on Augustine Volcano before (*A*) the 1976 eruption, (*B*) the 1986 eruption, and (*C*) the 2006 eruption. Solid triangles represent short-period stations, solid squares represent permanent broadband sensors, open squares are temporary broadband stations deployed in late 2005, and the open circle is a strong motion instrument deployed in early 2006. Sea-level, 1,000-ft, 2,000-ft, and 3,000-ft contours are shown in map view.

Table 1. Seismic stations operated on Augustine Island between 1971 and 2007.

Station	North Latitude[1]	West Longitude[1]	Elevation (m)	Installation Date	Termination Date
AU1	59 22.39	153 25.23	508	08/01/1970	01/01/1976
AU2[2]	59 22.22	153 22.68	195	06/15/1971	01/01/1976
AU3	59 20.05	153 25.62	282	1972	04/06/1978
AU4	unknown	unknown	unknown	1972	07/1974
AU4[3]	59 21.79	153 26.19	890	07/1974	01/01/1976
AU5	59 23.19	153 27.35	152	1972	01/01/1976
AUI[4]	59 20.11	153 25.66	293	04/06/1978	current
AUH[5]	59 21.83	153 26.59	890	12/01/1978	current
AUL[6]	59 22.937	153 26.142	360	08/27/1978	current
AUE	59 21.531	153 22.365	172	10/29/1980	10/01/1988
AUE[7]	59 22.309	153 22.50	168	10/01/1988	current
AUP[8]	59 21.805	153 25.210	1033	06/26/1988	current
AUS[9]	59 21.599	153 25.840	1226	09/01/1990	01/11/2006
AUW	59 22.205	153 28.249	276	107/01/986	current
AUC	59 21.596	153 25.469	1175	09/13/1995	12/27/2000
AUR[9]	59 21.766	153 25.876	1204	11/01/1995	01/11/2006
AUB[10]	59 22.937	153 26.142	360	12/21/1995	09/28/1998
AUSE	59 20.481	153 23.850	152	02/10/2006	current
AUNW	59 22.694	153 28.609	160	03/30/2006	current
AU10[11]	59 20.974	153 23.126	219	12/20/2005	12/20/2005
AU11	59 21.576	153 28.818	234	12/20/2005	02/11/2006
AU12[12]	59 23.009	153 27.114	210	12/20/2005	01/30/2006
AU13	59 20.781	153 26.046	518	12/20/2005	05/30/2006
AU14	59 22.268	153 23.811	303	12/21/2005	08/07/2006
AU15	59 21.042	153 29.134	168	12/21/2005	08/10/2006
AU20	59 22.216	153 21.245	102	01/01/2006	08/31/2006
AU22	59 22.247	153 21.301	105	09/01/2006	current

[1] Datum is NAD27; numbers are in degrees and decimal minutes.

[2]Station had a single horizontal component of unknown orientation.

[3] Station relocated in July 1974, but name retained.

[4]Horizontal components added in 1987.

[5]Station destroyed by explosion on January 27, 2006, repaired August 7, 2006.

[6]Station destroyed by explosion on January 27, 2006, reinstalled on September 4, 2006.

[7]Station relocated on October 1, 1988, but name retained.

[8]Station destroyed by explosion on January 13, 2006, reinstalled on September 6, 2006.

[9]Station destroyed by explosion on December 15, 2006.

[10]Broadband station that replaces short-period station AUL on September 28, 1998.

[11]Station did not function properly and returned no useful data.

[12]Station overrun by a pyroclastic flow on January 30, 2007, data recovered from seismometer on August 15, 2006.

velocity model with six horizontal layers with boundaries at depths of –1.2, –0.7, 0.0, 1.0, 9.0, and 44.0 km. The top of the model at –1.2 km depth corresponds roughly with the summit of the volcano. The respective P-wave velocity for each layer is 2.3, 2.6, 3.4, 5.1, 6.3 and 8.0 km/s. These layer boundaries and velocities were determined using the results of the 1975 active source seismic experiment (Kienle and others, 1979) and were found to minimize residuals in a number of test runs of HYPOELLIPSE. For the precursory seismic sequences of the 1976, 1986, and 2006 eruptions we have then relocated the hypocenters using the two-dimensional ray tracing procedure described by Lalla and Power (this volume). This relocation technique uses the three-dimensional velocity model derived by Kienle and others (1979) for Augustine Island and station corrections calculated from the 1975 active source seismic experiment (Lalla and Power, this volume). This technique calculates theoretical traveltimes from grid points with a 0.25-km grid spacing embedded within the Augustine velocity structure and assigns the hypocenter to the grid point that most closely matches the observed arrival times. This technique accounts for the topography of the volcanic edifice when calculating traveltimes and allows hypocenters to be located above sea level. An evaluation of the accuracy of hypocenter determination using this technique indicates that hypocenters can be resolved within 0.25 km for shocks located above sea level and within 0.5 km for shocks located from sea level to 2 km b.m.s.l. (Lalla and Power, this volume). We have chosen this relocation technique for this study as it can be applied in a similar manner to the seismic data collected by both the analog and digital acquisition systems in use during the 1976, 1986, and 2006 eruptions of Augustine. Additionally, this relocation technique provides a means to determine absolute rather than relative locations. Deshon and others (this volume) studied earthquake families using waveform cross correlation techniques between 1993 and 2006. They found multiple earthquake families that occurred between 1993 and 2006

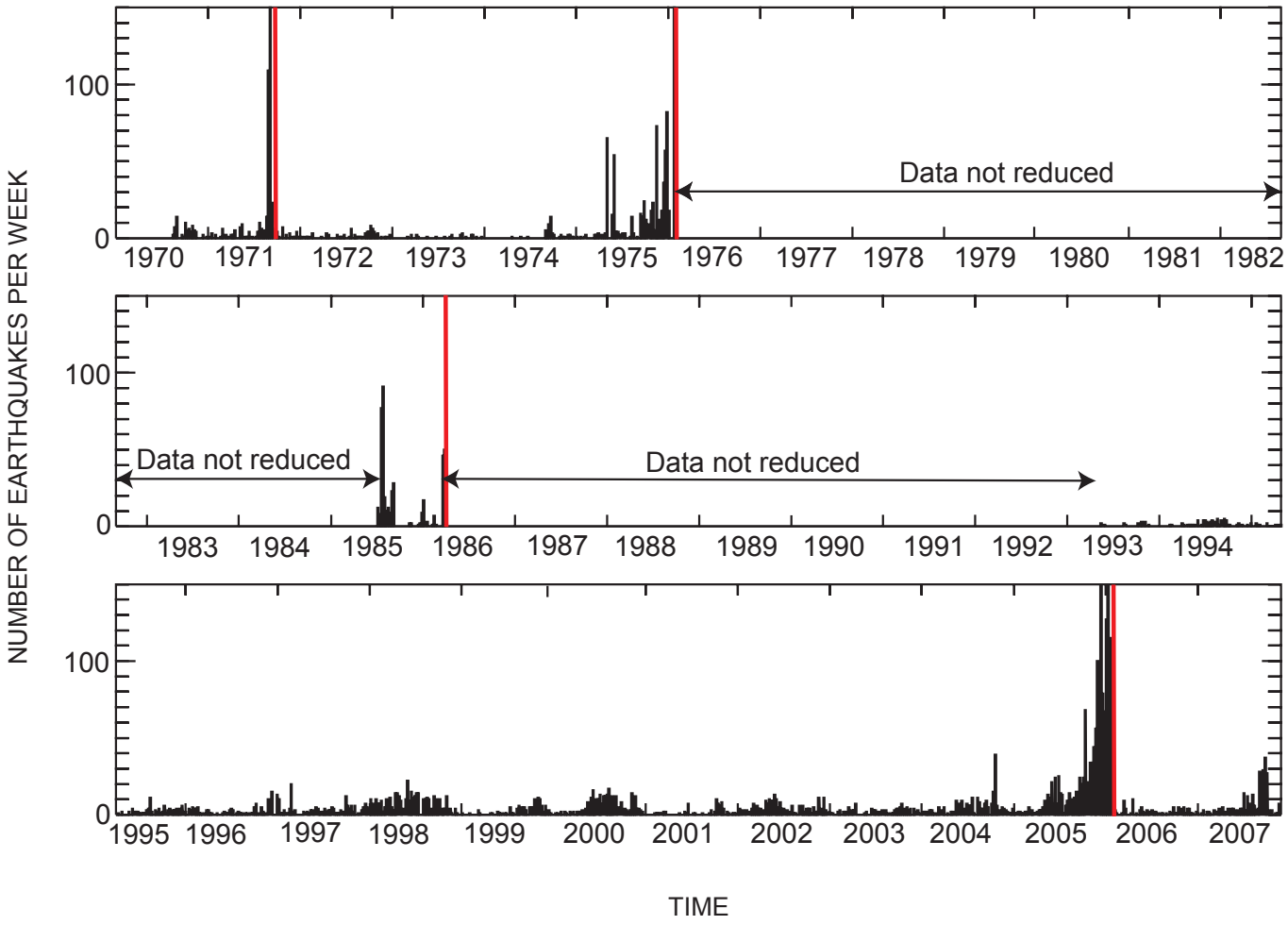

Figure 3. Histograms of the number of earthquakes located at Augustine Volcano per week between 1970 and 2007. Before installation of the full network in 1972 (table 1), data simply reflect number of earthquakes detected. Periods when earthquakes were not routinely located (January 1976 to July 1985 and March 1986 to May 1993) are noted. Red lines correspond to onsets of eruptions in 1971, 1976, 1986, and 2006.

and identified several families that occurred at progressively shallower depths in the weeks prior to the onset of eruptive activity in 2006.

Earthquake magnitudes at Augustine were calculated using several methodologies during the period of this study. From 1970 through 1976 a coda magnitude scale was used for earthquakes located beneath the central volcanic edifice, above 0.25 km a.m.s.l. For earthquakes at greater depth or those with hypocenters located away from the central edifice a local magnitude (M_L) was calculated using frequency-amplitude measurements in the manner described by Lahr (1999). This methodology was adopted to overcome strong attenuation affects observed for earthquakes with deeper hypocenters (Lalla and Kienle, 1978). For larger earthquakes that clipped all local stations on Augustine Island during this period, local magnitudes were determined at station CKK (fig. 1) assuming a hypocentral depth of sea level. Since 1985 we use frequency-amplitude measurements to calculate M_L using HYPOELLIPSE (Lahr, 1999). These methodologies were chosen to provide the most reliable magnitude information possible given the data available during the respective time period. During intereruptive periods, the largest earthquakes at Augustine generally do not exceed magnitude 1.2. The largest earthquakes recorded at Augustine during the period of this study reached magnitude 2.75 and occurred on January 22 and 23, 1976, in a 22-hour sequence that accompanied the onset of explosive activity in 1976 (fig. 4). A study of *b* values for Augustine earthquakes between 1993 and 2007 is given by Jacobs and McNutt (this volume).

Augustine Seismicity

The dominant seismic activity seen at Augustine Volcano between 1970 and 2007 are small VT earthquakes. These events generally have impulsive to emergent P arrivals and

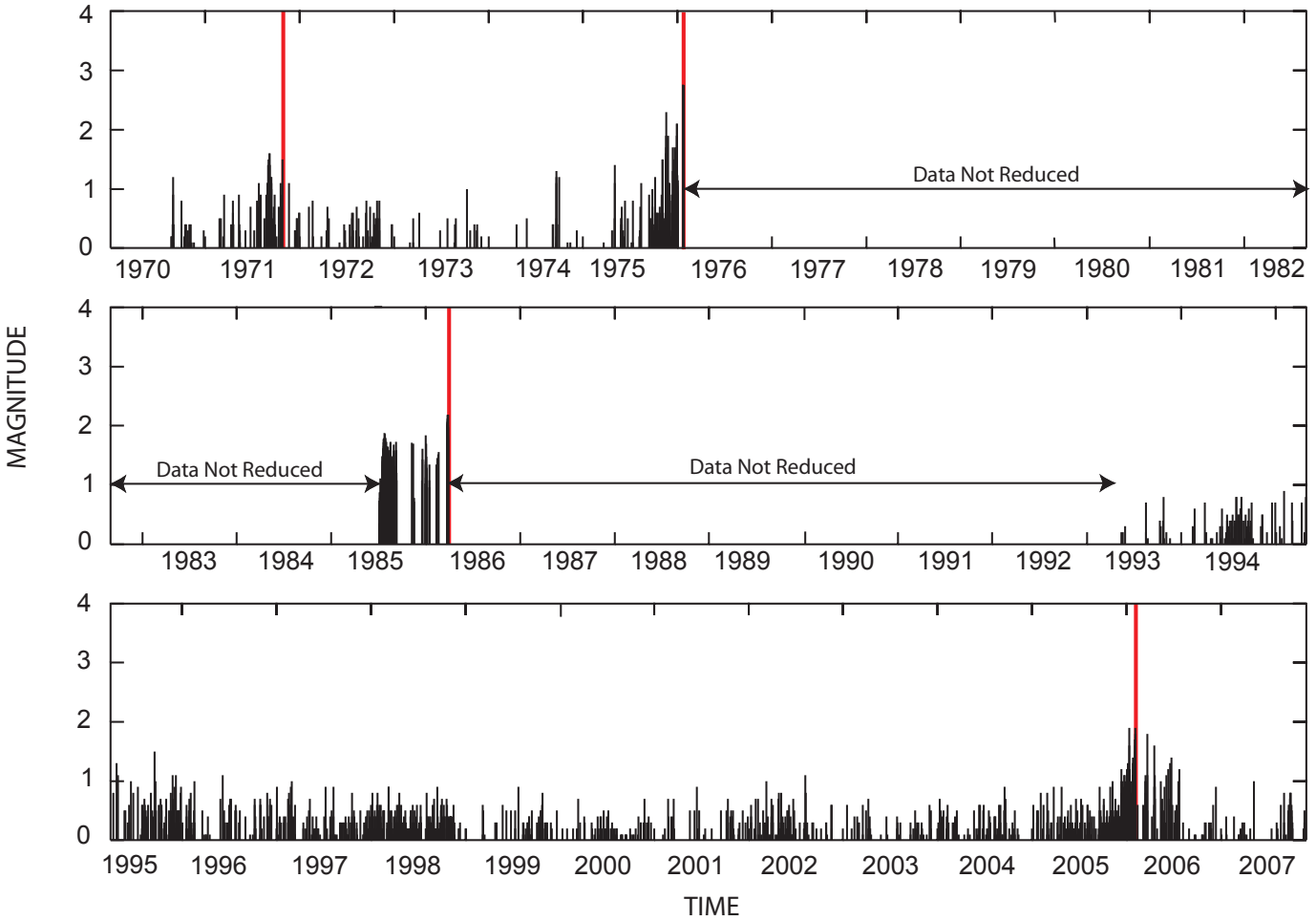

Figure 4. Summary of the magnitudes of detected earthquakes located at Augustine Volcano between 1970 and 2007. Magnitudes that are greater than magnitude (M_L) 0.0 are shown as individual vertical lines. Periods when earthquakes were not routinely located (January 1976 to July 1985 and March 1986 to May 1993) are noted. Red lines correspond to onsets of eruptions in 1971, 1976, 1986, and 2006.

poorly defined S arrivals and a broad spectrum with significant energy between 1 and 15 Hz (fig. 5*A*). At Augustine, waveforms from these earthquakes have well-defined phases on stations located high on the volcanic edifice, and the waveforms degrade rapidly on stations located on the pyroclastic apron (fig. 6). During intereruptive periods epicenters of these earthquakes generally occur within 1 to 2 km of the volcano's summit and range in depth from 1 km b.m.s.l. to 1.2 km a.m.s.l. (the volcano's summit). Infrequently, small VT earthquakes also occur on the south and north flanks of the volcano (fig. 7). Deshon and others (this volume) found that only 30 to 40 percent of located earthquakes occurred in event clusters, or earthquake families, between 1993 and 2006, suggesting that VT earthquake activity is widely distributed throughout the Augustine cone during this period.

At Augustine, LP events are comparatively rare; their occurrence is generally restricted to periods surrounding eruptive episodes. These events usually have emergent to poorly developed phases and have a strong peak frequency near 2 Hz (fig. 5*B*). Well-recorded LP events locate within 1 to 2 km of the volcano's summit at depths of sea level or above. At Augustine we also see a variety of waveforms that have a mix or range of frequencies similar to the hybrid events described by Lahr and others (1994). In this report we do not attempt to classify events as hybrids. Studies of event classifications during the 2006 eruption are given by Buurman and West (this volume) and Jacobs and McNutt (this volume).

Several times during the 1986 and 2006 eruptions, we recorded sequences of small repetitive regularly spaced events that often had similar waveforms. These earthquakes can occur at rates that range from 1 event every few minutes to as high as 8 to 10 events per minute or possibly higher. Similar small repetitive events have been reported at numerous volcanoes, typically during the effusive eruption of magma that ranges from high-silica andesite to dacite in composition. These volcanoes include Mount Usu, Japan (Okada and others, 1981), Mount St. Helens (Fremont and Malone, 1987; Moran and others, 2008; Thelen and others, 2008), Mount Redoubt (Power and others, 1994), Guagua Pichincha, Ecuador (Villagomez, 2000), and Soufriere Hills Volcano, Montserrat (Rowe and others, 2004). As a result of the repetitive character of these earthquakes they have recently been termed "drumbeats" at Mount St. Helens (Moran and others, 2008). At Augustine, drumbeat earthquakes typically have poorly defined phases and fairly narrow spectra, with most energy concentrated between 1 and 6 Hz (fig. 5*C*).

Seismic signals generated by explosive eruptions at Augustine generally have emergent onsets, extended high-amplitude codas, and fairly broad spectrums with peak frequencies near 2 to 3 Hz (fig. 5*D*). Explosive eruptions generally are quite powerful and register well on distant stations such as OPT and CKK (fig. 1). At Augustine, explosive eruptions are often accompanied by seismic signals associated with pyroclastic flows and lahars. These signals generally have a broad spectrum and can be very strong on individual stations on various quadrants of the volcano. A parametric study of explosive eruptions at Augustine in 2006 has been prepared by McNutt and others, (this volume).

Seismic signals from rock avalanches or rockfalls observed at Augustine are generally emergent and have a broad spectrum with energy between 1 and 6 Hz (fig. 5*E*). These signals are most prevalent when the lava dome and associated flows are actively growing and shedding material down the steep upper flanks of the volcano.

A unique type of low-frequency seismic event generated at Augustine results from the interaction of shore–fast sea ice and the ocean tides. During periods of cold winter weather (–15 to –30° C or 5 to –20° F), low frequency seismic events with emergent waveforms, a distinct lack of identifiable phases, and extended codas are often observed. The dominant frequency of these events is generally between 1 and 5 Hz (fig. 5*F*). The largest amplitudes occur on the stations closest to the shoreline and the seismic waves generally do not propagate well enough to be identified on stations high on the volcanic edifice or on the opposite side of the island. Between 1993 and 2007 we have observed these events being generated on all quadrants of the island, although they seem to be most often observed at station AUI (fig. 2*B*), suggesting a frequently active source area along the southern shoreline. We have visited the island when these events were occurring in February 1993 and March 2007 and have noted large accumulations of sea ice along the island's coastline. Mauk and Kienle (1973) found that events with these characteristics were most common during the ocean tide high, although they attributed them to volcanic activity. Because we only observe these events during periods of very cold weather, we believe they most likely reflect the breakage or movement of shore fast sea ice in response to the changing ocean tides in Cook Inlet. A similar explanation was advanced by Lalla and Kienle (1980).

Eruption Chronologies

In this section we describe the sequence of seismic events that accompanied the minor eruption in 1971 and the major eruptions in 1976, 1986, and 2006. For these chronologies we combine seismic information with visual, geological, and geophysical observations of the volcano to provide as much context for the seismic observations as possible. We focus on the periods from the time when seismicity first began to increase to the time when unrest ceased following the eruption. These periods are August 30, 1971, to December 21, 1971; May 2, 1975, to April 24, 1976; July 5, 1985, to September 10, 1986; and April 30, 2005, to March 18, 2006. The number of located earthquakes and the reported periods of eruptive activity for the 1976, 1986, and 2006 eruptions are shown on a comparative time scale in figure 8. In this paper the times of specific events are referenced to either Alaska Standard Time (AKST) or Alaska Daylight Time (AKDT). To convert to UTC before January 1, 1983, subtract 10 hours

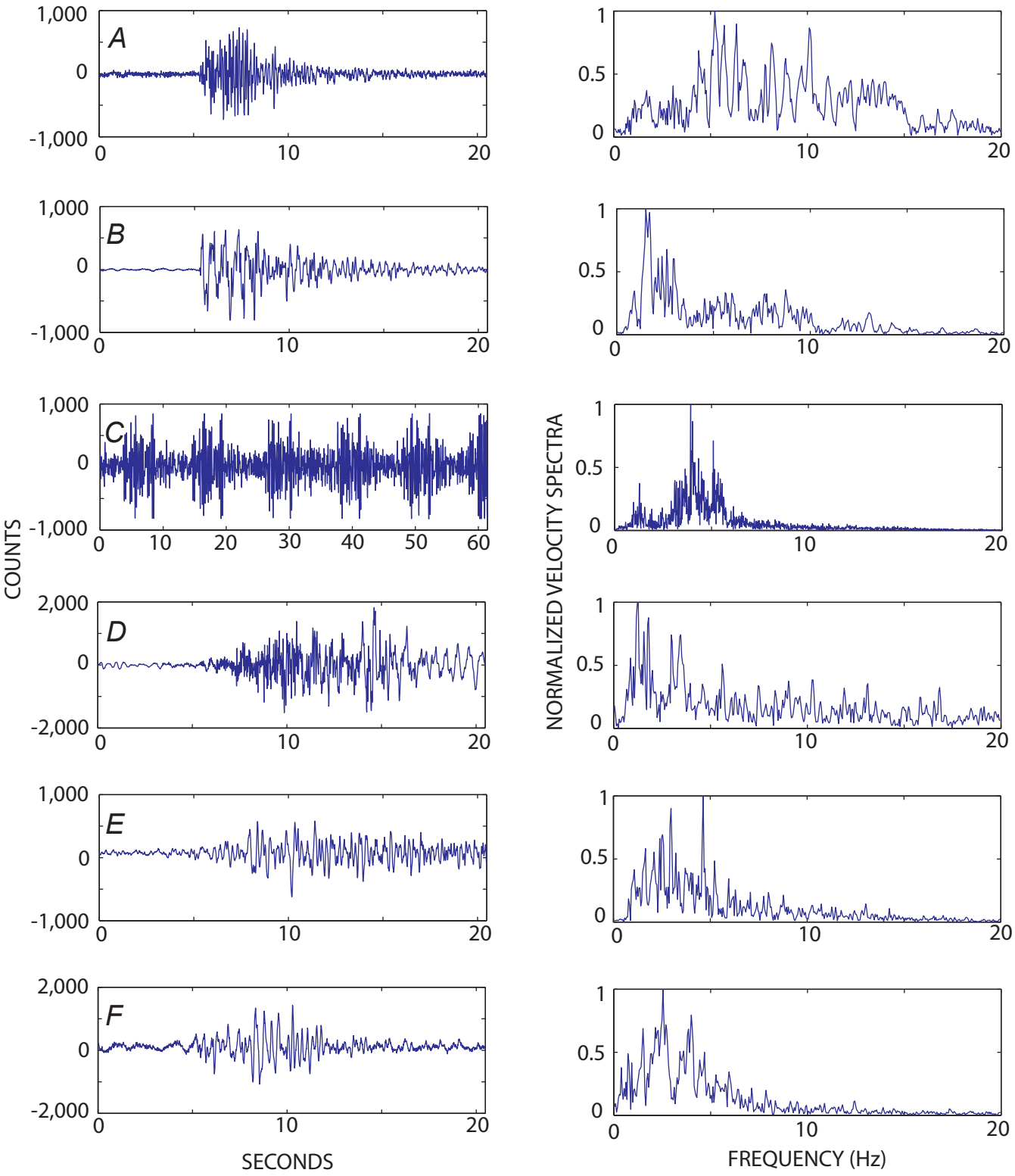

Figure 5. Waveforms and normalized velocity spectra of typical seismic events recorded at Augustine Volcano. Individual events represent, (*A*) volcano-tectonic earthquake at station AUH on May 26, 2005, 1601 AKST, M_L = 0.2, Z = 0.98 km a.m.s.l., station; (*B*) long-period event at station AUH on October 10, 2005, 0410 AKST, ML = 0.2, Z = 0.48 km a.m.s.l.; (*C*) drumbeats at station AUW on March 8, 2006, 1500 AKST; (*D*) explosion recorded at station AU13 on January 11, 2006, at 0514; (*E*) Rockfall on station AUE May 26, 2006, 0006 AKST; (*F*) ice event seen at station AUI on January 10, 2005, 1948 AKST. Spectra were calculated using a 20.48 second sample, except for the drumbeat earthquakes shown in panel *C*, which uses a 61.44-second sample.

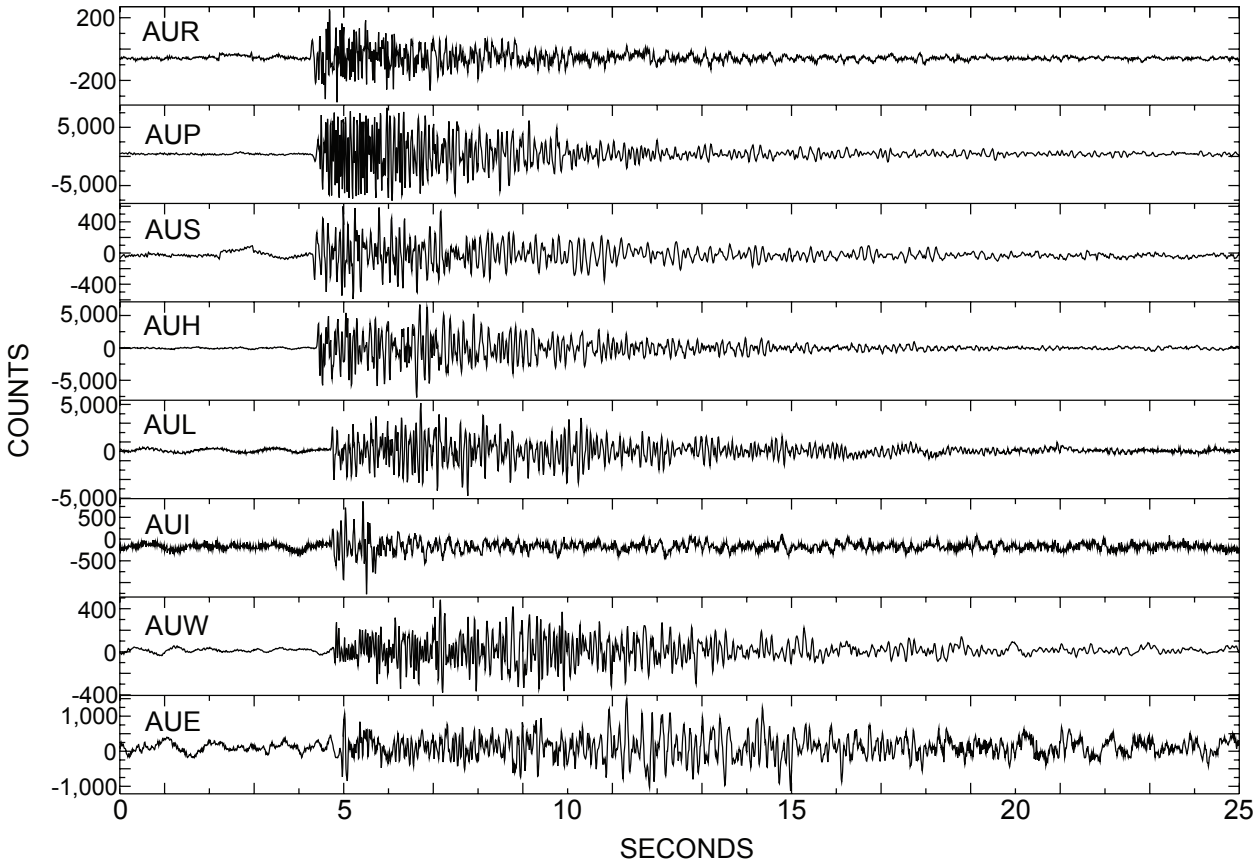

Figure 6. Velocity waveforms of a volcano-tectonic earthquake with magnitude (M_L) 0.1 that occurred on October 10, 2005, at 0037 UTC at a depth of 0.22 km a.m.s.l. beneath the summit of Augustine Volcano as recorded on various seismic stations on Augustine Island.

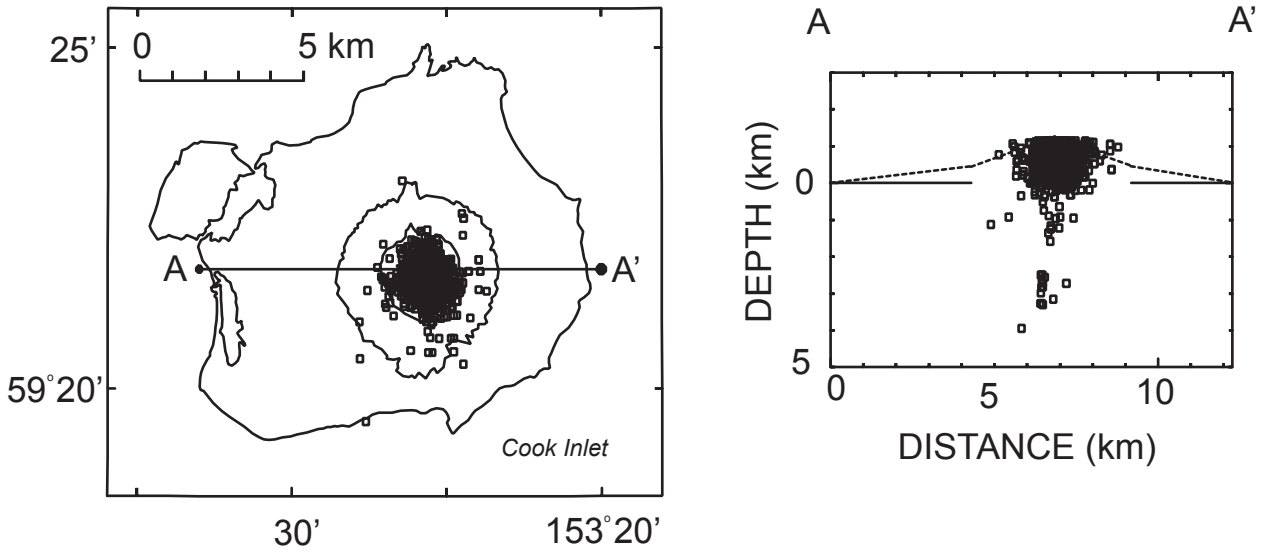

Figure 7. Map and west-east cross section (A to A') showing earthquake hypocenters at Augustine Volcano between 1993 and 2007. Only hypocenters with standard horizontal and vertical errors of less than 5 km are shown. Sea level, 1,000-ft and 2,000-ft contours are shown in map view. Dotted line in cross section represents approximate surface elevation along cross section A–A'. The hypocenters between 2 and 4 km depth all occurred between March 15 and August 16, 2006, following the end of the 2006 eruption.

from AKST and 9 hours from AKDT. After January 1, 1983, subtract 9 hours AKST and 8 hours from AKDT.

To provide a consistent measure of earthquake activity during these precursory seismic sequences we have relocated many earthquakes with the 2-dimensional ray tracing algorithm described by Lalla and Power (this volume). This was not possible for the 1971 eruption, because only two stations were operating on the volcano at that time. Histograms of the number of relocated earthquakes per day during the precursory sequences of the 1976, 1986, and 2006 eruptions are shown in figure 9. Relocated earthquake hypocenters for each precursory period are shown in map and east-west cross section in figure 10, and plots of focal depth versus time are shown in figure 11. Seismic events such as explosive eruptions, rock avalanches, and pyroclastic flows are more difficult to describe because the seismic stations operating on the volcano and the

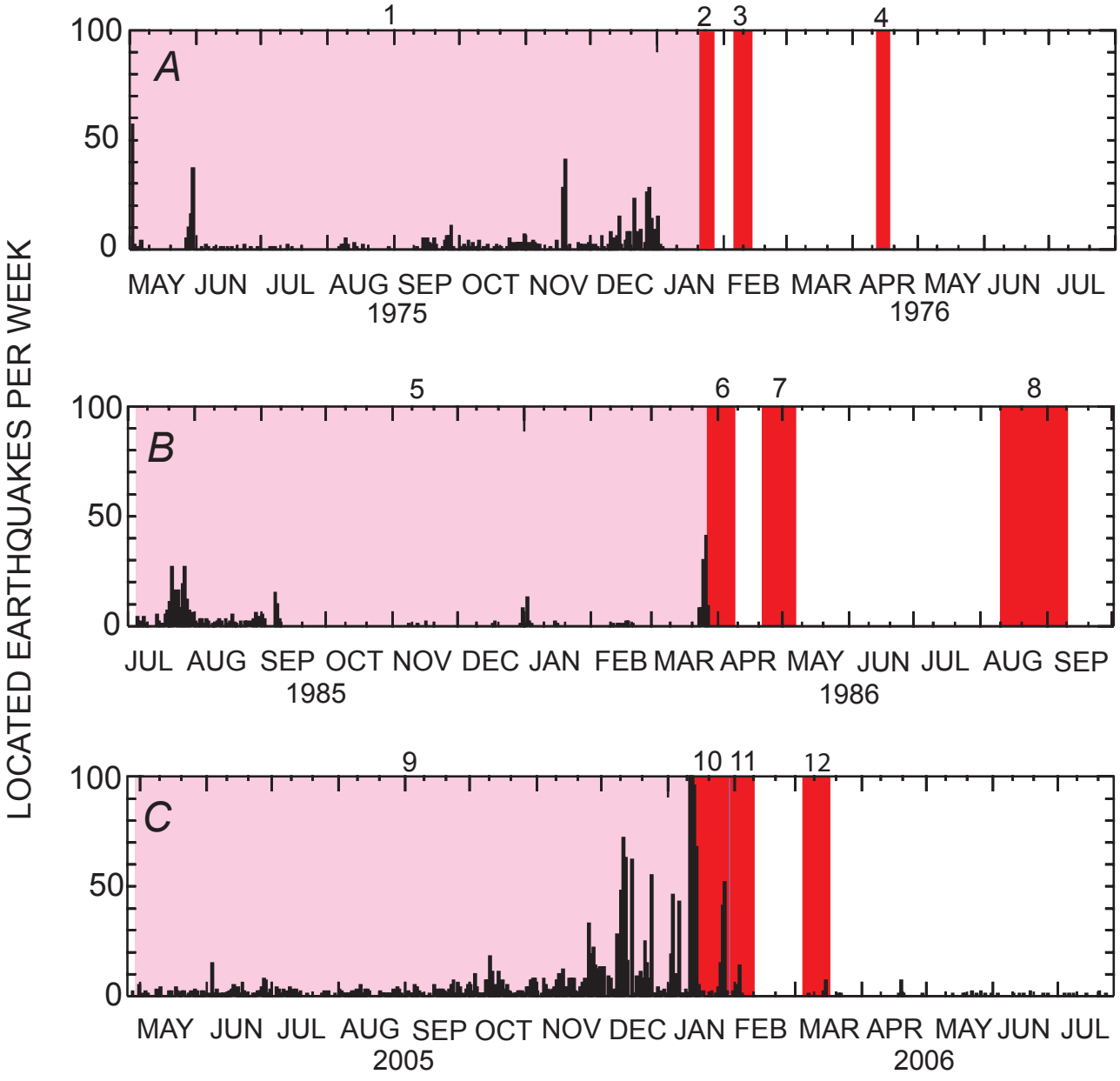

Figure 8. Comparative time lines of the eruptive phases of (*A*) 1976, (*B*) 1986, and (*C*) 2006 eruptions based on histograms of the number of located earthquakes each week. Pink shading corresponds to precursory periods, and red shading corresponds to eruptive periods. Numbers correspond to: 1, 1976 precursory phase; 2, the first 1976 explosive phase; 3, the second 1976 explosive phase; 4, 1976 effusive phase; 5, 1986 precursory phase; 6, 1986 explosive phase; 7, 1986 initial dome building phase; 8, 1986 second dome building phase; 9, 2006 precursory phase; 10, 2006 explosive phase; 11, 2006 continuous phase; and 12, 2006 effusive phase.

resolution of the recording media changed drastically between 1970 and 2007. For earlier time periods we rely on descriptions developed by Reeder and Lahr (1987) for the 1976 eruption and Power (1988) for the 1986 eruption.

The 1971 Eruption

On August 30, 1971, an intense earthquake swarm began that lasted until September 6, 1971 (fig. 3). These earthquakes had broad-spectrum VT waveforms and were of much larger magnitude than those previously recorded at Augustine. During the peak in activity between September 2 and 4, more than 300 identifiable earthquakes per day were recorded on station AU1. Seismic records from AU1 and AU2 on September 6 show the high level of VT earthquake activity recorded during this swarm (fig. 12). A photograph taken by Austin Post of the volcano on September 3, 1971, shows vigorous steaming on the east side of the volcano's summit (Kienle and Swanson, 1985). Smaller earthquake swarms were recorded November 28–30 and December 19–21, 1971 (fig. 3).

On October 7, 1971, a fishing boat 38 km north of the volcano reported a small ash eruption and red glow from the summit. This report coincides with a 2 hour period of volcanic tremor recorded on October 7 and 8 between 2300 and 100 (AKDT) (Kienle and Swanson, 1985). No information exists on the extent or type of eruptive products that may have been produced by this event. The red glow reported by

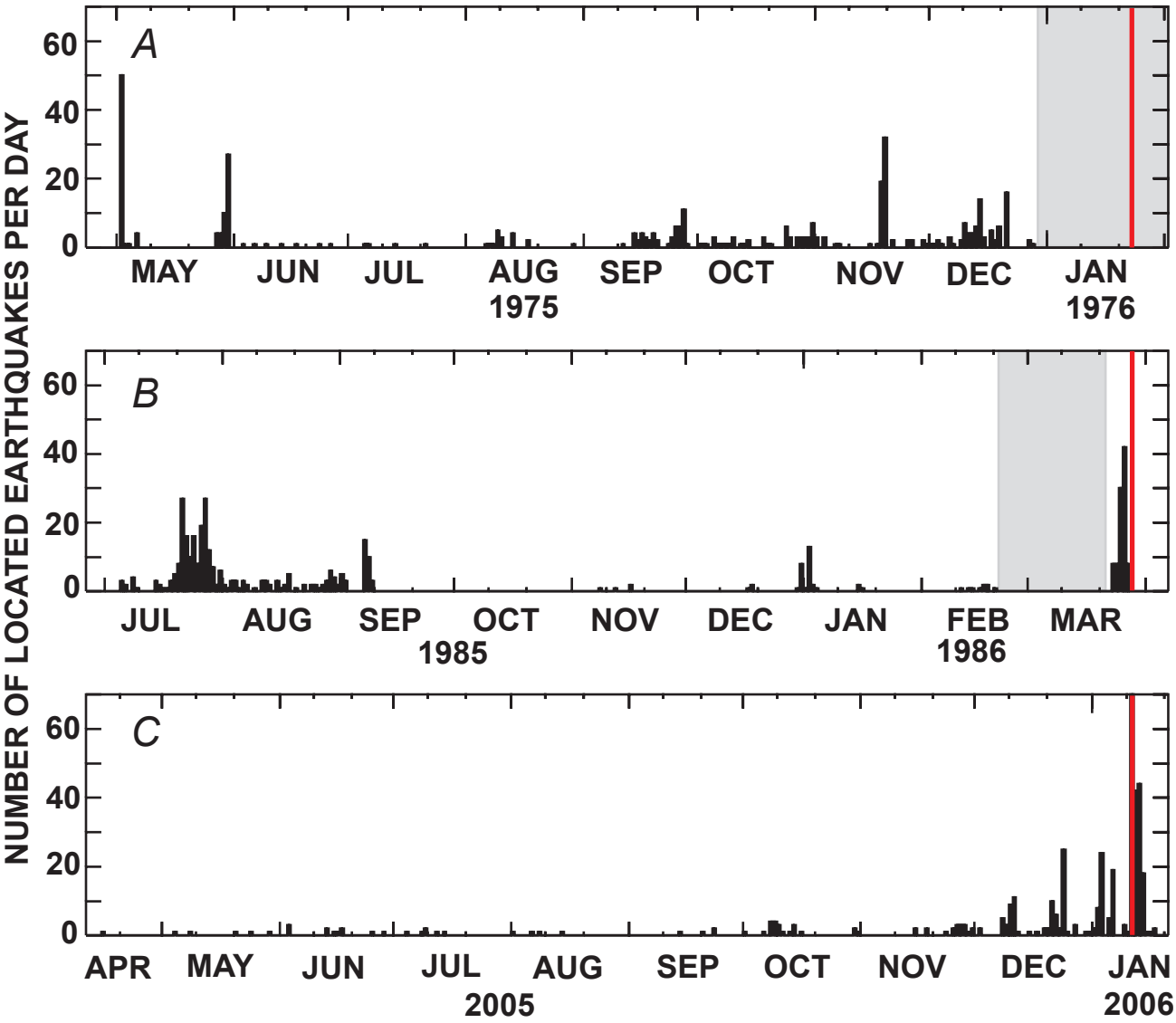

Figure 9. Histograms showing the number of relocated earthquakes that occurred before the *(A)* 1976, (*B*) 1986, and (*C*) 2006 eruptions of Augustine Volcano. The time periods when the Augustine seismic network was not operating sufficiently to relocate earthquakes are shown in gray. Red lines correspond to the onset of explosive events in the 1976, 1986, and 2006 eruptions.

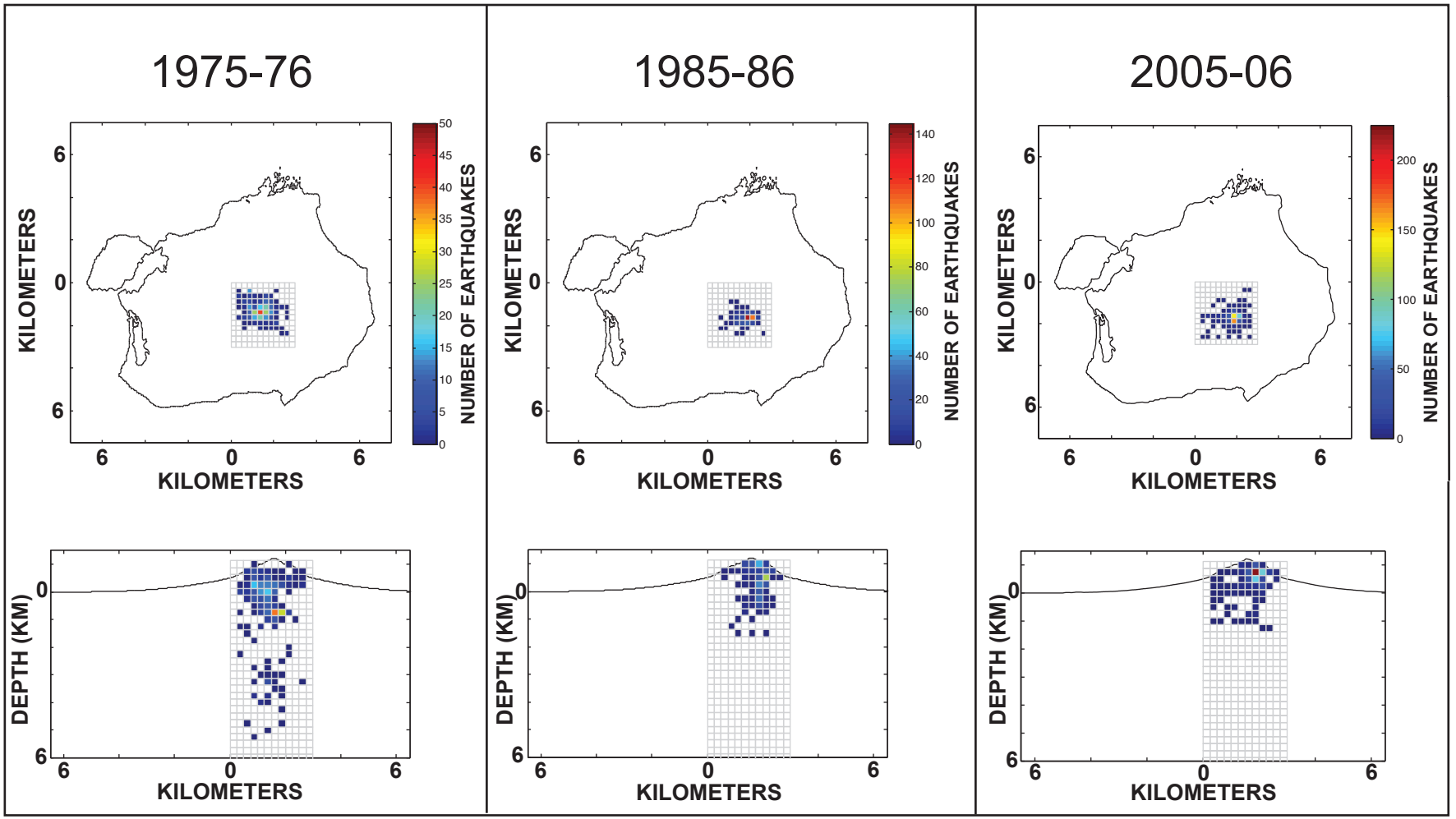

Figure 10. Map and east-west cross sections of relocated earthquakes at Augustine Volcano during precursory phases of the 1976, 1986, and 2006 eruptions. Color scales indicate the number of earthquakes located in each grid square.

the fishing boat suggests that it represents more than a simple phreatic explosion, perhaps mild explosive activity and a small lava extrusion near the volcano's summit.

The 1976 Eruption

Seismic activity associated with the 1976 eruption of Augustine Volcano was closely observed by the five stations on the island (fig. 2*A*) and the additional stations surrounding southern Cook Inlet (fig. 1). Unfortunately, all the stations on the island failed in early December 1975 as a result of severe winter weather (Johnston, 1978). However, station CKK on the Alaska Peninsula (fig. 1) operated at an unusually high gain and provided a means of tracking earthquakes at Augustine Volcano as small as magnitude (M_L) 0.25. The 1976 eruption consisted of four distinct phases based on the character of seismic activity and eruptive behavior. For this discussion we define the phases as follows:

1. Precursory phase (May 2, 1975, to January 23, 1976).
2. Explosive phase (January 22 to 25, 1976).
3. Second explosive phase (February 6 to 14, 1976).
4. Effusive phase (April 13 to 18, 1976).

These time periods were selected on the basis of descriptions of seismicity and eruptive activity provided by Reeder and Lahr (1987), Kienle and Shaw (1977), and Kienle and Swanson (1985).

Precursory Phase—May 2, 1975, to January 22, 1976

The precursory phase began with a pronounced swarm of VT earthquakes on May 2, 1975 (fig. 8). These shocks had impulsive arrivals and well-defined phases compared to most Augustine earthquakes. Relocated hypocenters clustered near sea level, and the largest magnitude was 1.4. This swarm quickly died off, with the last locatable event occurring on May 6, 1975. The volcano was then seismically quiet until May 27, when a second pronounced swarm of earthquakes began. This swarm consisted of 67 earthquakes large enough to be relocated (fig. 9), and the largest event had a magnitude of 0.7 (fig. 4). Seismicity following this swarm continued at a new higher rate of 5 to 10 relocated events per month. On September 14 the rate of seismicity climbed to a higher rate of tens of earthquakes located each month. This rate climbed again in late November to 100 to 200 events per month

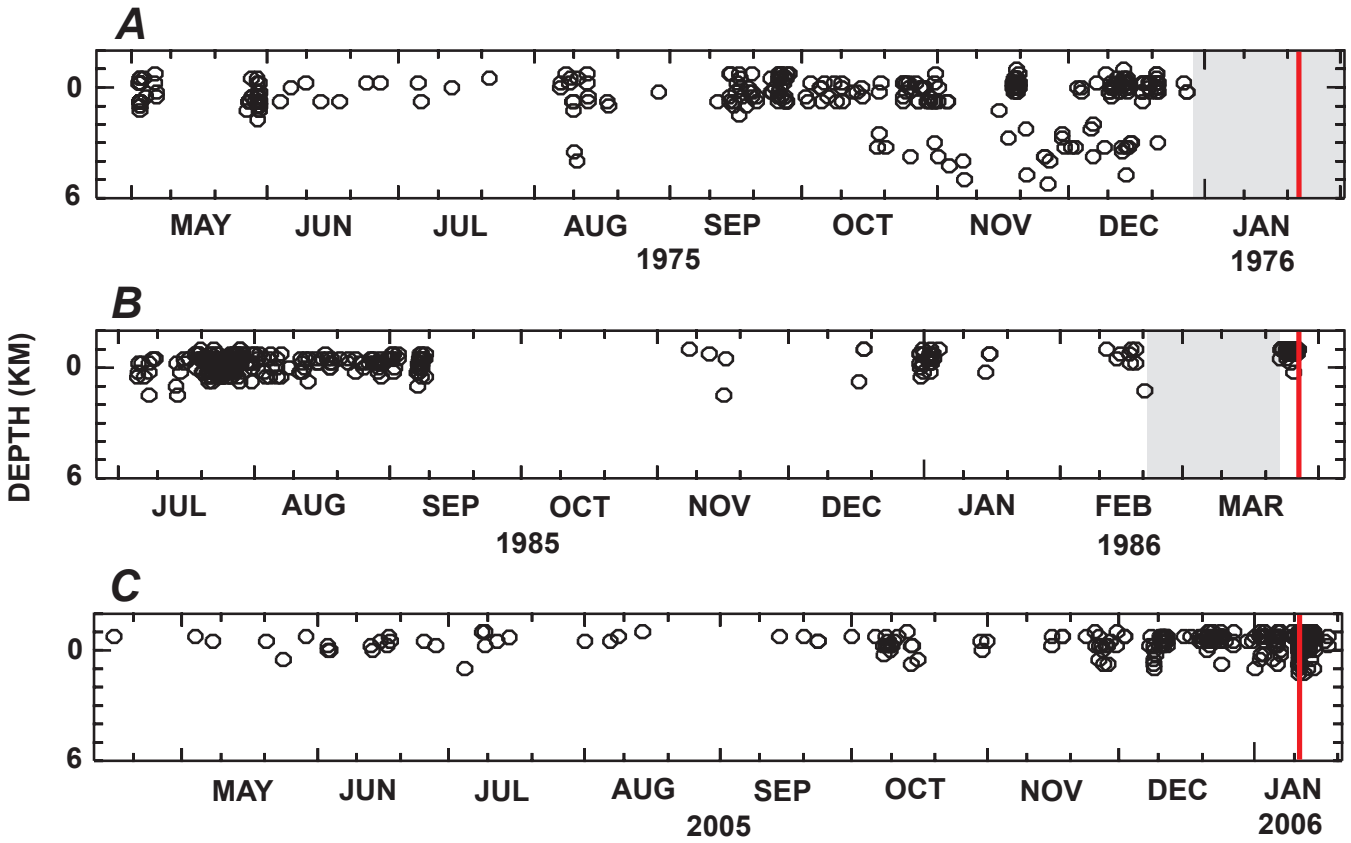

Figure 11. Plots of focal depth versus time for earthquakes relocated during the precursory phases of the (*A*) 1976, (*B*) 1986, and (*C*) 2006 eruptions of Augustine Volcano. The time periods when the Augustine seismic network was not operating sufficiently to relocate earthquakes are shown in gray. Red lines correspond to the onset of major explosive events in 1976, 1986, and 2006.

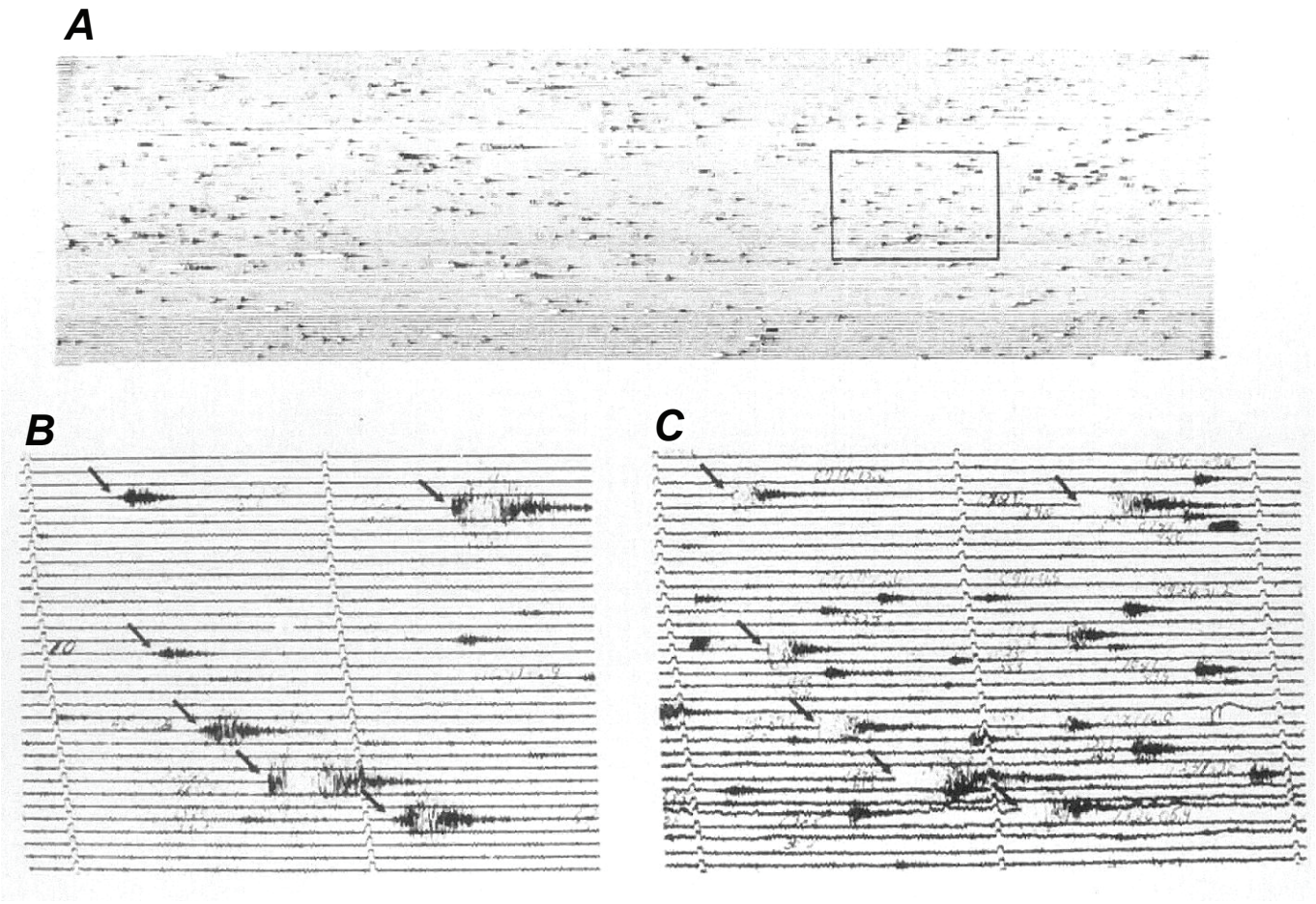

Figure 12. Drum records showing the character of earthquake activity prior to the 1971 eruption of Augustine Volcano. *A*, 24-hour drum record from seismic station AU1 on September 6, 1971. Small box in *A* denotes time periods shown in *B* and *C* on stations AU2 and AU1, respectively. Time marks represent 1 minute intervals.

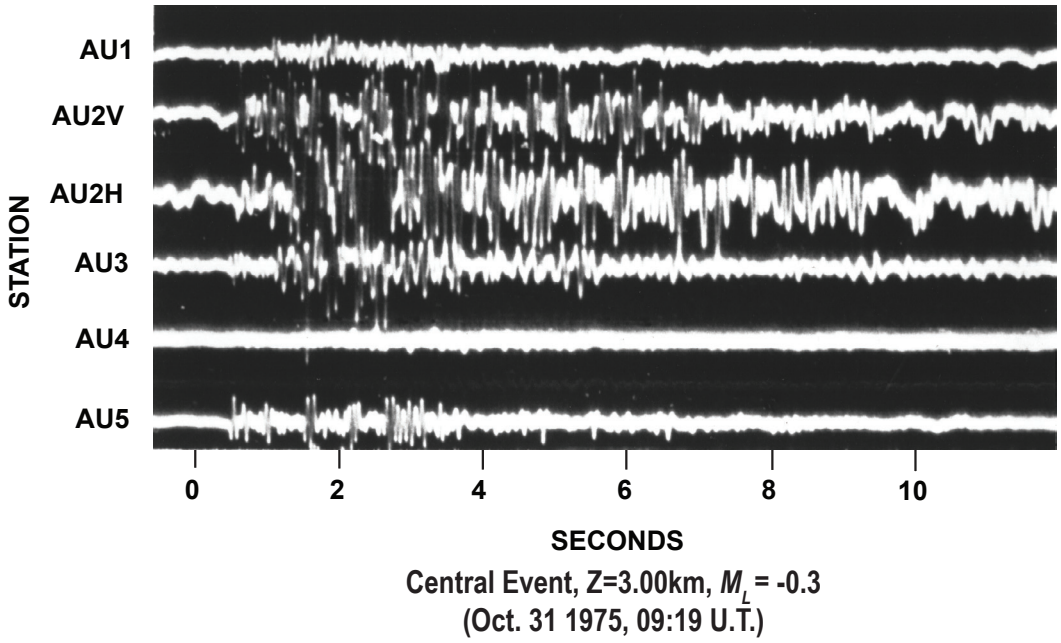

Figure 13. Seismograms from various seismic stations on Augustine Island of a magnitude (M_L) –0.3 earthquake located at a depth of 3 km below sea level on October 30, 1975 at 2319 AKST. Note small amplitudes observed at station AU4 (fig. 2*A*), which is near the summit, compared with other stations that are located on the flanks of the volcanic edifice. Stations AU2H and AU2V represent the horizontal and vertical components of station AU2, respectively.

(fig. 3). This high rate of earthquake activity continued until the network failed on December 22, 1975.

On August 10, earthquakes with hypocentral depths ranging from 2.75 to 5.25 km b.m.s.l. began to occur. Two of these deeper events were located on August 10 and 29, and additional events were located between October 18 and December 21, 1975 (fig. 11). The waveforms of these earthquakes have well-defined P and S phases and broader frequency content typical of VT earthquakes (fig. 13). Earthquakes in this depth range were found to have characteristically higher amplitudes on the flank stations such as AU2 and AU3 and lower amplitudes on the higher station AU4 (fig. 2*A*). This is the opposite of relative amplitudes observed for earthquakes with hypocentral depths of 1 km b.m.s.l. and above. Magnitudes of the deeper events ranged from –2.0 to 1.3. Increased steaming and fumorolic activity was reported by Johnston (1978) beginning in October of 1975.

Initial Explosive Phase—January 22 to 25, 1976

The 1976 eruption of Augustine began with a large explosion at 1759 AKST on January 22 which produced an ash plume that rose to 14 km a.m.s.l. (Kienle and Shaw, 1977; Reeder and Lahr, 1987). This explosion initiated a 22-hour-long sequence of more than 668 earthquakes that ranged in magnitude from 1.6 to 2.75 as determined by amplitude measurements on station CKK (fig. 1) located on the Alaska Peninsula. The rate and magnitudes of earthquakes recorded at station CKK and the times of explosive eruptions reported by Kienle and Shaw (1977) are shown in figure 14. This energetic swarm is the most vigorous recorded at Augustine Volcano between 1970 and 2007. The swarm was most intense between 0300 and 0600 AKST and was declining in intensity when the larger explosive events occurred (fig. 14). The explosive eruptions on January 23, 1976, as described by Kienle and Shaw (1977) were clearly the most powerful observed at Augustine during the 38 years of this study.

Kienle and Shaw (1977) report 12 additional Augustine explosions between 0353 on January 23 and 0457 AKST on January 27 that produced detectible infrasonic signals in Fairbanks. Reported plume heights for these explosions ranged from 6 to 12 km a.m.s.l. Reeder and Lahr (1987) report the occurrence of "large tremors" at station CKK associated with all 12 of these explosions. They report the occurrence of 22 additional "small tremors" recorded at station CKK between January 22 and 25 that may represent smaller explosions. Ashfall from these eruptions covered many areas surrounding Cook Inlet including Anchorage, Kenai, Homer, Seldovia, and Iliamna (Johnston, 1978).

The strong explosions in January 1976 removed a significant portion of the summit lava dome emplaced at the end of the 1964 eruption, leaving a crater that was estimated to be 200 m deep (Johnston, 1978). On the basis of coordinates of benchmarks located on the remnant crater rim (Power and Iwatsubo, 1998), we estimate the size of this crater to be roughly 550 by 350 m.

Second Explosive Phase—February 6 to 14, 1976

Eruptive activity resumed at 1444 AKST on February 6 with a powerful seismic signal recorded on station CKK. Activity continued at a sustained rate through February 14. Larger seismic signals were recorded late February 8 (Reeder and Lahr, 1987, figure 22). This phase of the eruption again produced large plumes that deposited ash on communities on the Kenai Peninsula, as well as numerous block-and-ash flows that moved down the north side of the volcano (Johnston,

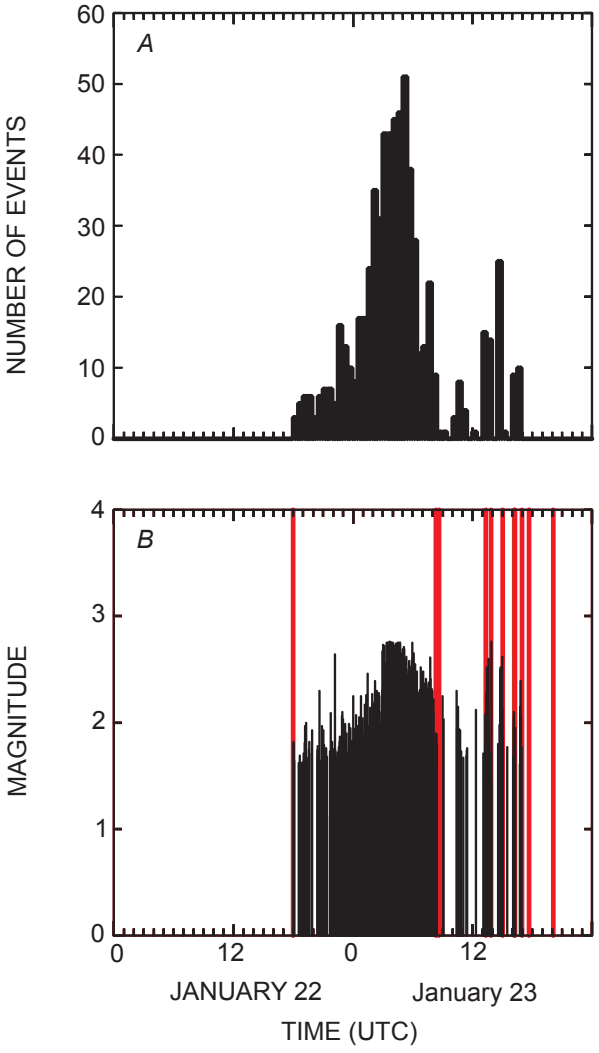

Figure 14. Time history of earthquake occurrence, magnitude, and explosive eruptions at Augustine Volcano on January 22 and 23, 1976. *A*, Number of earthquakes detected at station CKK during each 30-minute period. *B*, Each vertical line represents the magnitude of one earthquake as determined at station CKK. Red lines indicate times of explosive eruptions reported by Kienle and Shaw (1977). Time is referenced to UTC; to convert to AKST subtract 10 hours.

1978). Kienle and Swanson (1985) report that a new lava dome within the summit crater was first observed on February 12, 1976.

Effusive Phase—April 13 to 18, 1976

Seismic activity consisting of small tremors and shallow earthquakes resumed on April 13 and continued through April 18 (Reeder and Lahr, 1987, figure 24). Kienle and Swanson (1985) report that three seismic stations were reestablished on the island in February and these recorded numerous signals associated with block and ash flows that continued until April 24.

The 1986 Eruption

The 1986 eruption was well observed seismically by the network of four to five stations that was operating on the volcano throughout this eruption (fig. 2*B*). Descriptions of the 1986 eruption based on observations from individuals in the vicinity of the volcano, radar, observational overflights, satellite photographs, and a qualitative analysis of the seismic record were prepared by Yount and others (1987) and Swanson and Kienle (1988). A more detailed discussion of the seismic activity associated with the 1986 eruption was prepared by Power (1988).

Power (1988) divided the eruption into four phases based on the character of seismic activity and eruptive activity as follows:

1. Precursory phase (July 5, 1985 to March 26, 1986).
2. Explosive phase (March 26 to April 8, 1986).
3. Initial dome-building phase (April 21 to May 7, 1986).
4. Second dome-building phase (August 10 to September 10, 1986).

The character of seismicity changes dramatically from the precursory to the eruptive phase, and there are also significant differences among the remaining eruptive phases.

Precursory Phase—July 5, 1985 to March 26, 1986

The precursory phase to the 1986 consisted of several distinct swarms separated by long periods of seismic quiescence (Power, 1988). This phase began with a very energetic swarm of VT earthquakes that started on July 5, 1985, and continued until September 9, 1985. Relocated hypocenters in this swarm appear to have begun at depths of 0.2 to 0.4 km b.m.s.l. and quickly migrated to depths of 0.1 to 0.5 km a.m.s.l. The largest earthquake had a magnitude of 1.5. The swarm reached maximum intensity in late July 1985 (fig. 8).

Following this swarm the volcano went through a period of seismic quiescence from roughly September 10 to December 18. No other unusual behavior of the volcano was noted (Yount and others, 1987; Power, 1988). A small increase in the number of earthquakes began on December 18. This increase culminated in a short but intense swarm from December 31, 1985 to January 2, 1986. A magnitude 1.3 (M_L) earthquake on January 1 was the largest event of this period. Except for a small increase in mid-January, the volcano then remained relatively quiet until February 10 (fig. 8).

On February 10, 1986, the number of earthquakes increased an order of magnitude to tens of events per day. Unfortunately, on February 20 station AUI (fig. 2*B*) failed and earthquakes could not be located until it was repaired on March 22. To track seismicity during this period Power, (1988, figure 21) counted earthquakes from helicorder records of station AUH that were larger than M_L 0.25. Although, the number of events fluctuated greatly from day to day, the overall level of seismicity did not drop from this level until after the eruption. Earthquake activity during this period consisted of highly clustered bursts with 20 to 100 earthquakes occurring in a period of one to four hours. Earthquake activity of this character has been referred to as spasmodic bursts by Hill and others (1990). Figure 15 shows a helicorder record from station AUH illustrating a typical spasmodic burst on March 17, 1986. Individual spasmodic bursts can be separated by as much as 24 to 48 hours of relative quiescence. This increase in seismicity, coupled with reports of increased steaming, prompted the U.S. Geological Survey in Anchorage to make a series of observational overflights on February 22 and 28, and March 14 and 21. Increased fumorolic activity and snow melt were observed on successive flights (Yount and others, 1987).

A second order-of-magnitude increase in the seismicity rate to over 100 earthquakes per day greater than M_L 0.25 occurred on March 22. A ground party visited the volcano on this day to repair station AUI and to install station AUT. Vigorous steaming in the summit area and a strong sulfur smell downwind from the volcano were observed. The repair of station AUI allowed us to locate earthquakes again (fig. 9). Hypocentral depths of relocated earthquakes between March 22 and March 26 all cluster at 0.75 and 1.0 km a.m.s.l. (fig. 11). Late on March 24, a number of spasmodic bursts occurred that raised the rate of earthquake occurrence even higher (fig. 16). The largest events recorded during the 1986 eruption of Augustine Volcano occurred on March 26 and 27 and ranged in magnitude from 1.3 to 2.1 (fig. 4). Seismic signals with waveforms that resemble explosion events began to appear at 0957 AKST on March 26 (Power, 1988) (fig. 16). Power (1988) reported an upward migration of average hypocentral depth from 0.21 to 0.82 km a.m.s.l. during the precursory phase.

Explosive Phase—March 26 to April 8, 1986

The start of the eruption on March 26 marked a dramatic change in the character of the seismicity. However, analysis of this period is difficult because the film and helicorder records are saturated by the high levels of seismic activity. Before the

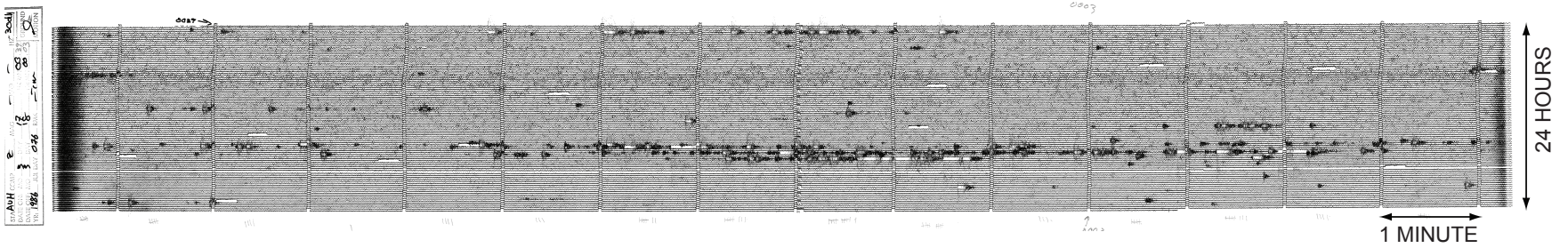

Figure 15. Drum record from seismic station AUH for March 17, 1986, showing a prominent spasmodic burst of earthquake activity composed of more than 75 earthquakes between 0630 and 0845 AKST. Note relative quiescence before and after spasmodic burst.

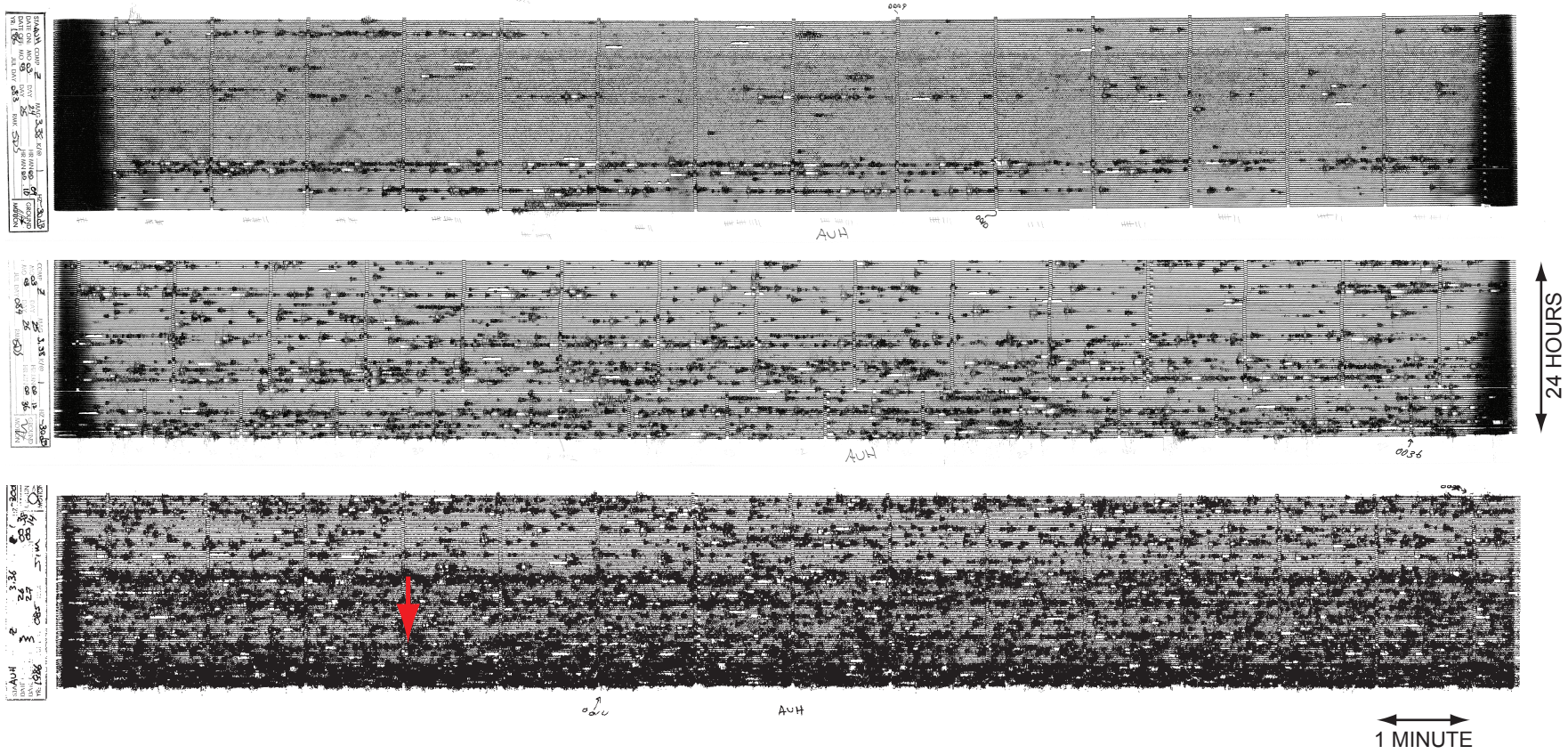

Figure 16. Drum records from seismic station AUH (fig. 2*B*) for March 24 through March 26, 1986, showing the strong buildup in earthquake activity before the onset of explosive activity in 1986. The red arrow notes the approximate onset of explosive activity at 0957 AKST on March 26, 1986.

explosive phase of the eruption, the seismic record is dominated by small VT earthquakes, generally of magnitude less than 1.3. Beginning at 0957 AKST on March 26 small explosions began to be interspersed with the earthquake signals. By 1711 AKST these explosions became strong enough to be recorded at station OPT, 25 km to the north of Augustine Volcano (fig. 1). As these explosion events began to increase in both amplitude and duration, the number of earthquakes began to diminish. By 0335 AKST on March 27 VT earthquakes were only occurring 5 to 10 minutes before the explosion events. Finally, by 1023 AKST on March 27 explosion events were taking place with no preceding earthquake activity. This sequence of intermixed earthquakes and explosions suggests that the Augustine vent opened rather slowly in 1986. This phase of the eruption produced widespread tephra throughout south-central Alaska and pyroclastic flows and lahars on Augustine Island (Yount and others, 1987).

To determine the relative size and rate of occurrence of explosions, Power (1988, figure 22) measured the onset and duration of the seismic signal at station OPT (fig. 1). These data show the relative intensity of explosive activity during this phase. The duration of individual events and the intensity of explosive activity increased slowly to a maximum on March 28 and then slowly decreased until March 31. At 0955 AKST on March 31 the largest single explosion occurred; the duration of this event was greater than 13 minutes at station OPT (Power, 1988). This explosion produced an eruption column that rose to more than 12 km above sea level, and spread ash over a wide area to the east of the volcano. Small explosions were also observed at OPT through April 4, and explosion events continued to be recorded on the island stations through April 8. Observations of these explosions, plume heights, and trajectories are discussed by Yount and others (1987). In addition to explosions, many events which could be related to pyroclastic flows and rock avalanches were also recorded during this phase.

Initial Dome Building Phase—April 21 to May 7, 1986

During this phase of the eruption a new lava dome was emplaced on the volcano's summit and a small lava flow moved down the upper northeast face of the volcano. Seismic activity was dominated by the occurrence of small repetitive earthquakes or drumbeats (Power, 1988, figure 29). A detailed description of observations of the volcano during this phase of the eruption is given by Yount and others (1987).

Drumbeat earthquakes first became apparent as a small increase above background noise at station AUH (fig. 2*B*) on April 21. By roughly 2000 AKST on April 21 the earthquakes were visible on helicorder records on all stations on the volcano and the signals from individual earthquakes began to run together, forming a continuous disturbance. To quantify this activity, Power (1988; figure 28) made hourly measurements of the signal amplitude on develocorder film on station AUH and identified periods when the signal was continuous or composed of identifiable discrete events. These measurements indicate that the drumbeat earthquakes increased in amplitude from April 22 to 27, then rapidly declined and disappeared completely by April 30. A second but less energetic period of drumbeats occurred from May 2 to 6 (Power, 1988). During this second period of drumbeats, individual events could be identified within the signal. On April 25 the approximate frequency of the signal was determined to be between 3 and 4 Hz.

Second Dome-Building Phase—August 10 to September 10, 1986

During this phase, dome building activity resumed and a peleean spine developed on the volcano's summit (Swanson and Kienle, 1988). This eruptive phase began about August 10, when Power (1988) reports that the number of avalanche signals began to increase gradually. Most of these signals were generated as small portions of the actively growing lava dome sloughed off the north side of the volcano's summit, forming pyroclastic flows (Kienle and Swanson, 1985). The seismic record became saturated with these signals on August 20. A count of surface events remained high until roughly September 10 (Power, 1988; figure 25). No associated increase in earthquake activity was noted (Power, 1988).

The 2006 Eruption

The 2006 eruption of Augustine Volcano received a much higher degree of monitoring and observation than earlier eruptions in 1971, 1976, and 1986. In addition to the increased seismic instrumentation (fig. 2*C*), a network of six continuous GPS receivers (CGPS) had been installed on the volcano by the Alaska Volcano Observatory (AVO) and EarthScope's Plate Boundary Observatory (PBO) (Pauk and others, this volume). Once unrest began, AVO deployed six temporary broadband seismometers, a strong-motion seismometer (AU20) (table 1), and five additional temporary CGPS (Cervelli and others, this volume) on the volcano. AVO also began a series of overflights to make visual observations, measure volcanic gas (McGee and others, this volume), and obtain thermal imagery (Wessels and others, this volume). AVO also deployed time-lapse and Web cameras (Paskievitch and others, this volume), and took high-resolution aerial photographs (Coombs and others, this volume). Researchers from the University of Alaska Fairbanks deployed a low-light camera in Homer, Alaska (Sentmen and others, this volume), and researchers from the New Mexico Institute of Mining and Technology deployed a lightning detection system (Thomas and others, this volume). Subsequent investigations of the deposits from the 2006 eruption are described by Coombs and others, (this volume), Vallance and others, (this volume), Larsen and others, (this volume), and Wallace and others (this volume).

The 2006 eruption of Augustine, like the 1976 and 1986 eruptions, consisted of four distinct phases defined by the character of seismicity, geophysical unrest, and eruptive activity, which are described below. The time periods for these phases are:

1. Precursory phase (April 30, 2005 to January 11, 2006).
2. Explosive phase (January 11 to 28, 2006).
3. Continuous phase (January 28 to February 10, 2006).
4. Effusive phase (March 3 to 16, 2006).

The number of located earthquakes per week, approximate times of phreatic and magmatic explosions, RSAM values from station AU13, ground deformation, measured SO_2 output, erupted volume, and the time periods of the four eruptive phases are summarized in figure 17.

Precursory Phase—April 30, 2005 to January 11, 2006

The precursory phase began as a slow, steady increase in microearthquake activity beneath the volcano on April 30, 2005. These earthquakes were all classified as VT earthquakes during standard AVO processing (Dixon and others, 2008). An earlier swarm in October of 2004 (fig. 3) developed seismicity rates that exceeded any observed since the 1986 eruption; however, the six-month-long period of quiescence between this swarm and April 30, 2005, makes any connection to the 2006 eruption uncertain. The number of located VT earthquakes slowly increased from an average of one to two per day in May 2005 to five to six per day in October 2005 to 15 per day in mid-December 2005 (fig. 3). Relocated hypocenters had average depths generally between 0.1 and 0.6 km a.m.s.l. between April and December of 2005. These hypocentral depths are shallower than those observed during the initial precursory stages of both the 1976 and 1986 eruptions (fig. 11). In July 2005, geodetic baselines measured by the CGPS receivers began to lengthen, showing a clear radial pattern indicative of a pressurization source beneath the volcano's summit near sea level (Cervelli and others, 2006).

On November 17 there was a clear offset in the GPS data (fig. 17) that Cervelli and others (2006) attribute to the onset of the upward propagation of magma or associated volatiles in a dikelike structure. This was followed on December 2 by the onset of a series of small phreatic explosions that were clearly recorded on the Augustine seismic network. The largest of these explosions occurred on December 10, 12, and 15. An observational overflight on December 12 revealed vigorous steaming from the summit area, a new vigorous fumarole on the summit's southern side at roughly 3,600 feet elevation, and a light dusting of ash on the volcano's southern flanks. A strong plume of steam and

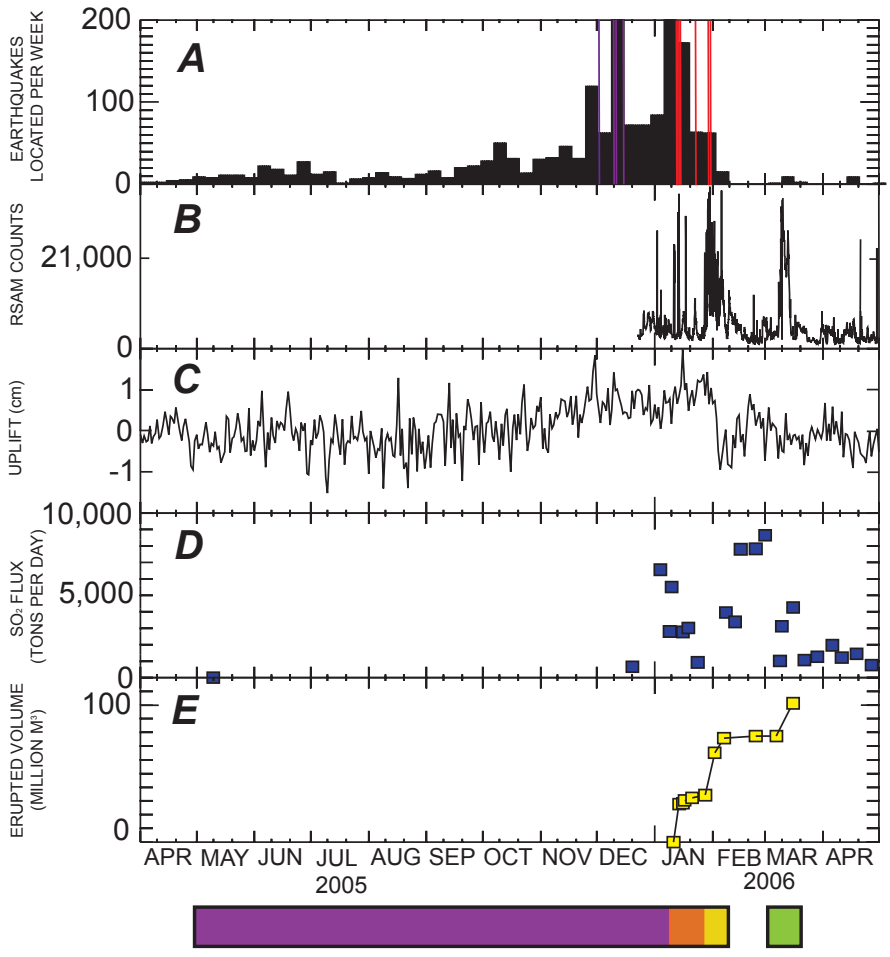

Figure 17. Summary of the 2006 eruption that shows (*A*) the number of earthquakes located each day, (*B*) the hourly RSAM record from station AU13, (*C*) the displacement measured between GPS stations A59 and AV02 (Cervelli and others, this volume), (*D*) the measured SO_2 flux (McGee and others, this volume), and (*E*) the erupted volume determined by Coombs and others (this volume). Purple and red lines in *A* correspond to approximate times of phreatic and magmatic explosions, respectively. Colors in bar at base of figure (purple, orange, yellow, and green) correspond to the precursory, explosive, continuous and effusive phases, respectively. Gap in bar represents hiatus in eruptive activity.

gas extended to the southeast. The explosion on December 15 disabled seismic stations AUS and AUR, the two highest seismic stations (fig. 2*C*). The ash was sampled on December 20 and was found to be a mix of weathered and glassy particles; the latter appear to be remobilized 1986 tephra (Wallace and others, this volume). Measurements of SO_2 flux on December 20, 2005, and January 4 and 9, 2006, returned values of 660, 6,700, and 2,800 tons per day, respectively (McGee and others, this volume).

Between December 12, 2005, and January 10, 2006, seismicity rates were strongly elevated, with more than 420 earthquakes located by the AVO (Dixon and others, 2008). Much of this activity occurred in spasmodic bursts similar to those observed before the 1986 eruption (fig. 15). Jacobs and McNutt (this volume) determined a *b* value of 1.85 for earthquakes during this period. Relocated hypocenters continued to cluster between 0.4 and 0.8 km a.m.s.l. On the basis of geodetic data, Cervelli and others (2006) suggest that magma and/or volatiles continued to move to progressively shallower depths within the Augustine edifice during this period.

On January 10 at roughly 1535 AKST, a 13-hour long swarm of VT earthquakes began that would culminate in two large explosions at 0444 and 0512 AKST on January 11, marking the onset of the explosive phase of the eruption (fig. 18). AVO would eventually locate more than 300 earthquakes during this swarm. Relocated hypocenters cluster beneath the volcano's summit at depths of 0.5 to 1.0 km a.m.s.l. The swarm began slowly, with locatable earthquakes occurring roughly every 2 minutes and magnitudes smaller than 1.0 (fig. 9). The seismicity rate peaked twice during the swarm at roughly 1800 January 10 and 0200 AKST January 11, and the magnitudes of located events also followed a similar progression (fig. 19).

Explosive Phase—January 11 to January 28, 2006

The two explosions on January 11 produced ash plumes, reported by the U.S. National Weather Service (NWS) to have reached heights greater than 9 km a.m.s.l. that moved slowly to the north and northeast (Bailey and others, this volume). Ash sampled on January 12 was primarily dense or weathered fragments, suggesting the involvement of little or no juvenile magma (Wallace and others, this volume). Over the next 36 hours, several sequences of drumbeat earthquakes occurred at rates as high as three to four per minute. Each of these sequences of drumbeats lasted 2 to 3 hours (fig. 18). These earthquakes suggest that magma may have begun to move within the shallow portions of the Augustine edifice, possibly forming a new lava dome if material reached the surface.

Explosive activity resumed on January 13 with a series of six powerful explosions that occurred at 0424, 0847, 1122, 1640, 1858 on January 13 and 0014 AKST on January 14 (fig. 18). The first explosion destroyed the seismometer at AUP (fig. 2*C*). Plumes reached altitudes of 14 km a.m.s.l. and deposited traces of ash on southern Kenai Peninsula communities. Ash from these eruptions was more heterogeneous than that from the January 11 explosions and contained dense particles as well as fresh glass shards, indicating the eruption of new magma (Wallace and others, this volume). Satellite imagery tracked these plumes as they moved eastward and disrupted commercial airline traffic to and from Alaska (Bailey and others, this volume). These explosions opened a new vent in the top of the 1986 lava dome that was estimated to be roughly 100 by 200 m in diameter (Coombs and others, this volume).

A January 16 overflight revealed a small new lava dome at the summit partially filling the new crater. An explosive eruption at 0758 AKST on January 17 sent ash to 13 km a.m.s.l. in a plume that moved westward. This explosion left a 20- to 30-meter-diameter crater in the new dome and produced ballistic fields on the volcano's western flanks (Coombs and others, this volume; Wallace and others, this volume; Schneider and others, 2006).

The eruptions of January 13–17 generated pyroclastic flows, snow avalanches, and lahars that moved down most flanks of the volcano. The January 17 explosion was followed by roughly 9 days of relative seismic quiescence. Brief periods of drumbeat earthquakes occurred throughout this period, and lava again filled the new crater and formed a small lava flow that moved to the east (Coombs and others, this volume; Vallance and others, this volume).

Explosive activity resumed on January 27 with two explosions at 2024 and 2337 and two on January 28 at 0204 and 0742 AKST (fig. 20) that generated ash plumes to heights of 9 km a.m.s.l. Ash moved southward and fell in trace amounts on Kodiak Island (Bailey and others, this volume; Wallace and others, this volume). The explosion at 2024 AKST on January 27 generated the largest single pyroclastic flow of the eruption, which moved down the north flank of the volcano (Coombs and others, this volume; Vallance and others, this volume). This explosion destroyed seismic stations AUH and AUL on the west and north flanks of the volcano. Destruction of these two final stations on the upper flanks of the volcano compromised AVO's ability to assign reliable hypocentral depths to earthquakes in near real-time.

Continuous Phase—January 28 to February 10, 2006

The volcano entered a period of more continuous eruptive activity starting at about 1430 AKST on January 28, 2006, with a roughly 2-hour period of volcanic tremor (fig. 20) that was accompanied by a significant ash plume that reached 9 km a.m.s.l. (Wallace and others, this volume). This phase of the eruption was characterized by continuous lower level ash production that gradually transitioned to the effusion of lava. Early in this phase the volcano erupted a more silicic magma (62.5 weight percent SiO_2) that formed a rubbly dome atop the remnants of the 1986 dome. By early February the composition of erupted magma had shifted back to a more andestic composition that formed a short lava flow that moved a short distance down the volcano's north side (Coombs and others, this volume).

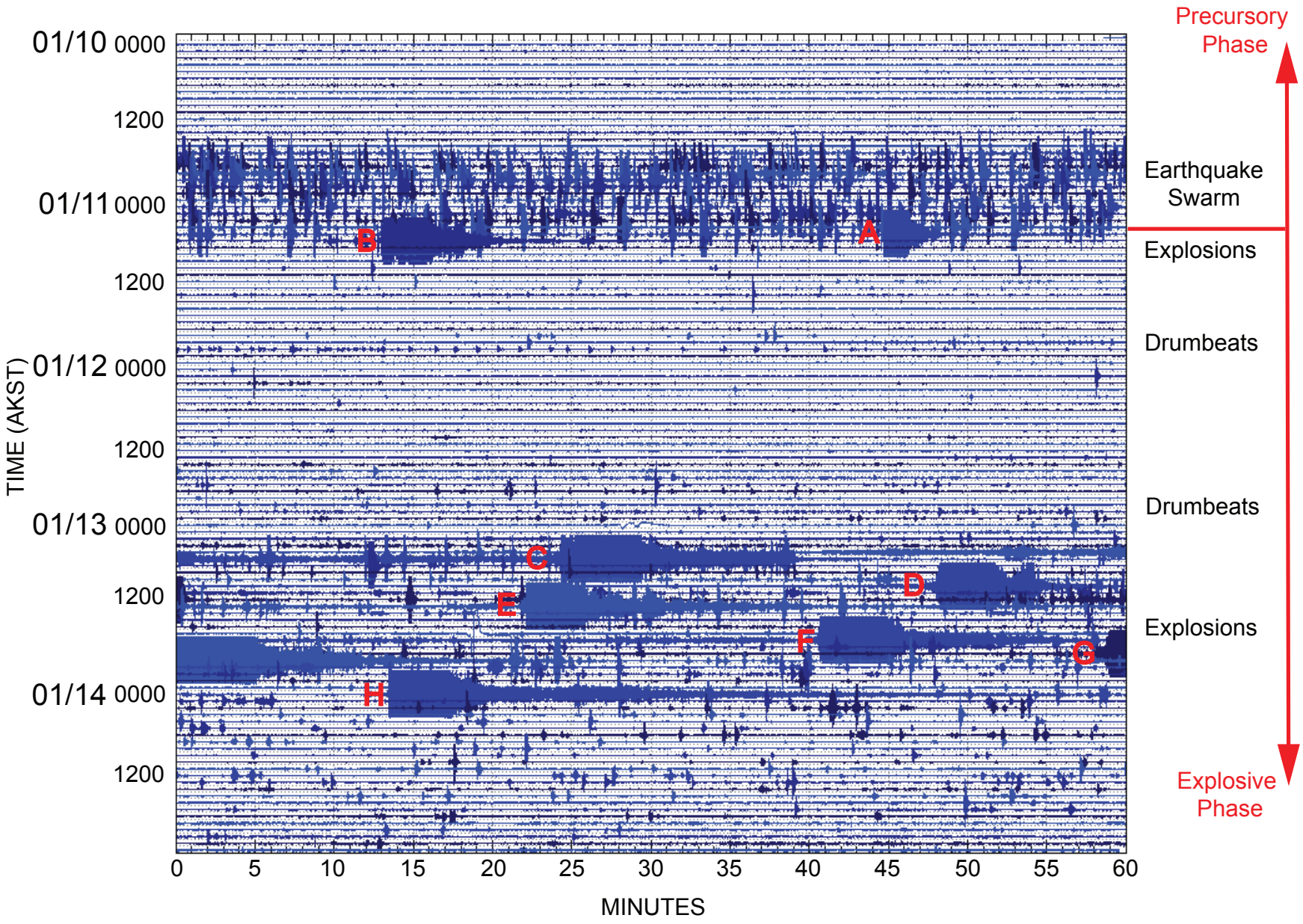

Figure 18. A 5-day velocity seismic record from station AU13 that shows the precursory earthquake swarm on January 11, 2006, the first eight explosions on January 11, 13, and 14, and the intervening periods of drumbeat earthquakes. Labeled events are A, explosion at 0444 AKST on January 11; B, explosion at 0512 AKST on January 11; C, explosion at 0424 AKST on January 13; D, explosion at 0847 AKST on January 13; E, Explosion at 1122 AKST on January 13; F, explosion at 1640 AKST on January 13; G, explosion at 1858 AKST on January 13; H, explosion at 0014 AKST on January 14.

At approximately 2200 AKST on January 28, the seismic network began to detect numerous signals associated with rock falls and block-and-ash flows generated by small failures of the growing lava dome and flows, cascading down the volcano's northern flanks (fig. 20). These signals generally have emergent onsets, extended codas, and a broad spectrum between 1 and 10 to 15 Hz. Numerous LP events are also observed during this time. Automatic event classification by Buurman and West (this volume) indicates that most seismic events had a lower frequency content or LP character during this phase of the eruption. One of these flows swept over seismic station AU12 at 0329 AKST on January 30, 2006, destroying the station's batteries. Fortunately, the seismometer and internally recorded data were recovered on August 11, 2006. Signals from rockfalls and small pyroclastic flows, as well as individual shallow LP events, declined markedly on February 3 at about 1500 AKST and then gradually decreased through the remainder of this phase.

Data from the remaining CGPS stations indicated that the volcano reversed its long inflationary trend on January 28 and began a sharp deflation that continued until 10 February. Modeling suggests the locus of deflation was at about 3.5 km b.m.s.l. (Cervelli and others, this volume).

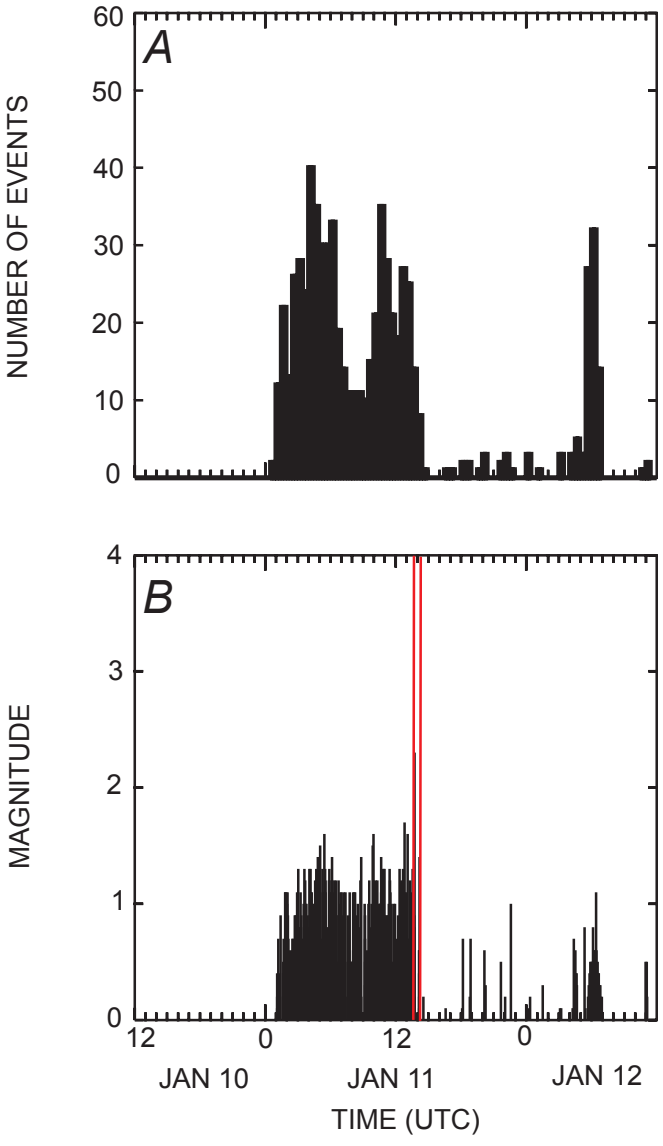

Figure 19. Time history of earthquake occurrence, magnitude, and explosive eruptions on January 10 through 12, 2006. *A,* Number of earthquakes located in each 30-minute period. *B,* Each vertical line represents the magnitude of one located earthquake. Red lines indicate times of explosive eruptions. Time is referenced to UTC; to convert to AKST subtract 9 hours.

Effusive Phase—March 8 to16, 2006

Following the end of the continuous phase, the volcano then entered a period of relative seismic quiescence that continued until March 3, 2006. This period is characterized by only an occasional rockfall signal. Visual observations of the volcano indicate that the period from February 10 to March 3 represents a cessation in eruptive activity. Geodetic data indicate that the volcano slowly inflated between February 10 and March 1 and then entered an 11-day period of deflation between March 1 and 12, 2006. The strength of this signal on the remaining CGPS instruments was not sufficient to accurately model a source depth for this episode of deflation (Cervelli and others, this volume).

On March 3 the number of rockfalls seen on the remaining seismic stations began to slowly increase. This activity peaked on March 6 and early on March 7. Starting on March 8, small repetitive drumbeat-style seismic events began to slowly emerge from the seismic background. The rate and size of the drumbeat events waxed and waned several times before forming a nearly continuous signal late on March 8 (fig. 21). Between 0500 and 2000 AKST on March 8 the rate of individual drumbeat events varied from two to as many as six per minute. After 2000 AKST on March 8, the events were occurring so rapidly (eight or more per minute) that they formed a continuous signal and it is no longer possible to distinguish individual events. RSAM records from station AU13 indicate that the amplitude of the continuous signal reached a maximum late on March 10 (fig. 17). This continuous signal lasted until about 1200 AKST on March 13 when the amplitude began a slow decline and individual events could again be distinguished occurring at a rate of about 5 per minute. The rate of events slowly declined, and by roughly 1200 AKST on March 16 they could no longer be identified.

Lava extrusion at the summit increased markedly in association with these drumbeat events, and two blocky lava flows moved down the north and northeastern flanks. Observations indicate that the effusion of lava had stopped by mid-March. The estimated volume of erupted material during this phase is 23 million cubic meters (Coombs and others, this volume).

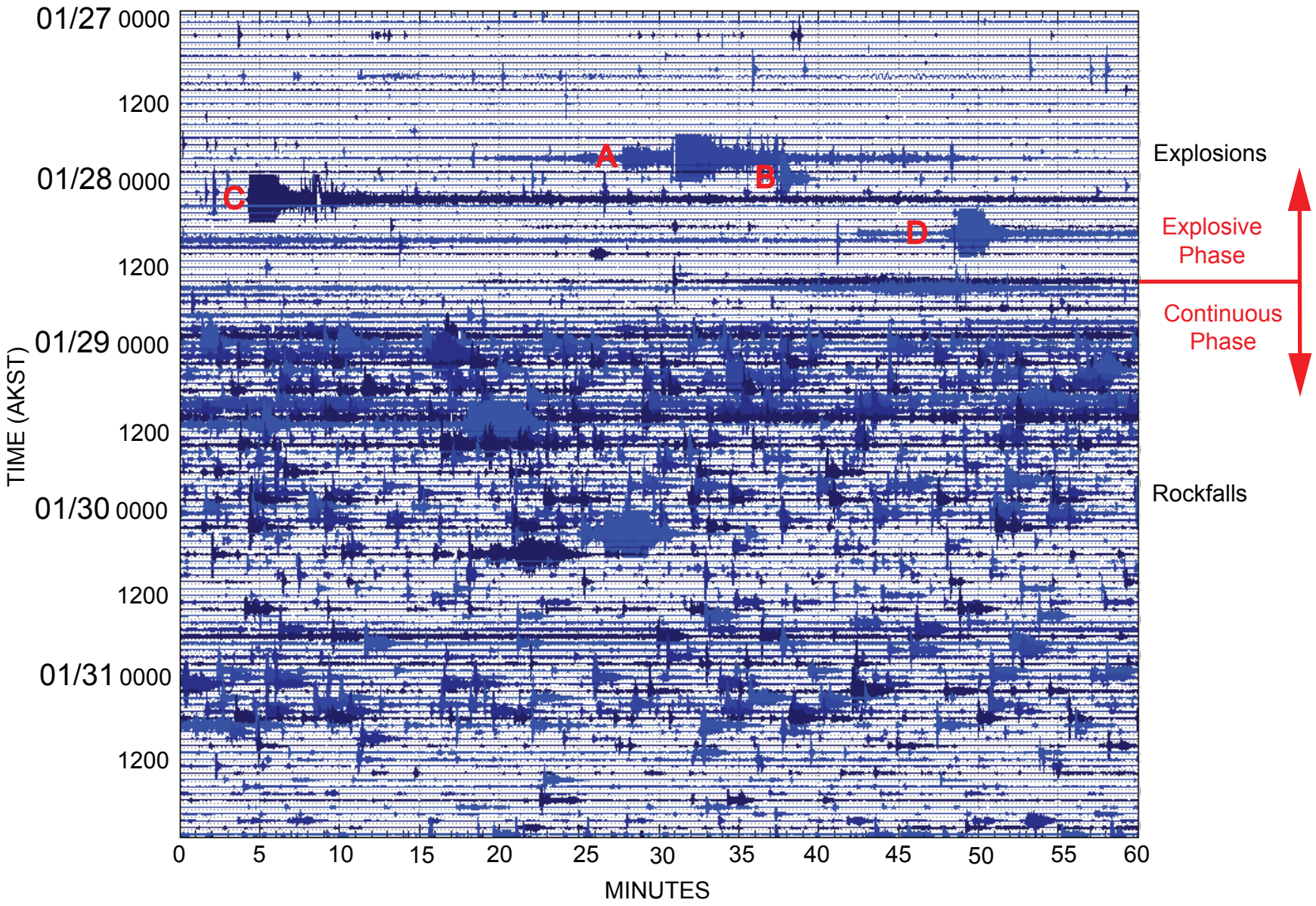

Figure 20. A 5-day velocity seismic record from station AU13 that shows the transition from the explosive to the continuous phase of the 2006 eruption. Labeled events are A, explosion at 2024 AKST on January 27; B, explosion at 2337 AKST on January 27, C, explosion at 0204 AKST on January 28; and D, explosion at 0742 on January 28, 2006.

Posteruptive Seismicity

On March 15, 2006, two earthquakes were located beneath the summit with hypocentral depths of 2.8 and 2.4 km b.m.s.l. Earthquakes with hypocenters between 2.3 and 3.75 km b.m.s.l. continued at a low rate until mid-August, by which time 18 shocks at this depth had been identified. These earthquakes had well-defined phases and a broad spectrum between 2 and 15 Hz, typical of VT earthquakes that represent a brittle failure source. To accurately locate these shocks we incorporated S-phases from the horizontal components of stations AU13, AU14, and AU15 (fig. 2*C*). Deshon and others (this volume) found that 11 of these earthquakes formed a single family suggestive of a common source, while the remaining 7 shocks had unique waveforms. These were the first earthquakes identified with hypocenters in this depth range at Augustine since December 1975. A representative waveform and a time history of these deeper earthquakes are shown in figure 22.

The seismic signals from rockfalls and the number of locatable earthquakes continued to decline throughout the summer of 2006. Small fluctuations in the rate of shallow VT earthquakes continued at Augustine throughout 2007 (figs. 3 and 4). These were generally small magnitude earthquakes that were most visible on station AUH. A pronounced increase in locatable VT earthquakes occurred between July and October, 2007 (fig. 3). Magnitudes of these earthquakes were less than 1.0 (fig. 4).

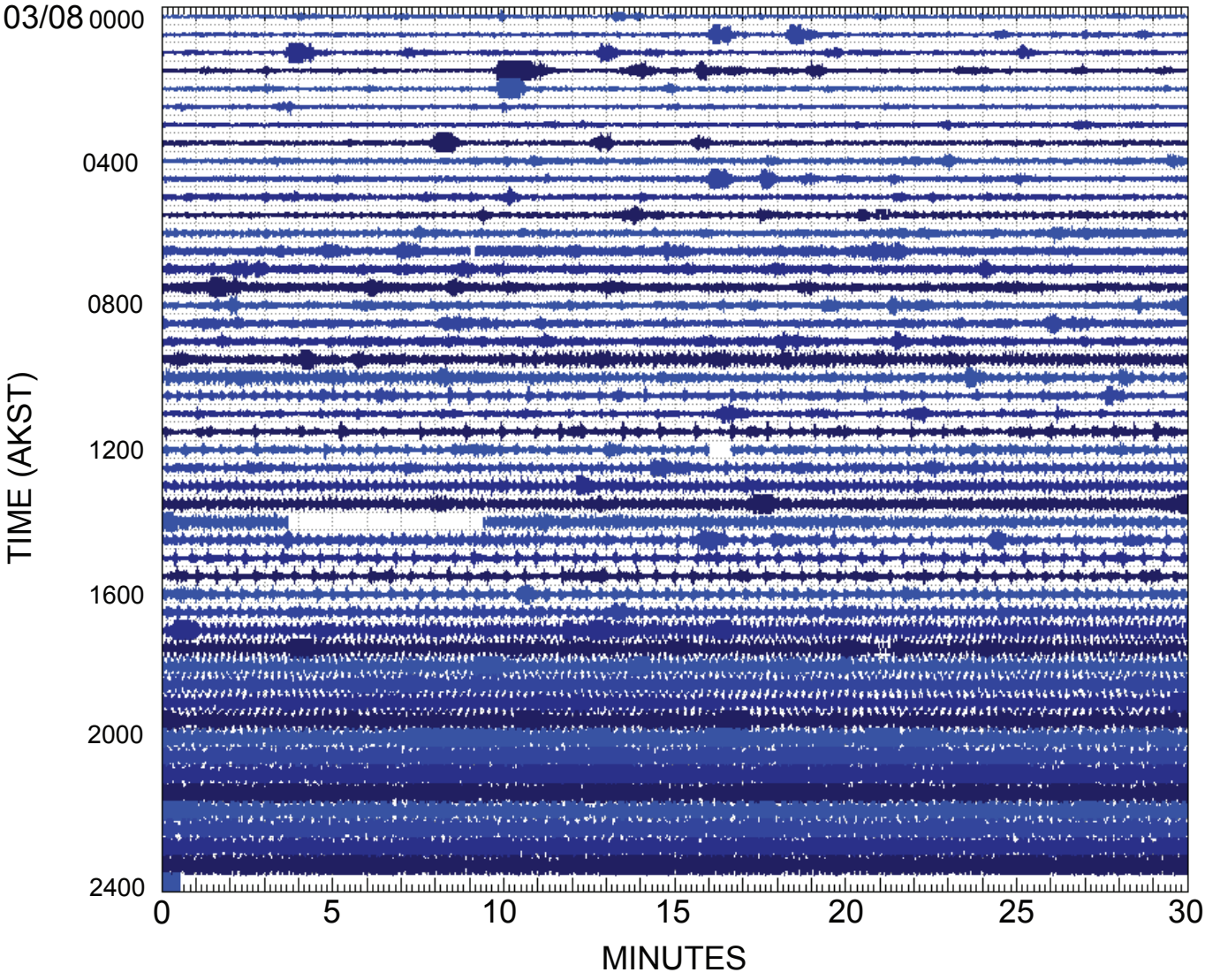

Figure 21. Velocity seismic record from station AUW on March 8 showing the onset of drumbeat earthquakes during the 2006 eruption. The rate and size of individual events changes several times until they form a nearly continuous signal at roughly 2330 AKST on March 8, 2006.

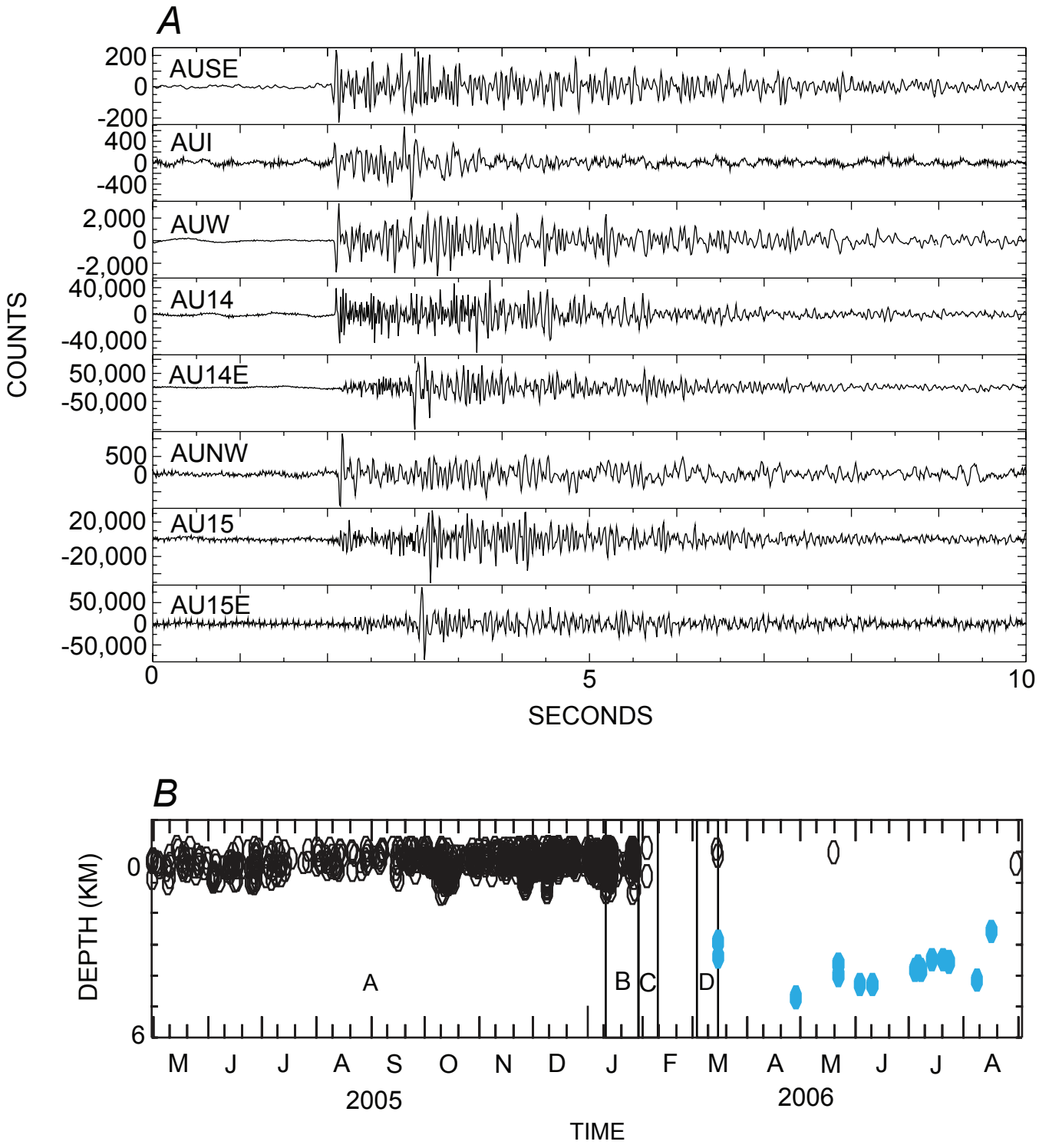

Figure 22. Representative waveform and plot of earthquake focal depth versus time, highlighting the occurrence of earthquakes between 2 and 5 km depth during the 2006 eruption sequence. *A*, Waveform of a magnitude 0.2 earthquake located at 3.55 km depth b.m.s.l. under the summit of Augustine on July 6, 2006. Individual station names are shown at left, east-west horizontal components are noted by "E" suffix. *B*, Plot of time versus focal depth showing the time history of the deeper earthquakes, noted by blue symbols, that followed the 2006 eruption. Labels A, B, C, and D note the precursory, explosive, continuous, and effusive phases of the 2006 eruption.

Discussion and Interpretation

This section relates the observed seismicity to the structure and subsurface configuration of the Augustine magmatic system and to the magmatic processes during the 1971, 1976, 1986, and 2006 eruptive sequences as well as the intervening quiescent periods. We will use the seismic patterns, waveform characteristics, and earthquake locations to infer both the geometry of the Augustine magmatic system and the evolution of the system during the three major eruptions. This discussion relies principally on the seismic record from 1970 through 2007 and secondarily on geophysical, geological, and visual observations reported by other authors.

Quiescent Periods

We think that the small shallow VT earthquakes most commonly seen at Augustine Volcano during quiescent periods, such as 1972 to 1975 and 1993 to 2004, represent small-scale adjustments within the upper portions of the volcanic edifice and summit dome complex. Deshon and others (this volume) find that only 30 to 40 percent of these earthquakes have similar waveforms, suggesting that seismicity is well distributed throughout the cone during quiescent periods. The stress regime responsible for the generation of these earthquakes is perhaps either thermal contraction of the cooling lava dome or gravitational slumping of the summit dome complex. Geodetic data from 1986 to 2000 indicate that portions of the summit dome complex can subside as much as 8 cm per year (Pauk and others, 2001). This process is relatively steady state, as evidenced by the relatively constant rate of VT earthquake activity observed between 1993 and 2004 (fig. 3).

Magmatic System Geometry

We think that the magmatic system beneath Augustine Volcano consists of a magma storage or source zone between 3.5 and 5 km b.m.s.l. that is connected by a largely aseismic conduit system to a shallower system of cracks that is centered near sea level. This shallower system roughly corresponds to the area where most earthquakes are located during the early precursory seismic sequences and may extend from as much as 0.9 km b.m.s.l. to several hundred m a.m.s.l. This shallower system of cracks is perhaps connected to the surface by a system of interconnected conduits or cracks that coalesce to a single north-south-trending dike at the volcano's summit. An idealized sketch of the inferred components of the Augustine magmatic system is shown in figure 23.

The deeper magma source area is only poorly defined seismically by the small number of earthquakes between 2 and 5 km b.m.s.l. that occurred in 1975 before the 1976 eruption (figs. 10 and 11) and following the 2006 eruption (figs. 7, 11 and 22). We speculate that the 1975 hypocenters most logically lie above the magma source zone, because they occurred before the 1976 eruption, and may reflect

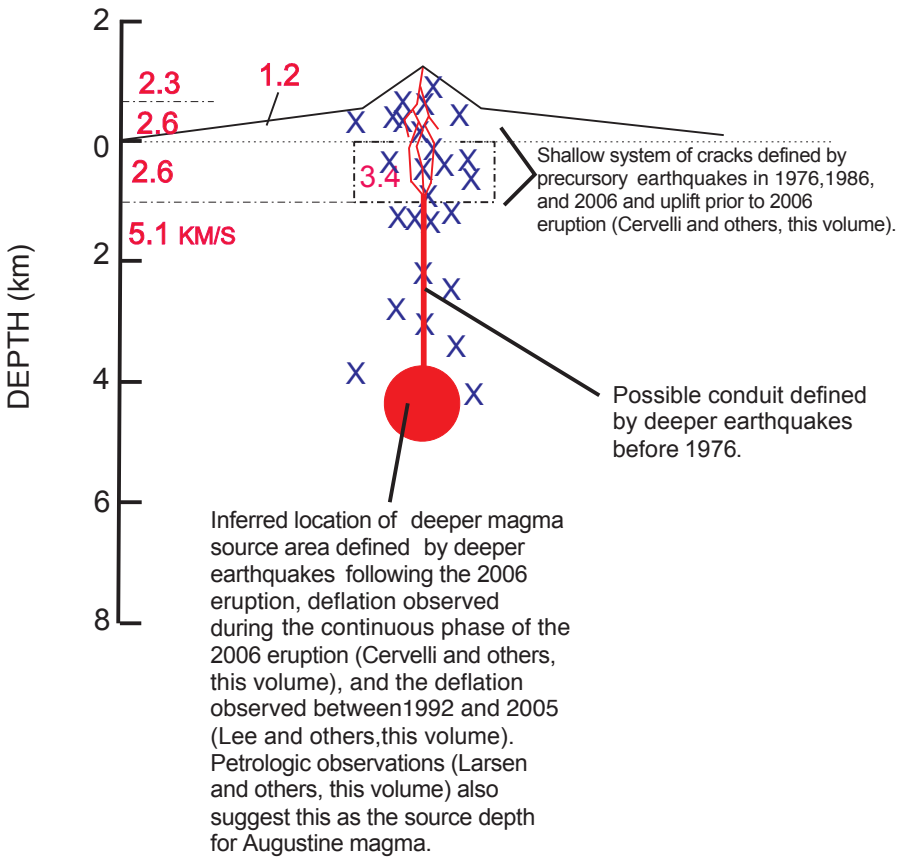

Figure 23. Inferred cross section of the Augustine Volcano magmatic system based on seismic and supporting geophysical information. Principal components of the system are a shallow system of cracks that may extend from depths of 0.9 km below sea level to a few hundred meters above sea level, a deeper magma source area at 3.5 to 5.0 km depth, and a possible conduit defined by deeper earthquake hypocenters observed in 1975 and 2006. Xs note areas of VT earthquake hypocenters. P-wave seismic velocities determined by Kienle and others (1979) are shown on the left and beneath the volcano.

the upward movement of magma and associated volatiles along a conduit system or magma pathway. The 1976 eruption was both more explosive and more voluminous than the 1986 or 2006 eruptions. Perhaps the deeper precursory earthquakes in 1975 reflect the ascent of either a greater volume of magma or a more volatile rich and consequently more explosive magma. We have no compelling explanation for the lack of earthquakes in this 2-to-5-km depth range before the 1986 and 2006 eruptions. The 2006 precursory sequence was much more closely monitored than either the 1976 or 1986 precursory phases (fig. 2) and we located many more earthquakes in 2005 and 2006 than before either the 1976 or 1986 eruptions. On the basis of the appearance of deeper earthquakes' waveforms in 1975 and 2006 (figs. 12 and 22) and the increased station coverage in 2006 (fig. 2*C*), we think the lack of observed activity in this depth range before the 1986 and 2006 eruptions is not a reflection of network aperture, station geometry, or preferential data acquisition or processing. Consequently we suggest it is most likely that earthquakes in this depth range did not occur before either the 1986 or 2006 eruption.

The deeper earthquakes at 2 to 5 km b.m.s.l. that followed the 2006 eruption most likely reflect a stress response to the removal of magma from this area (fig. 22). Earthquakes at mid to upper crustal depths are often observed to begin beneath a volcanic edifice following the onset of eruptive activity. Such a stress response has been observed at numerous volcanoes, including Mount St. Helens, Washington (Weaver and others, 1981), Redoubt Volcano, Alaska (Power and others, 1994), and Mount Pinatubo, Philippines (Mori and others, 1996). The small numbers and magnitudes of these deeper (2 to 5 km b.m.s.l.) VT earthquakes may be a reflection of a smaller change in stress or strain rate associated with the more frequently active magma system at Augustine. Additional support for this source zone comes from the synthetic-aperture radar (InSAR) measurements from 1992 through 2005 that suggest the presence of a relatively subtle inflationary source at roughly 2 to 4 km depth (Lee and others, this volume) and the deflationary pressure source at 3.5-km depth that was active during the continuous phase of the 2006 eruption (Cervelli and others, this volume). Taking these observations together, we suggest that the magma source zone might most logically lie at 3.5 to 5.0 km depth. This depth is also consistent with petrologic evidence that suggests the source zone at 4 to 6 km depth b.m.s.l. for magmas erupted in 2006 (Larsen and others, this volume). Similar earthquakes in this depth range would not have been located following the 1976 eruption, because only three stations were operating during this period (table 1). Earthquakes in this depth range could easily have been missed following the 1986 eruption, when the network was relatively sparse and the data were recorded on photographic film.

We think the shallower system of cracks likely extends from about 0.9 km b.m.s.l. to a few hundred m a.m.s.l. and is the source zone for most of the VT earthquakes located at Augustine during precursory periods (figs. 7, 10 and 11). The concentration of earthquake hypocenters at this depth range may in part be governed by changes in the density that would accompany the P-wave velocity boundaries observed at 0.9 km b.m.s.l. and sea level. These changes in P-wave velocity are thought to reflect changes from zeolitized sediments to intrusive volcanic rocks beneath the Augustine cone (Kienle and others, 1979). These changes in density and lithology may cause magma and associated volatiles to pause in this area on their rise to the surface. This area of high earthquake activity is coincident with the inflation source modeled by Cervelli and others (this volume) that was active during the 2006 precursory phase.

We find no seismic expression of the deeper inflationary source at 7 to 12 km b.m.s.l. modeled by Lee and others (this volume). The only possible seismic expression of the Augustine magmatic system at mid- to lower-crustal depths is a single magnitude (M_L) 1.5 LP event at 26-km depth that occurred on April 15, 2008 (Dixon and Stihler, 2009).

Magmatic System Activation

Seismicity prior to the 1976, 1986, and 2006 eruptions all began within 0.5 km of sea level. We believe the onset of this seismic activity likely reflects the arrival of magmatic volatiles into the shallow system of cracks (fig. 23). The onset of seismic activity in this depth range began roughly 9 months before all three major eruptions and suggests that the processes that allow volatiles to accumulate in this area were active on a similar time scale before all three major eruptions. Confirmation of this interpretation comes from the uplift observed near sea level beneath the volcano's summit starting in July 2005 (Cervelli and others, 2006). The only seismic expression of movement of magma from greater depths are the shocks between 2 and 5 km depth below sea level that occurred between August and December 1975 (fig. 11) and between March and August 2006 (fig. 22).

As the system of cracks near sea level progressively pressurized, it likely forced some volatiles into the upper portions of the Augustine edifice. This is the process we suspect is responsible for the upward migration of hypocenters reported before the 1976 (Lalla and Kienle, 1980) and 1986 (Power, 1988) eruptions. Confirmation of this process comes from the progressive shallowing of the pressure source revealed by geodetic data between November 2005 and January 11, 2006 (fig. 17), reported by Cervelli and others (this volume). Additionally, increased fumorolic activity was reported 1 to 3 months before the 1976, 1986, and 2006 eruptions. All of these observations suggest that magmatic volatiles had moved upward through the Augustine cone in the months prior to each major eruption.

While the upward migration of earthquake hypocenters is expected, confirmed observations of this phenomenon are

somewhat rare. This is perhaps more a reflection of deficiencies of volcano seismic networks, seismic velocity models, and processing methodology than an absence of physical process. The upward propagation of earthquake hypocenters has been reported at Mount Etna, Italy (Castellano and others, 1993), Mount Pinatubo (Harlow and others, 1995), Mount St. Helens (Moran and others, 2008; Thelen and others, 2008), and elsewhere. Propagating earthquake hypocenters have also often been observed associated with the intrusion of dikes in Hawaii (Klein and others, 1987). To examine this phenomenon at Augustine we use the methodology developed by Miller and others (2004) to track the progression of earthquake hypocenters driven by the migration of CO_2 in fold and thrust belts. First we smoothed our relocated hypocenter depths by calculating a 10-point running average of hypocentral depths similar to a convolution with a rectangular window or boxcar filter in the manner described by Oppenheim and Schafer (1975). We then calculated a best fit line to the relocated hypocenters of the precursory sequences of the 1976, 1986, and 2006 eruptions. The resultant data, best fit line, and linear correlation coefficient for each earthquake sequence are shown in figure 24. This analysis suggests that hypocenters moved upwards at a rate of approximately 1 km/yr before the 1976 and 1986 eruptions. A similar long-term upward progression of hypocenters was not observed during the 2006 precursory phase. This result is not unexpected, because the relocated earthquake depths in the 2006 precursory sequence began at a shallower level than in either the 1976 or 1986 precursory sequences (fig. 11). However, we do observe a short-term upward progression in hypocentral depth from 0.2 to 0.6 km a.m.s.l. between December 8 and 12, 2005 (fig. 24). A similar best-fit line for relocated hypocenters on these 4 days has a linear correlation coefficient of 0.9442 and a slope corresponding to 56 km/yr (150 m/d). Deshon and others (this volume) also found that earthquakes migrated upwards at this time on the basis of differential traveltimes measured between summit and flank stations. Geodetic data also indicate that magma and associated volatiles migrated upward between November 17, 2005, and January 10, 2006 (Cervelli and others, 2006). We note that a similar short-term upward migration in hypocenters may have occurred during the 1986 precursory phase between December 30, 1985 and January 1, 1986, when hypocenters migrated upwards from 0.2 to 0.6 km a.m.s.l. (fig. 24). The varying time scales (months and days) of these observed upward migrations suggests that separate physical processes or different conduit geometries may be responsible for generating the earthquake activity.

We did not observe any significant seismic activity under the flanks of the volcano throughout the period of this study, including the precursory sequences of the1976, 1986, or 2006 eruptions (fig. 10). Throughout the 38-year period of this study only a relatively small number of earthquakes were located under the volcano's flanks at distances of 3 to 10 km from the summit vent (fig. 7). This suggests that magma can

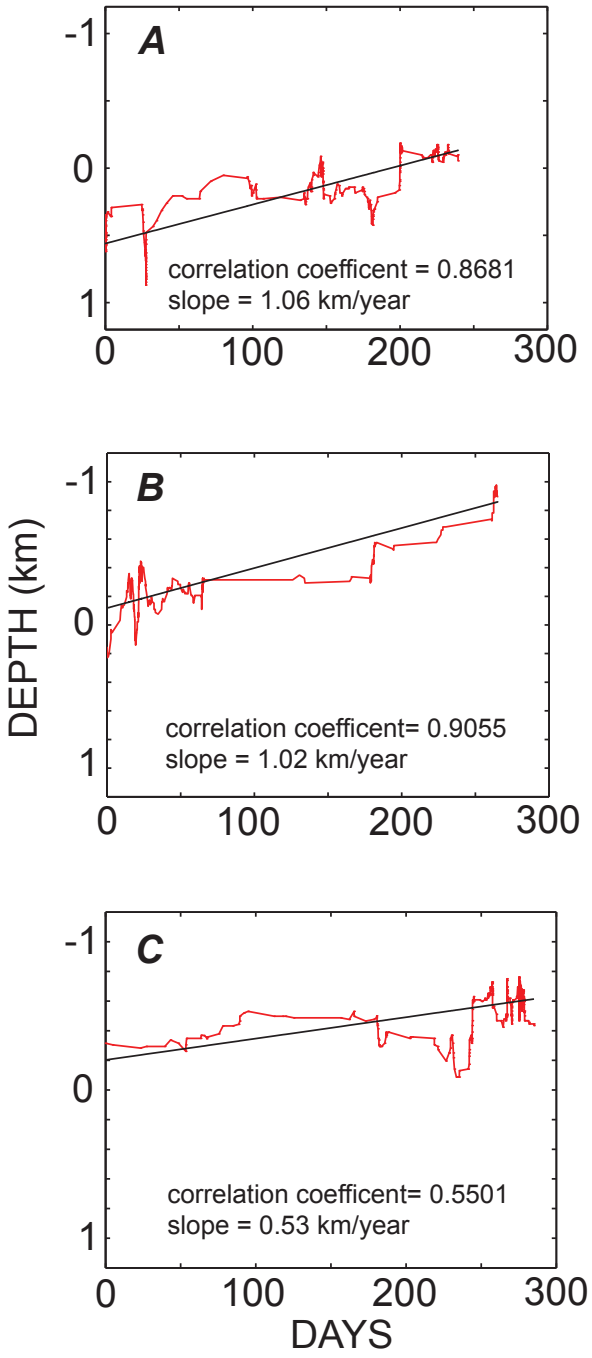

Figure 24. Smoothed hypocentral depths for relocated earthquakes (red lines) under the summit of Augustine Volcano from *(A)* May 2 to December 22, 1975, (*B*) July 4, 1985 to March 26, 1986, and (*C*) April 30, 2005 to January 11, 2006, plotted against the number of days in each sequence. These time periods correspond to the precursory seismic sequences for the 1976, 1986, and 2006 eruptions. Black lines represent least-squares fit to each set of hypocenters. Correlation coefficient and apparent rate of upward propagation of hypocentral depth are shown in each plot. The earthquake hypocenters in 2006 begin at shallower depth, and the resultant fit for the 2006 data (*C*) is poor.

move and erupt at Augustine without significantly stressing the surrounding crust. However, Fisher and others (this volume) did notice an increase in earthquake activity 25 km northeast of Augustine Island in the 6 months prior to the onset of the 2006 eruption and suggest that these earthquakes were triggered by magmatic processes at Augustine Volcano.

Eruption Initiation

The initial vent opening or onset of explosive activity appears to vary a great deal between the 1976, 1986, and 2006 eruptions. The onset of explosive activity in 1976 was extremely energetic seismically and was accompanied by a series of several hundred earthquakes on January 22 and 23, 1976 with larger magnitudes ($M_{L\max} \sim 2.75$) than any observed at Augustine between 1970 and 2007 (fig. 4). The most intense period of earthquake activity preceded the largest explosive eruptions reported by Kienle and Shaw (1977) by more than three hours (fig. 14). In contrast, explosive activity in 1986 was preceded by 3 days of increasing earthquake activity (fig. 16). The 1986 explosive sequence began with relatively small explosions that increased in size over 2 days (Power, 1988, fig. 22). Explosive activity in 2006 was immediately preceded by a 12-hour-long VT swarm (fig. 18) with a maximum magnitude of 1.6 (fig. 20), which is smaller than reported magnitudes of earthquakes that immediately preceded eruptions in 1976 or 1986 (figs. 4, 13).

The observed differences in the magnitudes and durations of earthquake swarms immediately preceding the three major eruptions suggest that the final ascent of magma and associated volatiles occurred differently in 1976, 1986, and 2006. The size of earthquakes does seem to scale roughly with the size of explosions and the amount of modification to the volcano's summit.

Drumbeat Events

The appearance of small, repetitive low- to medium-frequency seismic events or drumbeats at Augustine is very similar to seismicity often observed during effusive eruptions at Mount St. Helens (Moran and others, 2008; Thelen and others, 2008), Redoubt Volcano in Alaska (Power and others, 1994), Usu Volcano in Japan (Okada and others, 1981), Soufriere Hills Volcano in Montserrat (Rowe and others, 2004) and elsewhere. Often events with these frequency characteristics are referred to as hybrids (Lahr and others, 1994). The source mechanism of drumbeat seismicity has been the subject of vigorous research since their recent appearance at Soufriere Hills Volcano and Mount St. Helens. Proposed source models for drumbeat-style seismicity include a pressure transient in a fluid filled crack (Chouet, 1996; Waite and others, 2008), resonance of a fluid within a crack or conduit initiated by a stick-slip event within the magma (Neuberg and others, 2006), and stick-slip along the conduit magma interface (Iverson and others, 2006, Harrington and Brodsky, 2007; Iverson, 2009). It is not possible to fully characterize the source of repetitive events or drumbeats at Augustine given the observations and analysis presented here. However, the repeated occurrence of drumbeat seismicity during several eruptive events at Augustine allows us make some inferences about their source and significance.

Drumbeat-style seismicity was observed at Augustine associated with active periods of lava extrusion during both the initial dome building phase of the 1986 eruption (Power, 1988) and during the effusive phase of the 2006 eruption (fig. 21). In each case the drumbeats quickly coalesced into a continuous high-amplitude signal that persisted for roughly 8 days in both 1986 and 2006. At the end of each episode the high-amplitude signal slowly diminished until individual events could again be distinguished and then slowly faded into the normal seismic background. The initial dome building phase of the 1986 eruption had a second pulse of drumbeat seismicity that consisted only of discrete events and continued for 5 days. This second episode followed a 2 day hiatus in drumbeat activity (Power, 1988). In each of these cases of drumbeat style seismicity, the effusion of magma was actively occurring at the summit, building a lava dome.

Short episodes of drumbeat earthquakes lasting several hours were also observed briefly on January 11 and 12 during the early portions of the explosive phase of the 2006 eruption (fig. 18). These drumbeats provide some constraint on the source depth because they occur before many of the seismic stations were destroyed and we can determine their hypocentral depth relatively well. Relocated hypocenters using the 2D relocation method of Lalla and Power (this volume) suggest depths of 0.25 to 0.5 km a.m.s.l., while Deshon and others (this volume) have determined that a depth of 0.2 km a.m.s.l. or shallower for these events. The strongest sequence occurred between 2036 and 2206 AKST, and Buurman (2009) found these events to consist of a single family of events whose source migrates roughly 20 m over 1.5 hours.

The occurrence of repetitive events or drumbeats on January 11 and 12, 2006 suggests that magma may have reached the surface and a small lava dome may have begun to form as early as January 11. Unfortunately, insufficient visual observations of the summit of the volcano between January 11 and 13 do not allow us to confirm that new magma reached the surface at this time (Wessels and others, this volume). However, the strongest drumbeats begin at about 2036 AKST on January 11, which corresponds with the end of shallow deformation of the summit area. This change in deformation has been attributed to the possible onset of lava extrusion (Cervelli and others, this volume). Further, the deposits from the early explosions on January 13 contain a high percentage of dense low-silica andesite clasts, suggesting that these explosions may have partially removed new dome material (Vallance and others, this volume). The most likely explanation for these observations is that a new lava dome possibly began to form

as early as late on January 11, 2006, in association with this sequence of drumbeats. Alternatively, these early drumbeats may only reflect the shallow movement of magma that may not have reached the surface.

During the effusive phase of the 2006 eruption, roughly 23 million m^3 of low-silica andesite (57 weight percent SiO_2) was erupted (Coombs and others, this volume). The average rate of extrusion during the 8 day period of drumbeat activity, assuming that magma effusion is restricted to periods when drumbeats are occurring, is roughly 33 m^3/s. We note that this extrusion rate exceeds the reported rates for Mount St. Helens in November 2004 through March 2005 of 4 to 5 m^3/s (Shilling and others, 2008) when drumbeat events were occurring at rates of 0.3 to 3 per minute (Moran and others, 2008). The rate of magma extrusion and drumbeat events (3 to 6 per minute) at Augustine greatly exceed the rates at Mount St. Helens, suggesting that the rate of drumbeat events may reflect the extrusion rate of magma. Unfortunately, the calculations of erupted volume at Augustine lack the temporal resolution to establish a specific relationship between magma flux and drumbeat rate and size. The drumbeats at Mount St. Helens occurred while lava was actively forming large peleean spines that were coated with fault gouge (Iverson and others, 2006). At Augustine there were no observations of notable fault gauge or spine development during the effusive phase of the 2006 eruption, suggesting that these are not required for generating drumbeat seismicity. No obvious periods of drumbeat activity were observed during the continuous phase of the 2006 eruption when magma with composition of 62.5 weight percent SiO_2 was dominant (Coombs and others, this volume). Oddly, magma erupted during the 2006 continuous phase at Augustine most closely matches the 65 weight percent SiO_2 of magma erupted at Mount St. Helens (Pallister and others, 2008) in 2004 when drumbeats were prevalent. This suggests that the occurrence of drumbeat style seismic events is not simply related to the magma's composition.

At the start of the 2006 effusive phase, drumbeats were observed to increase discontinuously in both rate and amplitude over a 16-hour period (fig. 21). At the end of the effusive phase drumbeats slowly decreased in rate and size between March 13 and 16. During most of this phase, the drumbeats formed a continuous high-amplitude signal that clipped many of the short-period stations on the island. Visual observations of the growing lava dome suggest that the high-amplitude drumbeat signal roughly corresponds to the period of maximum extrusion rate (Coombs and others, this volume; Wessels and others, this volume). These observations suggest that the rate and amplitude of drumbeats at Augustine in at least the 2006 effusive phase may correspond to the rate of magma extrusion.

It is also apparent from observations of the 2006 eruption of Augustine that lava domes can be emplaced on the summit without the occurrence of drumbeats. This was the case for the small dome observed on January 16, 2006 (Coombs and others, this volume). This dome was emplaced while stations as close as AUH (fig. 2*C*) were in operation without identifiable drumbeat seismicity. This indicates that magma of similar composition can move at shallow depths without accompanying drumbeat seismicity.

Observations of Augustine drumbeat-style seismicity suggest that its source is associated with the shallow movement of magma. The source is likely a complex process governed by a number of variables, such as the extrusion rate, ascent rate, gas content, compressibility and rigidity of magma as it moves at shallow depth. The best estimations of hypocentral depth suggest that drumbeats take place at 0.2 to 0.5 km a.m.s.l. These depths suggest that the actual source is within the Augustine cone and is not associated with a specific process related to the effusion of magma or formation of a lava dome at the volcano's summit. At Augustine the shallow movement of magma is closely associated temporally with the effusion of lava and emplacement of a lava dome at the summit of the volcano. The absence of obvious fault gauge or peleean spines at the summit of Augustine, as was observed at Mount St. Helens during drumbeat seismicity (Iverson, 2008; Moore and others, 2008) would lead us to prefer the models of Waite and others, (2008) or Neuberg and others (2006) for the source of Augustine drumbeats. At Augustine this style of seismicity is closely associated with effusion of magma at the summit.

Eruption Forecasting

In this section, we review the role that seismic observations played in formulating eruption forecasts and public warnings and the factors that influenced our interpretations during the 2006 eruption sequence, and we provide recommendations for evaluating future episodes of seismic unrest at Augustine Volcano. Neal and others (this volume) provide a detailed account of the specific warnings issued by AVO and the communication protocols used to disseminate the warnings, while Adleman and others (this volume) describe how AVO communicated with the news media and general public during the 2006 eruption. The forecasting strategy used by AVO relied on the synthesis of data from a number of different monitoring techniques, which include seismic (hypocenters, seismicity rate, RSAM, continuous spectral measurements, and waveform characteristics), visual observations, satellite observations, gas-flux measurements, and CGPS data. These observational data streams were supplemented by well-developed chronological information on the two most recent eruptions in 1976 (Johnston, 1978; Swanson and Kienle, 1985; Reeder and Lahr, 1987) and 1986 (Yount and others 1987; Power, 1988; Kienle and Swanson, 1988). The most important information for forecasting in 2006 was that the progression of unrest and eruptive events in 1976 and 1986 were strikingly similar. Both the 1976 and 1986 eruptions were preceded by roughly 9 months of slowly escalating VT earthquake activity. Each of these eruptions consisted of an initial explosive phase followed by two additional periods of eruptive activity

characterized by milder explosive eruptions and effusive activity (fig. 8). Although the overall progression of seismic activity and eruptive events during the 1976 and 1986 eruptions were similar, there are notable differences that were considered in developing forecasts of the 2006 eruption. The most important differences were that the 1976 eruption was much more voluminous than the 1986 eruption, the 1976 precursory seismic sequence contained earthquakes with hypocenters in the 2 to 5 km depth range while the 1986 eruption did not, and the 1976 eruption progressed to completion much faster than the 1986 eruption (fig. 8).

The long-term AVO seismic monitoring program allowed us to identify the initial increase in VT earthquake activity and heighten our surveillance of the volcano as the shocks were occurring in the spring of 2005. Long-term seismic monitoring (fig. 3) allowed us to recognize that the initial subtle increase was significant, even though the early portions of the 2006 precursory seismicity were milder than either the 1976 or 1986 sequences (figs. 3, 4, 8). The prominent earthquake swam in October 2004 had a much shorter duration than the seismic increase in the spring of 2005.

This early identification of increased seismicity focused our attention on Augustine and allowed us to identify the uplift that began in July 2005 (Cervelli and others, 2006) at an early stage. Continued increases in both seismicity and uplift (fig. 17) provided a strong basis for the first public warning of possible renewed eruptive activity on November 29, 2005 when AVO moved the color code to yellow (Neal and others, this volume). Although some uncertainty persisted at this time about the eventuality of an eruption, the color code change positioned AVO to respond to the further escalations in unrest that were to follow shortly.

The continued increases in seismicity rate and geodetic uplift, combined with the phreatic explosions in early to mid December, the greatly increased fumorolic activity, opening of extensional cracks on the volcano's summit, and the greatly increased gas flux (McGee and others, this volume), served only to focus more of our attention on Augustine. During this period we greatly intensified our monitoring of Augustine by adding broadband seismometers, temporary CGPS receivers, time lapse cameras, Web cams (Paskievitch and others, this volume), and a pressure sensor (Petersen and others, 2006). In hindsight much of this equipment should have been deployed on the volcano earlier in the precursory phase when snow cover would have been lighter and we could have benefited from longer daylight hours.

The energetic earthquake swarm that began late on January 10 (fig. 18) was an unequivocal sign that eruptive activity should be expected in the short term. The level-of-concern color code was raised to orange at 2105 AKST on January 10, and AVO began 24-hour monitoring in both the Anchorage and Fairbanks offices. Although it was recognized on January 10 that the 2006 swarm had a more sudden onset than the earthquake swarm that immediately preceded eruptive activity in 1986 (compare figures 15 and 17). Unfortunately no warning was issued immediately following the first explosive event at 0444 AKST on January 11. The waveform of this explosion resembles a large VT earthquake in the short-period velocity record (fig. 18), and the relatively small amount of ash generated by this explosion only produced a short radar return (Schneider and others, 2006). The waveform of the second explosion at 0512 was much less ambiguous, and the level-of-concern color code was raised to red at 0550 AKST.

Following the onset of explosive activity on January 11, careful monitoring of seismic activity, along with radar and satellite imagery, allowed AVO to issue warnings of explosive eruptions on January 13, 14, 17, 27, and 28, often within seconds of the explosion's onset (Neal and others this volume). Further warnings were issued during the later phases of the eruption, again often formulated on the basis of the similar patterns in eruption progression observed during the 1976 and 1986 eruptions. The onset of drumbeat earthquakes on March 8 was especially noteworthy, because we were immediately able to associate this seismic activity with renewed lava extrusion. AVO lowered the level-of-concern color code from orange to yellow on April 28 and from yellow to green on August 9, 2006 (Neal and others, this volume).

A significant problem during the 2006 eruption was that all telemetered seismic and CGPS instruments near the volcano's summit and on the north side of the volcano were eventually destroyed by eruptive activity. This made it impossible to reliably calculate earthquake hypocentral depths in near-real time and track deformation of the upper portions of the edifice. To some extent, station loss is unavoidable; however, if stations had been operating high on the south and east flank of the volcano in 2006 these stations would likely have survived the eruption. In future years we recommend installing telemetered stations in locations near the site of AU13 and similar higher locations on all quadrants of the volcano. Ideally these seismometers would be three-component instruments.

In evaluating future episodes of unrest at Augustine, the following observations should be considered:

1. The 1976, 1986, and 2006 eruptions were all preceded by roughly 9 months of slowly escalating earthquake activity (figs. 3, 8) and hypocentral depths were observed to migrate slowly upward before the 1976 and 1986 eruptions (fig. 24). Shorter term upward migrations were also observed before the 1986 and 2006 eruptions.

2. Each of the three major eruptions began explosively and was followed by several months of discontinuous effusive activity. Although the overall character of each major eruption was similar, they progressed to completion on different time scales. The total duration of eruptive activity from beginning to end was approximately 85, 178, and 67 days for the 1976, 1986, and 2006, eruptions respectively (fig. 8).

3. Historical reports (Davidson, 1884; Coats, 1950; Determan, 1968; Johnston and Detterman, 1979), as well as the geologic record (Waythomas and Waitt, 1998), indicate

that past eruptions show more variability in eruptive size and duration than we have seen in 1976, 1986, and 2006.

4. Smaller eruptions similar to that seen in 1971 should also be expected, and the period of precursory activity may be shorter than what was observed in 1976, 1986, and 2006.

5. Earthquakes at 2 to 5 km depth b.m.s.l. preceded the more explosive onset of the 1976 eruption (fig. 11). Procedures should be developed to closely monitor earthquake activity in this depth range.

6. The duration and size of earthquakes over the 24 to 48 hours immediately preceding the eruption's explosive onset in 1976, 1986, and 2006 showed great variability. Such variability in the onset of explosive activity should be expected in future eruptions.

7. Drumbeat seismicity was observed during the initial dome-building phase of the 1986 eruption and during the effusive phase of the 2006 eruption, when new magma was being actively extruded at the volcano's summit. Drumbeats were also observed during several brief periods of the explosive phase of the 2006 eruption. However, drumbeats were not observed in association with active lava extrusion during the second dome-building phase of the 1986 eruption or several periods of the 2006 eruption. Drumbeats should be taken as a strong indicator that magma is moving at shallow depth within the edifice and is likely forming a lava dome at the summit.

Summary and Conclusions

This paper summarizes the primary observations of seismic activity at Augustine Volcano between 1970 and 2007. During this period, Augustine Volcano experienced one minor and three major eruptions. Judging from the spatial and temporal development of earthquake hypocenters in association with a minor eruptive event in 1971 and three major eruptions in 1976, 1986, and 2006, we suggest that the subsurface magmatic system consists of a source region between 3.5 and 5 km depth b.m.s.l., and a system of cracks near sea level where magma and magmatic volatiles pause as they ascend to the surface. The position of these cracks may be controlled by density contrasts associated with rock types that are observed in changing P-wave velocities. These two magma storage areas are perhaps connected by a system of dikes or conduits that also extend to the surface.

The last three major eruptions at Augustine were all preceded by roughly 9 months of seismic activity. Hypocenters were observed to migrate upwards before the 1976 and 1986 eruptions over the length of the precursory period. However, before the 2006 eruption hypocenters began at a shallower depth, and a longer term upward migration was not observed. Relocated earthquake hypocenters and continuous geodetic data tracked a shorter term upward progression late in the precursory phase of the 2006 eruption (Cervelli and others, 2006; Cervelli and others, this volume). Each of these eruptions also followed a similar progression from explosive to effusive activity, although the time from onset to completion of eruptive activity varied considerably. Petrologic evidence also suggests that the magma-mixing events thought to have triggered the 1976, 1986, and 2006 eruptions involved magmas of similar composition. This overall similarity suggests that the physical processes responsible for the accumulation, rise, and eruption of magma at Augustine are roughly constant or change only slowly with time. If conditions do not change, future eruptions of Augustine might be expected to follow a similar pattern.

Acknowledgments

In compiling a long-term study of seismicity such as this we have relied on the hard work of many individuals over nearly a 40-year period. We gratefully acknowledge the early contributions of Jurgen Kienle, John Davies, Robert Forbes, Chris Pearson, Elliot Endo, Hans Pulpan, Dave Stone, and David Harlow. Many individuals, including Steve Estes, Guy Tytgat, John Benevento, Kaye Lawson, John Paskievitch, Ed Clark, John Lahr, and Tom Murray, managed to keep the Augustine seismic instrumentation and various acquisition systems operational over long periods of time. Scott Stihler, Jim Dixon, Tom Parker, and many others assisted with processing and archiving seismic data from 1993 through 2007. During the preparation of this manuscript we had useful conversations with Matt Haney, Phil Dawson, Bernard Chouet, Seth Moran, Greg Waite, Scott Stihler, Jim Dixon, Heather Deshon, Cliff Thurber, Helena Buurman, Katherine Jacobs, Stephanie Prejean, Mike West, Steve McNutt, Peter Cervelli, Michelle Coombs, Dave Schneider, Kristi Wallace, Tom Murray, Christina Neal, Kate Bull, Jessica Larsen, Game McGimsey, and many others. Peter Cervelli and Matt Haney provided extra assistance and guidance in preparing figures 10 and 24. We benefited from formal reviews of the text and figures by Diana Roman, Fred Klein, and Jeff Freymueller.

References Cited

Adleman, J.N., Cameron, C.E., Snedigar, S.F., Neal, C.A., and Wallace, K.L., 2010, Public outreach and communications of the Alaska Volcano Observatory during the 2005–2006 eruption of Augustine Volcano, *in* Power, J.A., Coombs, M.L., and Freymueller, J.T., eds., The 2006 eruption of Augustine Volcano, Alaska: U.S. Geological Survey Professional Paper 1769 (this volume).

Bailey, J.E., Dean, K.G., Dehn, J., and Webley, P.W., 2010, Integrated satellite observations of the 2006 eruption of Augustine Volcano, *in* Power, J.A., Coombs, M.L., and Freymueller, J.T., eds., The 2006 eruption of Augustine Volcano, Alaska: U.S. Geological Survey Professional Paper 1769 (this volume).

Barrett, S.A., 1978, A three-dimensional magnetic model of Augustine Volcano: University of Alaska Fairbanks, M.S. thesis, 175 p.

Buurman, H.M., 2009, Seismicity preceding volcanic explosions during the 2006 eruption of Augustine Volcano: University of Alaska Fairbanks, M.S. thesis, 85 p.

Buurman, H., and West, M.E., 2010, Seismic precursors to volcanic explosions during the 2006 eruption of Augustine Volcano, *in* Power, J.A., Coombs, M.L., and Freymueller, J.T., eds., The 2006 eruption of Augustine Volcano, Alaska: U.S. Geological Survey Professional Paper 1769 (this volume).

Castello, M., Ferrucci, F., Godano, C., Imposa, S., and Milano G., 1993, Upwards migration of seismic foci; a forerunner of the 1989 eruption of Mt. Etna (Italy): Bulletin of Volcanology, v. 55, p. 35–361.

Cervelli, P.F., Fournier, T., Freymueller, J.T., and Power, J.A., 2006, Ground deformation associated with the precursory unrest and early phases of the January 2006 eruption of Augustine Volcano, Alaska: Geophysical Research Letters, v. 33, doi: 10.1029/2006GL027219.

Cervelli, P.F., Fournier, T.J., Freymueller, J.T., Power, J.A., Lisowski, M., and Pauk, B.A., 2010, Geodetic constraints on magma movement and withdrawal during the 2006 eruption of Augustine Volcano, *in* Power, J.A., Coombs, M.L., and Freymueller, J.T., eds., The 2006 eruption of Augustine Volcano, Alaska: U.S. Geological Survey Professional Paper 1769 (this volume).

Chouet, B.A., 1996, Long-period seismicity; its source and use in eruption forecasting: Nature, v. 380, p. 309–316.

Coats, R.R., 1950, Volcanic activity in the Aleutian Arc: U.S. Geological Survey Bulletin, 974-B, p. 35–49.

Coombs, M.L., Bull, K.F., Vallance, J.W., Schneider, D.J., Thoms, E.E., Wessels, R.L., and McGimsey, R.G., 2010, Timing, distribution, and volume of proximal products of the 2006 eruption of Augustine Volcano, *in* Power, J.A., Coombs, M.L., and Freymueller, J.T., eds., The 2006 eruption of Augustine Volcano, Alaska: U.S. Geological Survey Professional Paper 1769 (this volume).

Daley, E.E., 1986, Petrology, geochemistry, and the evolution of magmas from Augustine Volcano, Alaska: University of Alaska Fairbanks, M.S. thesis 106 p.

Davidson, G., 1884, Notes on the volcanic eruption of Mount St. Augustine, Alaska, October 6, 1883: Science, v. 3, p. 186–189.

Detterman, R.L., 1968, Recent volcanic activity on Augustine Island, Alaska: U.S. Geological Survey Professional Paper 600-C, p. 126–129.

DeShon, H.R., Thurber, C.H., and Power, J.A., 2010, Earthquake waveform similarity and evolution at Augustine Volcano from 1993 to 2006, *in* Power, J.A., Coombs, M.L., and Freymueller, J.T., eds., The 2006 eruption of Augustine Volcano, Alaska: U.S. Geological Survey Professional Paper 1769 (this volume).

Dixon, J.P., Power, J.A., and Stihler, S.D., 2004, A comparison of seismic event detection with IASPEI and Earthworm acquisition systems at Alaskan volcanoes: Seismological Research Letters, v. 26, no. 2., p. 168–176.

Dixon, J.P., Stihler, S.D., Power, J.A., and Searcey, C., 2008, Catalog of earthquake hypocenters at Alaskan Volcanoes; January 1 through December 31, 2006: U.S. Geological Survey Data Series 326, 78 p.

Dixon, J.P., and Stihler, S.D., 2009, Catalog of earthquake hypocenters at Alaskan Volcanoes: January 1 through December 31, 2008: U.S. Geological Survey Data Series 467, 88 p.

Dzurisin, D., Iwatsubo, E.Y., Kleinman, J.W., Murray, T.L., Power, J.A., Paskievitch, J.F.,1994, Deformation monitoring at Augustine Volcano, AK: Eos, (American Geophysical Union Transactions), v. 75, abs. p. 166.

Endo, E.T., and Murray, T.L., 1991, Real-time seismic amplitude measurement (RSAM); a volcano monitoring and prediction tool: Bulletin of Volcanology, v. 53, p. 533–545.

Fisher, M.A., Ruppert, N.A., White, R.A., Sliter, R.W., and Wong, F.L., 2010, Distal volcano-tectonic seismicity near Augustine Volcano, *in* Power, J.A., Coombs, M.L., and Freymueller, J.T., eds., The 2006 eruption of Augustine Volcano, Alaska: U.S. Geological Survey Professional Paper 1769 (this volume).

Fremont, M., and Malone, S.D., 1987, High precision relative locations of earthquakes at Mount St. Helens, Washington: Journal of Geophysical Research, v. 92, p. 10233–10236.

Gorshkov, G., 1959, Gigantic eruption of the volcano Bezymianny: Bulletin of Volcanology, v. 21, p. 77–109.

Harlow, D.H., 1971, Volcanic earthquakes: Dartmouth College, M.A. thesis, 66 p.

Harlow, D.H., Power, J.A., Laguerta, E.P., Ambubuyog, G., White, R.A., and Hoblitt, R.P., 1995, Precursory seismicity and forecasting of the June 15, 1991 eruption of Mount Pinatubo, *in* Newhall, C.G., and Punongbuyan, R.S., eds., Fire and Mud, eruptions and lahars of Mount Pinatubo, Philippines: University of Washington Press, p. 258–306.

Harrington, R.M., and Brodsky, E.E., 2007, Volcanic hybrid earthquakes that are brittle-failure events: Geophysical Research Letters, v. 34, L06308, doi:10.1029/2006GL028714.

Harris, G.W., 1994, The petrology and petrography of lava from the 1986 eruption of Augustine Volcano: University of Alaska Fairbanks, M.S. thesis, 131 p.

Hill, D.P., Ellsworth, W.L., Johnston, M.J.S., Langbein, J.O., Oppenheimer, D.P., Pitt, P.A., Reasenberg, P.A., Sorey, M.L., and McNutt, S.R., 1990, The 1989 earthquake swarm beneath Mammoth Mountain, California; an initial look at the 4 May through 30 September activity: Bulletin Seismological Society of America, v. 80, p. 325–339.

Holasek, R.E., and Rose, W., 1991, Anatomy of 1986 Augustine Volcano eruptions as recorded by multispectral image processing of digital AVHRR weather satellite data: Bulletin of Volcanology, v. 53, p. 420–435.

Iverson, R.M., 2008, Dynamics of seismogenic volcanic extrusion resisted by a solid surface plug, Mount St. Helens, 2004–2005, *in* Sherrod, D.R., Scott, W.E., and Stauffer, P.H., eds, A volcano rekindled; the renewed eruption of Mount St. Helens, 2004–2006: U.S. Geological Survey Professional Paper 1750, p. 425–460.

Iverson, R.M., Dzurisin, D., Gardner, C.A., Gerlach, T.M., LaHusen, R.G., Lisowski, M., Major, J.J., Malone, S.D., Messerich, J.A., Moran, J.C., Pallister, J.S., Qamar, A., Schilling, S.P., and Vallance, J.W., 2006, Dynamics of seismogenic volcanic extrusion at Mount St. Helens in 2004–2005: Nature, v. 444, p. 439–443.

Jacobs, K.M., and McNutt, S.R., 2010, Using seismic *b*-values to interpret seismicity rates and physical processes during the preeruptive earthquake swarm at Augustine Volcano 2005–2006, *in* Power, J.A., Coombs, M.L., and Freymueller, J.T., eds., The 2006 eruption of Augustine Volcano, Alaska: U.S. Geological Survey Professional Paper 1769 (this volume).

Johnston, D.A., 1978, Volatiles, magma mixing, and the mechanism of eruptions of Augustine Volcano, Alaska: University of Washington, Ph. D. dissertation, 177 p.

Johnston, D.A., and Detterman, R.L., 1979, Revision of the recent eruptive history of Augustine Volcano; elimination of the "1902 eruption": U.S. Geological Survey Circular, 804-B, p. 80–84.

Jolly, A.D., Power, J.A., Stihler, S.D., Rao. L., Davidson, G., Paskievitch J.F., Estes, S., and Lahr, J.C., 1996, Catalog of earthquake hypocenters for Augustine, Redoubt, Iliamna, and Mount Spurr volcanoes, Alaska; January 1, 1991–December 31, 1993: U.S. Geological Survey Open-file Report 96-007, 89 p.

Kienle, J., and Shaw, G.E., 1977, Plume dynamics, thermal energy and long distance transport of vulcanian eruption clouds from Augustine Volcano, Alaska: Journal of Volcanology and Geothermal Research, v. 6, p. 139–164.

Kienle, J., Lalla, D.J., Pearson, C.F., and Barrett, S.A., 1979, Search for shallow magma accumulations at Augustine Volcano: University of Alaska Fairbanks, Geophysical Institute, Final Report to U.S. Department of Energy, 157 p.

Kienle, J., and Swanson, S.E., 1983, Volcanism in the eastern Aleutian Arc; late quaternary and Holocene centers, tectonic setting and petrology; Journal of Volcanology and Geothermal Research, v. 17, p 393–432.

Kienle, J., and Swanson, S.E., 1985, Volcanic hazards from future eruptions of Augustine Volcano, Alaska: Geophysical Institute, University of Alaska Fairbanks, Rep. UAG R-275, 2nd ed., 122 p.

Klein, F.W., Koyanagi, R.Y., Nakata, J.S., and Tanigawa, W.R., 1987, The seismicity of Kilauea's magma system, *in* Decker, R.W., Wright, T.L., and Stauffer, P.H., eds., U.S. Geological Survey Professional Paper 1350, p. 1019–1186.

Lalla, D.J., and Kienle, J., 1978, Evolution of seismicity at Augustine Volcano, 1970 to 1976 eruption: Geological Society of America, Abstracts With Programs, v. 10, p. 113.

Lalla, D.J., and Kienle, J., 1980, Problems in volcanic seismology on Augustine Volcano, Alaska: Eos (American Geophysical Union Tranactions), v. 61 p. 68.

Lalla, D.J., and Power, J.A., 2010, A two-step procedure for calculating earthquake hypocenters at Augustine Volcano, *in* Power, J.A., Coombs, M.L., and Freymueller, J.T., eds., The 2006 eruption of Augustine Volcano, Alaska: U.S. Geological Survey Professional Paper 1769 (this volume).

Lahr, J.C., 1999, HYPOELLIPSE; A computer program for determining local earthquake hypocentral parameters, magnitude and first motion pattern: U.S. Geological Survey Open-File Report 99-361, 48 p.

Lahr, J.C., Chouet, B.C., Stephens, C.D., Power, J.A., and Page, R.A., 1994, Earthquake classification, location and error analysis in a volcanic environment; implications for the magamatic system of the 1989–1990 eruptions of Redoubt Volcano, Alaska: Journal of Volcanology and Geothermal Research, v. 62, p. 137–151.

Larsen, J.F., Nye, C.J., Coombs, M.L., Tilman, M., Izbekov, P., and Cameron, C., 2010, Petrology and geochemistry of

the 2006 eruption of Augustine Volcano, *in* Power, J.A., Coombs, M.L., and Freymueller, J.T., eds., The 2006 eruption of Augustine Volcano, Alaska: U.S. Geological Survey Professional Paper 1769 (this volume).

Lee, C.-W., Lu, Z., Jung, H.-S., Won, J.-S., and Dzurisin, D., 2010, Surface deformation of Augustine Volcano, 1992–2005, from multiple-interferogram processing using a refined small baseline subset (SBAS) interferometric synthetic aperture radar (InSAR) approach, *in* Power, J.A., Coombs, M.L., and Freymueller, J.T., eds., The 2006 eruption of Augustine Volcano, Alaska: U.S. Geological Survey Professional Paper 1769 (this volume).

Lee, W.H.K., Tottingham, D.M., and Ellis, J.O., 1988, A PC-based seismic data acquisition and processing system: U.S. Geological Survey Open-file Report 88-751, 31 p.

Mauk, F.J., and Kienle, J., 1973, Microearthquake triggering at St. Augustine Volcano, Alaska, triggered by earth tides: Science, v. 182, p. 386–389.

McGee, K.A., Doukas, M.P., McGimsey, R.G., Neal, C.A., and Wessels, R.L., 2010, Emission of SO_2, CO_2, and H_2S from Augustine Volcano, 2002–2006, *in* Power, J.A., Coombs, M.L., and Freymueller, J.T., eds., The 2006 eruption of Augustine Volcano, Alaska: U.S. Geological Survey Professional Paper 1769 (this volume).

McNutt, S.R., Tytgat, G., Estes, S.A., and Stihler, S.D., 2010, A parametric study of the January 2006 explosive eruptions of Augustine Volcano, using seismic, infrasonic, and lightning data, *in* Power, J.A., Coombs, M.L., and Freymueller, J.T., eds., The 2006 eruption of Augustine Volcano, Alaska: U.S. Geological Survey Professional Paper 1769 (this volume).

Miller, S.A., Colletti, C., Chlaraluce, L., Cocco, M., Barchi, M., and Kaus, B.J.P., 2004, Aftershocks driven by a high pressure CO_2 source at depth: Nature, v. 427, p. 724–727.

Moore, P.L., Iverson, N.R., and Iverson, R.M., 2008, Frictional properties of the Mount St. Helens Gouge, *in* Sherrod, D.R., Scott, W.E., and Stauffer, P.H., eds, A volcano rekindled; the renewed eruption of Mount St. Helens, 2004–2006: U.S. Geological Survey Professional Paper 1750, p. 415–424.

Moran, S.C., Malone, SD., Qamar, A.I., Thelen, W., Wright, A.K.,and Caplan-Auerbach, J., 2008, Seismicity associated with renewed dome-building at Mount St. Helens, 2004–2005, *in* Sherrod, D.R., Scott, W.E., and Stauffer, P.H., eds, A volcano rekindled; the renewed eruption of Mount St. Helens, 2004–2006: U.S. Geological Survey Professional Paper 1750, p. 27–60.

Mori, J., White, R.A., Harlow, D.H., Okubo, P., Power, J.A., Hoblitt, R.P., Laguerta, E., Lanuza, A., and Bautista, B., 1996, Volcanic earthquakes following the 1991 climactic eruption of Mount Pinatubo; strong seismicity during a waning eruption, *in* Newhall, C.G., and Punongbayan, R.S., eds, Fire and Mud, Eruptions and Lahars of Mount Pinatubo, Philippines: University of Washington Press, p. 339–350.

Neal, C.A., Murray, T.L., Power, J.A, Adleman, J.N., Whitmore, P.M., and Osiensky, J.M., 2010, Hazard information management, interagency coordination, and impacts of the 2005–2006 eruption of Augustine Volcano, *in* Power, J.A., Coombs, M.L., and Freymueller, J.T., eds., The 2006 eruption of Augustine Volcano, Alaska: U.S. Geological Survey Professional Paper 1769 (this volume).

Neuberg, J.W., Tuffen, H., Collier, L., Green, D., Powell, T., and Dingwell, D., 2006, The trigger mechanism of low-frequency earthquakes on Montserrat: Journal of Volcanology and Geothermal Research, v. 154, p. 37–50.

Okada, H., Watanabe, H., Yamashita, H., and Yokoyama, I., 1981, Seismologcal signifigance of the 1977–1978 eruptions and magma intrusion process of Usu Volcano, Hokkaido: Journal of Volcanology and Geothermal Research, v. 9, p. 311–334.

Oppenheim, A.V., and Schafer, R.W., 1975, Digital signal processing, Englewood Cliffs, New Jersey, Prentice Hall, 278 p.

Pallister, J.S., Thornber, C.R., Cashman, K.V., Clynne, M.A., Lowers, H.A., Mandeville, C.W., Brownfield, I.K., and Meaker G.P., 2008, Petrology of the 2004–2006 Mount St. Helens Lava Dome—implications for magmatic plumbing and eruption triggering, *in* Sherrod, D.R., Scott, W.E., and Stauffer, P.H., eds, A volcano rekindled; the renewed eruption of Mount St. Helens, 2004–2006: U.S. Geological Survey Professional Paper 1750, p. 647–702.

Paskievitch, J., Read, C., and Parker, T., 2010, Remote telemetered and time-lapse cameras at Augustine Volcano, *in* Power, J.A., Coombs, M.L., and Freymueller, J.T., eds., The 2006 eruption of Augustine Volcano, Alaska: U.S. Geological Survey Professional Paper 1769 (this volume).

Pauk, B.A., Power, J.A., Lisowski, M., Dzurisin, D., Iwatsubo, E.Y., and Melbourne, T., 2001, Global positioning system (GPS) survey of Augustine Volcano, Alaska, August 3-8, 2000; Data processing, geodetic coordinates and comparison with prior geodetic surveys: U.S. Geological Survey Open-File Report 01-99, 20 p.

Pauk, B.A., Jackson, M., Feaux, K., Mencin, D., and Bohnenstiehl, K., 2010, The Plate Boundary Observatory permanent global positioning system network on Augustine Volcano before and after the 2006 eruption, *in* Power, J.A., Coombs, M.L., and Freymueller, J.T., eds., The 2006 eruption of Augustine Volcano, Alaska: U.S. Geological Survey Professional Paper 1769 (this volume).

Pearson, C.F., 1977, Seismic refraction study of Augustine Volcano: University of Alaska Fairbanks, M.S. thesis, 131 p.

Petersen, T., De Angelis, S., Tytgat, G., and McNutt, S.R., 2006, Local infrasound observations of large ash explosions at Augustine Volcano, Alaska, during January 11–28, 2006: Geophysical Research Letters, v. 33 , doi 10.1029/2006GL026491.

Power, J.A., (1988), Seismicity associated with the 1986 eruption of Augustine Volcano, Alaska: University of Alaska Fairbanks, M.S. thesis, 142 p.

Power, J.A., and Iwatsubo E.Y., 1998, Measurements of slope distances and zenith angles at Augustine Volcano, Alaska, 1986, 1988, and 1989: U.S. Geological Survey Open-File Report 98-145, 17 p.

Power, J.A., Lahr, J.C., Page, R.A., Chouet, B.A., Stephens, C.D., Harlow, D.H., Murray, T.L., and Davies, J.N., 1994, Seismic evolution of the 1989–1990 eruption sequence of Redoubt Volcano, Alaska: Journal of Volcanology and Geothermal Research, v. 62, p. 69–94.

Power, J.A., Nye, C.J., Coombs, M.L., Wessels, R.L., Cervelli, P.F., Dehn, J., Wallace, K.L., Freymueller, J.T., and Doukas, M.P., 2006, The reawakening of Alaska's Augustine Volcano: Eos (American Geophysical Union Transactions), v. 87, p. 373, 377.

Reeder, J.W., and Lahr, J.C., 1987, Seismological aspects of the 1976 eruptions of Augustine Volcano, Alaska: U.S. Geological Survey Bulletin 1768, 32 p.

Robinson, M., 1990, XPICK users manual, version 2.7: Seismology Lab, Geophysical Institute, University of Alaska Fairbanks, 93 p.

Roman, D.C., Cashman, K.V., Gardner, C.A., Wallace P.J., and Donovan, J.J., 2006, Storage and interaction of compositionally heterogeneous magmas from the 1986 eruption of Augustine Volcano, Alaska: Bulletin of Volcanology, v. 68, p. 240–254, doi10.1007/s00445-005-003-z.

Rowe, C.A., Thurber, C.H., and White, R.A., 2004, Dome growth behavior at Soufriere Hills Volcano, Montserrat, revealed by relocation of volcanic event swarms, 1995–1996: Journal of Volcanology and Geothermal Research, v. 134, p. 199–221.

Schneider, D.J., Scott, C., Wood J., and Hall T., 2006, NEXRAD weather radar observations of the 2006 Augustine volcanic eruption clouds: Eos (American Geophysical Union Transactions) v. 87, abs. V51C-1686.

Sentman, D.D., McNutt, S.R., Stenbaek-Nielsen, H.C., Tytgat, G., and DeRoin, N., 2010, Imaging observations of thermal emissions from Augustine Volcano using a small astronomical camera, *in* Power, J.A., Coombs, M.L., and Freymueller, J.T., eds., The 2006 eruption of Augustine Volcano, Alaska: U.S. Geological Survey Professional Paper 1769 (this volume).

Shilling, S.P., Thompson, R.A., Messerich, J.A., and Iwatsubo, E.Y., 2008, Use of digitial aerophotogrammetry to determine rates of lava dome growth, Mount St. Helens, Washington, 2004–2005, *in* Sherrod, D.R., Scott, W.E., and Stauffer, P.H., eds, A volcano rekindled; the renewed eruption of Mount St. Helens, 2004–2006: U.S. Geological Survey Professional Paper 1750, p. 145–167.

Siebert, L., Beget, J.E., and Glicken, H., 1995, The 1883 and late-prehistoric eruptions of Augustine Volcano, Alaska: Journal of Volcanology and Geothermal Research, v. 66, p. 367–395.

Swanson, S.E., and Kienle, J., 1988, The 1986 eruption of Mount St. Augustine; Field test of a hazard evaluation: Journal of Geophysical Research v. 93, p. 4500–4520.

Thelen, W.A., Crosson, R.S., and Creager, K.C., 2008, Absolute and relative locations of earthquakes at Mount St. Helens, Washington using continuous data: implications for magmatic processes, *in* Sherrod, D.R., Scott, W.E., and Stauffer, P.H., eds, A volcano rekindled; the renewed eruption of Mount St. Helens, 2004–2006: U.S. Geological Survey Professional Paper 1750, p. 71–96.

Thomas, R.J., McNutt, S.R., Krehbiel, P.R., Rison, W., Aulich, G., Edens, H.E., Tytgat, G, and Clark, E., 2010, Lightning and electrical activity during the 2006 eruption of Augustine Volcano, *in* Power, J.A., Coombs, M.L., and Freymueller, J.T., eds., The 2006 eruption of Augustine Volcano, Alaska: U.S. Geological Survey Professional Paper 1769 (this volume).

Vallance, J.W., Bull, K.F., and Coombs, M.L., 2010, Pyroclastic flows, lahars, and mixed avalanches generated during the 2006 eruption of Augustine Volcano, *in* Power, J.A., Coombs, M.L., and Freymueller, J.T., eds., The 2006 eruption of Augustine Volcano, Alaska: U.S. Geological Survey Professional Paper 1769 (this volume).

Villagomez, D., 2000, Sismicidad del volcan Guagua Pichincha 1998–1999: Quito, Ecuador, Escuela Politecnica Nacional, M.S. thesis.

Waite, G.P., Chouet, B.A. and Dawson P.B., 2008, Eruption dynamics at Mount St. Helens imaged from broadband seismic waveforms; Interaction of the shallow magmatic and hydrothermal systems: Journal of Geophysical Research, v. 113, B02305, doi:10.1029/2007JB005259.

Waitt, R.B., and Begét, J.E., 2009, Volcanic processes and geology of Augustine Volcano, Alaska: U.S. Geological Survey Professional Paper 1762, 78 p., 2 map plates [http://pubs.usgs.gov/pp/1762/].

Wallace, K.L., Neal, C.A., and McGimsey, R.G., 2010, Timing, distribution, and character of tephra fall from the 2005–2006 eruption of Augustine Volcano, *in* Power, J.A.,

Coombs, M.L., and Freymueller, J.T., eds., The 2006 eruption of Augustine Volcano, Alaska: U.S. Geological Survey Professional Paper 1769 (this volume).

Waythomas, C.F., and Waitt, R.B., 1998, Preliminmary volcano-hazard assessment for Augustine Volcano, Alaska, U.S. Geological Survey Open-File Report 98-106, 39 p.

Wessels, R.L., Coombs, M.L., Schneider, D.J., Dehn, J., and Ramsey, M.S., 2010, High-resolution satellite and airborne thermal infrared imaging of the 2006 eruption of Augustine Volcano, *in* Power, J.A., Coombs, M.L., and Freymueller, J.T., eds., The 2006 eruption of Augustine Volcano, Alaska: U.S. Geological Survey Professional Paper 1769 (this volume).

Weaver, C.S., Grant, W.C., Malone, S.D., and Endo, E.T., 1981, Post-May 18 seismicity; volcanic and tectonic applications, *in* Lipman, P.W., and Mullineaux, D.R., eds., The 1980 eruptions of Mount St. Helens, Washington: U.S. Geological Survey Professional Paper 1250, p. 109–122.

Yount, M.E., Miller, T.P., and Gamble, B.M., 1987, The 1986 eruptions of Augustine Volcano, Hazards and effects: U.S. Geological Survey Circular 998, p. 4–13.

The 2006 Eruption of Augustine Volcano, Alaska
Power, J.A., Coombs, M.L., and Freymueller, J.T., editors
U.S. Geological Survey Professional Paper 1769

Chapter 2

Seismic Precursors to Volcanic Explosions During the 2006 Eruption of Augustine Volcano

By Helena Buurman[1] and Michael E. West[1]

Abstract

The 2006 eruption of Augustine Volcano, Alaska, generated more than 3,500 earthquakes in a month-long time frame bracketing the most explosive period of activity. We examine two quantitative tools that, in retrospective analysis, were excellent indicators of imminent eruption. The first tool, referred to as the frequency index (*FI*), is based on a simple ratio of high- and low-frequency energy in an earthquake seismogram. It is a metric that allows us to quantify the differences between the canonical high-frequency, hybrid, and low-frequency volcanic earthquakes. *FI* values greater than –0.4 indicate earthquakes classically referred to as high-frequency or volcano-tectonic events. *FI* values less than –1.3 correspond to events usually referred to as low-frequency earthquakes. Because the *FI* is based on a ratio and not a spectral peak, hybrid earthquakes are successfully assigned *FI* values intermediate to these two classes. In this eruption, we find a remarkable correlation between events with *FI* less than –1.8 and explosive eruptions. The second tool we examine is based on repeating seismic waveforms identified through waveform cross-correlation. Although the vast majority of earthquakes during this eruption have unique waveforms, subsets of events exhibiting a high degree of similarity occur and are closely tied to explosive eruption events. Of the 13 large explosion events, seven were preceded by clusters of highly similar earthquakes. We apply the *FI* and correlation tools together to identify changes in high- and low-frequency earthquake occurrences and examine their relations to the precursory, explosive, and continuous phases of the eruption. We find that earthquakes that have low *FI* values and earthquakes exhibiting high degrees of similarity occur almost exclusively within hours of explosive eruptions and postulate that they occur as a result of the final ascent of magma in the volcanic edifice. Because neither of these methods requires analyst-reviewed earthquake locations, we believe that they have considerable potential as automated real-time volcano monitoring tools.

Introduction

Seismicity has long been one of the most commonly monitored aspects of active volcanoes. Different volcanic processes produce very different types of earthquakes, varying in waveform duration, onset, frequency content, and amplitude. Earthquakes with impulsive P and S arrivals and peak frequencies between 5 and 15 Hz, for example, are typically the result of brittle failure of rock within the volcanic edifice (McNutt, 1996). They often occur at high rates during episodes of volcanic unrest, although they are also part of the natural background seismicity found at volcanoes. Another type of earthquake routinely observed during episodes of volcanic activity has an emergent P arrival and often lacks a distinct S arrival. This type of earthquake is dominated by frequencies between 1 and 5 Hz, has little energy at frequencies greater than 15 Hz, and is thought to result from the resonance of fluid-filled cracks (Chouet, 1988). Numerous trigger mechanisms exist for such a process, and we refer to the summaries of Neuberg and others (2005) and Petersen (2007) for excellent overviews.

Certain volcanic processes can cause earthquakes to have remarkably similar waveform characteristics. For one waveform to appear the same as another it must originate in approximately the same place and from the same process. Nondestructive processes such as stick-slip movement along a fault or conduit or destructive mechanisms such as the incremental opening of cracks are possible sources for such earthquakes. The low-frequency resonant sources can be particularly rich in similar waveforms because of their inherently nondestructive source (for example, Stephens and Chouet, 2001; Petersen, 2007).

Perhaps the most basic metric for tracking volcanic seismicity is the overall rate of earthquakes. Eruptions are

[1]Alaska Volcano Observatory, Geophysical Institute, University of Alaska Fairbanks, 903 Koyukuk Drive, Fairbanks, AK 99775.

almost always preceded by some type of earthquake swarm. The swarm may last hours or months and may contain a variety of earthquake types or consist of just one style of event (Benoit and McNutt, 1996). The wide range of swarm characteristics reflects the wide range of processes thought to produce them. However, the nearly ubiquitous existence of precursory seismic swarms is one of the foundations of volcano monitoring.

Quantifying seismic activity is an effective method for inferring the level of unrest and the type of activity occurring at a volcano. This can be challenging in a real-time setting because the rate of seismic activity in a precursory swarm typically exceeds the rate at which events can be processed by any sort of analyst-reviewed process. Earthquakes are often classified manually, and this is usually based on the experience and interpretation of the analyst in subjective method that can lead to inconsistencies across or even within datasets (Langer and others, 2006). The manual review of earthquakes is impossible to accomplish in real time during rapid seismic sequences, even though assessing earthquake parameters such as frequency content is precisely what is needed in order to know whether or not such swarms are building towards an eruption.

We present a method for differentiating between earthquake types based on their frequency content. Our approach is simple and can be applied without user intervention. We apply this method to the explosive sequences of the 2006 eruption of Augustine Volcano, Alaska. The method is largely independent of earthquake locations and is robust to changes in seismic network coverage. The only assumption we make is that the seismic events are being generated by the volcano—a reasonable assumption given the high rates of seismicity during most eruptions. This is particularly relevant to Augustine, where the earthquakes are clustered together such that the first-order earthquake locations (which at some volcanoes exhibit a clear rise to the surface before eruption; for example, Harlow and others, 1994) provided limited information about the eruptive processes.

We also investigate patterns of repeating earthquakes and examine how they relate to eruptive behavior. The classification of seismic events combined with the identification of repeating earthquakes provides a different insight into the processes that occur at an erupting volcano. We show that an automated analysis of this type could provide key observations and even identify precursors to explosive activity.

Augustine Volcano

Augustine Volcano is a 10-km-wide island located in Cook Inlet between the Kenai Peninsula and Cape Douglas, 115 km from the town of Homer, in south-central Alaska. It has an historical eruptive history dating back to 1812 and erupted four

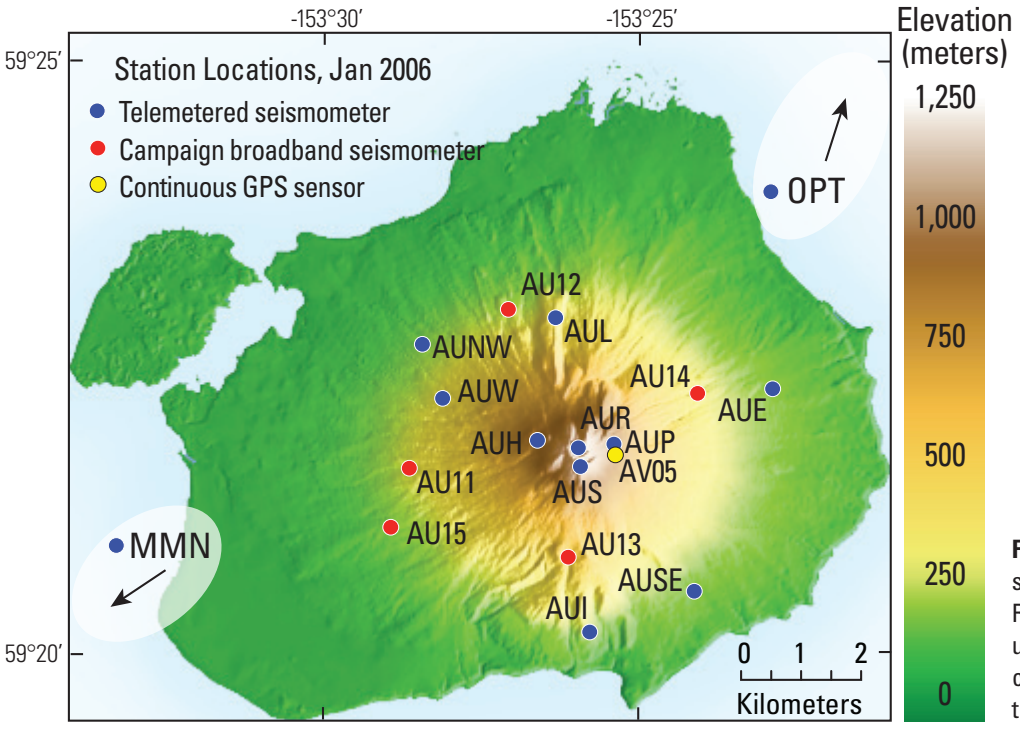

Figure 1. Locations of seismic stations on Augustine Island. Reference stations MMN and OPT used during the compilation of the catalog are located on the mainland; their directions are indicated.

times in the twentieth century alone, with the most recent eruption occurring in 1986 (Power and Lalla, this volume).

The 2006 eruption of Augustine began on January 11, following an 8.5-month period of precursory seismic activity (Jacobs and McNutt, this volume; Power and Lalla, this volume). An earthquake swarm occurred on January 10–11, 2006, which culminated in two phreatic explosions (Wallace and others, this volume) and heralded the onset of the explosive eruption sequence. On the basis of the character of unrest and the resultant eruptive deposits, Coombs and others (this volume) divide the eruption into several different phases. The explosive phase occurred between January 11 and January 28, during which time the eruptive activity was characterized by 2 largely phreatic and 11 magmatic explosions that generated ash plumes to heights greater than 9 km above sea level (asl) (Bailey and others, this volume), with repose periods between events lasting hours to days. These events recorded peak amplitudes greater than 20 Pa on the local pressure sensor located at station AUE (fig. 1), 3.5 km east of the volcano's summit. The explosions in the latter half of January were also strong enough to be recorded on the 153US infrasonic array at Fairbanks, 675 km north of Augustine (Wilson and others, 2006). A period of continuous eruptive activity (the continuous phase) began on January 28. This was characterized by a persistent ash plume up to 5 km asl (Bailey and others, this volume), produced by discrete but frequent (minutes to hours apart) minor explosions measuring less than 20 Pa at pressure sensor AUE. A gradual transition to effusive behavior followed, in which the small explosive events became fewer in number during the first week of February and the eruptive activity became dominated by dome growth with associated rockfalls and block and ash flows. Finally, a period of dome growth and lava flow (the effusive phase) between March 3 and March 16 brought the 2006 eruption sequence to a close.

The dataset used in this study spans the last 11 days of the precursory phase, which terminates with a vigorous seismic swarm of over 780 earthquakes, the entire explosive phase from January 11 to January 28, and the majority of the continuous phase from January 28 to February 6. By February 6 the seismic activity had begun to wane considerably and the volcano was moderately quiet until a short effusive dome-building phase occurred in early March 2006.

Data

Augustine was one of the more densely instrumented volcanoes in Alaska before 2006 as a result of its recent eruptive history and its proximity to settlements. The real-time seismic network on the island consisted of 10 short-period seismic stations at distances between 0 and 3.5 km from the summit and a broad-band seismometer 2.5 km from the summit. In late December 2005 the Alaska Volcano Observatory (AVO) deployed five campaign broad-band seismometers with on-site recording, as well as a telemetered strong motion sensor at a distance of 4.5 km. Over the course of the eruption, the five telemetered seismometers closest to the summit were destroyed, along with broad-band seismometer AU12. The loss of the summit seismic stations compromised AVO's ability to locate earthquakes during the latter portions of the eruption. The summit stations also provided the means with which to track the microseismicity occurring within the edifice, which was detectable only at those stations. Although not available in real time, the campaign broad-band data provided three-component records of high dynamic range with a flat response in the frequencies of interest. The 24-bit dynamic range allowed the entire eruption sequence to be recorded on scale.

The seismic data collected from the 2006 eruption of Augustine Volcano provide an excellent dataset for calibrating event classification schemes. A wide range of nonseismological observations complement this dataset, including deformation and visual records, as well as surface temperatures measured via satellite, all of which serve as independent verifications of volcanic processes observed in the seismic dataset. Perhaps most importantly, the eruption exhibited several types of activity, including a precursory earthquake swarm, vulcanian explosions, and sustained ash emission, in a 1-month time frame. This complexity provides the opportunity to benchmark tools against a variety of volcanic events in a single dataset.

Our analysis is based on a custom earthquake catalog. The analyst-reviewed earthquake catalog produced by AVO is limited to events that meet specific quality criteria (Dixon and others, 2008). For the current analysis we wished to include emergent earthquakes that cannot be located by traditional methods. We also wanted coverage of the final explosions and the transition into the continuous phase, even though the loss in summit stations compromised earthquake location during those periods. To accomplish this, we compiled a custom catalog of earthquakes for the period of time between January 1 and February 6. We scanned the full set of continuous waveforms and included in the catalog all earthquakes observed on a minimum of three stations including AU13, regardless of whether the trace was impulsive or emergent. Requiring a clear signal on station AU13 introduced a minor station bias in the data. In practice, however, there were few earthquakes visible away from the summit that were not well recorded on AU13. By requiring all arrivals to appear on one consistent station, we were able to catalog events by their arrival time at AU13 instead of the traditional method of cataloging events by their modeled origin time. This allowed us to analyze earthquakes that were not locatable, either because of poor station coverage or emergent onset. Of the 3,514 events in this catalog, 39 percent were included in the AVO analyst-reviewed catalog. This difference helped insulate the analysis from network changes and allowed a more comprehensive inclusion of earthquake types—at the notable expense of earthquake locations. We chose AU13 as our master station because it had the lowest signal-to-noise ratio of the campaign broadband stations and, unlike most of the telemetered stations located at similar distances, recorded continuously through the eruption. All broadband stations at Augustine were instrumented with Guralp CMG-6TD (30 s) seismometers recording at 100 Hz.

Teleseismic signals (including regional earthquakes) were identified by referring to mainland seismic stations OPT and MMN, situated at sufficiently great distances from Augustine Island so as not to record the volcanogenic signals, and were not included in the catalog.

Frequency Index Analysis

Method

The frequency content of an earthquake is a first-order metric with which to infer different source processes. The frequency with the greatest amplitude in the Fourier spectrum, the so-called dominant frequency, can be used as a general proxy for spectral content. Dominant frequency has been used in studies to characterize waveform types (for example, Latter, 1980; McNutt, 2002), but several shortcomings arise when using dominant frequency as a measure of the overall frequency content. Earthquakes with low signal-to-noise ratios are subject to low-frequency noise contamination (a particular issue for broadband data); the high-frequency earthquake shown in figure 2, for example, has a dominant frequency of 1.27 Hz, despite its considerable high-frequency content. The dominant frequency measure is also unable to identify earthquakes with bimodal frequency distributions, measuring only one peak in the spectra and therefore grouping it with other single-peaked events. This is a particular issue for hybrid-type earthquakes. Our early attempts to classify waveforms on the basis of dominant frequency were unsuccessful, in large part because hybrid events were arbitrarily grouped with either the high- or low-frequency groups, depending on which peak in the spectrum happened to be largest. These uncertainties associated with dominant frequency led us to seek a more robust metric for discriminating between different types of earthquake.

We develop the frequency index (*FI*) based on the ratio of energy in low and high frequency windows. Because the resulting measure spans many orders of magnitude, we use a base-ten logarithm to reduce the index to a simple number, typically between –3 and 1 for this dataset. The logarithm is intuitively appealing because waveforms with equal amounts of high and low energy (as defined by the frequency windows) have a frequency index of 0. A negative *FI* means the waveform is dominated by low-frequency energy, while a positive *FI* demonstrates a majority of energy in the high-frequency band.

We define the frequency index as

$$FI = \log_{10}\left(\frac{mean(A_{upper})}{mean(A_{lower})}\right), \quad (1)$$

where A_{upper} are the spectral amplitudes across a band of high frequencies and A_{lower} are the spectral amplitudes measured across a lower range of frequencies. To calculate the *FI* in a consistent manner on thousands of waveforms, we use unfiltered waveforms with durations of 7 seconds: 1 second prior to the earthquake onset and 6 seconds after, ensuring that the high frequency P-wave onset is fully captured in the Fourier analysis. This is a sufficient time window over which to sample both the shorter duration, smaller magnitude earthquakes recorded, as well as the more emergent, lower frequency events. Linear trends and offsets are removed from the waveforms, and they are transformed to the frequency domain using a Tapered Fourier Transform. There is no need to correct for instrument response during this particular analysis, because the data were recorded on sensors with a flat response across our bandwidth of interest.

To determine suitable ranges for A_{lower} and A_{upper} we compiled a set of calibration waveforms. Using standard, if subjective, visual criteria, we selected high quality examples of three types of earthquake, based on the canonical high-frequency, low-frequency, and hybrid volcanic earthquake classification scheme (for example, Minikami, 1960; Lahr and others, 1994; McNutt, 1996). The high-frequency earthquakes contain energy up to 30 Hz; the low-frequency earthquakes contain a range of frequencies predominantly between 1 and 4 Hz; while the hybrid-type earthquakes sample both. Figure 2 shows example waveforms of high-frequency, hybrid and low-frequency type waveforms from this set. The frequency spectra for each event type were stacked to produce the spectra in figure 3*A*. The spectra were normalized to the area below each spectral curve prior

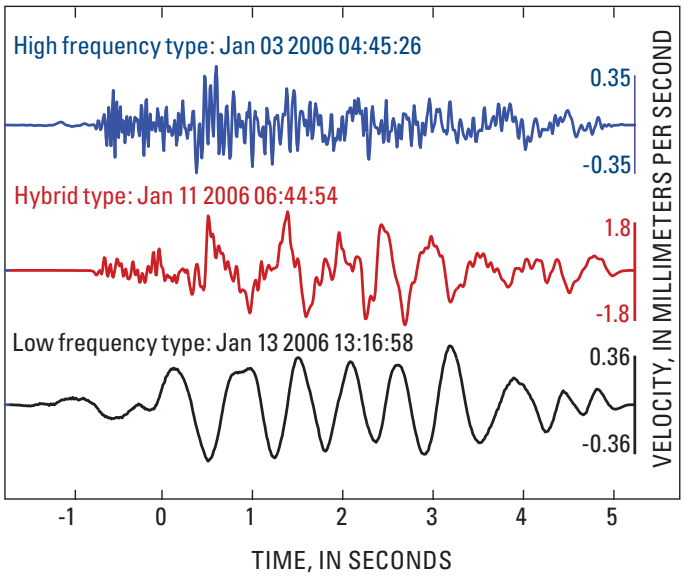

Figure 2. Selection of seismic waveforms from the "calibration set" used to translate between Frequency Index (*FI*) and the high-frequency, hybrid, and low-frequency earthquake classification. Waveforms were selected on the basis of visual criteria.

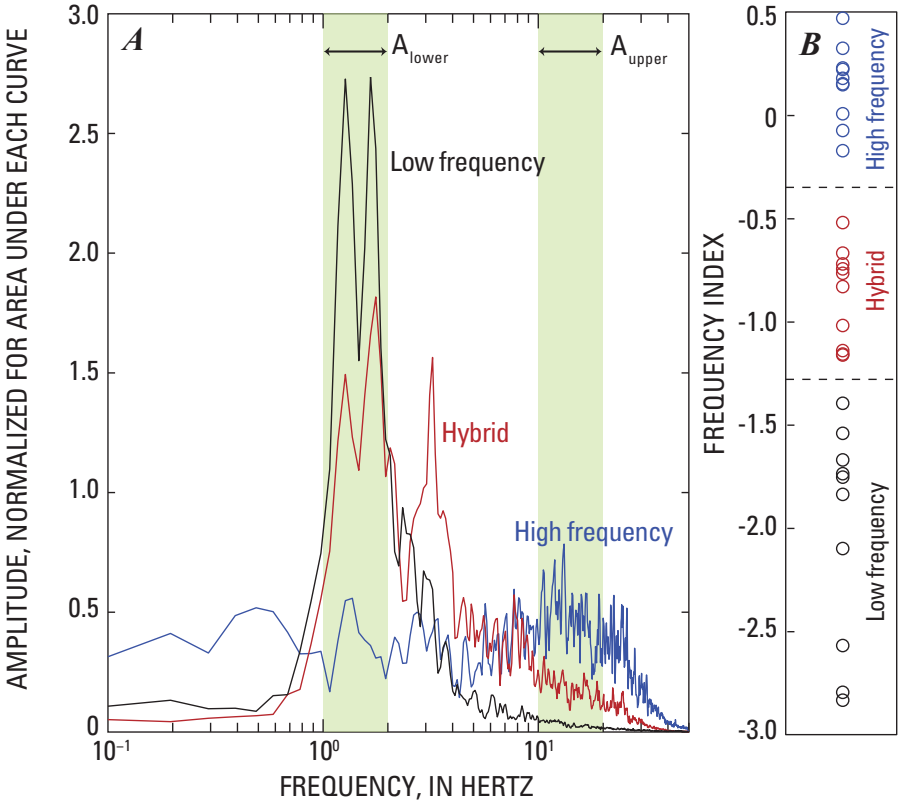

Figure 3. Frequency spectra and *FI* values for the "calibration set" of waveforms used to translate between Frequency Index (*FI*) and the high-frequency, hybrid, and low-frequency earthquake classification. *A*, Stacked frequency spectra of 10 high frequency, 10 low frequency and 10 hybrid "calibration waveforms," normalized for area beneath the curve. Ranges for A_{upper} and A_{lower} are displayed as shaded areas. *B*, *FI* values for each waveform, with dashed black lines indicating the half-distance between earthquake types.

to stacking. The intervals for A_{lower} and A_{upper} were defined across frequencies where the differences between the high-frequency, low-frequency and hybrid earthquake spectra were most pronounced: A_{lower} was attributed the range of 1-2 Hz, while A_{upper} was set to the range of 10-20 Hz, as shown in figure 3*A*. The *FI* values were calculated for the sample set and are shown in figure 3*B*. Although the frequency ranges in equation 1 are subjectively defined, the *FI* provides a repeatable quantitative measure of the frequency content inherent to the waveform. The calibration earthquakes provide an approximate translation between *FI* and the more traditional high-frequency, low-frequency, hybrid paradigm.

The high frequency, low frequency and hybrid groups fall within distinct *FI* limits, showing no overlap between groups, and exhibit an overall range of *FI* values between –2.9 and 0.5. Black dashed lines in figure 3*B* mark the half-distance between the group end-members at –0.4 for the transition from high frequency to hybrid earthquakes and at –1.3 for the transition from hybrid to low frequency earthquakes. The threshold for high frequency earthquakes is less than 0, which is not intuitive, since the 0 *FI* represents equal amplitudes at high and low frequencies. Indeed, the overall distribution of *FI* is biased towards the lower frequencies. There are two causes for this. The first is the greater attenuation of high frequencies with distance from the earthquake source. The second is the generally low signal-to-noise ratio of the high frequency earthquakes. This is due to the small magnitude of the seismicity (the largest located earthquake during the entire eruption had M_L 1.5, Dixon and others, 2008) and high levels of low-frequency noise resulting from the location of Augustine Island. These two factors tend to amplify the low frequency end of the spectrum. An examination of larger magnitude high-frequency earthquakes in other settings suggests that *FI* values of 1 and 2 should be common outside of this particular dataset.

FI Analysis for the Eruption Sequence

The distribution of *FI* values shows a distinct pattern with the eruptive phase (fig. 4). Before the swarm on January 10–11, the majority of events had significant amounts of high frequency energy as indicated by the *FI* values greater than –0.5, with rare events as low as –1.8. The earthquakes during the preeruptive swarm were different, exhibiting *FI* values between 0.6 and –1.7, with 80 percent between 0.2 and –0.8. These ranges indicate that the earthquakes still contain significant amounts of high frequency energy, but that lower frequencies are present too; less that 10 percent of the earthquakes show dominantly low frequency (below *FI* –1.3) energy content. After the first two explosions on January 11, the earthquakes shift to a lower *FI* , between –0.2 and –1.2, indicating that they are predominantly hybrid-type earthquakes. In the 12 hours before the first magmatic explosion on January 13 (Wallace and others, this volume), the *FI* range drops further to *FI* s of –0.5 to –1.6. In the hour prior to the first of the explosions on January 13, the *FI* drops as low as –2.9. Throughout

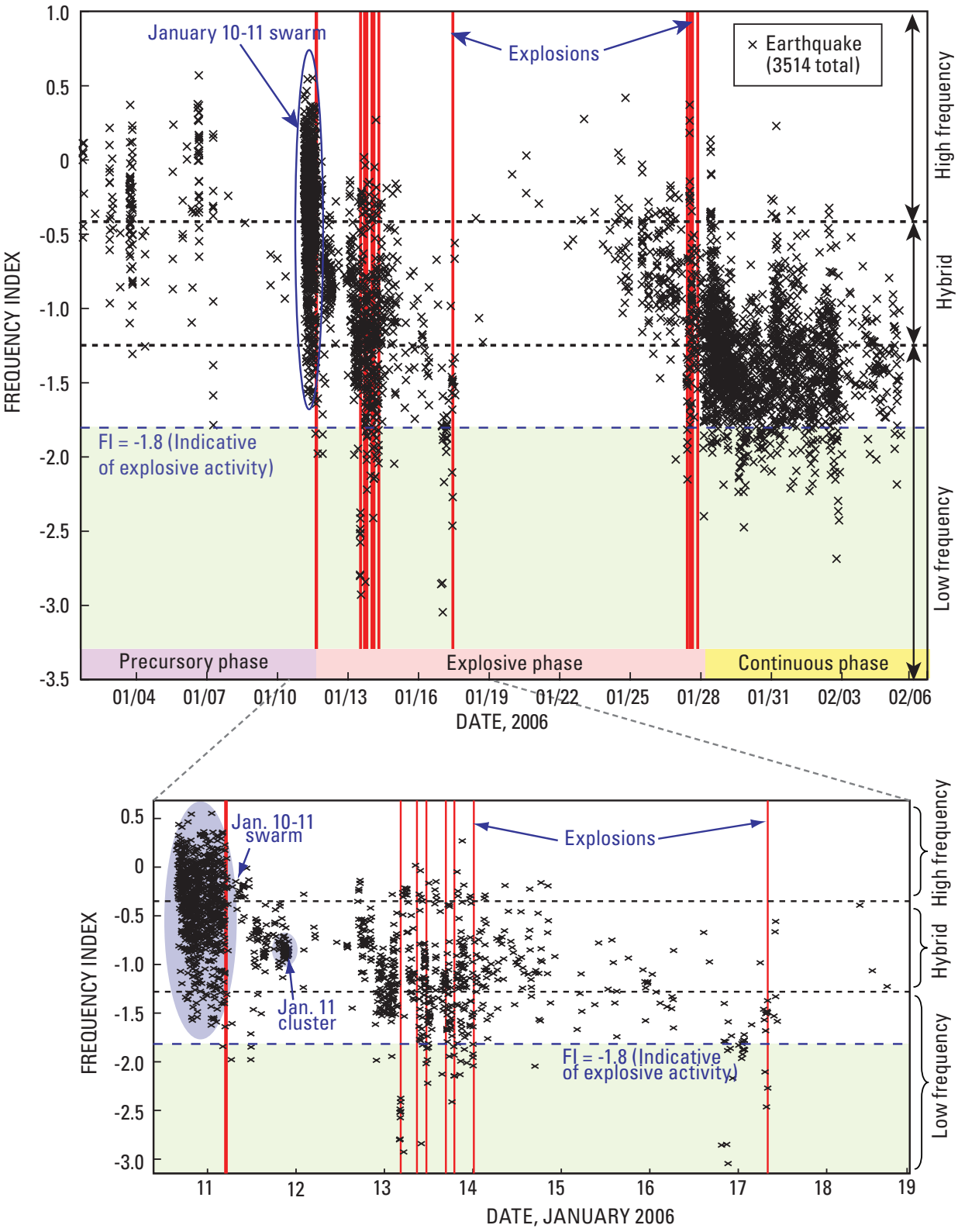

Figure 4. Distribution of Frequency Index (*FI*) with time at station AU13 for all earthquakes in the custom Augustine earthquake catalog. The *FI* range for the Augustine dataset is between 0.57 and –3.05. Explosions are marked with vertical red lines. *FI* = –1.8 (dashed line at the top of the shaded area) indicates the threshold *FI* for earthquakes as precursors to explosive eruptions. Translation to the traditional high-frequency, hybrid, and low-frequency classification scheme is marked by dashed black lines at *FI* –0.35 and *FI* –1.28.

the six explosions on January 13–14 the *FI* ranges from 0 to –2.9, with the majority of events between –0.7 and –2. Once the explosive activity ceases, the range diminishes somewhat, with most earthquakes falling within the *FI* range of –0.5 and –1.8, indicating hybrid and low frequency earthquake activity. A drop in *FI* is observed in the 12 hours prior to the explosion on January 17, with values as low as –3. After this explosion the seismicity decreases, and few events occur between January 17 and 25. Seismic activity resumes after January 25, and there is a systematic decline in the *FI* from 0.4 and –2 leading up to the magmatic explosions on January 27–28. Following the last of the 5 explosions on January 28, the *FI* remains low. The earthquake activity from January 28 through February 6 falls mostly between the *FI* values of –0.4 and –2.

Path and site effects can cause the frequency content of waveforms to vary significantly between stations. To verify the trends observed within the *FI* results, *FI* analysis was carried out at station AU15 located 3.5 km southwest of the edifice (fig. 1). The *FI* for these earthquakes was calculated using the same procedure described for the AU13 arrivals, with results shown in figure 5. The *FI* trends observed at station AU15 are similar to those found at station AU13, showing the same high *FI* values prior to the eruption sequence and a significant drop after the precursory swarm. The same association between low *FI* events and explosions is observed at AU15. In general, however, the upper *FI* values at AU15 are lower than those at AU13. Another difference between the *FI* at these stations is observed during the continuous phase. The majority of earthquakes at AU13 have *FI* values between –1 and –2, whereas the majority of events at station AU15 fall between –0.5 and –1.5, and the pronounced drop in *FI* seen at station AU13 after January 28 is scarcely evident at AU15. Strong wind can increase the *FI* of an earthquake, because it introduces high frequency noise into the spectrum and lowers the signal-to-noise ratio. It is possible that the poor weather conditions during the continuous phase had a greater effect on the signal-to-noise ratio at station AU15 than at AU13, given that the prevailing northwesterly wind direction affords minimal shelter to a site on the west of the island such as AU15. We consider wind noise to be one possibility for the 0.5 *FI* variation between these two stations.

Interpretation of Eruptive Sequence in Terms of *FI*

One of the most notable features of the eruption was the energetic swarm of earthquakes characterized by high *FI* values (up to 0.5) in the hours preceding the first explosive eruption on January 11. The predominance of high frequencies suggests that much of the energy was released by fracturing rock. We interpret this as the final opening of the conduit pathways to the surface, which facilitated the first of the explosions. The first two explosions were predominantly gaseous and contained little ash (Wallace and others, this volume),

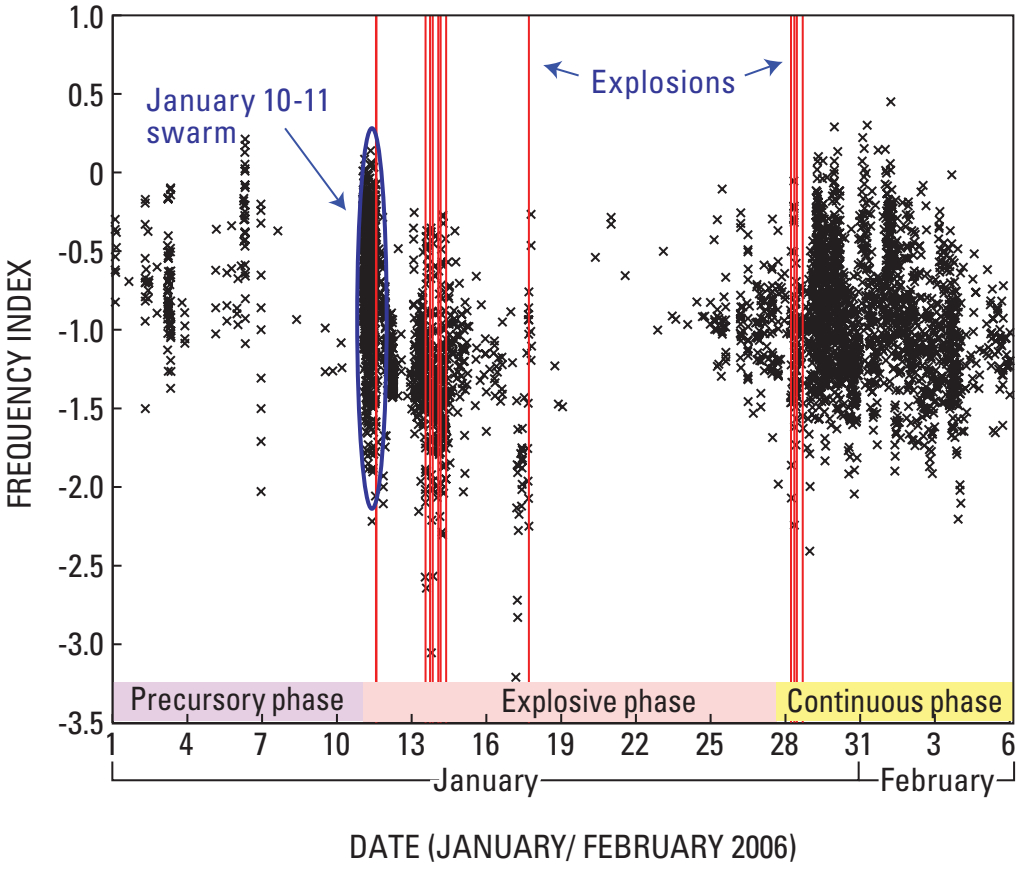

Figure 5. Frequency Index (*FI*) for the catalog recorded at station AU15. Explosions are marked with vertical red lines.

Table 1. Summary of earthquake clusters and *FI* associated with volcanic explosions at Augustine Volcano, Alaska, January 11-28, 2006.

[AKST, Alaska Standard Time; FI, Frequency Index]

Day, 2006	Time, AKST	Number of events in cluster prior to explosion	Length of cluster	Time between end of cluster and explosion	Maximum correlation within cluster	*FI* range of cluster	Number of events with *FI*<–1.8 since last explosion	Plume height, kilometers above sea level
Jan. 11	0444	<swarm>	-	13 min	-		1	9
Jan. 11[1]	0512	0	-	-	-		0	9
Jan. 13	0424	5	10 min	1 min	0.97	–2.35 -> -2.8	9	10
Jan. 13	0647	9	56 min	1 hr 17 min	0.96	–1.03 -> -1.3	2	>9
Jan. 13	1122	11	15 min	16 min	0.98	–0.93 -> -1.28	3	11
Jan. 13	1640	5	17 min	13 min	0.92	–1.07 -> -1.28	6	10
Jan. 13	1858	0	-	-	-		6	9
Jan. 14	0014	0	-	-			9	no data
Jan. 17	0758	6	37 min	6 hr 23 min	0.91	–1.78 -> -1.92	15	14
Jan. 27	2024	29	81 hr 13 min	9 hr 24 min	0.95	–0.5 -> -1.5	1	9
Jan. 27	2337	0	-	-	-		4	<3
Jan. 28	0204	0	-	-	-		0	8
Jan. 28	0742	0	-	-	-		0	8

[1] Disregarded because this explosion occurs within half an hour of the previous event.

suggesting that the high frequency fracturing preceding the eruption was driven by high-pressure gas moving ahead of the magma that followed in later eruptions. The precursory swarm on January 10-11 also contained a small number of events with *FI* as low as –1.6. These events are more consistent with a source generated from the migration of fluids. One possibility is that on January 10-11 magma within the Augustine edifice began to move slowly upwards. As the pressure on the magma decreased, additional water exsolved from the magma, creating a gas phase. This high-pressure gas phase migrated rapidly to the summit ahead of the magma, opening pathways and enabling magma to follow in the subsequent eruptive sequence.

These first two explosions were followed by a 2-day repose period, during which the average *FI* dropped to values between –0.2 and –1.2, with a notable 2-hour-long cluster of repeating earthquakes all with *FI* values near –0.9 (fig. 4). These hybrid and low frequency events were likely caused by the movements of magma into shallow levels of the edifice in anticipation of explosive eruption. The presence of hybrid earthquakes (*FI* –0.4 to –1.3)—and therefore some amount of high frequency energy—suggests that pathways to the surface were still not entirely open and brittle fracture continued as magma continued to force open conduits and/or squeeze through constrictions. The net effect, however, was to bring magma into shallow levels in the volcano. Cervelli and others (this volume) reach a similar conclusion, based on the deformation signals recorded at the summit, and suggest an upward propagating magma-filled crack near GPS station AV05 (fig. 1). Coombs and others (this volume) further propose that a small and relatively degassed lava dome effused on January 12, which was subsequently destroyed during the sequence of magmatic explosions on January 13–14.

FI as an Eruptive Precursor

Earthquakes with *FI* values lower than –1.8 are seen exclusively within 17 hours of the larger explosions in January 2006 and occur frequently during the continuous eruptive activity in late January and early February, diminishing in number with the gradual decline of explosive activity. Such a close association between explosions and low-*FI* earthquakes strongly suggests that these earthquakes are directly related to the explosive process. These results are summarized in table 1.

Low frequency earthquakes prior to eruption sequences are not unique to Augustine and have been observed in a variety of places, including Redoubt (for example, Chouet and others, 1994), Galeras (for example, Fischer and others, 1994), and Pinatubo (Harlow and others, 1994). The time scales over which these events occur vary between systems, ranging from hours to weeks, and are thought to depend on the amount

of pressurization within the magmatic/hydrothermal system below the volcano (Chouet, 1996). The time scale of 17 hours at Augustine Volcano is similar to the build-up observed before the December 1989 eruption of Redoubt and is consistent with a system which has become pressurized.

The occurrence of low-*FI* earthquakes prior to explosive eruptions suggests that they are linked to the movement of magmatic fluids preceding extrusion. This is a significant observation from a monitoring perspective, as it presents a tool with which explosive eruption events might be anticipated. An empirical threshold of $FI<-1.8$ for this dataset, as indicated on figure 4, successfully anticipates explosive events or sequences. One earthquake with an *FI* of –2.1 occurred late on January 14, 17 hours after the final explosion of the January 13–14 eruptive sequence and did not occur as an explosion precursor. However its occurrence so soon after the powerful January 13–14 explosion sequence could mean that it was the final low-*FI* event from that sequence. Regardless, it is clear from table 1 that the limit of –1.8 never failed to indicate a pending explosion series, being successful for 10 of the 13 individual large explosions.

The Role of Attenuation

Because the *FI* analysis is based on waveform amplitude in different frequency bands, it will be influenced by attenuation effects. Seismic waves are diminished as a function of distance and frequency by a combination of intrinsic attenuation and scattering attenuation. The attenuating character of the Earth can be expressed through the quality factor *Q*, which is related to the seismic amplitude by

$$A(\omega, r) = A_0 r^{-n} \exp(-\omega r/2Qv), \quad (2)$$

where $A(\omega, r)$ is the spectral amplitude as a function of angular frequency ω and distance *r* from the source (Aki and Richards, 1980). A_0 is the amplitude at the source, *v* is the propagation velocity, and r^{-n} is the geometric spreading factor, where n=1 for body waves and n= ½ for surface waves. To determine the influence of attenuation on *FI*, we combine equations 1 and 2. We simplify the system by approximating the lower and upper frequency ranges by their center (angular) frequencies, ϖ_{upper} and ϖ_{lower}:

$$FI(Q,r) = \log_{10}\left[\frac{A_{upper_0} r^{-n} exp(-\varpi_{upper} r/2Qv)}{A_{lower_0} r^{-n} exp(-\varpi_{lower} r/2Qv)}\right], \quad (3)$$

$$FI(Q,r) = \log_{10}\left[\exp\left(-\frac{r}{2Qv}(\varpi_{upper} - \varpi_{lower})\right)\right] + \log_{10}\left[\frac{A_{upper_0}}{A_{lower_0}}\right], \quad (4)$$

$$FI(Q,r) = \log_{10}\left[\exp\left(-\frac{r}{2Qv}(\varpi_{upper} - \varpi_{lower})\right)\right] + FI_0, \quad (5)$$

where FI_0 is the *FI* at the source. The form of equation 5 is significant because it demonstrates that attenuation will reduce *FI* by a fixed term but will not change trends in the *FI* data coming from a single source region. In other words, if one is willing to assume an attenuation and velocity, *FI* can be corrected for distance by a static correction term. This result is shown in figure 6, where we consider the case when *FI* is 0 and vary the distance for different values of *Q*. *FI* decreases linearly with distance, and the effect is increasingly more pronounced at low *Q* values. In fact, this relation can be used in reverse to estimate attenuation directly using *FI* measured at a range of epicentral distances.

The above analysis makes several assumptions. We do not take into account the differential effect of attenuation within the frequency ranges specified by A_{upper} and A_{lower}. Since our frequency ranges are narrow, we approximate attenuation effects at the center frequencies across A_{upper} and A_{lower}, 15 and 1.5 Hz, respectively. The error introduced by this assumption is smaller than the variations introduced by an assumed *Q* value. We also assume a constant value of *Q*, contrary to the findings of studies of attenuation in other volcanic areas (such as Patanè and others, 1994), where *Q* is found to vary across orders of magnitude within single volcanic complexes.

Shortcomings of the *FI* Method

The Frequency Index technique worked well for the Augustine 2006 eruption, showing trends in seismicity that were otherwise difficult to quantify. Its success is largely due to the high-quality, close range dataset. The method would

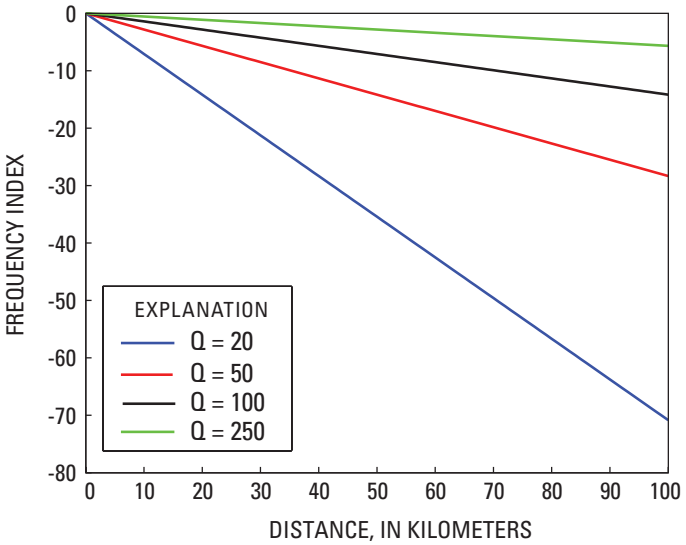

Figure 6. Frequency Index plotted against distance for different (fixed) values of the quality factor *Q*. The subsurface velocity was set to 1.3 km/s.

have been less successful at stations with poorer signal-to-noise ratios. The low-frequency bias evident in the model waveform set reflects this problem and indicates a fundamental challenge to quantifying the frequency content of small-amplitude seismic signals. It is possible that other datasets will be less contaminated by low-frequency noise than this dataset because the location of Augustine Island and the North Pacific wintertime storm conditions that prevailed during much of the eruption make for a seismically noisy environment. It is clear that site effects must be carefully considered when evaluating trends in *FI*, because they introduce an inherent bias within the *FI* calculation. This is demonstrated through the differences between figures 4 and 5 where station AU15, located in a particularly windy area of the island, yields much noisier data and lower values of *FI*.

Volcanic tremor could also influence the *FI* analysis. Our interval for A_{lower} (1–2 Hz) is within the common frequency range for volcanic tremor (for example, Gordeev, 1992), and it is possible that background tremor could add a low-frequency bias to the *FI*. Although potentially detrimental to the *FI* analysis, this may prove to be useful from a monitoring perspective. Volcanic tremor is often (although not always) associated with volcanic eruptions (Chouet, 1981), and an earthquake with a low *FI* due to tremor is also likely to be associated with a volcanic eruption. It therefore does not necessarily detract from the association between low *FI* and imminent eruption.

Repeating Earthquakes

Waveform similarity is another method for investigating trends in earthquake activity within large datasets. Recurring waveforms are significant because they are the product of earthquakes occurring in nearly the same place with the same mechanism. Not only do repeating events reveal the characteristic time of the seismogenic source, they can also be exploited for high-resolution mapping of the source volume. Stephens and Chouet (2001) and Green and Neuberg (2006) have used repeating low-frequency earthquakes to demonstrate that the sources of some low-frequency events are long lived, despite changes in a volcano's eruptive state. These events have been attributed to recurring interactions between magma and a fixed conduit geometry. Recurring high-frequency waveforms have been exploited by several authors to obtain precise relative relocations that define the timing and spatial extent of dike and fault structures within a volcanic edifice (for example, Got and others, 1994; Rowe and others, 2004; Thelen and others, 2008; DeShon and others, this volume). Here we explore the role of repeating earthquakes as precursors to explosive eruptions.

Method

We use cross-correlation to measure the similarity of waveforms in the event catalogue discussed above, again using station AU13. Focusing on a single station precludes the use of location techniques (see DeShon and others, this volume) but allows us to work with a more comprehensive catalog, improving time resolution and allowing us to extend the analysis into the latter portions of the eruption when all of the summit stations had been destroyed. Except for a handful of earthquakes at depths between 3.5 and 4.5 km, the located earthquakes all emanate from a relatively tight source region (Dixon and others, 2008; Power and Lalla, this volume), suggesting that the same is true for our more extensive catalog.

To calculate waveform cross-correlation, we extract a 6-second window of vertical component data beginning at the picked arrival time. Six seconds of data following the pick is sufficient to capture the largest amplitude sections of most waveforms (which dominate the cross-correlation) while minimizing the influence of background noise on short high-frequency waveforms. Changes in the window length of a few seconds showed only a minor influence on the correlation coefficients (not shown).

Each waveform in the dataset is correlated against all other waveforms using an algorithm tailored to large datasets using the newly developed waveform correlation toolbox for MATLAB (http://www.giseis.alaska.edu/Seis/EQ/tools/GISMO, accessed September 7, 2009). In the first step, all waveforms are transformed into the frequency domain. The first frequency-domain waveform is then multiplied against every other waveform, equivalent to convolution in the time domain. Exploiting the symmetry of the problem, the second waveform need only be multiplied by the third and subsequent waveforms, and so forth. This is equivalent to filling in the upper matrix triangle in figure 7 and completing the rest through a symmetry argument. The resulting cross-correlation series are transformed back to the time domain, where second-order polynomial interpolation is used to estimate the sub-sample maximum cross-correlation value. The maximum of the cross-correlation is normalized, following convention, to the scale of –1 to 1. The maximum value and its associated lag time are saved into n by n matrices, where n is the number of traces. Hereafter we refer to the normalized maximum of the cross-correlation function as simply the correlation value. The lag values are used to align the traces in time.

Figure 7 shows the similarity matrix for all events, chronologically left to right and top to bottom (not evenly spaced in time), with one pixel for each pair of waveforms. The matrix is symmetric with unity on the diagonal. Although figure 7 hardly does justice to the 10 million correlation values that form the matrix, it is clear that the majority of earthquakes throughout the eruption show little similarity. (Because we search for the optimum correlation lag times, even unrelated waveforms will often correlate at 0.5 or better.) Within this dataset, however, there are numerous clusters and time patterns with direct implications for volcanic processes (Buurman and West, 2006). The challenge is to mine the dataset in intuitive ways. We identify clusters using a hierarchical clustering method similar to that used by Rowe and others (2002). First we link all events on the basis of their correlations (fig. 8). Branches within the hierarchy are joined

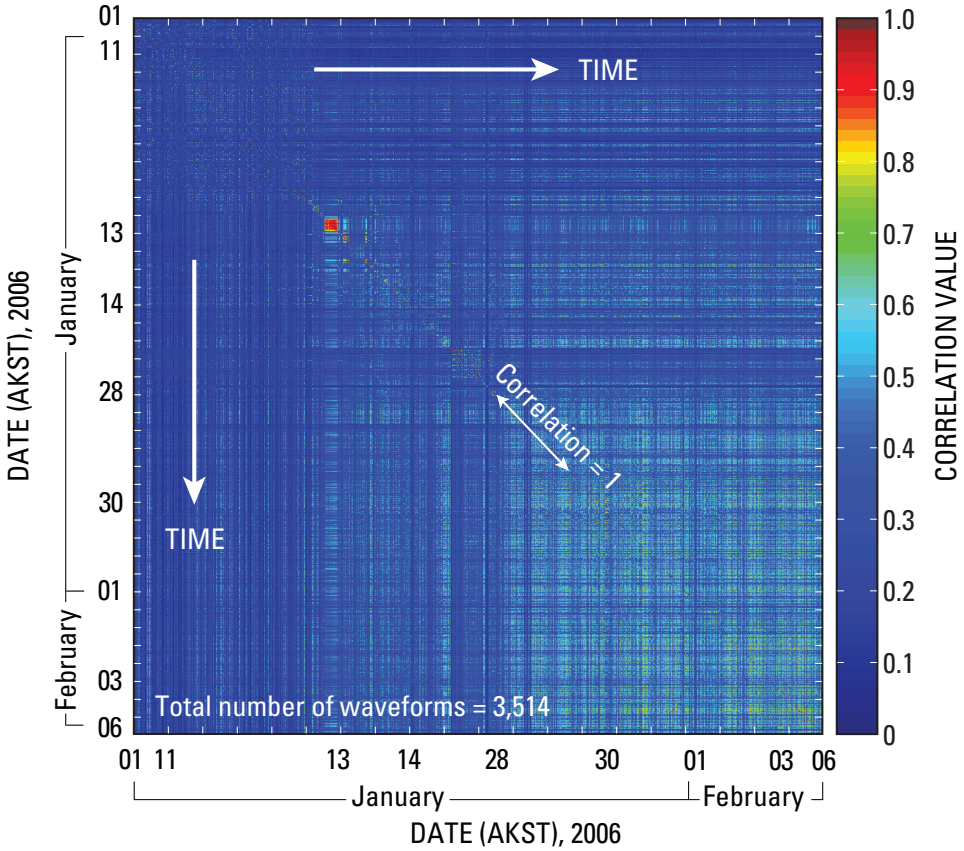

Figure 7. Correlation matrix for the entire Augustine 2006 catalog. Each point represents an earthquake correlation pair. The matrix is symmetric, with time progressing left to right and top to bottom. The correlations on the diagonal are equal to one as each waveform is auto correlated, although they appear muted because of the size of the matrix. The majority of cross-correlations in the dataset are poor, with values less than 0.6.

at nodes whose height is the mean correlation value between each pair of events spanning the two groups. That is,

$$C_{p,q} = \frac{1}{n_p n_q} \sum_{i=1}^{n_p} \sum_{j=1}^{n_q} C_{pi,qj}, \qquad (6)$$

where Cp,q is the mean correlation between the nth events in groups p and q. These links may be between individual events or between clusters of events, depending solely on which linkage has the highest mean correlation. The formation of discrete clusters is then just a matter of selecting branches from the hierarchical cluster tree. Because the correlation value is influenced by the trace length, filter parameters, and frequency content of the waveforms, the choice of correlation threshold is somewhat arbitrary. Given the wide variety of earthquake types in our catalog, we choose a threshold of 0.8 based on visual inspection to define clusters in lieu of a more adaptive approach, such as that of Rowe and others (2002). The value 0.8 is on par with or somewhat higher than in comparable studies (Petersen, 2007; Green and Neuberg, 2006; Stephens and Chouet, 2001).

We refer to groups of similar waveforms as clusters. "Multiplet" and "clones" (for example, Frémont and Malone, 1987; Geller and Mueller, 1980; Thelen and others, 2008) are comparable terms. We prefer the term cluster because of the implied spatial proximity and avoid the term "swarm" because it suggests a similarity in time. We use cluster to indicate a

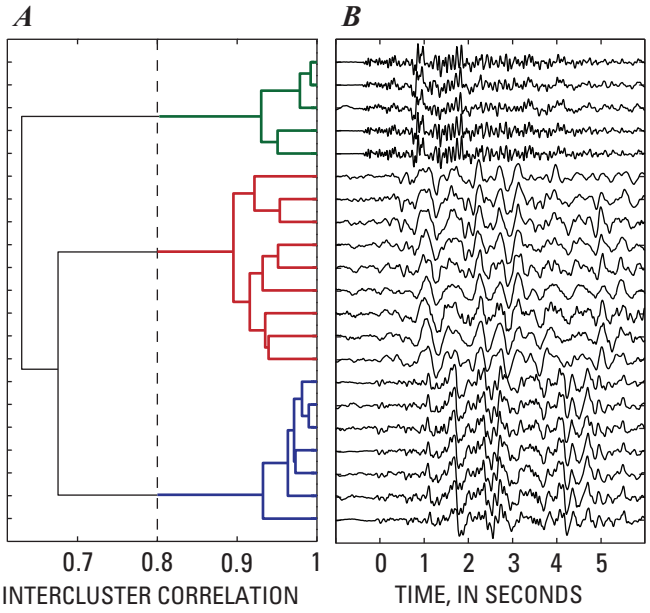

Figure 8. Illustration of the hierarchical clustering method used to group sample waveforms. *A*, The two most similar events are joined at a node, which yields a new correlation value. This value is then used to search the catalog for the next most similar event, pair, or group of events. Individual clusters are defined by assigning a minimum intercluster correlation value, indicated by the dashed line at 0.8. *B*, Waveforms corresponding to correlations in *A*.

similarity in waveform and, by extension, source location and mechanism. If a cluster occurs in a short period, it may also be a swarm, although this is not always the case.

In subsequent analyses we use a subset of data that includes the 40 largest clusters. This includes clusters of four or more events. By culling unrelated traces, trends not observed in figure 7 emerge as clear patterns that can be tied directly to different stages within the eruption (fig. 9*A*).

Clusters of Similar Events Before Explosive Eruptions

The most important pattern in the subset matrix is the presence of repeating events in the hours preceding explosive eruptions. More than half of the ash-producing explosions during the explosive phase were immediately preceded by small clusters of highly similar earthquakes ("precursory clusters"). The two phreatic explosions at the beginning of the explosive phase were closely spaced in time and occurred at the end of the seismic swarm, which itself contained several clusters of earthquakes, discussed later. The first four explosions in the sequence of six ash-producing events on January 13–14 were preceded by small clusters (5–11 events) of similar earthquakes. These clusters occurred in short periods of time, some lasting only 10 minutes (table 1), and all occurred within 2.5 hours of eruption. The explosion on January 17 was preceded by a cluster that occurred 7 hours prior to eruption. The last four eruptions of the explosive phase, which occur immediately prior to the transition to continuous activity, show different seismic precursors than the other large explosions; they are preceded by an 81-hour swarm of earthquakes, not all of which are as strikingly similar as the previous precursory clusters. These results are summarized in table 1.

The largest cluster occurred on January 11 within the space of 2 hours and contained 57 events with exceedingly high correlation values (fig. 9*D*). This cluster was followed by a smaller but more protracted cluster that ended only 14 minutes before the first of the ash-producing explosions of the explosive phase. Earthquakes in the second cluster also showed similarity (values greater than 0.7) with the largest cluster, suggesting that the two clusters were slight variations of the same mechanism.

The occurrence of repeating clusters immediately prior to explosions indicates that they represent either the mobilization of magma, the opening of conduits to the surface, or both. The interaction of magma with surrounding rock is well known to produce repeating events. This association is most convincing during periods of dome growth, when magma extrusion is observed at the surface accompanied by repeating event clusters (for example, Thelen and others, 2008; Green and Neuberg, 2006). The same patterns were observed during the March 2006 lava effusion at Augustine (not shown). Conduit opening prior to explosive eruptions is another viable option for the source of event clusters. In order for magma to erupt explosively, an open conduit to the surface is required. The magma ascent and gas exsolution that precedes explosions may well be responsible for creating (or reopening) such pathways to the surface (fig. 10). The progressive fracturing of a crack pathway, driven by high-pressure gas or fluid, is thought to be a mechanism for earthquake swarms (for example, Hill, 1977) and could produce nearly the same waveform. Although cracking is an inherently destructive process, a series of small progressive fractures on the same pathway would have the same mechanism and nearly the same seismic raypath. This would be an unlikely mechanism to explain many thousands of repeating events (for example, Petersen, 2007), but it is a more reasonable mechanism at Augustine, considering the modest size of the clusters preceding explosive eruptions.

Recurring Clusters

Figure 9*A* reveals a few occasions when a cluster of events pauses and resumes at a later time. A striking example of recurring clusters occurs on January 13 (fig. 9*E*). Two clustered swarms are separated by a gap of 3 hours but have events correlating as high as 0.9. This is seen by the high off-diagonal correlation values between the two swarms. These two small clusters occur immediately after explosions, suggesting that they are caused by posteruptive processes related to relaxation of eruptive stresses in the edifice. Alternatively, they may be related to a final release of gas or magma from the explosion.

Contemporaneous Groups of Repeating Events

Some clusters occur contemporaneously with other unrelated clusters. The repeating events in the preeruptive swarm on January 11 provide a good example. Within this group there are two main families of waveforms, referred to here as *A* and *B* (fig. 9*C*). The waveforms in group A contain significant amounts of high-frequency energy, indicated by their range in *FI* of –0.2 to –1.4. Waveforms in the B cluster have lower frequency content ($FI < -2.5$ for nine of the waveforms, with one outlier), although they also contain some portion of high-frequency content. Because both families occur during the same time period, the similarity matrix shows deceiving scatter when sorted chronologically (fig. 9*B*). The presence of two families, one rich in high frequencies, the other rich in low frequencies, demonstrates the coexistence of different seismic processes. Considering the vigor of this preeruptive swarm and its occurrence prior to the first explosive eruption, cluster A likely represents the brittle failure of rock caused by the incremental opening of cracks as a result of a new intrusion of fluids or gases in the shallow edifice. We attribute cluster *B*, rich in low-frequency energy, to resonances caused by this same movement of gas or fluid to shallow depths.

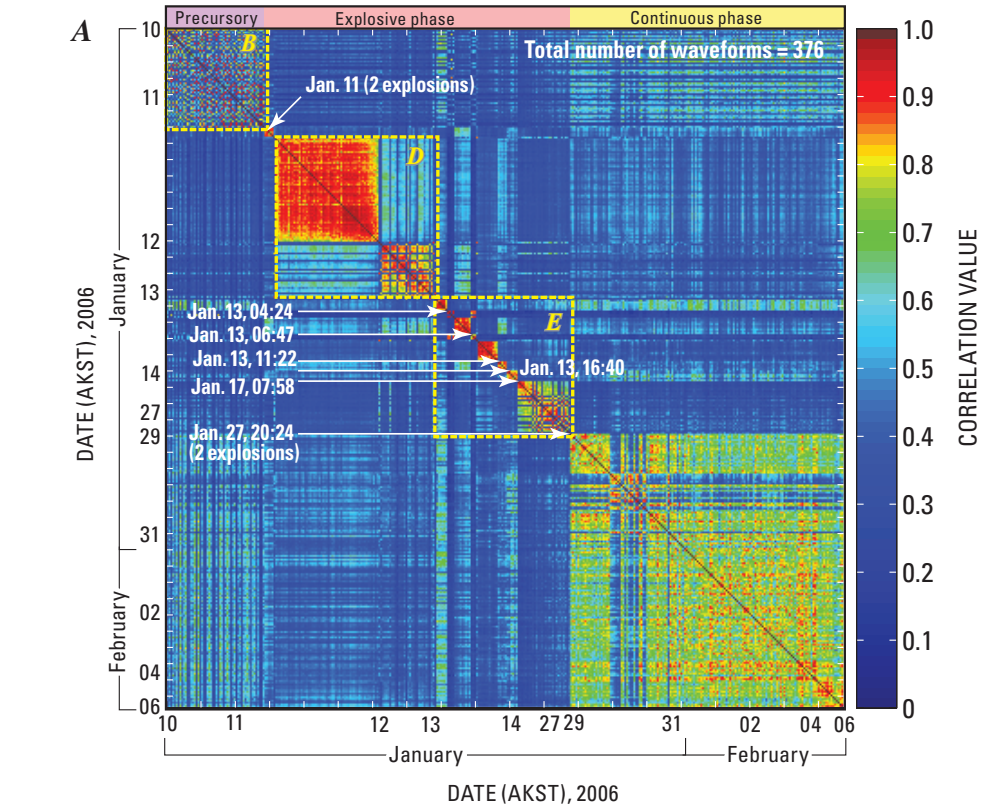

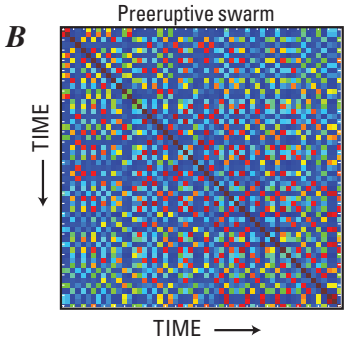

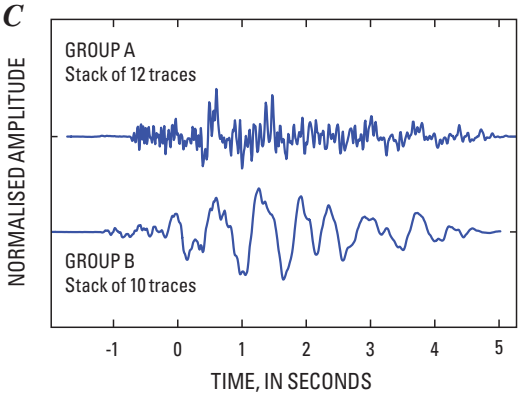

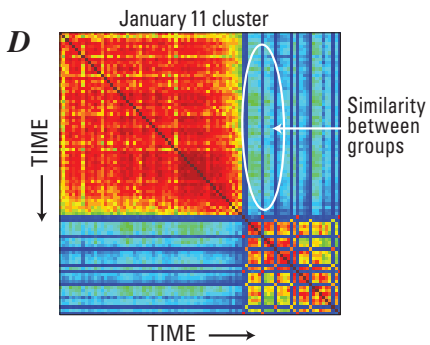

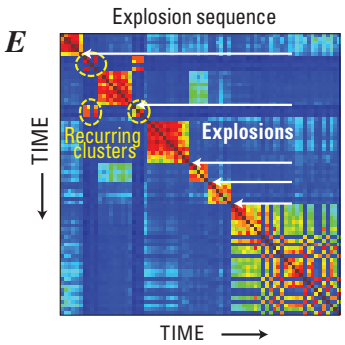

Figure 9. Refined correlation matrix (*A*), with sample waveforms (*C*), and enlarged sections of the matrix (*B, D, E*). *A*, Refined correlation matrix showing the 40 largest clusters. Explosions are marked with white arrows. Dashed yellow lines indicate enlarged areas (panels *B, D,* and *E*). *B*, Enlargement of the preeruptive swarm time period, showing disparate clusters of repeating events. *C*, Stacks of the two largest groups of waveforms present during the preeruptive swarm shown in *B. D*, Enlargement of the large clusters on January 11, containing correlation values as high as 0.97. E, Enlargement of the explosive phase, with recurring clusters circled. Explosions are marked with arrows.

Repeating Earthquakes During Continuous Eruptive Activity

The character of the repeating earthquakes changes with the transition to the continuously explosive phase on January 28, 2006. Whereas the earlier explosive phase was characterized by intermittent swarms of highly clustered events lasting minutes to hours, repeating events during the continuous phase are more variable but seem to follow one general waveform type. Our arbitrary correlation criterion of 0.8 groups these events into several small clusters. However, the subset similarity matrix (fig. 9*A*) suggests that there is one dominant cluster beginning on January 28 that extends beyond the end of our analysis on February 6 as seismicity began to taper significantly. This cluster is interspersed by a smaller cluster of 21 events on January 29 and 30.

Poor weather during much of the continuous phase prevented visual and satellite-based observations for all but the largest explosive events. The emergent broad-spectrum seismic data was at times enigmatic. In the absence of corroborating evidence it was challenging to separate how much of the seismicity represented rockfall activity on the new dome and how much was generated by the emplacement of new lava at the surface. Although both sources were surely present, the retrospective similarity analysis demonstrates that a subset of the events can be tied directly to magma extrusion. Rockfall events, including pyroclastic flows and avalanches, are inherently dissimilar because of their chaotic and destructive mechanism. The repeating sequence could be stick-slip behavior associated with dome growth, as has been documented in the 2004 Mount St. Helens sequence (Moran and others, 2008). However, the low frequency nature (fig. 4) of the events, combined with their registration at all on-island stations and on the pressure sensor at AUE (not shown), suggest that vulcanian explosions are a more plausible source. Indeed, as the number of explosions declined during early February (evident on the pressure sensor at AUE, not shown), so too did the number of repeating earthquakes.

Discussion

Combining *FI* Data and Correlation Data

In order to gain further insight into the seismic activity using the similarity matrix in figure 9*A* It is helpful to compare these results with the *FI* analysis. Table 1 presents the *FI* values of the clusters that occurred prior to explosions ("precursory clusters"), as well as listing the number of earthquakes with *FI* below –1.8 that occurred prior to each of the large explosion events. It is interesting to note that the very low *FI* earthquakes do not appear to occur in large clusters. Although events with *FI* below –1.8 show a unique correspondence to explosive eruptions (see section on "*FI* as an eruptive precursor"), they are a separate phenomenon from the repeating earthquakes. This suggests that they should be tracked independently and even that small numbers of very low *FI* events may have significant implications.

Not all explosions were preceded by precursory clusters or very low *FI* earthquakes. Almost all were preceded by one of the two, however. We disregard the second explosion of the sequence (table 1) because it occurs less than half an hour after the first. It is significant that 10 of the first 11 eruptions during the explosive phase were preceded by either repeating earthquakes or those with very low *FI*. Neither technique exhibits a significant change preceding the final two magmatic explosions of the explosive phase, which occurred immediately prior to the change to sustained eruptive activity. We suspect that by the time these explosions occurred, the volcano had already established a clear open conduit to the surface that allowed magma and gas to reach the surface without the constrictions present in early explosions. This suggests that both the frequency-based and correlation-based techniques (and likely all precursory seismic techniques) may perform better with initial eruptive activity than with ongoing repeat eruptions.

We hypothesize that both precursory clusters and very low *FI* earthquakes are associated with the movement of magma or, in some cases, gas. Specifically, we propose that the low frequency earthquakes are the result of the movement of magmatic fluids rising from the magma chamber (as proposed by Chouet, 1996), while the precursory hybrid clusters originate from the interaction between the advancing body of magmatic fluids and the brittle edifice (figure 10).

Although low frequency earthquakes and repeating earthquakes are commonly observed at volcanoes without eruption, the Augustine sequence provides unmistakable ground truth for these associations. By combining the two techniques, we see that although very low *FI* earthquakes can occur as precursory clusters, it is not generally the case and the two styles usually represent separate earthquakes.

Adaptations for Real-Time Use

The *FI* technique shows promise as an indicator of explosive magmatic eruptions. It is also a useful all-purpose tool for quantifying trends in seismicity. *FI* is particularly useful in tracking changes in large numbers of earthquakes where manual inspection of waveforms is quickly overwhelmed. Examples include the transition from explosive to continuous activity at Augustine, or the changes from high-frequency to hybrid and lower frequency events observed during the early stages of the 2004–8 Mount St. Helens dome building eruption (Moran and others, 2008). It provides a repeatable, quantifiable measure that is simple to calculate and faithfully reduces the overall frequency content of a waveform to a single parameter.

The correlation approach is similarly well suited to large datasets where the pattern matching required to identify repeating clusters of events is all but impossible without

computational aids. Figure 7 provides an excellent example of how these rich correlation patterns in the Augustine sequence can be buried by high rates of scattered seismicity.

Both tools are readily adaptable to real-time use, and both techniques operate on short waveform segments encompassing a detected event but do not require event locations. This distinction is significant. A seismic event detection system is one of the most basic monitoring tools available at nearly all monitored volcanoes. Fully automated event locations, though existent, are still the exception at most volcanoes.

The *FI* parameter can be used in real time in its current form. All that is required is a real-time module to perform the trivial Fourier transform and ratio calculation and a database to store and track the progression of these values.

The correlation tool needs to be adapted slightly. In the analysis presented here, the complete seismic history of the eruption was already available, so that for a given moment in the eruption all events from the past and future could be used in the correlation. As a real-time tool, the correlation analysis must be limited to events that have already occurred. The easiest implementation would store the waveforms from detected events (or preferably store pointers to these waveforms in a continuous waveform archive). When a new event is detected, it would be correlated against other events in the recent past. This could include all events in a fixed time frame (say, 12 hours), or it may be more computationally appropriate to include a fixed number of events (say, the past 100 detected waveforms). The only significant challenge in implementing a real-time correlation tool is computational expense, although this could be minimized by storing the most recent waveforms in memory. Storing the Fast Fourier Transform of each waveform would be even more efficient. By correlating each incoming event against recent waveforms instead of the entire dataset, the resulting similarity matrix would be limited to a strip of data within n steps of the diagonal, where n is the number of recent events included in the correlation calculation. In many cases this may be sufficient to reveal the basic similarity patterns, as demonstrated by Umakoshi and others (2008). In the Augustine 2006 dataset, for example, most correlation patterns are fully revealed when only the previous 150 events are included.

Both tools are simplistic in that they operate on single channels of data, though more comprehensive multichannel versions can be envisioned. The single-channel requirement makes them straightforward to implement, however, and given this simplicity we believe the frequency index and correlation tools can be readily incorporated into most processing systems. Although both tools have limitations and will not always be as insightful as they have proven for the Augustine 2006 eruption, we believe that they have the potential to become indispensable additions to the suite of seismic volcano monitoring tools.

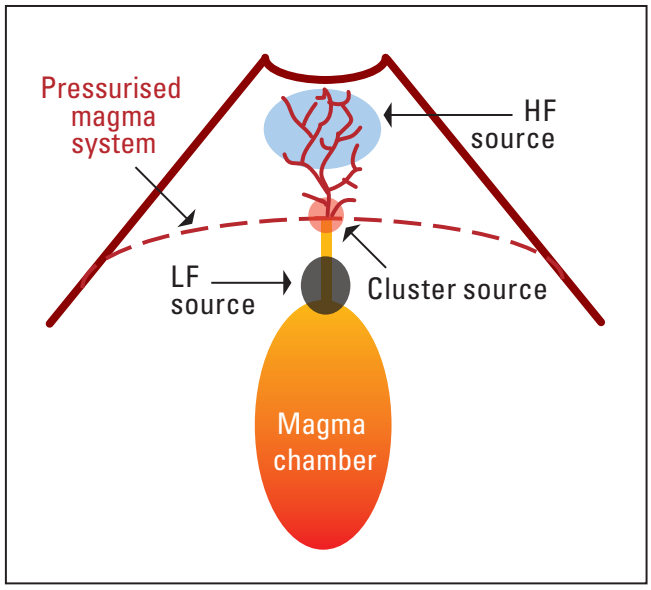

Figure 10. Schematic model showing the origins of high-frequency (HF) earthquakes, low-frequency (LF) earthquakes, and the (hybrid) clusters. Low-frequency earthquakes are generated by the movement of magmatic fluids, as proposed by Chouet (1996). Earthquake clusters have a tight source region, where both brittle fracture and fluid resonance occurs, at the head of the advancing body of magma. High-frequency earthquakes, such as those in the precursory swarm, are the result of the brittle fracture of rock in the edifice, where volatiles from the degassing body of magma break new pathways to the surface.

Acknowledgments

We thank Stephanie Prejean and Rick Aster for their helpful comments and suggestions. We also thank John Power, Kate Bull, and Katie Jacobs for several useful discussions that also improved the manuscript.

References Cited

Aki, K., and Richards, P.G., 1980, Quantitative seismology: New York, W.H. Freeman, 700 p.

Bailey, J.E., Dean, K.G., Dehn, J., and Webley, P.W., 2010, Integrated satellite observations of the 2006 eruption of Augustine Volcano, *in* Power, J.A., Coombs, M.L., and Freymueller, J.T., eds., The 2006 eruption of Augustine Volcano, Alaska: U.S. Geological Survey Professional Paper 1769 (this volume).

Benoit, J.P., and McNutt, S.R., 1996, Global volcanic earthquake swarm database, 1979–1989: U.S. Geological Survey Open-File Report 96-0069, 333 p.

Buurman, H., and West, M., 2006, Integrated seismic observations of the 2006 eruption of Augustine Volcano: Eos

(American Geophysical Union Transactions), v. 87(52), Fall Meeting supp., abs V51C-1683

Cervelli, P.F., Fournier, T.J., Freymueller, J.T., Power, J.A., Lisowski, M., and Pauk, B.A., 2010, Geodetic constraints on magma movement and withdrawal during the 2006 eruption of Augustine Volcano, *in* Power, J.A., Coombs, M.L., and Freymueller, J.T., eds., The 2006 eruption of Augustine Volcano, Alaska: U.S. Geological Survey Professional Paper 1769 (this volume).

Chouet, B.A., 1981, Ground motion in the near field of a fluid-driven crack and its interpretation in the study of shallow volcanic tremor: Journal of Geophysical Research, v. 86, no. B7, p. 5985–6016.

Chouet, B.A., 1988, Resonance of a fluid-driven crack; radiation properties and implications for the source of long-period events and harmonic tremor: Journal of Geophysical Research, v. 93, p. 4375–4400.

Chouet, B.A., 1996, Long-period volcano seismicity; its source and use in eruption forecasting: Nature, v. 380, p. 309–316.

Chouet, B.A., Page, R.A., Stephens, C.D., Lahr, J.C. and Power, J.A., 1994, Precursory swarms of long-period events at Redoubt Volcano (1989–1990), Alaska—their origin and use as a forecasting tool: Journal of Volcanology and Geothermal Research, v. 62, p. 95–135.

Coombs, M.L., Bull, K.F., Vallance, J.W., Schneider, D.J., Thoms, E.E., Wessels, R.L., and McGimsey, R.G., 2010, Timing, distribution, and volume of proximal products of the 2006 eruption of Augustine Volcano, *in* Power, J.A., Coombs, M.L., and Freymueller, J.T., eds., The 2006 eruption of Augustine Volcano, Alaska: U.S. Geological Survey Professional Paper 1769 (this volume).

DeShon, H.R., Thurber, C.H., and Power, J.A., 2010, Earthquake waveform similarity and evolution at Augustine Volcano from 1993 to 2006, *in* Power, J.A., Coombs, M.L., and Freymueller, J.T., eds., The 2006 eruption of Augustine Volcano, Alaska: U.S. Geological Survey Professional Paper 1769 (this volume).

Dixon, J.P., Stihler, S.D., Power, J.A., and Searcy, C., 2008, Catalog of earthquake hypocenters at Alaskan volcanoes; January 1 through December 31, 2006: U.S. Geological Survey Data Series 326, 79 p. [http://pubs.usgs.gov/ds/326, accessed September 7, 2009].

Fischer, T.P., Morrissey, M.M., Calvache, M.L., Gomez, D., Torres, R., Stix, J., and Williams, S.N., 1994, Correlations between SO_2 flux and long-period seismicity at Galeras volcano: Nature, v. 368, p.135–137.

Frémont, M.J., and Malone, S.D., 1987, High precision relative locations of earthquakes at Mount St. Helens, Washington: Journal of Geophysical Research, v. 92, p. 10223–10236.

Geller, R.J., and Mueller, C.S., 1980, Four similar earthquakes in central California: Geophysical Research Letters, v. 7, p. 821–824.

Gordeev, E.I., 1992, Modeling of volcanic tremor wavefields: Journal of Volcanology and Geothermal Research, v. 51, p. 145–160.

Got, J.-L., Frechet, J., and Klein, F.W., 1994, Deep fault plane geometry inferred from multiplet relative relocation beneath the south flank of Kilauea: Journal of Geophysical Research, v. 99, p. 15375–15386.

Green, D.N., and Neuberg, J., 2006, Waveform classification of volcanic low-frequency earthquake swarms and its implication at Soufriere Hills Volcano, Montserrat: Journal of Volcanology and Geothermal Research, v. 153, p. 51–63.

Harlow, D.H., Power, J.A., Laguerta, E.P., Ambubuyog, G., White, R.A., and Hoblitt, R.P., 1994, Precursory seismicity and forecasting of the June 15, 1991, eruption of Mount Pinatubo, *in* Newhall, C.G., and Punongbayan, eds., Fire and mud; eruptions and lahars of Mount Pinatubo, Philippines: Philippine Institute of Volcanology and Seismology and University of Washington Press, p. 285–306.

Hill, D.P., 1977, A model for earthquake swarms: Journal of Geophysical Research, v. 82, no. 8, p. 1347–1352.

Jacobs, K.M., and McNutt, S.R., 2010, Using seismic *b*-values to interpret seismicity rates and physical processes during the preeruptive earthquake swarm at Augustine Volcano 2005–2006, *in* Power, J.A., Coombs, M.L., and Freymueller, J.T., eds., The 2006 eruption of Augustine Volcano, Alaska: U.S. Geological Survey Professional Paper 1769 (this volume).

Lahr, J.C., Page, R.A., Chouet, B.A., Stephens, C.D., Harlow, D.H., and others, 1994, Seismic evolution of the 1989-90 eruption sequence of Redoubt Volcano, Alaska: Journal of Volcanology and Geothermal Research, v. 62, p. 69–94.

Langer, H., Falsaperla, S., Powell, T., and Thompson, G., 2006, Automatic classification and a-posteriori analysis of seismic event identification at Soufriere Hills Volcano, Montserrat: Journal of Volcanology and Geothermal Research, v.153, p. 1–10.

Latter, J.H., 1980, Volcanic earthquakes and their relationship to eruptions at Ruapehu and Ngauruhoe volcanoes: Journal of Volcanology and Geothermal Research, v.9, p. 293–309.

Minikami, T., 1960, Earthquakes and crustal deformations originating from volcanic activities: Bulletin of the Earthquake Research Institute, v. 38, p. 497–544.

McNutt, S.R., 1996, Seismic monitoring and eruption forecasting of volcanoes; a review of the state-of-the-art and case histories, *in* Scarpa, R., and Tilling, R., eds.,

Monitoring and mitigation of volcano hazards: Berlin/Heidelberg, Springer-Verlag, p. 99–146.

McNutt, S.R., 2002, Volcano seismology and monitoring for eruptions, chap. 25 *of* Lee, W.H.K., Kanamori, H, Jennings, P.C., and Kisslinger, C., eds, International handbook of earthquake and engineering seismology: Academic Press, v. 81A.

Moran, S.C., Malone, S.D., Qamar, A.I., Thelen, W.A., Wright, A.K., and Caplan-Auerbach, J., 2008, Seismicity associated with renewed dome-building at Mount St Helens, 2004-2005, *in* Sherrod, D.R., Scott, W.E., and Stauffer, P.H., eds., A volcano rekindled; the renewed eruption of Mount St. Helens, 2004–2006: U.S. Geological Survey Professional Paper 1750, p.27–60.

Neuberg, J.W., Tuffen, H., Collier, L., Green, D., Powell, T., and Dingwell, D., 2005, The trigger mechanism of low-frequency earthquakes on Montserrat: Journal of Volcanology and Geothermal Research, v. 153, p. 37-50, doi: 10.1016/j.jvolgeores.2005.08.008.

Patanè, D., Ferrucci, F., and Gresta, S., 1994, Spectral features of microearthquakes in volcanic areas; attenuation in the crust and amplitude response on the site at Mt. Etna, Italy: Bulletin of the Seismological Society of America, v. 84, p. 1842–1860.

Petersen, T., 2007, Swarms of repeating long-period earthquakes at Shishaldin Volcano, Alaska, 2001–2004: Journal of Volcanology and Geothermal Research, v. 166, p. 177–192, doi:10.1016/j.volgeores.2007.07.014.

Power, J.A., and Lalla, D.J., 2010, Seismic observations of Augustine Volcano, 1970–2007, *in* Power, J.A., Coombs, M.L., and Freymueller, J.T., eds., The 2006 eruption of Augustine Volcano, Alaska: U.S. Geological Survey Professional Paper 1769 (this volume).

Rowe, C.A., Thurber, C.H., and White, R.A., 2004, Dome growth behavior at Soufriere Hills Volcano, Montserrat, revealed by relocation of volcanic event swarms, 1995–1996: Journal of Volcanology and Geothermal Research, v. 134, no. 3, p. 199–221.

Rowe, C.A., Aster, R.C., Borchers, B., and Young, C.J., 2002, An automative, adaptive algorithm for refining phase picks in large seismic data sets: Bulletin of the Seismological Society of America, v. 92, p. 1660–1674.

Stephens, C.D., and Chouet, B.A., 2001, Evolution of the December 14, 1989 precursory long-period event swarm at Redoubt Volcano, Alaska: Journal of Volcanology and Geothermal Research, v. 109, p. 133–148.

Thelen, W.A., Crosson, R.S., and Creager, K.C., 2008, Absolute and relative locations of earthquakes at Mount St. Helens, Washington, using continuous data; implications for magmatic processes, *in* Sherrod, D.R., Scott, W.E., and Stauffer, P.H., eds., A volcano rekindled; the renewed eruption of Mount St. Helens, 2004–2006: U.S. Geological Survey Professional Paper 1750, p.71–95.

Umakoshi, K., Takamura, N., Shinzato, N., Uchida, K., Matsuwo, N., and Shimizu, H., 2008, Seismicity associated with the 1991–1995 dome growth at Unzen Volcano, Japan: Journal of Volcanology and Geothermal Research, v. 175, p. 91–99.

Wallace, K.L., Neal, C.A., and McGimsey, R.G., 2010, Timing, distribution, and character of tephra fall from the 2005–2006 eruption of Augustine Volcano, *in* Power, J.A., Coombs, M.L., and Freymueller, J.T., eds., The 2006 eruption of Augustine Volcano, Alaska: U.S. Geological Survey Professional Paper 1769 (this volume).

Wilson, C.R., Olson, J.V., Szuberla, C.A.L., McNutt, S., Tytgat, G., and Drob, D.P., 2006, Infrasonic array observations at 153US of the 2006 Augustine Volcano eruptions: Inframatics, no. 13, p. 11–26.

This page intentionally left blank

The 2006 Eruption of Augustine Volcano, Alaska
Power, J.A., Coombs, M.L., and Freymueller, J.T., editors
U.S. Geological Survey Professional Paper 1769

Chapter 3

Using Seismic *b*-Values to Interpret Seismicity Rates and Physical Processes During the Preeruptive Earthquake Swarm at Augustine Volcano 2005–2006

By Katrina M. Jacobs[1] and Stephen R. McNutt[2]

Abstract

We use seismic *b*-values to explore physical processes during the Augustine Volcano 2005–6 preeruptive earthquake swarm. The preeruptive earthquake swarm was divided into two parts: the "long swarm," which extended from April 30, 2005, to January 10, 2006; and the "short swarm," which started 13 hours before the onset of explosive activity on January 11, 2006. Calculations of *b*-value for each of these swarms and for a background period were performed. The short swarm, directly preceding the eruption, had the lowest calculated *b*-value. In addition to the low value, the shape of the *b*-value plot for the short swarm appears to have two separate slopes, a shallower slope for magnitudes as great as 1.2 and a steeper slope for magnitudes greater than 1.2. Calculations of *b* were also run for three precursory deformation stages suggested by a separate investigation of deformation at Augustine Volcano. The highest *b*-value, found in stage 2, may indicate an increase in pore pressure and in thermal gradient, which matches the geodetic interpretation of a proposed dike intrusion. Finer resolution changes of *b* are explored through calculations of *b*-value versus time. An initial drop in *b*-value in late 2004 preceded the onset of increased seismicity. The temporal nature of this change and its timing are corroborated by atmospheric temperature data recorded on the summit of the volcano, which increased at approximately the same time. Stress at Augustine Volcano was also studied using 79 earthquakes that returned acceptable focal mechanisms between January 1, 2002, and January 10, 2006. These mechanisms and an attempted stress-tensor inversion imply that stresses within the Augustine edifice are highly variable and do not display a dominant faulting style. A population of high-frequency volcano-tectonic earthquakes during the short swarm is found to have accompanying very-long-period (20 seconds and greater) energy. Statistical analysis indicates that these earthquakes are a separate population of events. We interpret this population of earthquakes to represent a separate and distinct physical process that was not seen before the 13 hours preceding the eruption. The *b*-value time series also indicates that when changes in stress, pore pressure, and thermal gradient occur simultaneously, that stress effects dominate the observed *b*-value.

Introduction

The 2006 eruption of Augustine Volcano was preceded by 8 months of increased rates of volcano-tectonic (VT) earthquakes, similarly to previous eruptions in 1976 and 1986 (Power and Lalla, this volume). The eruption lasted from January 11 through mid-March, 2006, and was characterized by explosions, effusive activity, and pyroclastic flows. Only earthquakes that occurred before the onset of explosive activity on January 11 are examined here in hopes that we can gain insight about the sequence of processes that led up to the 2006 eruption. Study of this preeruptive period may provide better information for those monitoring future earthquake swarms at Augustine and other similar volcanoes. Although this study will focus on the earthquakes that occurred during the preeruptive earthquake swarm (April 30, 2005 to January 10, 2006), we also use Alaska Volcano Observatory (AVO) catalog data beginning in the year 2000 to establish background rates and a start date for the precursory swarm. A histogram showing

[1] School of Geography, Environment and Earth Sciences, Victoria University of Wellington, P.O. Box 600, Wellington, New Zealand.

[2] Alaska Volcano Observatory, University of Alaska Fairbanks Geophysical Institute, 903 Koyukuk Dr., Fairbanks, AK 99775.

located earthquakes per 30 days from January 1, 2000, through the January 11, 2006, eruptive activity can be seen in figure 1.

The concept of seismic *b*-values was first put forward by Ishimoto and Ida (1939) and was later recast in its more familiar form as the value of *b* in the Gutenberg and Richter relation, $\log N = a - bM$, where "*N*" is the cumulative number of events greater than or equal to magnitude "*M*", and "a" is an empirical constant (Ishimoto and Ida, 1939; Gutenberg and Richter, 1944). The *b*-value can also be thought of as a ratio of the number of small earthquakes to the number of larger earthquakes happening over a given period of time. Seismic *b*-values are often near one for tectonic areas and are found to be higher in volcanic areas (Bath, 1981; McNutt, 2005).

Seismic *b*-values have been shown to vary with several known physical parameters, including stress (Scholz, 1968), thermal gradient (Warren and Latham, 1970), pore pressure (Wyss, 1973), and fracture density (material heterogeneity) (Mogi, 1962). These physical parameters are likely to be affected by a variety of processes which are common at volcanoes. Given the links to these physical changes, investigating *b*-values has the potential to determine physical processes that are driving earthquake swarms.

Although *b*-values have been found to vary with four physical parameters, only three are considered here; material heterogeneity has been excluded from this study. Both Scholz (1968) and Warren and Latham (1970) suggest that some *b*-value changes initially thought to be due to material heterogeneity are in fact caused by stress differences or thermal gradient changes. Heterogeneity is often attributed to fixed rock properties, such as porosity or fracture density, and though it may vary slightly because of ongoing fracture formation and deformation, it is more likely to vary on long geologic time scales rather than short eruptive time scales (Zobin, 1979). Additionally, factors that make the material more heterogeneous, such as new fractures and injection of a magma body (fluid next to rock), are likely to produce transient signatures in the other three physical parameters.

Many *b*-values studies have been conducted at volcanoes. These investigations have covered both spatial mapping of *b*-values and temporal analyses. Spatial studies have identified small volumes of high *b*-values that have been interpreted as magma bodies (Wiemer and McNutt, 1997; Wiemer and others, 1998; Sanchez and others, 2004). At Long Valley caldera and at Martin and Mageik volcanoes significant temporal changes in *b*-value were observed during earthquake swarms (Wiemer and others, 1998; Jolly and McNutt, 1999). The small seismic volume at Augustine (fig. 2) makes it an ideal candidate for a temporal *b*-value study.

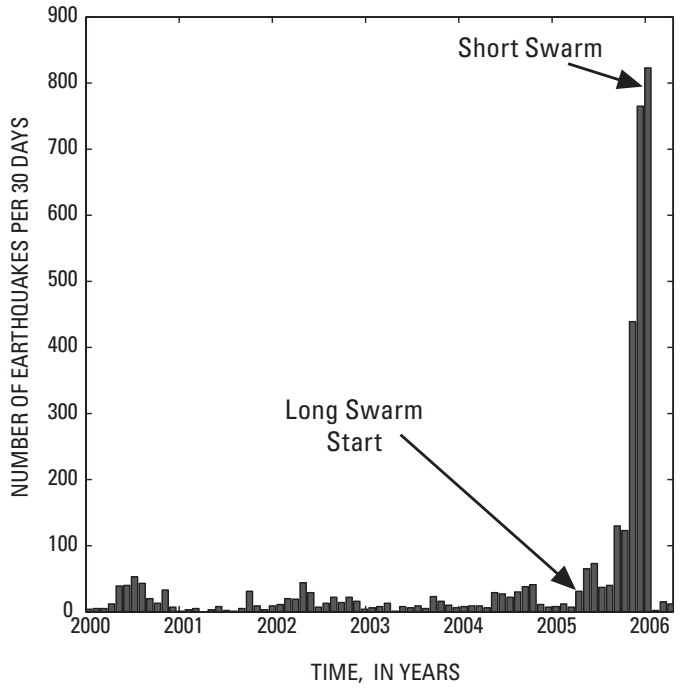

Figure 1. Histogram for located earthquakes per 30 days at Augustine Volcano from January 1, 2000, to January 11, 2006. Arrows point to the bins containing the start date of the long swarm (April 30, 2005) and the short swarm (January 10–11, 2006). Tick marks on the horizontal axis mark the beginning of each year.

Data

All located earthquakes at Augustine Volcano from 2000 through 2006 were selected from the AVO catalog. AVO maintains an earthquake catalog and publishes annual reports (for example, Dixon and others, 2008). The selected Augustine earthquake catalog has 2,945 located earthquakes between January 1, 2000, and the onset of the 2006 eruption on January 11, 2006. More than half (2,005) of the earthquakes are associated with the 2005–2006 preeruptive earthquake swarm. A rate histogram for the Augustine activity is shown in figure 1. Augustine earthquakes are located with an on-island seismic network that consists of 8 telemetered stations with 15 components (Dixon and others, 2008). Figure 2 shows a map of the island, its seismic instrumentation, and plots of the earthquake hypocenters selected from the AVO catalog. AVO catalog locations are determined using a one-dimensional six-layer velocity model derived from the model described by Lalla and Power (this volume). Processing is done using the XPICK seismic analysis software (Robinson, 1990) and the earthquake location program HYPOELLIPSE (Lahr, 1999). Magnitudes of completeness for Augustine Volcano ranged from 0.1 to -0.2 in 2005 (Dixon and others, 2008).

To use *b*-values to investigate temporal variations in physical processes we must assume, or demonstrate, that changes in *b*-value over time are meaningful. One potential problem is that if *b*-values are shown to change spatially, it may be difficult to determine whether they have also changed with time. The Augustine dataset presents us with a unique

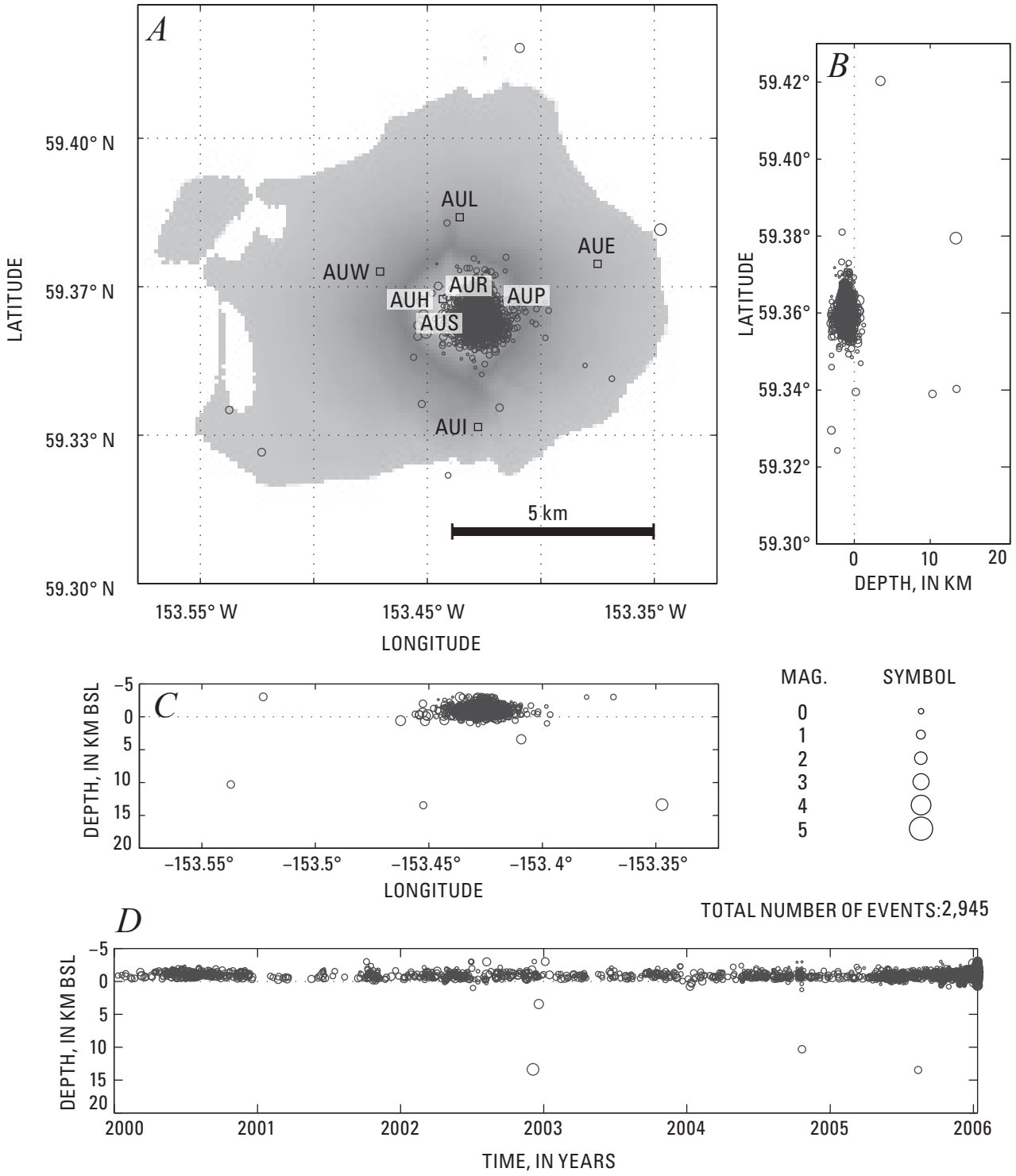

Figure 2. Summary plots of 2,945 earthquakes located by the Alaska Volcano Observatory near Augustine Volcano (shaded area is Augustine Island) from January 1, 2000, to January 11, 2006. Open circles show hypocenter locations. Hypocenters are scaled with magnitude (see scale). *A*, Earthquake epicenters in map view. *B* and *C*, north-south and east-west cross sections. *D*, Hypocenter focal depth plotted against time; a depth of 0 indicates sea level.

opportunity in this respect, because earthquakes located during the Augustine Volcano 2005–6 preeruptive swarm all occurred in a small seismic volume (fig. 2). The depth range for 95 percent of the earthquakes was confined to 0 to 2 km above sea level (asl), and depths appear to be constant over time. Despite the consistency, absolute depth control is poorly constrained and some earthquakes locate above the top of the volcano. In epicentral view the earthquakes span 1.5 km across the summit region. Some migration within this small volume is observed from late November 2005 to the onset of eruptive activity (DeShon and others, this volume; Power and Lalla, this volume). However, we believe that the seismic volume and the observed migration of events are small enough that we can consider the preeruptive swarm locations as essentially uniform in space.

The small seismic volume occupied by earthquakes at Augustine Volcano allows us to study the temporal evolution of *b*-values during the preeruptive earthquake swarm and compare our findings with information about temperature, pressure, and stress changes at Augustine. These other physical observations at the volcano will help to corroborate the temporal nature of observed *b*-value changes.

Methods

We first define a start date for the Augustine Volcano 2005–6 preeruptive earthquake swarm. Earthquake swarms are defined as increases in earthquake rates within a given volume over a relatively concentrated period of time without a single outstanding shock (Mogi, 1963). This is a rather loose definition and depends heavily on the opinions and perceptions of the reporter to define swarm durations. To lend a more quantitative element, we developed two algorithms, which used the daily number of located earthquakes to set a background rate and pick a swarm start date. We established the two algorithms to try to ensure that there was a real inflection or change at the selected point. Analysis of the years leading up to the 2005–6 activity was necessary to establish reliable background rates and give us a basis for determining change. A calendar year prior to the approximate onset of activity was used to establish background values used in each algorithm. Note that although only a single year is used to establish background rates in the algorithms, the earthquake rate at Augustine Volcano as seen in figures 1 and 2 appears to be relatively steady throughout the entire period from January 1, 2000, until the increase in activity in 2005. Late 2004 (October) is a possible exception to this statement; for details about this activity see Power and Lalla (this volume).

The first algorithm uses maximum daily event counts within a background period to establish a threshold for "increased activity." We call this method the largest-daily-count method (LDCM). In the case of Augustine all of these "counts" are located earthquakes, but the algorithm could potentially be used in places where earthquake locations are not possible. The second algorithm, the consecutive-days method (CDM), uses the low earthquake rate at Augustine Volcano to search for consecutive days with located earthquakes. Both the LDCM and CDM algorithms return a start date of April 30, 2005, for the beginning of the Augustine Volcano earthquake swarm. See appendix 1 for complete descriptions of the algorithms, flow chart diagrams, and additional details.

Using April 30, 2005, as the start date gives a total duration of 257 days for the preeruptive swarm. This long-building seismic swarm ultimately culminated in a very sharp increase in earthquake rate in the 13 hours directly preceding the eruption (Power and Lalla, this volume). For this paper we will term the 13-hour period of more energetic seismic activity on January 10–11, 2006, as the "short swarm" and refer to the swarm beginning April 30, 2005, as the "long swarm." This phenomenon of long and short swarms has been noted at many volcanoes (for both eruptive and non-eruptive swarm sequences), where either a long swarm, a short swarm, or both are present (Benoit and McNutt, 1996).

Calculations of *b*-value were carried out in ZMAP (Weimer, 2001). ZMAP is used to calculate a magnitude of completeness (M_c) for each *b*-value calculation, and only events above this threshold are used in the actual calculations (fig. 3). All *b*-values were determined using the maximum curvature method, which gives reasonable errors and is well suited for small earthquake catalogs and for temporal studies (Woessner and Wiemer, 2005). We also checked for station outages to ensure a uniform dataset. Although some station outages occur, we found no times when less than four seismometers were operating on Augustine Island. Four stations should generally be sufficient to determine consistent hypocenters and magnitudes (Lalla and Power, this volume).

To look for additional details, plots of *b*-value versus time were also generated using ZMAP (fig. 4). This calculation includes an automatic bootstrapping method to smooth the plot. A window size of 100 events with an overlap of 25 events was used to give the smallest time resolution possible. As with the standard *b*-value calculations, no cuts were made to the catalog, and the M_c was calculated for each time step.

Results

We found that the background (January 1, 2004–April 29, 2005) *b*-value was 1.51±0.1, the long swarm *b*-value was 1.26±0.04, and the short swarm *b*-value was 0.781±0.02 (fig. 3). A background calculation using all data between January 1, 2000, and April 29, 2005, yielded a *b*-value of 1.44±0.05, comparable to the background *b*-value which only uses data between January 1, 2004, and April 29, 2005. In addition to the low *b*-value for the short swarm, we also note the strange shape of its frequency-magnitude distribution curve (fig. 3*D*). The plot appears to have two separate slopes, a shallower slope for magnitudes up to 1.2 and a steeper slope for magnitudes greater than 1.2. The calculation of *b*-value with time shows an initial drop in *b*-value in mid-2004 and a dramatic

rise and fall in the *b*-value associated with the occurrence of the short swarm (fig.4).

To investigate the relationship between seismicity and deformation, we calculated the *b*-value for each of the three global positioning system (GPS) deformation stages as outlined by Cervelli and others (2006) (fig. 5). For stage 1 (constant slow inflation from June 1, 2005, to November 17, 2005) a *b*-value of 1.31±0.06 was calculated. The calculation for stage 2 (increased inflation possibly due to dike intrusion, from November 17, 2005 to December 10, 2005) yielded a *b*-value of 1.85±0.1. Finally, stage 3 (constant from December 10, 2005 to January 11, 2006) gave a *b*-value of 1.18±0.05. Data from the short swarm on January 10–11, 2006, was left out of this *b*-value calculation for stage 3 because of the odd frequency-magnitude distribution (fig. 3D).

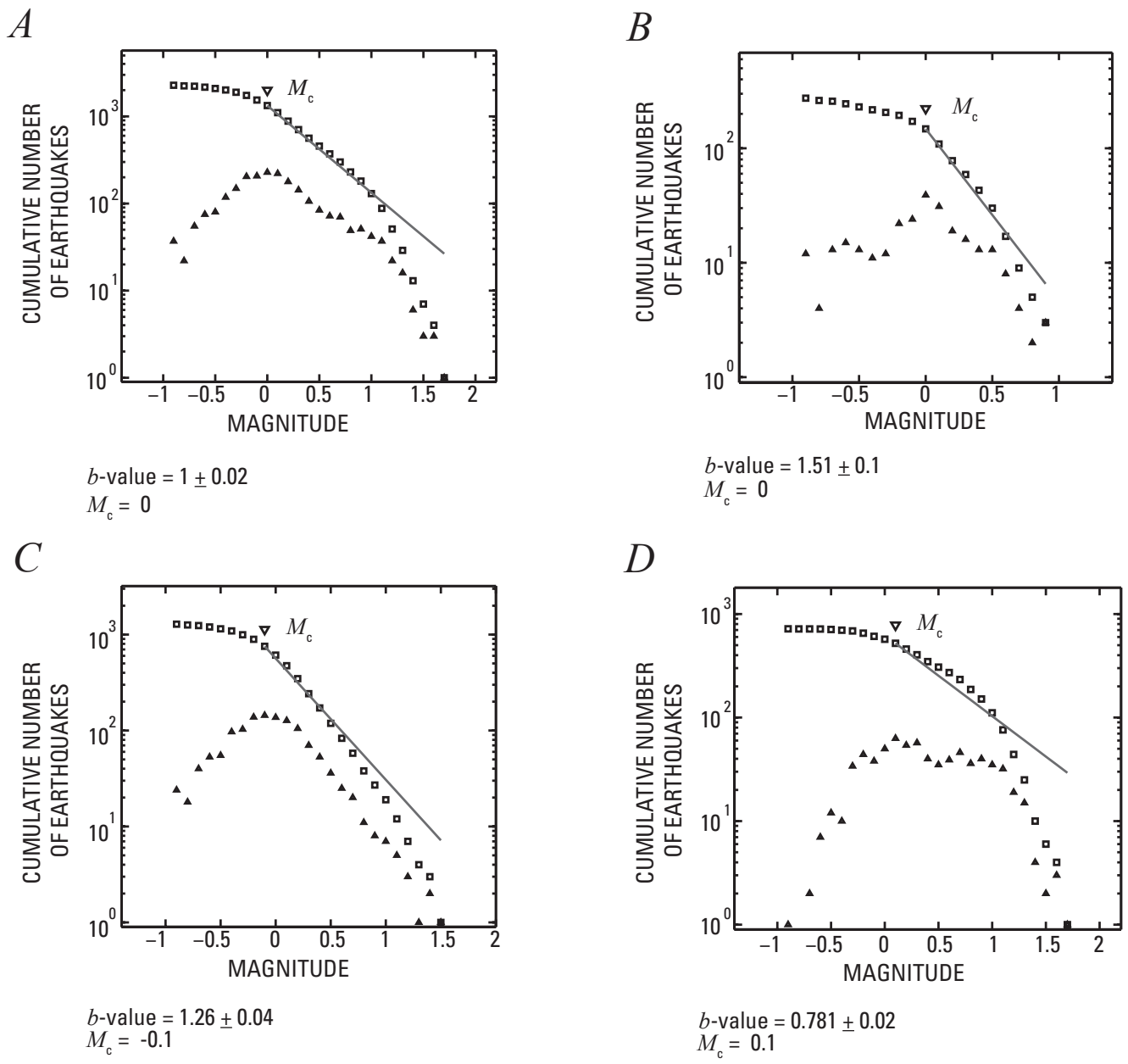

Figure 3. Cumulative frequency plots of Augustine earthquakes from January 1, 2000 to the initial eruption on January 11, 2006 with derived *b*-values. Triangles and squares show the number of earthquakes at each magnitude and the cumulative number of earthquakes, respectively. The magnitude of completeness (M_c) is shown by an inverted triangle; errors in *b*-value calculations reflect the 95-percent confidence interval of the maximum likelihood solution. *A*, The entire AVO earthquake catalog (January 1, 2000 to January 11, 2006). *B*, The background (January 1, 2000 to April 29, 2005). *C*, The long swarm (April 30, 2005 to January 10, 2006). *D*, The short swarm (13 hours prior to the initial eruption on January 11, 2006).

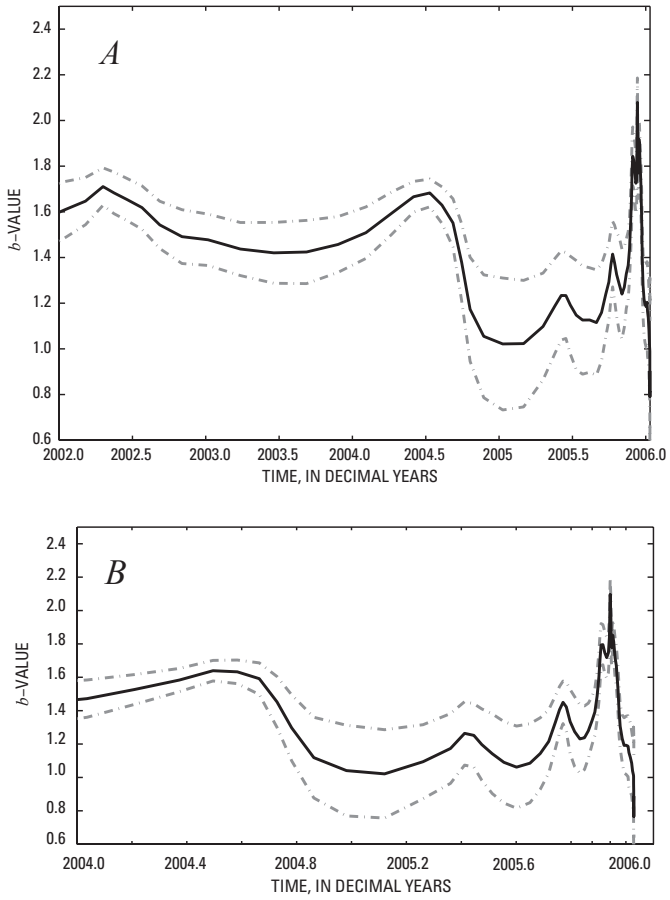

Figure 4. Plots of *b*-value with time for Augustine earthquakes. *A*, For time interval 2002–6. The calculation uses a moving window of 100 earthquakes with an overlap of 25 events. The solid line is the calculated *b*-value, and the dashed lines indicate the 95-percent confidence interval of the maximum likelihood solution. *B*, Data for 2004–6 expanded for more detail.

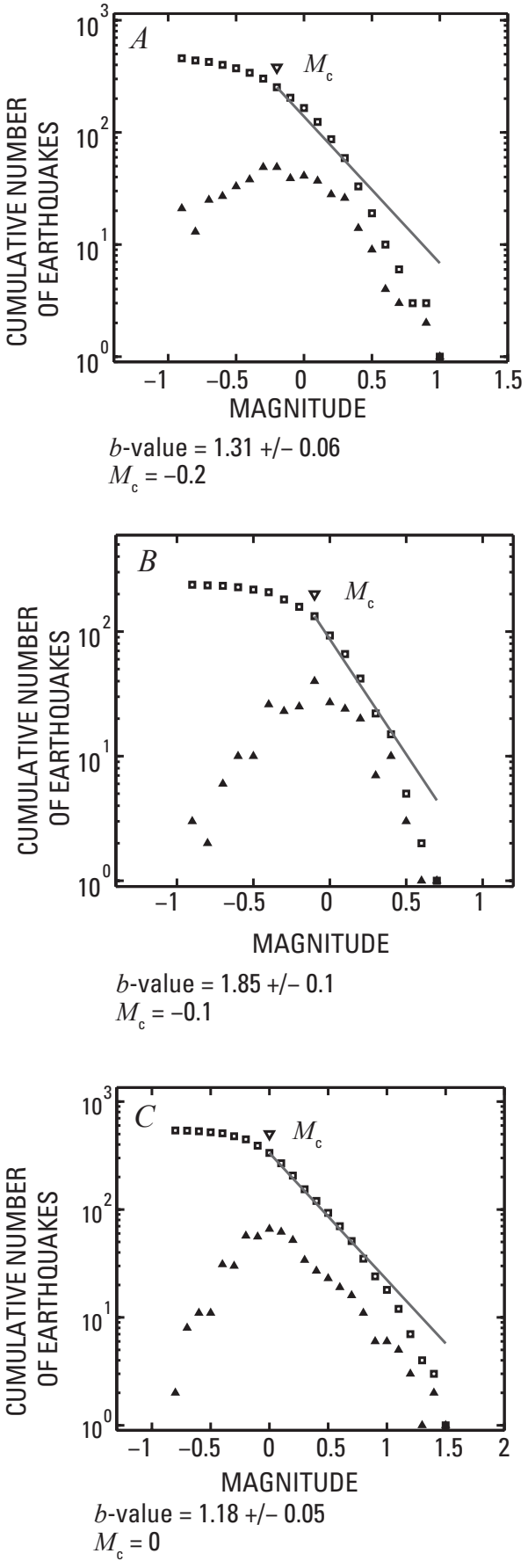

Figure 5. Results of *b*-value calculations for each precursory deformation stage outlined by Cervelli and others (2006). M_c is magnitude of completeness, and errors in *b*-value calculations reflect the 95-percent confidence interval of the maximum likelihood solution. *A*, Stage 1 (constant slow inflation from June 1, 2005, to November 17, 2005) *B*, Stage 2 (increased inflation possibly due to dike intrusion from November 17, 2005, to December 10, 2005) *C*, Stage 3 (continually increasing inflation from December 10, 2005, to January 11, 2006).

Discussion

Several physical processes could be associated with each part of an earthquake swarm. We expected to see an increase in stress in the surrounding region caused by pressurization of a deeper magma chamber during the long (building) swarm. This would lead to an overall decrease in the *b*-value. It was also expected that this would be followed by an increase in pore pressure and thermal gradient as the magma moved closer to the surface shortly before the eruption. These final changes would accompany the short swarm and cause an increase in the *b*-value above previous levels. These concepts are illustrated schematically in figure 6. Our results given earlier differ from this conceptual model. Neither the long swarm nor the short swarm shows an overall increase in *b*-value and it is the short swarm that has the lowest *b*-value of all the three periods. We will now examine these differences between our model and results by looking at the long and short swarms separately and then discussing our overall conclusions.

Long Swarm

We see in the plot of *b*-value versus time (fig. 4) that there is an initial drop in *b*-value in late 2004, but it precedes the actual seismic-swarm onset (April 30, 2005). A decrease in the *b*-value prior to the long swarm may explain why the long swarm does not have a *b*-value lower than the background period in the standard calculations. We will look to corroborate the timing of the *b*-value drop through correlation with other physical observations made at Augustine.

The *b*-values associated with the three precursory deformation stages help to identify some physical processes at work during the long swarm. The second stage of activity, from November 17, 2005, to December 10, 2005, has a higher *b*-value than the other two stages. Higher *b*-values are often associated with high thermal gradients and increases in pore pressure (Warren and Latham, 1970; Wyss 1973). At Augustine, the higher *b*-value could be explained as a result of pressurization that was caused by the inferred dike emplacement (Cervelli and others, 2006; Cervelli and others, this volume). An increase in pore pressure is likely to have occurred preceding the 75-km-long steam plume seen on December 12, 2005, in 250-m MODIS data (Bailey and others, this volume). The increase in *b*-value is also seen in figure 7, which shows the three deformation stages superimposed onto the plot of *b*-value with time. While the general trends in the *b*-value seem to correlate well, figure 7 also illustrates that they do not correlate exactly with the deformation changes, and there are additional changes in *b*-value that are not accompanied by any apparent changes in deformation.

Another physical observation at Augustine was an increase in temperature, at seismic station AUS (see fig. 2 for seismic-station locations). The hut at seismic station AUS contained a thermistor (LM335A thermocouple paired with a 3.3-kohm 5-percent resistor, manufactured by National Semiconductor) in the McVCO (a microcontroller-based frequency generator that replaces the voltage controlled oscillator (VCO) used in the analog telemetry of seismic data), which is used to test station health. The McVCO was located on a battery rack inside the AUS seismic hut, approximately 1.4 m off the ground. The LM335A works over a temperature range of –40 to 100°C and is accurate within 1°C. Temperature information from the thermistor was received with the calibration pulse, every 12 hours from late October 2000 through the eruption on January 11, 2006. No changes were made in the processing of this data from October 2000 through January 2006 when the AUS hut was destroyed (G. Tytgat, oral commun., 2006). Regional air temperature data from Homer, Iliamna, and Seldovia, courtesy of the Alaska Climate Data Center, and data from a National Oceanic and Atmospheric Administration (NOAA) weather station on Augustine Island

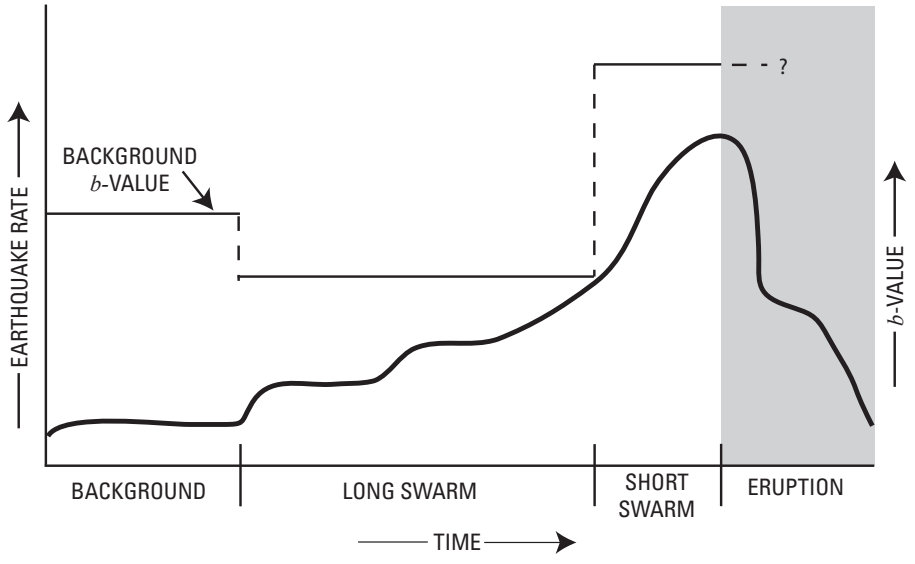

Figure 6. Schematic diagram illustrating how we expected the *b*-value to change over the course of the precursory earthquake swarm at Augustine Volcano. Curved line indicates the observed earthquake rate, and the straight horizontal lines indicate relative *b*-value changes expected for each part of the swarm activity.

were also processed for comparison with the recorded AUS temperatures.

The weather stations at Homer, Iliamna, Seldovia, and the Augustine NOAA station all gave temperatures that agreed with one another and varied systematically with the season. However, the changes seen at the AUS seismic hut differed from the others and are likely volcanic in origin. In figure 8 daily maximum temperatures from the three regional stations and the NOAA weather station on Augustine Island are plotted and overlain with weekly temperature averages from the AUS hut. Where data were unreported for a period, the average of the existing data within the 7-day period is shown instead. Periods where no data were reported are plotted as a zero value for both the regional stations and the AUS site. The long outage in AUS data in 2002 is a period when no data were received. Data were transmitted during the outage in 2004, but the temperature sensor did not report temperatures. These times do not correspond to the catalog-reported station outages (Dixon and others, 2008) and are more likely to be related to weather interference with the signal or a problem with the temperature sensor itself. Table 1 shows monthly average temperatures from January 2002 through January 2006. The monthly average shows a marked increase beginning in January 2005. A smaller increase of approximately 5°C is also seen in November and December 2004. This can also be seen in figure 9, where monthly averages of AUS hut temperatures from January 2002 through January 2006 are overlaid on the plot of *b*-values. Again, the monthly average shows a marked increase beginning in January 2005, and a smaller increase of approximately 5°C is also seen in November and December 2004.

Table 1. Monthly averaged temperatures at seismic station AUS on Augustine Volcano from January 2002 through January 2006.

[The value for January 2006 is only an average through January 11. All other values span the entire month. An asterisk indicates insufficient data to calculate the monthly average.]

	Average Temperature (°C)				
Month	**2002**	**2003**	**2004**	**2005**	**2006**
January	6.18	5.72	2.57	29.90	45.28
February	6.95	7.22	6.96	30.74	
March	5.74	2.83	1.55	35.75	
April	6.74	6.75	7.19	34.34	
May	4.31	8.82	11.00	28.35	
June	4.25	7.83	11.31	33.45	
July	*	13.51	15.04	39.03	
August	*	13.07	19.47	39.09	
September	6.96	8.78	12.09	33.39	
October	4.55	4.74	*	30.33	
November	5.28	3.87	13.70	24.26	
December	6.00	3.74	10.79	44.31	

An ASTER (advanced spaceborne thermal emission and reflection radiometer) image acquired on December 20, 2005, and the first FLIR (forward looking infrared radiometer) mission during the Augustine unrest on December 22, 2005, both revealed areas of warm, bare rock and active fumaroles. The FLIR observations recorded bare rock temperatures of 10°C and fumarole temperatures as high as 210°C (Wessels and others, this volume). These observations confirm that summit temperatures were

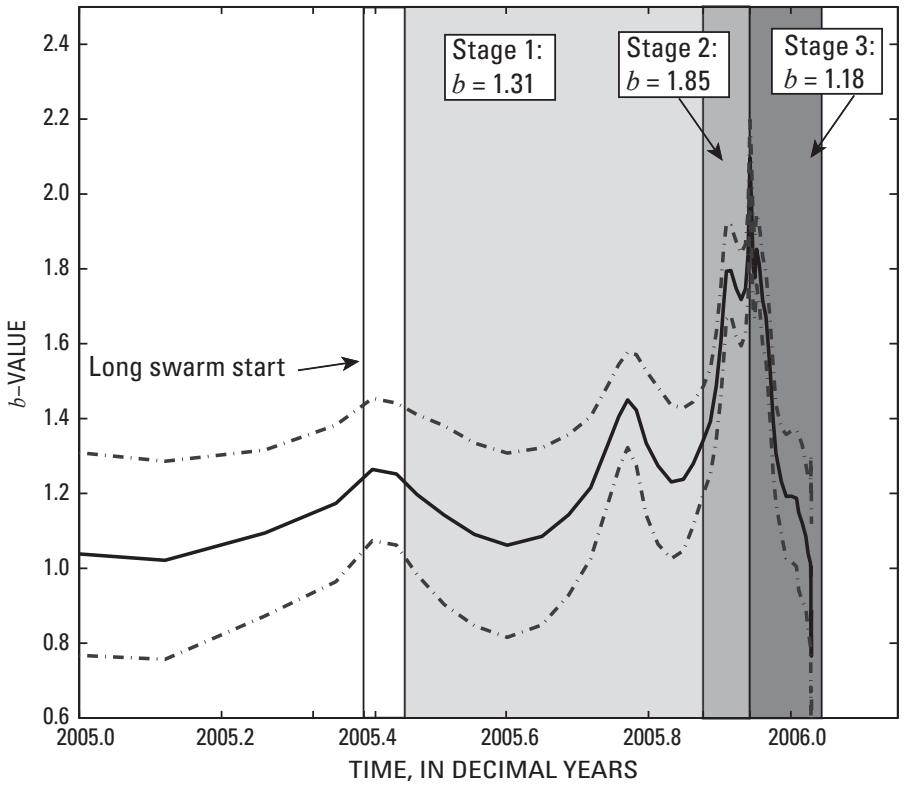

Figure 7. Plot of calculated *b*-value with respect to time for 2005–6, overlaid with shaded boxes indicating the periods of the long swarm and each of the three precursory deformation stages outlined in Cervelli and others (2006). The solid line is the calculated *b*-value, and the dashed lines indicate the 95-percent confidence interval of the maximum likelihood solution.

already elevated by late December. The AUS temperatures reported for those days were 44.6°C and 46.3°C, respectively. The consistency of data processing and a visit to the summit in December 2005 also provide evidence that this was a real thermal change (G. Tytgat and E. Clark, oral commun., 2006). The temperature change coincides with the initial *b*-value change in late 2004, which we see in our *b*-versus-time calculations. This change in *b*-value is possible evidence for a change in heat or fluid movement at depth at Augustine Volcano prior to the beginning of the seismic swarm.

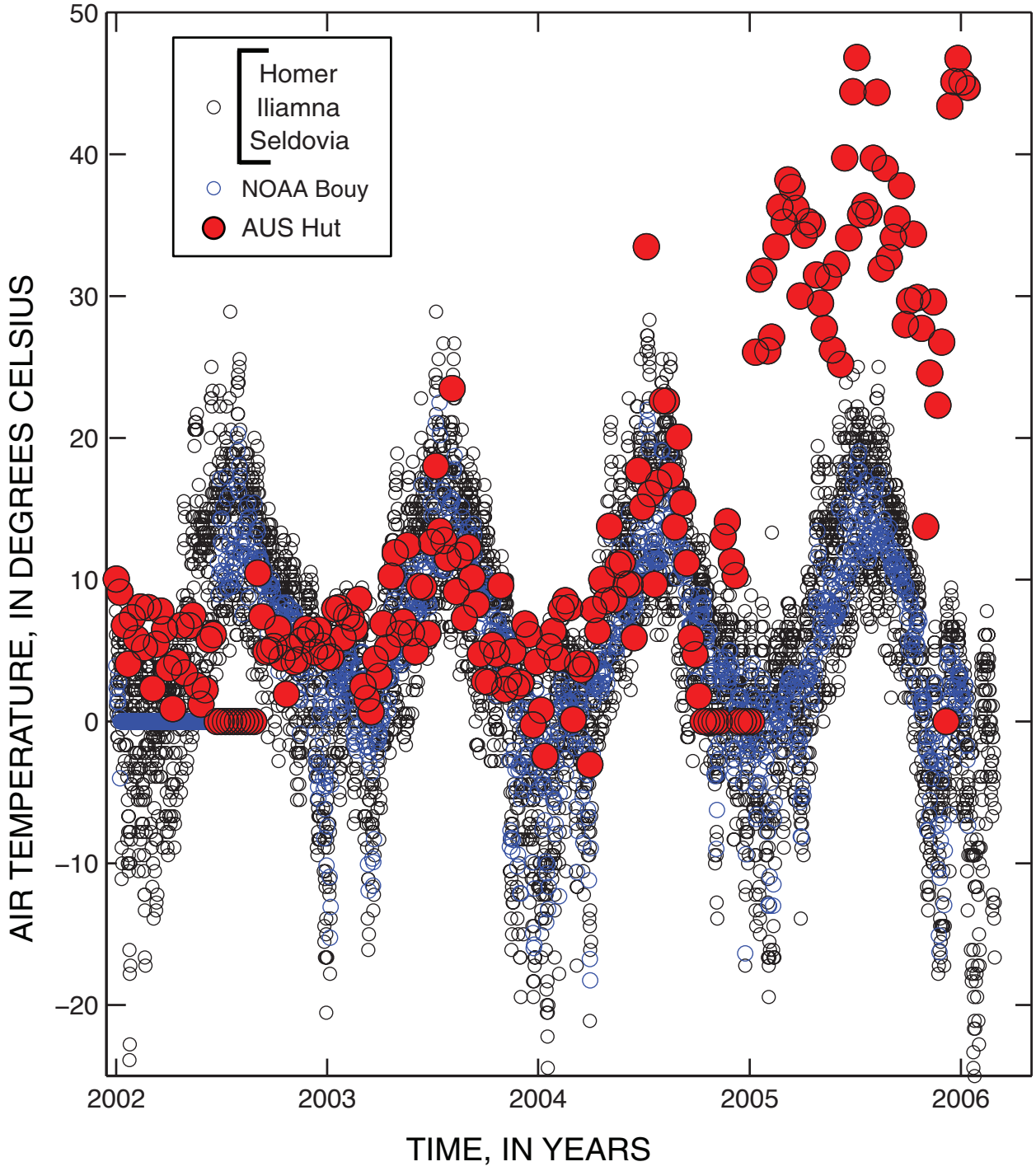

Figure 8. Plot of daily maximum air temperatures recorded in nearby communities (Homer, Iliamna, and Seldovia), at the Augustine Island NOAA weather station, and 7-day average temperatures from the seismic station AUS near the summit of Augustine Volcano. Tick marks on the horizontal axis mark the beginning of each year.

Given that the initial *b*-value decrease and temperature increase appear to be linked, we face the question, why does the *b*-value decrease? For *b*-value changes associated strictly with an increasing thermal gradient, the value of *b* should increase (Warren and Latham, 1970), the opposite of what we observe. We interpret this downward *b*-value trend to reflect an increase in stress throughout the seismic volume caused by the same physical process that is changing the thermal gradient. This suggests a possible influx of magma at depth or some other process that increases both thermal gradient and stress. Further support for a stress-induced *b*-value change is found in the slight time difference between the initial *b*-value change and the onset of the temperature increase seen in figure 9. A stress change would likely propagate instantaneously throughout the affected volume, whereas thermal (and pore pressure) effects take time to propagate through a volume of rock. Observing a stress change in *b*-values while we have evidence of thermal changes implies that stress effects dominate *b*-value observations when both parameters are changing simultaneously.

Because of the apparent importance of stress in overall *b*-value observations and past studies by Roman and others (2004), which suggest changes in stress tensors during periods of unrest and eruption, we undertook a study of focal mechanisms at Augustine. Determination of correct polarization of stations, normal or reversed, was made by looking at 37 large teleseisms from 2002 to 2006. *P*-wave polarities were then repicked for all located earthquakes for which at least six clear *P*-wave first motions were possible. Once the *P*-wave motions were repicked, the events were relocated using the same velocity model and processing steps as for the initial catalog locations (Dixon and others, 2008).

Focal mechanisms were computed for all earthquakes using FPFIT (Reasenberg and Oppenheimer, 1985). Solutions were judged acceptable if they had: a misfit of less than 0.15 (less than 15 percent of stations inconsistent with the preferred solutions); STDR (distribution around the hypocenter) ≥ 0.40; and an average uncertainty in strike, dip, and rake of $\leq 25°$.

After applying this criteria, 79 out of 201 earthquakes returned acceptable focal-mechanism solutions. There were 19 events (out of 61 picked) with acceptable solutions from 2002 through 2004 and 60 events (out of 140 picked) from the long swarm (all events with acceptable solutions in 2005 occurred during the long swarm). Appendix 2 shows all 79 acceptable

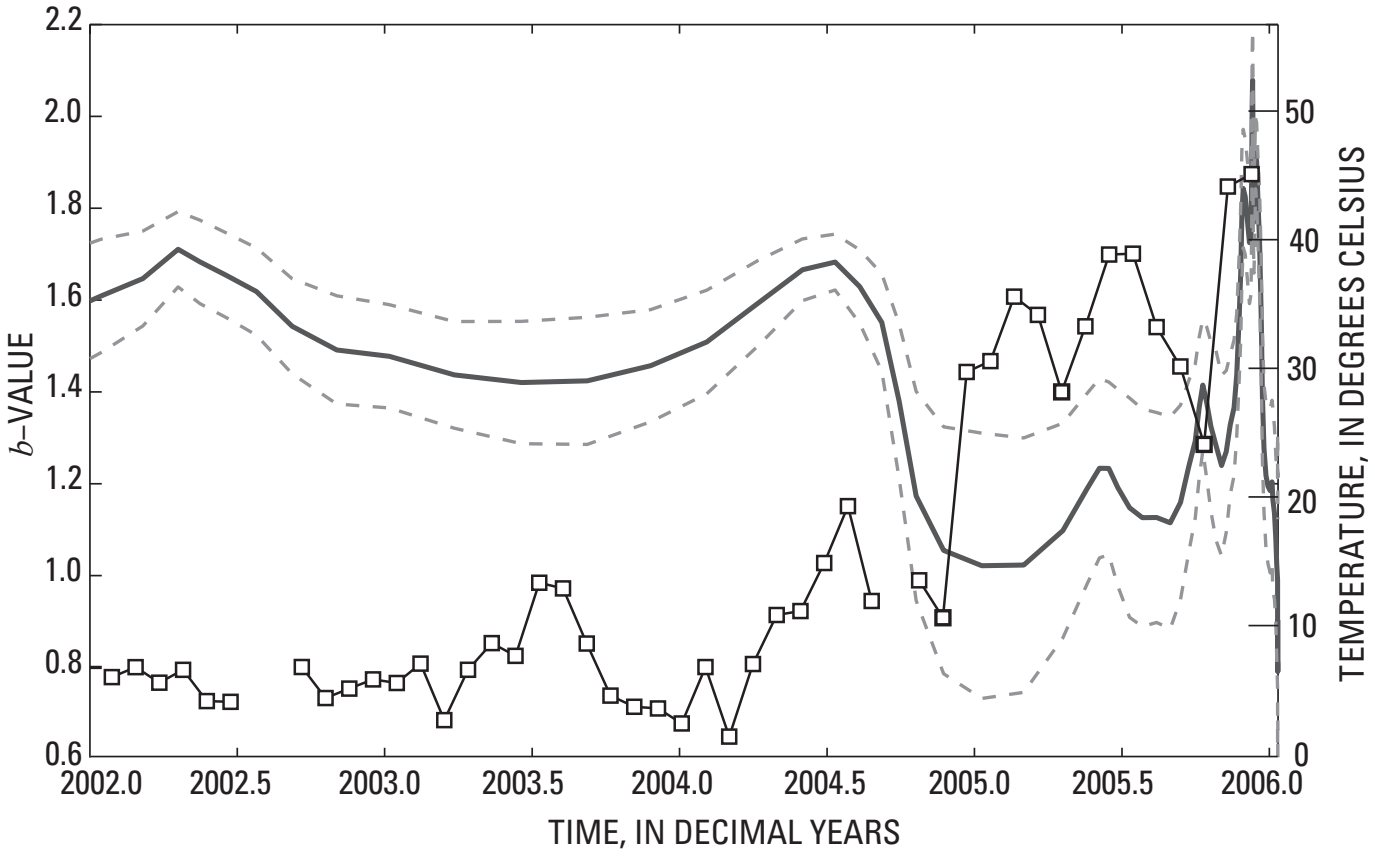

Figure 9. Plot of *b*-value with time from figure 4 (shown in boldline), overlaid with monthly average temperatures (as squares) from a thermistor at seismic station AUS. The *b*-value calculation uses a moving window of 100 earthquakes with an overlap of 25 events, and the dotted lines represent the 95-percent confidence interval of the maximum likelihood solution.

focal mechanisms. Stress tensor inversions were attempted in ZMAP for both the background data (2002 to 2004) and the long swarm (2005 through January 10, 2006) using the method of Michael (1987). The inversions had very high errors and do not display a dominant faulting style. The lack of any pattern or observable change in the focal mechanisms with time and the highly variable stress tensors agree with work by DeShon and others (this volume), which suggests no dominant faulting style or area within the Augustine Volcano seismic volume.

Short Swarm

In our conceptual model we expected the *b*-value of the short swarm to be the highest of all the time periods (fig. 6), and yet our results show that it is the lowest (fig. 3). We also see this low value in the calculation of *b*-value versus time, where there is a dramatic drop in *b*-value just before the eruption (fig. 4). We also note, however, that there is a strange bend or knee in the *b*-value curve (fig. 3*D*). This led us to question whether the low value was real and whether there was an "excess" of larger events occurring, or if this lower value was an artifact of a poor fit to a single distribution. Upon examining magnitudes with time, we find that the decrease in *b*-value leading into the eruption is real and appears to be caused by an increase in the number of $M_L \geq 1$ events (large earthquakes for Augustine) that occur in that time frame.

Having convinced ourselves that the observed low *b*-value for the short swarm is real, we look for ways to explain the observed knee in the frequency-magnitude distribution. Bends or knees like this one (fig. 3*D*) have been observed at other volcanoes, including Mount St. Helens (Qamar and others, 1983), Fernandina (Filson and others, 1973), and Usu (Okada and others, 1981; Okada 1983). At Fernandina the data are directly related to caldera collapse (Filson and others, 1973), so we will not seek comparisons with their conclusions. Okada and others (1981) outlined the appearance of odd frequency-magnitude plots at Usu and found that there were distinct earthquake families occurring in time. These earthquake families accounted for an unusually high number of earthquakes with similar magnitudes. Work by Buurman and West (this volume) and DeShon and others (this volume) indicates that earthquake families were occurring at Augustine from 1993 through 2006. Buurman and West (this volume) identified seven families on January 10–11, 2006, before the first eruption. Because only 41 out of 722 located earthquakes appear in the families on January 10–11, 2006, we conclude that earthquake families alone cannot explain the unusual shape of the frequency-magnitude plot.

The knee in the Mount St. Helens data corresponds to a group of earthquakes with magnitudes 4.5 and greater (Qamar and others, 1983). Low-frequency energy also accompanies many of the located earthquakes, and an increase in the low-to high-frequency amplitude ratio is observed leading up to the eruption. This has been interpreted as either the source of earthquakes becoming shallower or evidence of the magma chamber expanding (Qamar and others, 1983; Main, 1987).

A magnitude histogram for the short swarm is shown in figure 10. Most complete earthquake catalogs have a single normal-shaped distribution. The bell-shaped curve results from the lack of complete detection for magnitudes below the M_c and a similar reflected exponential decay of higher magnitudes resulting from decreasing frequency of occurrence. The histogram of the January 10–11, 2006, earthquakes is clearly not a single peaked bell-shaped curve and appears to be bimodal.

A separate study of very long period (VLP) energy was performed to investigate possible VLP energy associated with some of the high-frequency earthquakes during the short swarm, first observed by S. DeAngelis and J. Power (oral. commun., 2007). We looked for VLP signals during the short swarm (January 10–11, 2006) using data from temporary broadband stations AU11, AU12, AU13, AU14, and AU15 (for locations of these stations, see Power and Lalla, this volume). These seismometers were installed on Augustine Island in response to the increasing earthquake activity in December of 2005 and were not telemetered (Power and others, 2006). Initially we chose two different filters, a band pass filter from 0.01 to 0.2 Hz, and a second separate low pass filter of 0.05 Hz. The low pass filter

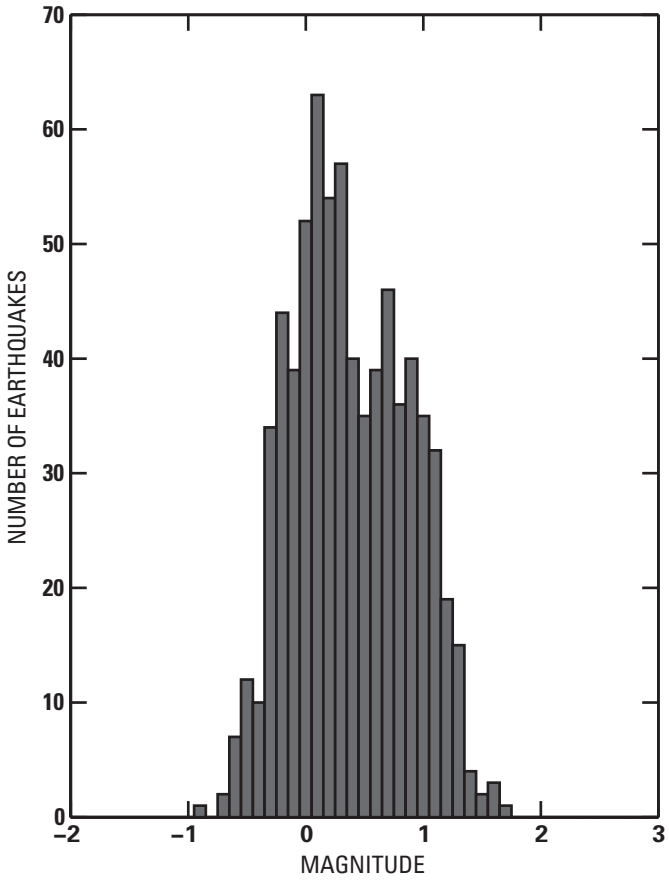

Figure 10. Histogram of magnitudes for located earthquakes at Augustine Volcano from the 13-hour short swarm on January 10–11, 2006.

of 0.05 Hz, corresponding to periods of 20 seconds and greater, showed the most consistent and largest amount of energy, and we chose that filter to examine all of the data.

To establish whether or not VLP energy was accompanying the high-frequency located earthquakes during the short swarm, we looked through continuous data at the time of each located earthquake, applied a 0.05 Hz low pass filter, and visually determined whether or not there was a pulse of VLP energy. No quantitative criteria were assigned for either amplitude or wavelength. Short-period stations AUP and AUW were used to verify the position of located earthquakes because the temporary broadband stations were not used for the location of earthquakes in the catalog. There were other long-period and VLP signals seen during this time frame, but no events without accompanying located high-frequency earthquakes were considered in this study. Figure 11 shows raw and filtered waveforms for several earthquakes at Augustine Volcano.

Using this method we found that 221 out of 722 located earthquakes during the short swarm had accompanying VLP energy. The events were separated according to this classification, and the individual properties of each group were examined. A magnitude histogram was created for each set of events, and these are plotted in figure 12. Both sets of events gave approximately normal distributions, indicating that they are complete populations of events. Furthermore, the two sets of events have notably different mean magnitudes. The smallest event without accompanying VLP energy is M_L 0.1, while the smallest event observed with VLP energy is M_L 0.9.

To test the significance of this apparent difference in mean magnitude, a Student t-test was run (Davis, 2002). This test examines the likelihood that two populations have come from a single parent population. The mean magnitude of the events with VLP energy was 0.91, and the mean magnitude of events without observed VLP energy was 0.16 (negative magnitudes

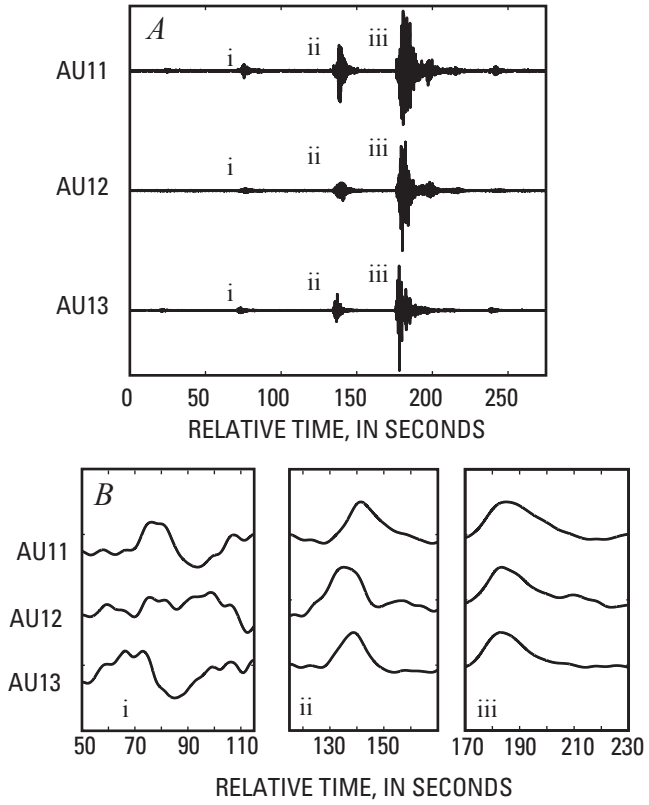

Figure 11. Waveforms for three located earthquakes at Augustine Volcano on January 10, 2006, as recorded on stations AU11, AU12, and AU13. The calculated origin time, depth, and magnitude are 19:48:58, 19:50:02, and 19:50:43 AKST; –0.57, –0.84, and –0.57 km below sea level; and 0.6, 0.6, and 1.4, respectively for the three earthquakes. *A,* Unfiltered waveforms at each station. *B,* Filtered waveforms around each earthquake that have been normalized to the maximum amplitude within the sample and low–pass filtered at 0.05 s for each station. Note that the first event shows no coherent VLP energy while the second and third events have significant VLP energy.

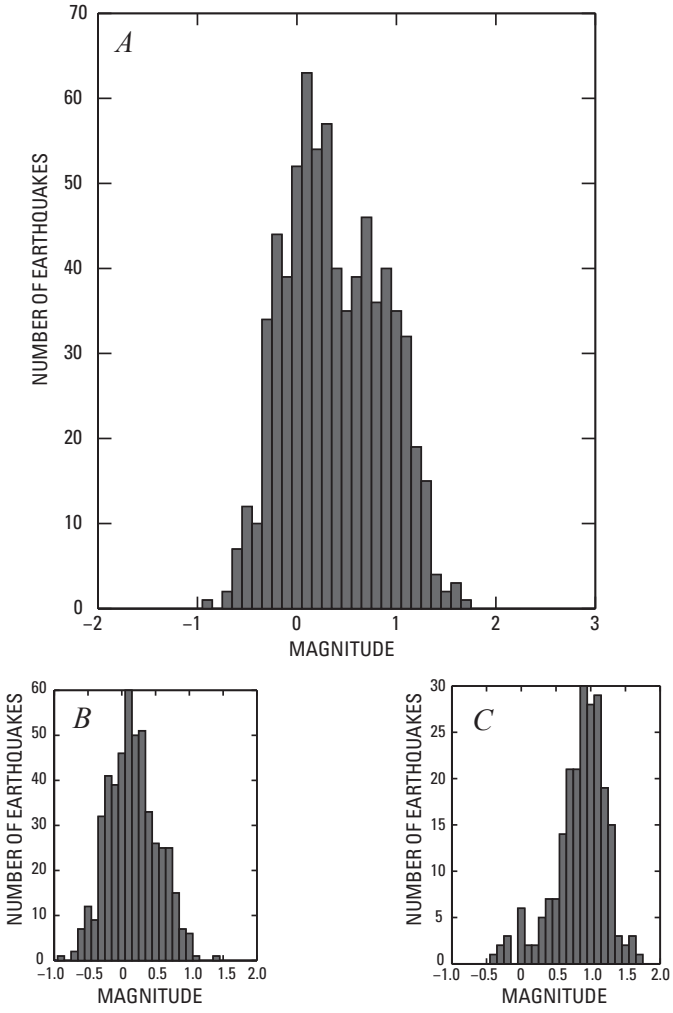

Figure 12. Magnitude histograms for (*A*) All events at Augustine Volcano during the short swarm (January 10–11, 2006), (*B*) Events with associated very long period energy, and (*C*) events without any associated very long period energy.

reduce the overall mean). The Student t-test produced a value of 26.3, well above the limit of 3.09 for a statistically significant difference between the means. Thus the two sets of earthquakes represent different parent populations.

To quantify the differences in energy implied by the differences in mean magnitude, we used ZMAP to calculate the cumulative moment for each earthquake population (fig. 13). The population with VLP energy has a moment of 1.01×10^{14} Nm, a factor of four larger than the cumulative seismic moment for the events without VLP energy (2.46×10^{13} Nm). The VLP events are also found to have more than half of the total moment for the entire seismic swarm and slightly more energy than all other earthquakes from January 1, 2000, through the January 11, 2006, eruption (9.49×10^{13} Nm).

Having observed that both events with and without VLP energy appear to have bell-shaped distributions (fig. 12), we note that the population without VLP energy represents earthquake activity on January 10–11, 2006, without the excess higher magnitude events that earlier made the observed magnitude histogram appear bimodal. The population with VLP energy, that has significantly higher magnitudes, corresponds to the $M \geq 1.0$ events that are seen to drive down the *b*-value for the short swarm. Essentially the population of VLP events is the "cause" of the bimodal magnitude histogram and of the associated low *b*-value for the short swarm.

The occurrence of VLP energy accompanying earthquakes and a bimodal *b*-value are in good agreement with the findings at Mount St. Helens (Qamar and others, 1983; Main, 1987), where both a bimodal frequency-magnitude distribution and the occurrence of lower frequency energy accompanying some of the recorded earthquakes were observed. Further comparison between these findings is ongoing.

The fact that the population of events without VLP energy has a similar M_c as the events in the long swarm suggests that the underlying process driving the long swarm continued during the short swarm and an additional population of earthquakes (those with VLP energy) was superimposed onto the existing seismicity trend. We believe that this is evidence of independent concurrent seismogenic processes at Augustine preceding the eruption. The fact that both sets of events appear to be happening in the same volume indicates that there is probably a difference in their mechanisms. Following Scholz (1968), we interpret the low *b*-values and larger event sizes of the VLP population to represent the formation of new fractures. The larger event size is required to accompany the low *b*-value because breaking rock, as opposed to failure along pre-existing fractures, requires much more energy.

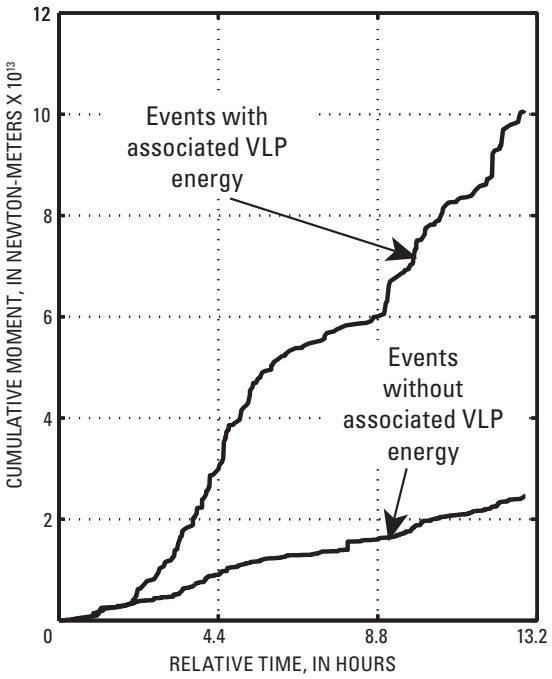

Figure 13. Cumulative seismic moment for earthquakes with and without associated very long period energy during the 13-hour short swarm on January 10–11, 2006. Time is shown in hours relative to the beginning of the short swarm at 1535 AKST on January 10.

A lull in earthquake rate is noted about 8 hours into the short swarm, and it appears in both populations of events (fig. 14). No major changes in depth or magnitude are seen in either population before or after the lull. Figure 15 shows several plots comparing the rate at which the two populations of events were occurring with time. We infer from the lack of change in either population that the individual processes causing each population of events did not change either. This indicates that the lull was not caused by a change in process and was probably the result of a mechanical, material, or thermal barrier present at Augustine Volcano.

Focal mechanisms were not attempted for the earthquakes during the short swarm. No clear stress tensor was produced from analysis of the background or long swarm, and so even if a stress tensor was produced from the short swarm, there would be no way to compare it to the preceding time periods.

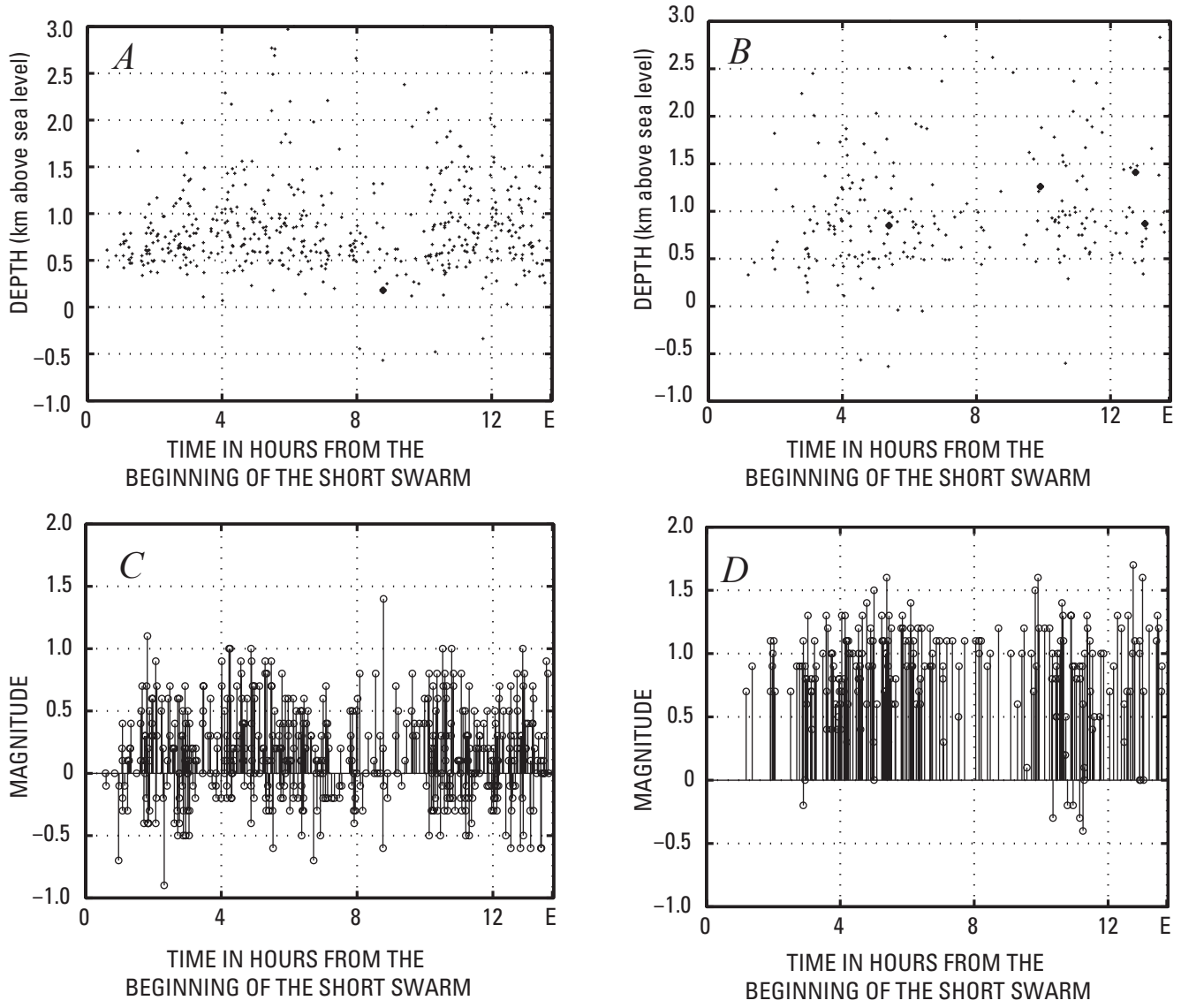

Figure 14. Plots of earthquake focal depth with time and of magnitude with time plots for events with very long period (VLP) energy (*A* and *C)* and without VLP energy (*B* and *D)*. The time axis reflects the time since the onset of the short swarm, taken to be at 1535 AKST on January 10, 2006. "E" marks the initiation of explosive activity.

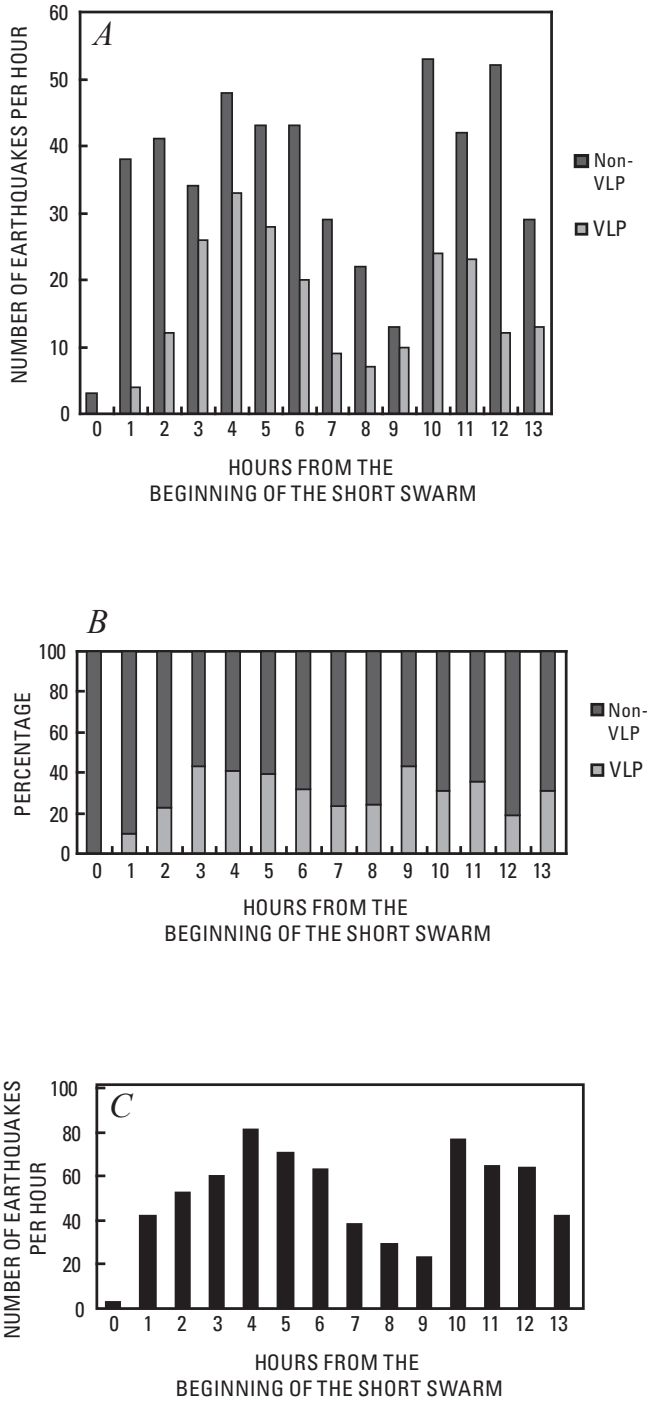

Figure 15. Summary plots the occurrence of earthquakes with very long period (VLP) and non-VLP energy during the 13-hour-long short swarm on January 10-11, 2006. *A*, histogram showing the number of earthquakes per hour with and without very-long-period energy. *B*, Percentage per hour of the two populations of earthquakes. *C*, Histogram showing the total number of earthquakes recorded per hour. Note that the total number of earthquakes in *C* tends to mirror the percentage of VLP events in *B* with a slight time delay.

Conclusions

We have been able to identify changes in *b*-value during the Augustine preeruptive earthquake swarm that we believe were caused by changes in thermal gradient, pore pressure, and stress. These changes have been substantiated through comparison with other physical observations at Augustine Volcano. Our observations in conjunction with temperatures recorded on Augustine Island suggest that when thermal-gradient and stress changes occur simultaneously, stress dominates the overall *b*-value observations. We have also been able to identify a unique set of high-frequency earthquakes that have associated VLP energy. These events are a complete and separate population from other high-frequency earthquakes occurring during the short swarm. The VLP events have significantly higher energy release than other earthquakes, and we believe that they may be the primary expression of magma moving towards the surface. We see preliminary evidence to suggest that *b*-value changes can precede other more obvious punctuations in activity, such as the onset of the seismic swarm. Changes in *b*-values can be used to corroborate other physical observations, such as the *b*-value changes that accompanied temperature changes or increased steaming before the large steam plume on December 12, 2005. These *b*-value changes may indicate that larger or deeper processes are occurring than can otherwise be observed. In this way *b*-value calculations can give us more information about the causes and physical process at work during earthquake swarms. Given these findings we suggest that systematic evaluation of *b*-values become a more regular part of monitoring efforts.

Acknowledgments

Thank you to Matt Haney, Seth Moran, and John Power for their reviews, which helped to shape this paper. We acknowledge the AVO staff, especially Scott Stihler, Guy Tytgat, Ed Clark, and Jim Dixon. During the course of this work we also had discussions with Mike West, Doug Christensen, Stephanie Prejean, Helena Buurman, Lea Burris, Celso Reyes, Matt Gardine, Nicole DeRoin, Tanja Peteresen, Silvio DeAngelis, and others.

References Cited

Bailey, J.E., Dean, K.G., Dehn, J., and Webely, P.W., 2010, Integrated satellite observations of the 2006 eruption of Augustine Volcano, *in* Power, J.A., Coombs, M.L., and Freymueller, J.T., eds., The 2006 eruption of Augustine Volcano, Alaska: U.S. Geological Survey Professional Paper 1769 (this volume).

Bath. M., 1981, Earthquake magnitude—recent research and current trends: Earth Science Review, v. 17, p. 315–98.

Benoit, J.P., and McNutt, S.R., 1996, Global volcanic earthquake swarm database, 1979–1989: U.S. Geological Survey Open-File Report 96-0069, 333 p.

Buurman, H., and West, M.E., 2010 Seismic precursors to volcanic explosions during the 2006 eruption of Augustine Volcano, *in* Power, J.A., Coombs, M.L., and Freymueller, J.T., eds., The 2006 eruption of Augustine Volcano, Alaska: U.S. Geological Survey Professional Paper 1769 (this volume).

Cervelli, P.F., Fournier, T.J., Freymueller, J.T., and Power, J.A., 2006, Ground deformation associated with the precursory unrest and early phases of the January 2006 eruption of Augustine Volcano, Alaska: Geophysical Research Letters, v. 33, doi: 10.1029/2006GL027219.

Cervelli, P.F., Fournier, T.J., Freymueller, J.T., Power, J.A., Lisowski, M., and Pauk, B.A., 2010, Geodetic constraints on magma movement and withdrawal during the 2006 eruption of Augustine Volcano, *in* Power, J.A., Coombs, M.L., and Freymueller, J.T., eds., The 2006 eruption of Augustine Volcano, Alaska: U.S. Geological Survey Professional Paper 1769 (this volume).

Davis, J.C., 2002, Statistics and data analysis in geology: New York, J. Wiley, p. 68–74.

DeShon, H.R., Thurber, C.H., and Power, J.A., 2010, Earthquake waveform similarity and evolution at Augustine Volcano from 1993 to 2006, *in* Power, J.A., Coombs, M.L., and Freymueller, J.T., eds., The 2006 eruption of Augustine Volcano, Alaska: U.S. Geological Survey Professional Paper 1769 (this volume).

Dixon, J.P., Stihler, S.D., Power, J.A., and Searcy, C., 2008, Catalog of earthquake hypocenters at Alaskan Volcanoes; January 1 through December 31, 2006: U.S. Geological Survey Data Series 326, 78 p.

Filson, J., Simkin, T., and Leu, L.-K., 1973, Seismicity of a caldera collapse—Galapagos Islands 1968: Journal of Geophysical Research, v. 34, p. 8591–8622.

Gutenberg, R., and Richter, C.F., 1944, Frequency of earthquakes in California: Bulletin of the Seismological Society of America, v. 34, p. 185–188.

Ishimoto, M., and Ida, K., 1939, Observations of earthquakes registered with the microseismograph constructed recently: Bulletin of the Earthquake Research Institute, University of Tokyo, v. 17, p. 443–478.

Jolly, A.D., and McNutt, S.R., 1999, Seismicity at the volcanoes of Katmai National Park, Alaska; July 1995–December 1997: Journal of Volcanology and Geothermal Research, v. 93, p. 173–190.

Lahr, J.C., 1999, HYPOELLIPSE; a computer program for determining local earthquake hypocentral parameters, magnitude, and first motion pattern (Y2K compliant version): U.S. Geological Survey Open-File Report 99-23, 48 p.

Lalla, D.J., and Power, J.A., 2010, A two-step procedure for calculating earthquake hypocenters at Augustine Volcano, *in* Power, J.A., Coombs, M.L., and Freymueller, J.T., eds., The 2006 eruption of Augustine Volcano, Alaska: U.S. Geological Survey Professional Paper 1769 (this volume).

Main, I., 1987, A characteristic earthquake model of the seismicity preceding the eruption of Mount St. Helens on 18 May 1980: Physics of the Earth and Planetary Interiors, v. 49, p. 283–293.

McNutt, S.R., 2005, A review of volcanic seismology: Annual Review of Earth and Planetary Science, v. 33, p. 461–491, doi: 10.1146/annurev.earth.33.092209.122459.

Michael, A.J., 1987, Use of focal mechanisms to determine stress; a control study: Journal of Geophysical Research, v. 92, p. 357–368.

Mogi, K., 1962, Magnitude-Frequency relation for elastic shocks accompanying fractures of various materials and some related problems in earthquakes (2nd paper): Bulletin Earthquake Research Institute, v. 40, p. 831–853.

Mogi, K., 1963, Some discussions on aftershocks, foreshocks and earthquake swarms, the fracture of a semi-infinite body caused by an inner stress origin and its relation to the earthquake phenomena (Third Paper): Bulletin of the Earthquake Research Institute-University of Tokyo, v. 41, p. 615–658.

Okada, Hm., Watanabe, H., Yamashita, H., and Yokoyama, I., 1981, Seismological significance of the 1977–1978 eruptions and the magma intrusion process of Usu volcano, Hokkaido: Journal of Volcanology and Geothermal Research, v. 9, p. 311–334.

Okada, Hm., 1983, Comparative study of earthquake swarms associated with major volcanic activities, *in* Shimozuru, D., and Yokoyama I., eds, Arc volcanism: physics and tectonics: Tokyo, TERRAPUB, p. 43–63.

Power, J.A., Nye, C.J., Coombs, M.L., Wessels, R.L., Cervelli, P.F., Dehn, J., Wallace, K.L., Freymueller, J.T., and Doukas, M.P., 2006, The reawakening of Alaska's Augustine Volcano: EOS (American Geophysical Union Transactions), v. 87, p. 373, 377.

Power, J.A., and Lalla, D.J., 2010, Seismic observations of Augustine Volcano, 1970–2007, *in* Power, J.A., Coombs, M.L., and Freymueller, J.T., eds., The 2006 eruption of Augustine Volcano, Alaska: U.S. Geological Survey Professional Paper 1769 (this volume).

Qamar, A., St. Lawrence, W., Moore, J.N., and Kendrick, G., 1983, Seismic signals preceding the explosive eruption of Mount St. Helens, Washington, on 18 May 1980: Bulletin of the Seismological Society of America, v. 73, p. 1797–1813.

Reasenberg, P., and Oppenheimer, D., 1985, FPFIT, FPPLOT, and FPPAGE; Fortran computer programs for calculating and displaying earthquake fault-plane solutions: U.S. Geological Survey Open-File Report 85-739, 25 p.

Robinson, M., 1990, XPICK users manual, version 2.7: Seismology Lab, Geophysical Institute, University of Alaska Fairbanks, 93 p.

Roman, D.C., Moran, S.C., Power, J.A., and Cashman, K.V., 2004, Temporal and spatial variation of local stress fields before and after the 1992 eruptions of Crater Peak vent, Mount Spurr Volcano, Alaska: Bulletin of the Seismological Society of America, v. 94, no. 6, p. 2366–2379.

Sanchez, J.J., McNutt, S.R., Power, J.A., and Wyss, M., 2004, Spatial variations In the frequency-magnitude distribution of earthquakes at Mount Pinatubo Volcano: Bulletin of the Seismological Society of America, v. 94, no. 2, p. 430–438.

Scholz, C.H., 1968, The frequency-magnitude relation of microfracturing in rock and its relation to earthquakes: Bulletin of the Seismological Society of America, v. 58, no. 1, p. 399–415.

Warren, N.W., and Latham, G.V., 1970, An experimental study of thermally induced microfracturing and its relation to volcanic seismicity: Journal of Geothermal Research, v. 75, no. 23, p. 4455–4464.

Wessels, R.L., Coombs, M.L., Schneider, D.J., Dehn, J., and Ramsey, M.S., 2010, High-resolution satellite and airborne thermal infrared imaging of the 2006 eruption of Augustine Volcano, *in* Power, J.A., Coombs, M.L., and Freymueller, J.T., eds., The 2006 eruption of Augustine Volcano, Alaska: U.S. Geological Survey Professional Paper 1769 (this volume).

Wiemer, S., 2001, A software package to analyze seismicity—ZMAP: Seismological Research Letters, v. 72, no. 2, p. 373–382.

Wiemer, S., and McNutt, S.R., 1997, Variations in the frequency-magnitude distribution with depth in two volcanic areas—Mount St. Helens, Washington, and Mt. Spurr, Alaska: Geophysical Research Letters, v. 24, no. 2, p. 189–192.

Wiemer, S., McNutt, S.R., and Wyss, M., 1998, Temporal and three-dimensional spatial analyses of the frequency-magnitude distribution near Long Valley Caldera, California: Geophysical Journal International, v. 134, p. 409–421.

Woessner, J., and Wiemer, S., 2005, Assessing the quality of earthquake catalogues; estimating the magnitude of completeness and its uncertainty: Bulletin of the Seismological Society of America, v. 95, no. 2, p. 684–698.

Wyss, M., 1973, Towards a physical understanding of the earthquake frequency distribution: Geophysical Journal of the Royal Astronomical Society, v. 31, p. 341–359.

Zobin, V., 1979, Variations of volcanic earthquake source parameters before volcanic eruptions: Journal of Volcanology and Geothermal Research, v. 6, p. 279–293.

Appendixes 1–2

Appendix 1. Start Date Algorithms

Algorithm Descriptions

Two algorithms were developed to quantitatively assign a start date for the Augustine 2005–6 preeruptive earthquake swarm. We call these algorithms the largest daily count method (LDCM), and the consecutive days method (CDM). Although the algorithms are written in a general format, they are tailored to Augustine Volcano. Each method requires a year of data to establish background rates. This period was chosen because earthquake rates at Augustine are generally steady for years at a time and the year–long period should eliminate any small seasonal or weather biases in the ability to locate earthquakes. Once the background rate has been established, we have a basis to look for increased rates of activity. Both algorithms assume that a swarm has already been detected; however, they could be run continuously on data with a moving background window to "search" for swarms. We use only located earthquakes in the algorithms; again, this is practical for Augustine, but isn't necessarily suitable for volcanoes where a large number of unlocated or long-period earthquakes occur. The CDM algorithm in particular is only suited to volcanoes with fairly low earthquake rates.

Both algorithms use the same initial background analysis to establish a trigger threshold for the selection of periods of increased activity or the occurrence of a swarm. We have chosen one–eighth of the total earthquakes from the previous year occurring in a period of 30 days as the trigger threshold for increased activity. The expected seismicity in an average 30-day period would be one–twelfth of the annual seismicity. Setting a threshold of one–eighth allows for monthly and seasonal variations within the yearly average, but also keeps the threshold low enough to detect small increases in rate. Later stages of the algorithms ensure that these initial triggers are not ordinary behavior. Once a trigger is found, another set of background calculations is performed on the 4 months prior to the beginning of the trigger to determine normal fluctuations in the earthquake rate.

The LDCM algorithm uses the daily number of located earthquakes. This is done by establishing another set of background criteria once a swarm is recognized. First the weekly average of the 4 months prior to the trigger is taken, and also the largest event count for a single day is found. These 4 months are then tested to see if there are any weeks within the 4 months that exceed three times the weekly average. If there is no week that exceeds three times the average in the 4 months, then the trigger period is searched for 7-day periods that exceed the weekly average. If a week is found within the trigger period that exceeds three times the weekly average, then the largest event count for that week is compared to the largest event count for the 4-month background. If there is a week that exceeds three times the weekly average of the previous 4 months and the highest daily event count in that week is equal to or exceeds the highest daily event count for the 4 months of background, then that day is taken as the swarm start date. Figure 17 is a flow chart diagram for the LDCM method.

Augustine Volcano has very low earthquake rates and many days without any located earthquakes. The CDM algorithm uses the number of consecutive days with located earthquakes as a second way to look for increased activity. Using the same initial trigger period as LDCM, we then define two more background parameters to search for the swarm start date. The first is the number of consecutive days with located earthquakes, and the second is the number of earthquakes found commonly within a short (1 to 5 days) span. For instance, at Augustine three earthquakes in 3 days is a common occurrence. The background period is analyzed to see how often this occurs and what the shortest time interval of reoccurrence is. Once this is established, the 30-day trigger period is searched for periods of time that meet the criteria of number of events in the shorter time frame. If the first instance found meets but does not exceed the number of earthquakes, then we look for another instance. If another instance is found, we look at the time interval between these instances and compare that to the occurrence information gathered from the background data. We continue searching for occurrences until one exceeds the thresholds of the background, or there are enough triggers in a short amount of time that we believe activity has increased, or activity returns to background for two weeks or more. Figure 18 is a flow chart diagram for the CDM method.

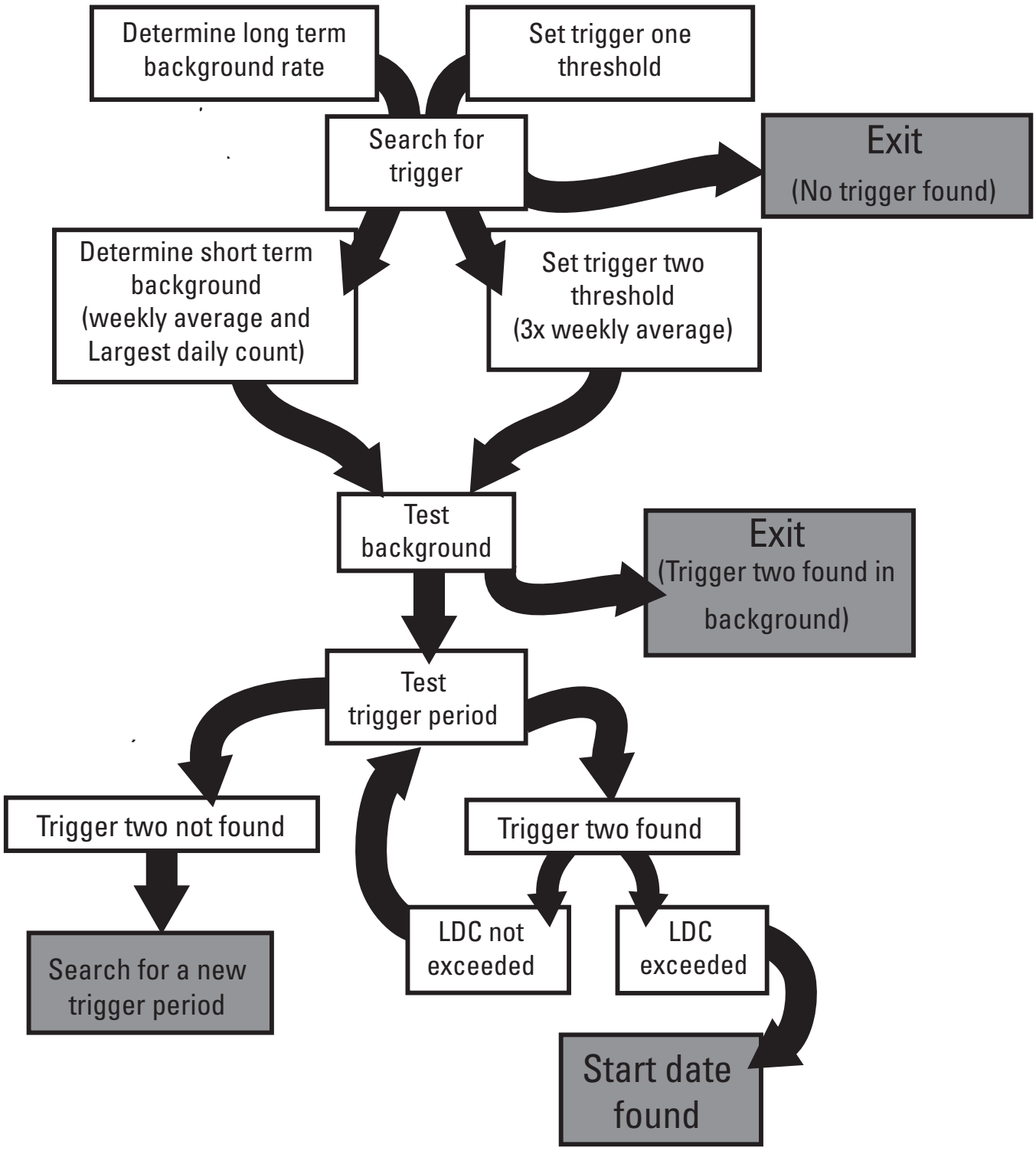

Figure 17. Flow–chart diagram illustrating the largest daily count method (LDCM) for swarm start–date determination.

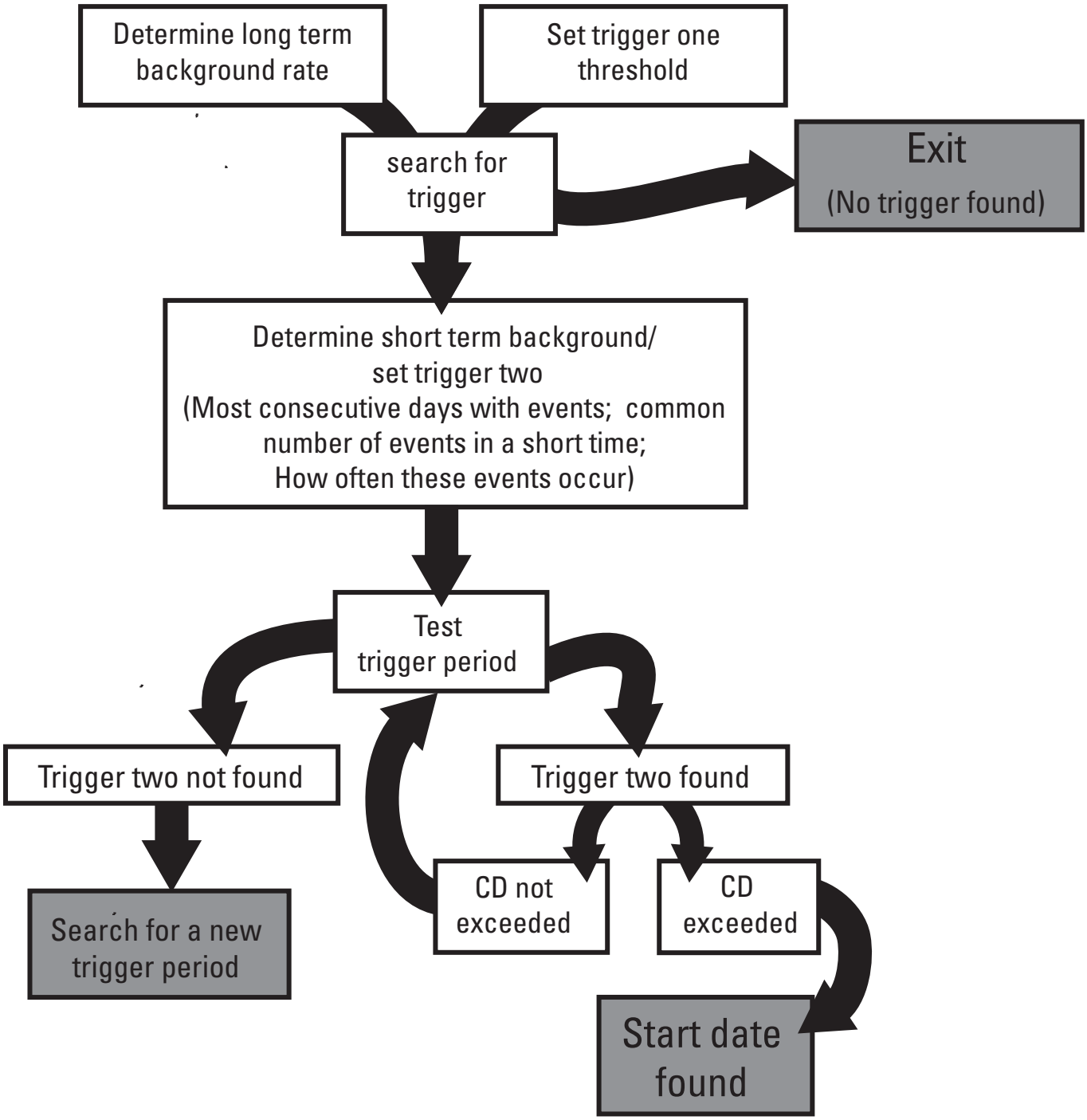

Figure 18. Flow–chart diagram illustrating the consecutive days method (CDM) for swarm start–date determination.

Results of LDCM and CDM Algorithms for the Augustine 2005–2006 Preeruptive Earthquake Swarm

Although the two algorithms use the same initial steps to classify earthquake activity as increased above background, they use unique secondary classifications to narrow down the start date. Both algorithms give a swarm start date of April 30, 2005. The detailed results for each step of the algorithms are given below.

Largest Daily Count Method

Define a reasonable background rate that is unbiased of previous swarms and annual weather phenomena:

- Calculate the previous calendar year's located earthquakes. Taking the average of an entire year's worth of data should eliminate most seasonal weather affects.
  Augustine: 238 located earthquakes total in 2004

Define a trigger to look for a swarm start date:

- Search for a 30-day period that exceeds 12.5 percent (1/8) of last year's earthquake total. Augustine: 238÷8 = 30 earthquakes
  Augustine: 4/14/2005–5/12/2005 = 31 earthquakes

If a trigger occurs, calculate the following data in order to define and test what is now taken to be the background seismicity rate:

- Take the weekly average for the 4 months prior to the 30 days of data in the trigger.
  Augustine: Two earthquakes per week
- Find the largest event count for a single day in those four months.
  Augustine: Three earthquakes in a single day

Test the background data calculated to see how representative the average daily located earthquake count is of the data:

- Search for weeks within the 4–month background period that exceed three times the weekly average calculated.
  Augustine: None
- If no week within the background period exceeds three times the weekly average of that period, then search for the first week in the 30-day trigger period that exceeds three times the background weekly average.
- If the weekly average and largest daily located earthquake counts are found to be unrepresentative of the time period, another method or calculation may be necessary.

Search the trigger period for deviations from the background averages:

- Search for the first week within the 30-day trigger period that exceeds three times the background weekly average.
  - If a week within the trigger period meets this criterion, find the largest daily earthquake count in that week.
    Augustine: Week of April 14th, six earthquakes, two in one day
- Compare this daily earthquake count to the largest daily earthquake count for the background period.
  - If the daily earthquake count for the trigger period week is less than the largest daily earthquake count for the background period, continue searching for another week that exceeds three times the weekly average and repeat as necessary.
    Augustine: Week of April 28th, nine earthquakes, five in one day
  - If the largest daily earthquake count for the trigger period is greater than or equal to the largest daily earthquake count for the background period, select that date as the start date.
    Augustine: Week of April 28th, nine earthquakes, five in one day (April 30th)
    Start Date: April 30th

Consecutive Days Method

Define a reasonable background rate that is unbiased of previous swarms and annual weather phenomena:

- Calculate the previous calendar year's located earthquakes. Taking the average of an entire year's worth of data should eliminate most seasonal weather affects.
  Augustine: 238 located earthquakes total in 2004

Define a trigger to look for a swarm start date:

- Search for a 30-day period that exceeds 12.5 percent (1/8) of last year's earthquake total.
  Augustine: 238÷8 = 30 earthquakes.Augustine: 4/14/2005-5/12/2005 = 31 earthquakes

If a trigger occurs, calculate the following data in order to define and test what is now taken to be the background seismicity rate:

- Define normal rates of continuous seismicity.
  - What is the longest string of consecutive days during normal activity?
    Augustine: 3 days
  - Find a value of consecutive days that is high, but occurs more than once.
    Augustine: 3 days (this is the longest string and occurs several times)
- Define normal numbers of earthquakes during the continuous seismicity.
  - Tally the highest number of events during these times.
    Augustine: Three earthquakes (in 3 days)
  - How often does this occur?
    Augustine: An average of every 13 days
  - What is the shortest time interval between occurrences?
    Augustine: One day (ranges to 30 days)

Search the trigger period for deviations from the background averages:

If there is a string of days that meets the consecutive day threshold or the events within a time threshold, look for a swarm.

- How many earthquakes are there?
- How does this compare to the normal number of earthquakes in a continuous period?
  Augustine triggers:
  April 14th: Three earthquakes, 3 days,
  Meets threshold
  April 18th: Three earthquakes, 2 days,
  Meets threshold
  ***April 24th: Three earthquakes, 1 day,**
  Meets threshold
  April 30th: Five earthquakes, 1 day,
  Exceeds threshold
  ***This is the shortest time between any three triggers in the background**
- Once a trigger is found that exceeds the threshold, this day (or the beginning of the set) is the swarm start date.

Start Date: April 30th

Appendix 2. Focal Mechanisms

Focal mechanisms were computed for all earthquakes using FPFIT (Reasenberg and Oppenheimer, 1985). Solutions were judged acceptable if they had: a misfit of less than 0.15 (less than 15 percent of stations inconsistent with the preferred solutions), STDR (distribution around the hypocenter) ≥ 0.40, and an average uncertainty in strike, dip, and rake of ≤ 25º. Below are 79 (out of 201) earthquakes that returned acceptable focal mechanisms. There were 19 events (out of 61 picked) with acceptable solutions from 2002 through 2004, and 60 events (out of 140 picked) from the long swarm (all events with acceptable solutions in 2005 occurred during the long swarm). If FPFIT returned two or more solutions for the same earthquake, we have retained the solution with the lowest combination of errors. Mechanisms are arranged with time starting from 2002 and getting later down each column and across each page.

Fault-plane solutions for 79 earthquakes occurring at Augustine volcano from May 24, 2002 to January 6, 2006. P, compressional axis; T, tensional axis. Open circles correspond to dilatational (down) first motions, crosses to compressional (up) first motions. Each solution is coded for date and time (UTC) in this format: YYYYMMDD hhmm. Z, depth, in kilometers; *M*, magnitude.

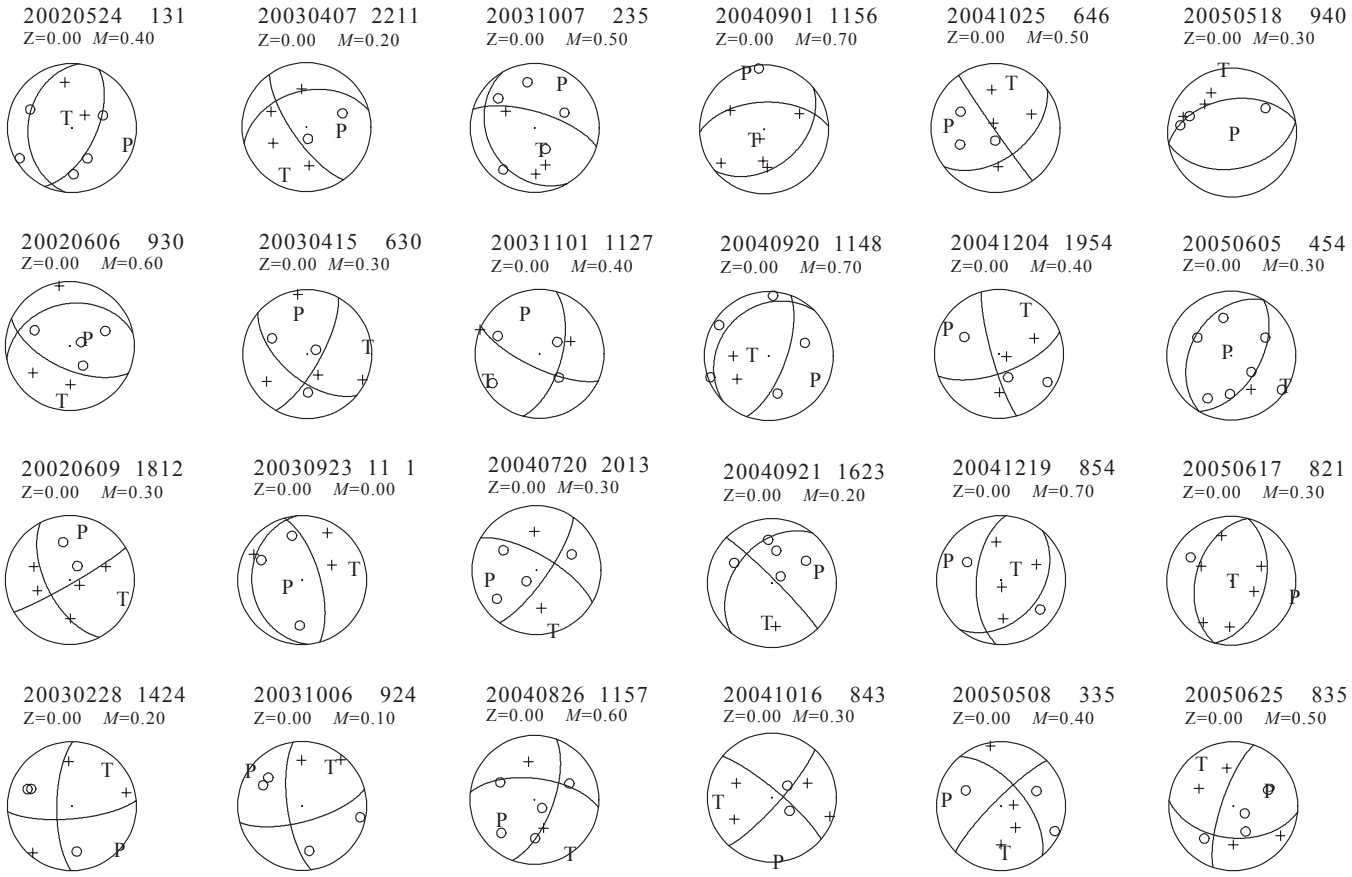

20050811 1732
Z=0.00 *M*=0.30

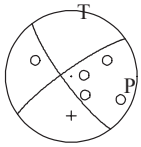

20051005 1329
Z=0.00 *M*=0.60

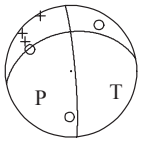

20051130 1047
Z=0.00 *M*=0.40

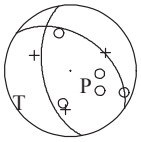

20051211 2358
Z=0.00 *M*=0.50

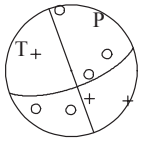

20051219 1126
Z=0.00 *M*=0.40

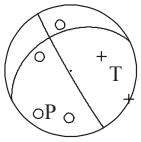

20051224 251
Z=0.00 *M*=1.10

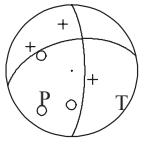

20050828 931
Z=0.00 *M*=0.30

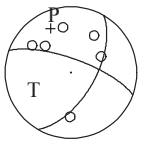

20051030 1939
Z=0.00 *M*=0.40

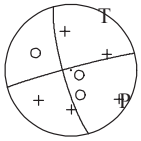

20051130 1639
Z=0.00 *M*=0.30

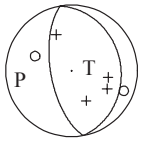

20051215 5 4
Z=0.00 *M*=0.80

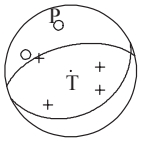

20051221 323
Z=0.00 *M*=0.80

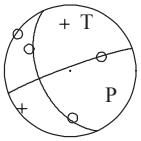

20051224 817
Z= 0.00 *M*=0.60

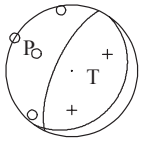

20050919 2046
Z=0.00 *M*=0.60

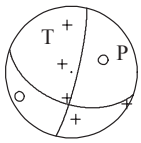

20051115 1740
Z=0.00 *M*=0.40

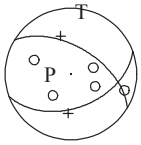

20051202 920
Z=0.00 *M*=0.70

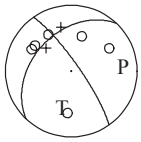

20051217 637
Z=0.00 *M*=0.60

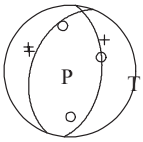

20051221 446
Z=0.00 *M*=0.70

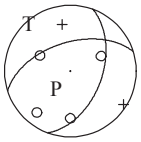

20051224 9 8
Z= 0.00 *M*=0.80

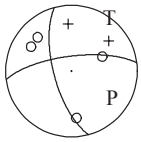

20050919 2051
Z=0.00 *M*=0.90

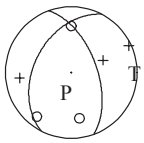

20051127 1821
Z=0.00 *M*=0.40

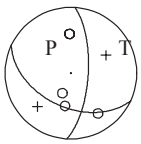

20051208 053
Z= 0.00 *M*=0.50

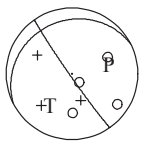

20051217 1149
Z=0.00 *M*=0.30

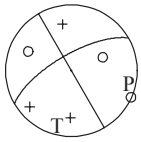

20051221 16 5
Z=0.00 *M*=0.60

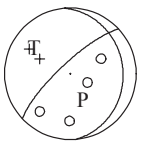

20051222 2241
Z=0.00 *M*=0.60

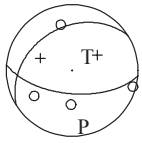

20051004 124
Z=0.00 *M*=0.30

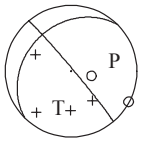

20051129 1641
Z=0.00 *M*=0.30

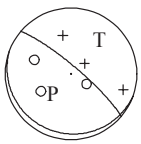

20051211 2222
Z= 0.00 *M*=0.40

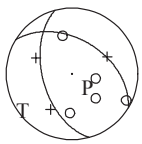

20051219 10 1
Z=0.00 *M*=1.00

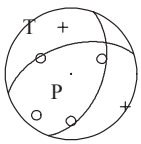

20051224 227
Z=0.00 *M*=0.60

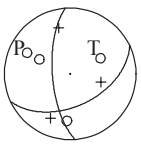

20051222 2242
Z=0.00 *M*=0.80

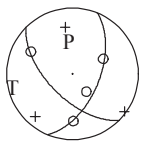

Continued.

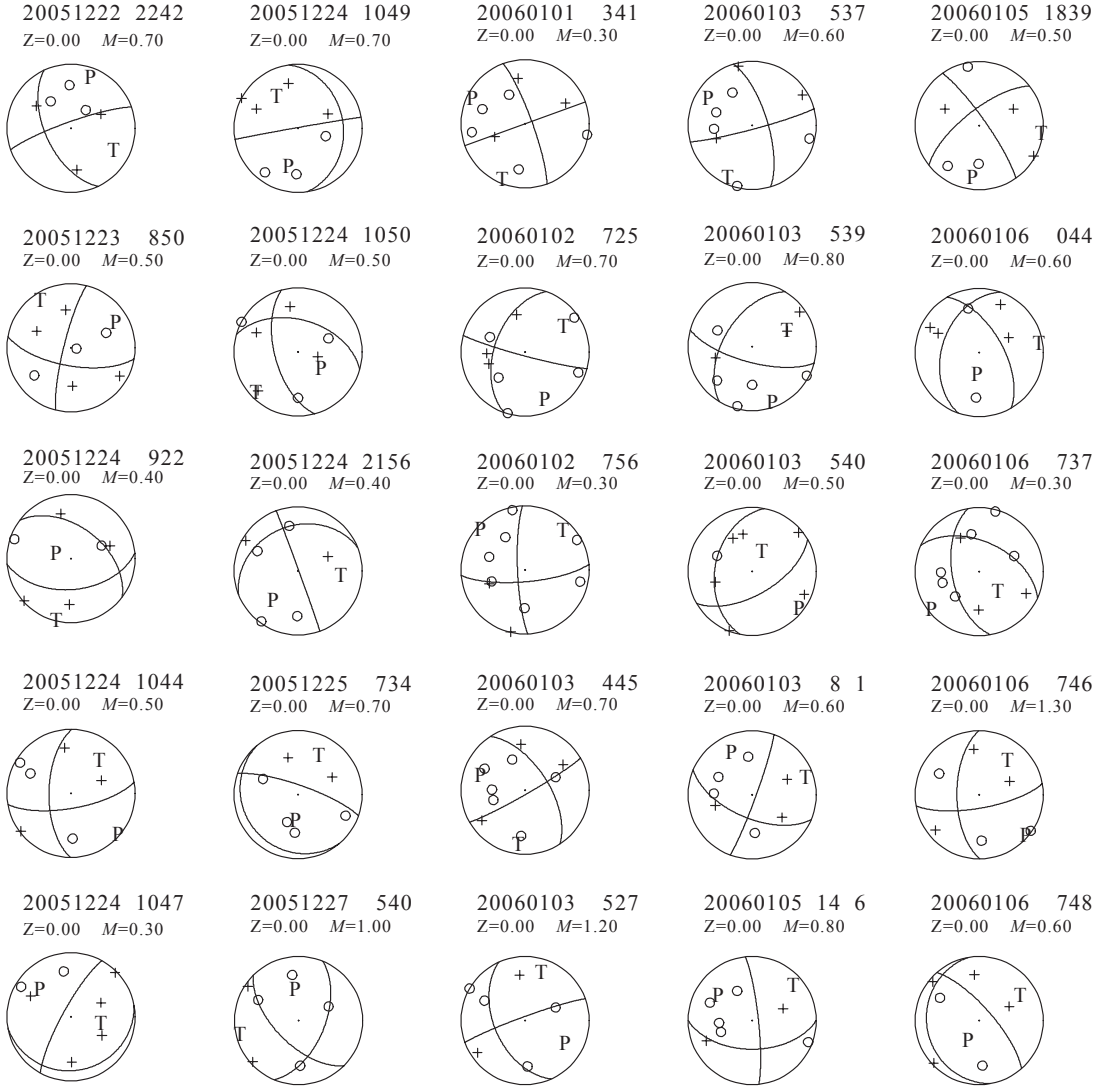
20051222 2242
Z=0.00 M=0.70
20051224 1049
Z=0.00 M=0.70
20060101 341
Z=0.00 M=0.30
20060103 537
Z=0.00 M=0.60
20060105 1839
Z=0.00 M=0.50
20051223 850
Z=0.00 M=0.50
20051224 1050
Z=0.00 M=0.50
20060102 725
Z=0.00 M=0.70
20060103 539
Z=0.00 M=0.80
20060106 044
Z=0.00 M=0.60
20051224 922
Z=0.00 M=0.40
20051224 2156
Z=0.00 M=0.40
20060102 756
Z=0.00 M=0.30
20060103 540
Z=0.00 M=0.50
20060106 737
Z=0.00 M=0.30
20051224 1044
Z=0.00 M=0.50
20051225 734
Z=0.00 M=0.70
20060103 445
Z=0.00 M=0.70
20060103 8 1
Z=0.00 M=0.60
20060106 746
Z=0.00 M=1.30
20051224 1047
Z=0.00 M=0.30
20051227 540
Z=0.00 M=1.00
20060103 527
Z=0.00 M=1.20
20060105 14 6
Z=0.00 M=0.80
20060106 748
Z=0.00 M=0.60

Continued.

This page intentionally left blank

The 2006 Eruption of Augustine Volcano, Alaska
Power, J.A., Coombs, M.L., and Freymueller, J.T., editors
U.S. Geological Survey Professional Paper 1769

Chapter 4

A Parametric Study of the January 2006 Explosive Eruptions of Augustine Volcano, Using Seismic, Infrasonic, and Lightning Data

By Stephen R. McNutt[1], Guy Tytgat[2], Steven A. Estes[1], and Scott D. Stihler[1]

Abstract

A series of 13 explosive eruptions occurred at Augustine Volcano, Alaska, from January 11–28, 2006. Each lasted 2.5 to 19 minutes and produced ash columns 3.8 to 13.5 km above mean sea level. We investigated various parameters to determine systematic trends, including durations, seismic amplitudes, frequency contents, signal characteristics, peak acoustic pressures, ash column heights, lightning occurrence, and lengths of pre-event and post-event quiescence. Individual tephra volumes are not known. There is no clear correlation between acoustic peak pressure and ash column height or between peak seismic amplitude and duration. However, several trends are evident. Two events, January 11 at 0444 AKST (1344 UTC) and January 27 at 2337 AKST (0837 UTC) are short (180 and 140 seconds) and have very impulsive onsets and high acoustic peak pressures of 93 and 105 Pa, as well as high peak seismic amplitudes. We interpret these to be mainly gas releases. Two of the largest events followed quiescent intervals of 3 days or longer: January 17 at 0758 AKST (1658 UTC), and January 27 at 2024 AKST (January 28 at 0524 UTC). These two events had reduced displacements (D_R) of 11.4 and 7.5 cm^2, respectively. Although these D_R values are typical for eruptions with ash columns to 9 to 14 km, most other D_R values of 1.6 to 3.6 cm^2 are low for the 7.0 to 10.5 km ash column heights observed. The combination of short durations, small D_R and high ash columns suggests that these events are highly explosive, in agreement with Vulcanian eruption type. Several events had long durations on individual seismic stations but not on others; we interpret these to represent pyroclastic or other flows passing near the affected stations so that tractions or momentum exchange from the cloud or flow adds energy to the ground only near those stations. The eruption on January 27 at 2024 AKST had more than 300 lightning flashes, whereas the following eruptions on January 28 at 0204 AKST and 0742 AKST had only 28 and 6 lightning flashes. The 2024 AKST eruption had a longer duration (1,180 versus <460 seconds), a higher ash column height (10.5 versus 7.0–7.2 km) and higher acoustic peak pressure (83 versus 66 and 24 Pa). The data suggest that the lightning-rich 2024 AKST eruption produced more tephra than the following eruptions, hence there were more charge carriers injected to the atmosphere. Seismic signals preceded the infrasound signals by 0 to 5 seconds with no obvious pattern in terms of the above groupings. The explosive eruption phase overlapped with the subsequent continuous phase by about 2 days. Parametric data may be useful to estimate eruption conditions in near real time.

Introduction

Following an 8.5-month period of precursory activity, Augustine Volcano began to erupt explosively on January 11, 2006 (Power and others, 2006). A series of 13 strong explosive eruptions occurred over the next 17 days, with most sending ash clouds to elevations of 10 km or more (table 1). New instrumentation added in December 2005 and January 2006 allows for a more comprehensive study of these eruptions than has previously been possible for explosive eruptions in Alaska. In particular, an infrasound pressure sensor located at AUE (fig. 1) recorded all 13 events on scale, temporary broadband seismometers remained on scale and complemented the permanent short-period network, and new lightning detection

[1] Alaska Volcano Observatory, Geophysical Institute, University of Alaska Fairbanks, Fairbanks, AK 99775.

[2] IRIS PASSCAL Instrument Center, New Mexico Tech, 100 East Road, Socorro, NM 87801.

equipment was installed on January 27, 2006, just before the last series of four strong explosive eruptions on January 27–28. This paper presents a systematic study of the 13 explosive eruptions, combining the new data to gain insights into processes contributing to observed variations in the explosivities of the eruptions, including plume heights, amounts of tephra, gas distribution, and electrical properties.

These new data (broadband seismic, infrasound, and lightning) are especially useful because for the 1976 and 1986 eruptions of Augustine Volcano only short-period seismic data were available. The seismic data for 1976 were recorded off island (Power and Lalla, this volume), and for 1986 only short-period data existed (Power, 1988). The short-period stations on the island in 2006 were all saturated (clipped), and several were damaged or destroyed by the eruptions, whereas the broadband stations remained on scale. Distant stations such as OPT (34 km north; fig. 1) remained on scale and provided a basis for comparisons. As will be shown, the new data streams provide many additional constraints on eruptive processes.

The 1976, 1986, and 2006 eruption sequences had remarkably similar precursory stages, which lasted 9, 9, and 8.5 months, respectively (Power and Lalla, this volume). The two previous eruption sequences began with explosive phases lasting 4 and 14 days, followed by effusive phases.

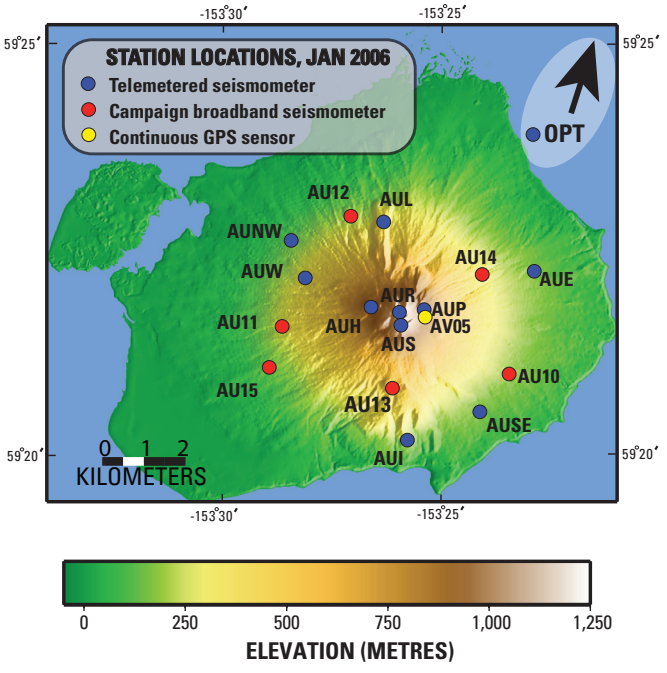

Figure 1. Map of seismic stations on Augustine Island. Stations shown have either short-period or temporary broadband seismometers. AUL has a permanent 3-component broadband station, and AUE has an infrasound sensor. Station OPT is on the Alaska mainland 34 km north of Augustine Volcano. (Image courtesy of H. Buurman.)

This pattern was repeated in 2006; however, the explosive phase lasted 18 days.

Augustine's Vulcanian eruptions are similar to eruptions at other volcanoes including Vulcano, Italy 1888–1890, Ngauruhoe, New Zealand 1975, Galeras, Colombia 1992–1993, Sakurajima, Japan 1985–1990, Asama, Japan 2004, and Montserrat, West Indies 1997 (Morrisey and Mastin, 2000; Ohminato and others, 2006; Druitt and others, 2002). A comparison is given in the discussion section of this paper, following presentation of the Augustine parameters.

Times in this paper are given in local time (Alaska Standard Time or AKST) followed by universal time (UTC) in parentheses where appropriate. At the time of the Augustine eruptions UTC was 9 hours ahead of local time; that is, 1200 (noon) AKST is equivalent to 2100 UTC.

Data and Methods

Seismic Data

The permanent seismic network on Augustine Island consisted of eight short-period stations and one broadband station (AUL; fig. 1). The short-period stations have a natural period of one second and use either Mark Products L4-C or Geotech S-13 vertical seismometers. The permanent broadband station uses a Guralp CMG-40T 3-component seismometer with a natural period of 30 seconds. Analog data from all short-period stations are telemetered to Homer, Alaska, by VHF radio, then by telephone and internet to the University of Alaska Fairbanks Geophysical Institute, where data are digitized at 100 Hz at 12-bit resolution. The broadband station is digitized on site at 100 samples per second and uses digital rather than analog radio telemetry. The permanent network was augmented by the addition of five temporary broadband stations that were recorded on site at 100 samples per second (fig. 1). All the short-period stations on the island were saturated (clipped) for all 13 of the large explosive eruptions. Station OPT, 33 km the north on the Alaskan mainland, is a short-period station that recorded all the events and remained on scale for all but one event (January 27 at 2337 AKST).

Seismic measurements include the duration and reduced displacement (D_R). Duration varies with the individual station used, and the gain, and distance. Because Augustine is a small island, all the local stations are close, within 5 km of the vent. All the short-period stations clipped during each of the 13 explosive eruptions. However, rather than being a problem, this actually afforded a convenient way to measure durations, which were estimated from the length of the continuously clipped (that is, strong) portion of the signal. This was measured from hard copies of seismograms at a standard scale of 600 seconds = 3.4 cm (figs. 2*A* and 2*B*; note the printed scale here is different). Several stations gave virtually identical durations, the most reliable being AUH and AUW. The closer station AUH gave preferred values early in the

Table 1. Parameters of the Augustine Volcano January 11–28, 2006, explosive eruptions.

[AKST, Alaska Standard Time; UTC, Universal Time; D_R, reduced displacement; OPT, Oil Point seismic station; I, impulsive; E, emergent]

Event Number	Date in 2006	Event Onset AKST (UTC)	Type	Pressure, in Pa	Duration: Acoustic, in seconds	Duration: Seismic, in seconds	D_R in cm² OPT	Preceding Quiescence, in days	Number of lightning flashes	Plume Height, in km[1]
1	January 11	0444 (1344)	I	93	25	180	139	---	---	6.5
2	January 11	0512 (1412)	E	14	100	385	1.8	0.02	---	10.2
3	January 13	0424 (1324)	E	22	130	915	7.7	1.97	---	10.2
4	January 13	0847 (1747)	E	35	100	400	2.4	0.18	---	10.2
5	January 13	1122 (2022)	I	32	150	520	2.6	0.11	---	10.5
6	January 13 (January 14)	1640 (0140)	E	29	150	570	3.3	0.22	---	10.5
7	January 13 (January 14)	1858 (0358)	E	52	170	765	1.6	0.09	---	13.5
8	January 14	0014 (0914)	I	65	100	430	3.6	0.23	---	10.2
9	January 17	0758 (1658)	E + I	93	50	410	11.4	3.32	---	13.5
10	January 27 (January 28)	2024 (0524)	E + I	83	250	1180	7.5	10.52	365	10.5
11	January 27 (January 28)	2337 (0837)	I	105	20	140	178	0.13	1	3.8
12	January 28	0204 (1104)	I	66	150	460	2.9	0.10	28	7.2
13	January 28	0742 (1642)	E	24	160	240	2.1	0.24	6	7.0

[1] Schneider and others, 2006.

eruption sequence but was destroyed on January 27 and had to be replaced by others (for example AUE and AUI) using bootstrapping methods to yield durations. Some adjustments were necessary when pyroclastic or other flows (for example, lahars, rockfalls) passed near stations, because these added extra energy to the ground and prolonged the codas at the stations nearest to the flows (figs. 3*A* and 3*B*).

For the 1976 and 1986 eruptions of Augustine Volcano, the stations on the island either were not operational or were mostly clipped (Reeder and Lahr, 1987; Power, 1988). Station OPT, a single-component, 1-second vertical seismometer located 33 km north of the vent, was far enough away that the signals had attenuated and remained on scale. Thus data from OPT are useful for direct comparison between the 1986 and 2006 eruptions. We determined magnitudes for the explosive eruptions using OPT by forcing the origin to be at Augustine's vent and measuring the highest amplitude portion of the signal. The maximum values obtained were M_L=2.3 and 2.6, which agree well with the largest events during the 1976 eruption, which were M_L=2.3, although these were considered to be earthquakes occurring simultaneously with large tremors and were recorded at station CKK, 82 km to the northwest (Reeder and Lahr, 1987). The 2006 M_L values were then converted to D_R; both are measures of ground motion that use the same seismic measurements but different normalizations. D_R is peak-to-peak root mean square displacement multiplied by the square root of wavelength times distance (Fehler, 1983). For the 2006 events, we assumed surface wave propagation using

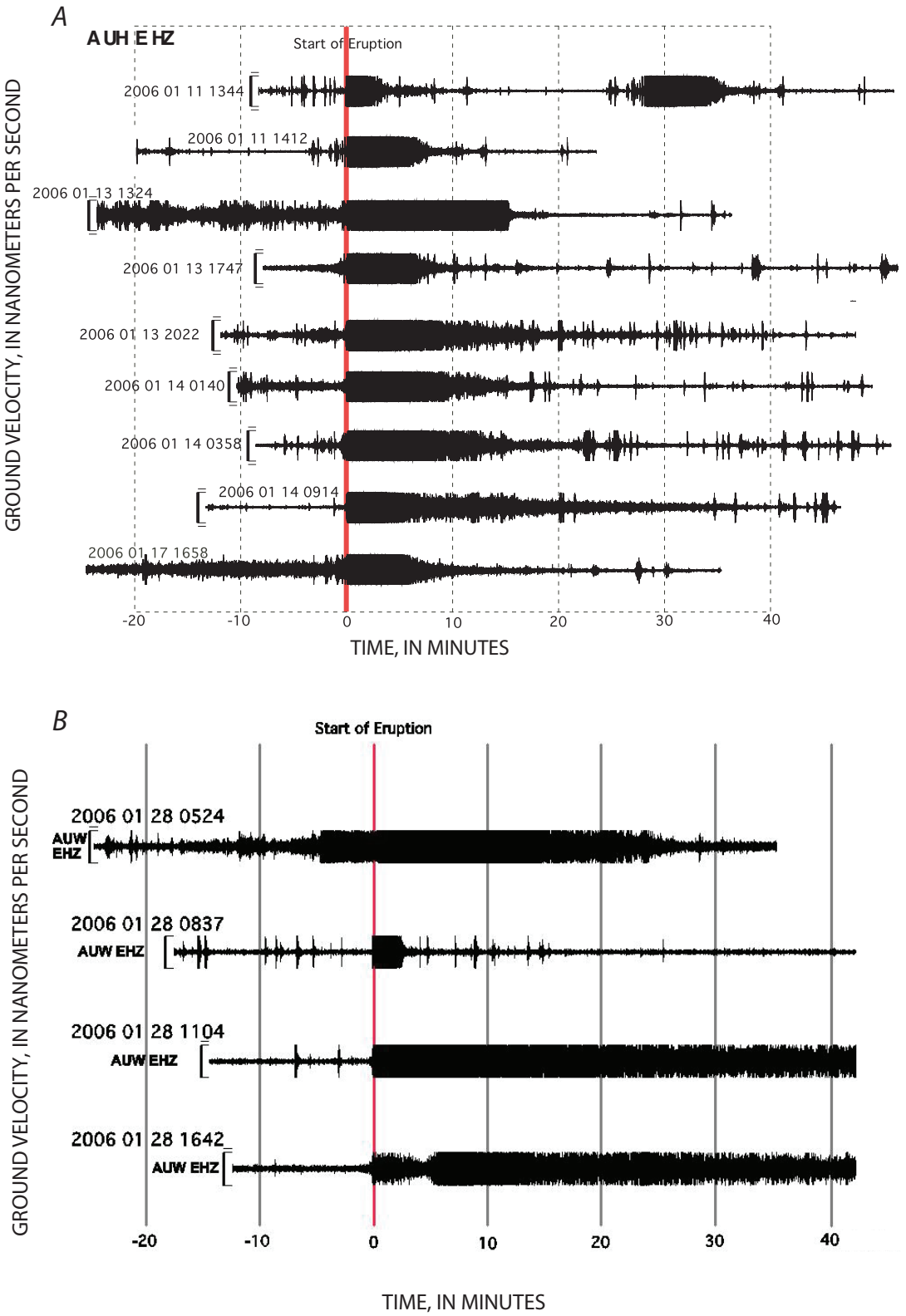

Figure 2. *A*, Seismograms (unfiltered) for the first 9 of 13 large explosive eruptions at Augustine Volcano in 2006. Data are from station AUH, which was destroyed on January 28, 2006. One hour of data is shown and the seismograms are aligned on the beginning of each explosive eruption. The durations of the clipped portion of the seismograms range from 3 to 15 minutes. *B*, Seismograms of the last 4 explosive eruptions. Data are from station AUW. Other features are as in part *A*. Time convention is YYYY MM DD HHMM. Times in UTC.

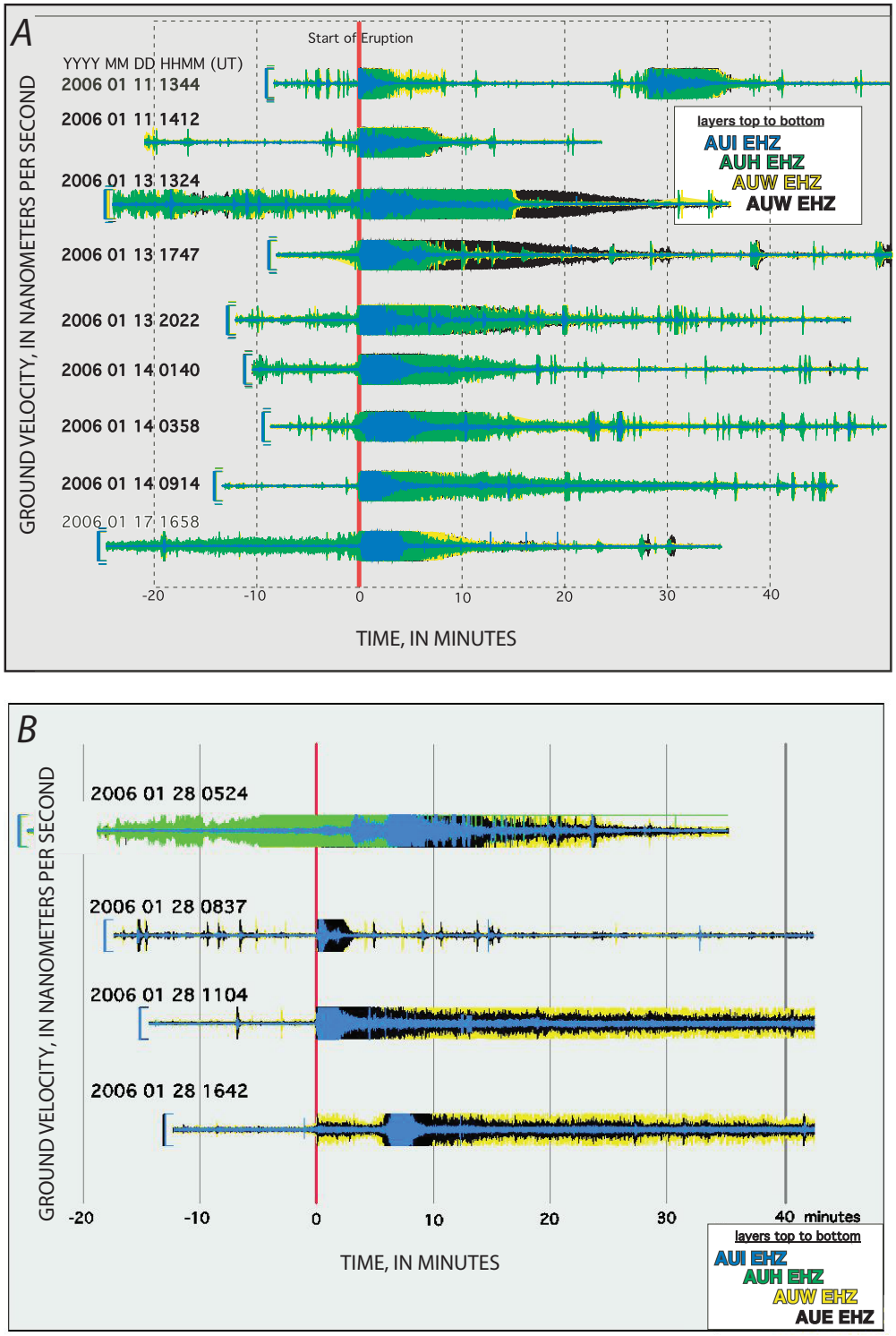

Figure 3. *A*, Overlaid seismograms for four stations (AUI, AUH, AUW, and AUE) on Augustine Island. Data are aligned on the beginning of each explosive eruption. Note that the codas for events 3 and 4 are much longer on station AUE than for the other stations, suggesting that pyroclastic or other flows passed near that station. *B*, Seismograms for four stations (AUI, AUH, AUE, and AUW) overlaid. Note that the colors and tiling are different than part A to better show the relative features of the different seismograms. Station AUH was destroyed during event 10 (top trace). EHZ is a code representing short-period seismic stations.

the same formulation, adjusted for differences in frequency content, as was used for the 1976 events to compare them with worldwide data (McNutt, 1994). The D_R values for the 2006 events are shown in table 1.

The D_R values computed here are systematically lower than those determined by van Manen and others (this volume). There are several reasons for this. Van Manen and others (this volume) used broadband stations on the island at close distances. Note that D_R corrects for geometrical spreading but does not correct for attenuation, so stations at distances of a few tens of km such as OPT generally give lower values than close stations. A clear example of this effect was observed for Pavlof Volcano (McNutt and others, 1991). A second effect is the choice of surface waves. Particle motions at many volcanoes show surface waves to be the most common component of tremor, so surface waves were assumed for Augustine Volcano. Further, the velocity of the high-amplitude portion of the signal at OPT is about 2 km/second, a value typical for surface waves. For the nearby broadband stations body waves may be more appropriate. Body waves always return higher values for D_R because of the way the formulations are set up (Fehler, 1983). A third factor is the narrow bandwidth of the short-period seismometer at station OPT; relatively high amplitude but very low frequency waves would not be visible. Finally, near-field terms may exist in the broadband data, which can be large near the source. Such waves would not appear in the OPT data. All these effects can give rise to quite different values for attempts to measure the same quantity using different stations. Because the purpose here is partly comparison with the previous eruptions, we used station OPT data as described above. The choice of other data may be more suitable for other purposes.

Broadband waveforms for all 13 explosive eruptions are shown in fig. 4*B* for temporary station AU14 (fig. 1). All seismograms are plotted at the same scale and the events are aligned on the start time to facilitate comparison.

Infrasound Data

A Chaparral Model 2.1 microphone was installed at AUE in early January 2006, and data were telemetered in the same manner as seismic data. This site has a direct distance of 3.2 km to Augustine Volcano's active vent (fig. 1). The laboratory calibrated pressure transducer system, consisting of the microphone, a voltage controlled oscillator (VCO) and a discriminator, has a flat response between 0.1 and 50 Hz and a linear response to pressures above 100 Pa. Both high-gain and low-gain channels were operated, with sensitivities of 0.171 and 0.0084 V/Pa, respectively (Petersen and others, 2006). The low gain channel remained on scale for all the explosive eruptions; peak values ranged from 14 to 105 Pa and are shown in table 1. A noise reduction system, consisting of eight microporous hoses spread out over a half circle, is connected to the microphone. Twelve of the large explosive eruptions were also recorded on the I53US infrasound array in Fairbanks, Alaska, 675 km north of Augustine (Olson and others, 2006). However, because atmospheric conditions varied so widely, it is not possible to use the I53US observations for comparative study of source processes (Olson and others, 2006). Thus, the discussion in this paper is mainly limited to the data from the local sensor, whose close distance of 3.2 km minimizes propagation effects.

For the infrasound data from station AUE (fig. 4*A*), durations were measured from the event onset to decay to the background (Petersen and others, 2006). These varied from 25 to 250 seconds (table 1). All the explosive eruptions remained on scale on the low gain channel, so maximum 0-peak (excess) pressures were measured directly from the waveforms. After the first event at 0444 AKST on January 11, with 93 Pa, the next ten events showed gradually increasing pressures from 14 Pa up to the maximum of 105 Pa at 2337 AKST on January 27 (Petersen and others, 2006). The next two events had lower pressures of 66 and 24 Pa and were followed by a continuous phase consisting of explosions with low pressures of 0.5 to 1 Pa occurring every few minutes for several days. These were only visible on the high-gain channel. Reduced pressures (Johnson 2000) may be obtained by multiplying the pressures by the distance to station AUE, which is 3.2 km. Only the 13 large explosions from January 11 to January 28 are considered in detail in this paper.

Infrasound waveforms for all 13 explosive eruptions are shown in fig. 4*A* for station AUE low-gain channel (fig. 1). All acoustigrams are plotted at the same scale and the events are aligned on the start time to facilitate comparison.

Lightning Data

Two New Mexico Tech Lightning Mapping Array (LMA) lightning detection stations were installed on January 27, 2006, in Homer and Anchor Point, 100 km east of Augustine Volcano (Thomas and others, 2007; Thomas and others, this volume). The stations record time of arrival of electromagnetic radiation in the unused channel 3 TV band (63 MHz) and constitute a minimal network capable of determining the azimuthal direction of impulsive radio emissions from electrical discharges (Thomas and others, 2004). The lightning stations detected both continuous electrical disturbances and lightning flashes in association with the last four explosive eruptions on January 27–28 (table 1) and with four stronger pulses on January 29–30 during the continuous phase. For the earlier eruptions (January 11–17), qualitative lightning reports were obtained from airline pilots, and two eruptions had data recorded by Bureau of Land Management (BLM) stations (Thomas and others, this volume).

The LMA stations recorded two main types of activity: lightning flashes and continuous electrical disturbances at the time of most vigorous eruption. We counted the number of discrete flashes associated with each of the eruptions on January 27–28 (table 1) and also measured the duration and peak radiated power of the continuous signals (Thomas and

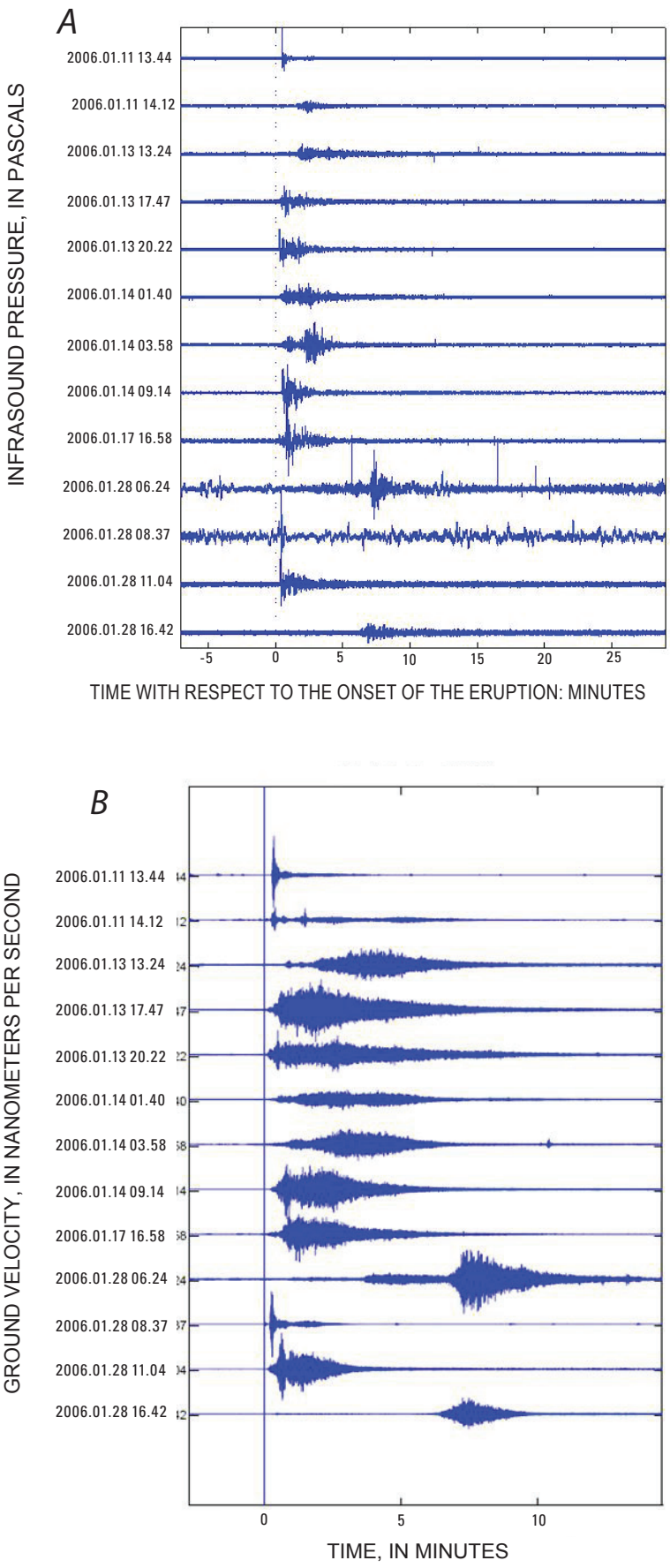

Figure 4. *A*, Acoustigrams of the 13 large explosive eruptions at Augustine Volcano in 2006. Data are from station AUE BDL (low gain). Thirty minutes of data are shown and the acoustigrams are aligned on the beginning of each explosive eruption (vertical dotted line). The durations of the strong portions of the signals range from 20 to 250 seconds. *B*, Seismograms of the 13 large explosive eruptions. Data are from broadband seismic station AU14 HHZ (vertical). Other features are as in part *A*. Times shown at left are UTC.

others, this volume). Because the lightning data were available only for the last four explosive eruptions, we can make only a few general conclusions about lightning.

Plume Heights and Quiescence Data

Two other parameters of interest are plume heights and the durations of preceding quiescence. Plume heights were determined from ground-based Nexrad Doppler radar measurements (Schneider and others, 2006) using data provided by the National Weather Service (NWS). Errors are discussed by Wallace and others (this volume). Resulting plume heights are shown in table 1. This method may not detect the diluted, uppermost parts of the plumes because the radar is tuned to see millimeter to centimeter sized particles; however, it provides an approximation that is consistent throughout the explosive eruption sequence. We measured the time interval between the start times of the events and show this in table 1 under the column labeled "preceding quiescence."

Results

This study compiles a set of measured parameters to describe and systematically compare the eruptions of Augustine Volcano in 2006. Once the parameters were measured, it became immediately obvious that the eruptions were not all the same, and that they fell into several clear groups. These are described and interpreted in this section. The infrasound pressure and D_R are shown in time sequence in figure 5. Because some of the explosive eruptions occurred closely spaced in time, the data appear bunched and are difficult to interpret. Thus, the same data are displayed in index order in figure 6. A comparison of the two figures allows for a complementary view of the data trends.

Short Strong Eruptions

The two shortest events were also two of the three events with the highest infrasound pressures and the two highest seismic amplitudes (table 1; figs. 4*A* and 4*B*). These were the first event on January 11 at 0444 AKST (event 1) and the January 27 event at 2337 AKST (event 11). These were quite short acoustically, only 20 to 25 seconds, whereas seismically they lasted 140 to 180 seconds. The periods of the highest amplitude seismic waveforms at OPT for each event were greater than 1 second each, longer than for any of the other events (the event at 0204 AKST on January 28 also had a long-period pulse near the onset, but this was not the highest amplitude pulse). Both events were very impulsive, with the initial pulse accounting for about 60 percent of the total energy of each event. Cumulative energy plots were used to make this estimate, as shown in figure 3 of Petersen and others (2006). Because they were strong, D_R=139 and 179 cm^2 (equivalent to M_L=2.25 and 2.55; both are measures of amplitude) one might suggest they were in some way the "biggest" of the eruptions. However, these two events appear to have produced the least amount of tephra. Event 11 had a plume only 3.8 km high that quickly dissipated, and event 1 mainly blew out old rock as it reamed out the vent. Its ash plume was the second smallest at 6.5 km high (Schneider and others, 2006). Photographs taken after the January 11 eruptions revealed small deposits near the summit and a few mixed avalanches or lahars. Observations and samples analyzed by Vallance and others (this volume), Wallace and others (this volume), and Coombs and others (this volume) suggest that little or no juvenile material was present in deposits from the January 11 eruptions. Taken together these observations suggest that these eruptions were gas rich and mainly erupted a large gas pocket or equivalent collection of gas charged magma.

Eruptions Preceded by 3 or More Days of Quiescence

Two of the eruptions followed inter-event quiescent periods of 3 days or more: January 17 at 0758 AKST (event 9) and January 27 at 2024 AKST (event 10). Both eruptions destroyed or partially destroyed new domes that had been emplaced during these quiescent intervals. The domes consisted of magma that had sat on the surface for some time and therefore lost much of its gas, forming a temporary plug. The new eruptions then pushed this material out of the way. Seismic data show that these two eruptions each had emergent onsets followed shortly by impulsive phases (Petersen and others, 2006; figure 4*A*); we suggest that the emergent part of the pressure record represents mostly old dome material being pushed out (gas poor) and that the impulsive phase of the pressure record represents the venting of a gas-rich parcel of magma that was previously

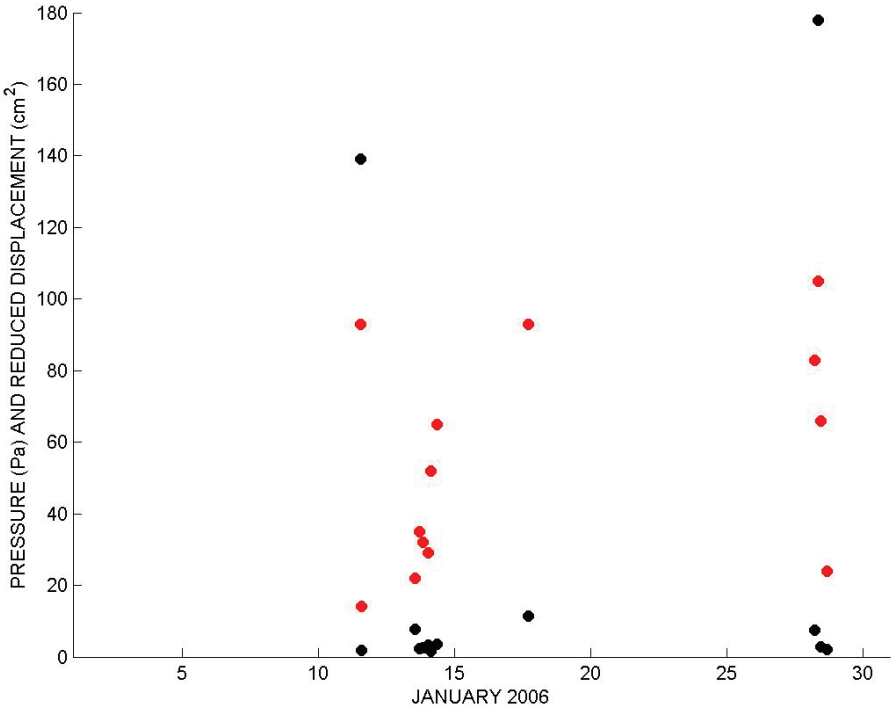

Figure 5. Acoustic peak pressure in Pa (red circles) and seismic reduced displacement in cm^2 (black circles) as a function of time for the 13 large explosive eruptions at Augustine Volcano in 2006.

beneath the dome. The eruptions produced the 3rd and 5th highest seismic amplitudes, the 2nd and 4th highest infrasound pressures (table 1; figs. 4*A* and 4*B*), and appear to be the two largest eruptions in terms of tephra production. The January 17 event was the only individual event to deposit significant tephra on land to the northwest of Cook Inlet, and the January 27 event produced a large pyroclastic flow, the Rocky Point flow (Coombs and others, this volume).

Low D_R but High Ash Column

Many of the eruptions shared the following characteristics: small D_R (1.6 to 3.6 cm^2), moderate infrasound pressures (14 to 66 Pa), a short time interval after the previous eruption (0.5 to 5.5 hours) and generally emergent signals on both seismic and infrasound data (table 1). These are the second event on January 11 at 0512 AKST (event 2), most of the events on January 13 and 14 (events 3 through 8) and the last two on January 28 (events 12 and 13). These events all had moderate durations of 100 to 170 seconds acoustically and 240 to 915 seconds seismically. Six of nine were emergent acoustically as determined by Petersen and others (2006), and the other three began with a weak impulsive phase that represented only about 15 percent of the total energy. The emergent character and moderate durations suggest that the gases are rather uniformly distributed in each batch of magma, so that the eruption is more of an intense "fizz" than a "pop." The data suggest that these are the most typical explosive eruption events and are most characteristic of the Vulcanian eruption style. The seismic and acoustic waveforms show some variation (figs. 4*A* and 4*B*), suggesting that although the events are similar, they are not identical to each other. Volcanic Explosivity Index (VEI; Newhall and Self, 1982) values of 2 to 3 would characterize these events, for which the plume heights were 7.0 to 13.5 km, but the volumes were small (<2 × 10^6 m^3, Coombs and others, this volume). Preliminary acoustic modeling by Fernandes and others (2007) suggests exit velocities of 50 to 300 m/second and volume flux rates of 10^3 to 10^4 m^3/second.

Lightning and Duration

The four eruptions on January 27–28 differed dramatically in their electrical activity. The first produced 365 lightning flashes, the second 1 flash, and the next two 28 and 6 flashes (table 1). The ash plume heights were similar for events 10, 12, and 13, whereas the plume for event 11 was the smallest of any of the explosive eruptions. This was also the event with the highest infrasound pressure. These observations can be reconciled by inferring that event 11 was mostly gas with very little tephra, an inference confirmed by radar observations (Schneider and others, 2006). Of the other

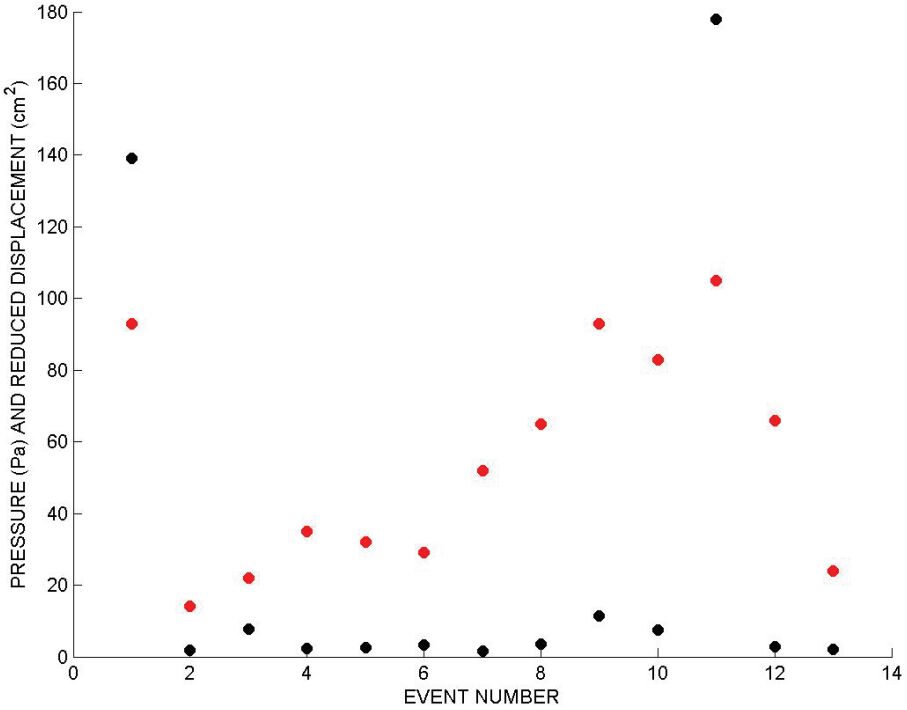

Figure 6. Acoustic peak pressure in Pa (red symbols) and seismic reduced displacement in cm^2 (black symbols) in index order for the 13 large explosive eruptions at Augustine Volcano in 2006.

parameters listed in table 1, the one that stands out as having the most direct correlation with the amount of lightning is the duration. This suggests that the tephra production is positively correlated with the duration, assuming that eruptions rates are similar. It also implies that the amount of tephra is proportional to the amount of lightning. The basic idea is that each tephra particle is a potential charge carrier, so the more particles, the higher total charge and greater potential to produce lightning. A detailed discussion of the lightning observations is given by Thomas and others (this volume).

End of Explosive Phase

An event that began on January 28 at 1430 AKST appears to be a transition event (fig. 7) between the period of discrete, moderate-large explosive events to nearly continuous, smaller explosions. It had smaller peak pressure (9 Pa) than any of the 13 explosive events and lasted much longer, about 1 hour 45 minutes compared to 15 minutes or less for the explosive events. After the transition event quiescence was observed for 6 hours, then at 1617 AKST on January 29 a series of small explosions (0.5 to 1 Pa) began to occur every few minutes for the next several days (fig. 7). A similar figure showing seismic data from station AU13 is given by Power and Lalla (this volume). Volcanic ash was observed in the air almost continuously starting at 1430 AKST on January 28 (Schneider and others, 2006) and lasting until February 2; this phase of the eruption is termed the continuous phase (Power and Lalla, this volume; Coombs and others, this volume). The continuous phase was punctuated by three larger events at 1119 AKST on January 29 (infrasound 13 Pa), and at 0328 AKST (13 Pa) and 0622 AKST (4.4 Pa) on January 30. These had durations of several minutes each and were accompanied by lightning (Thomas and others, this volume) but were all significantly smaller than all but one of the 13 numbered explosions. One may consider these events to be relatively large bursts of activity within the continuous phase. An alternative explanation is that these events were instead explosive eruptions (similar to the 13 numbered events), hence there was overlap rather than a clear separation between the explosive and continuous phases of the eruption.

Events Producing Pyroclastic Flows

Several of the 13 large explosive eruptions showed seismic evidence for the occurrence of pyroclastic or other flows, such as lahars or debris avalanches. These deposits have been described and mapped by Coombs and others (this volume) and Vallance and others (this volume). As shown in figure 3*A*, the events at 0424 AKST and 0847 AKST on January 13 had unusually long codas at station AUE (fig. 1). This suggests a primary part of the signal from the vent that appears on all stations, as well as a secondary part caused by pyroclastic material falling out of the cloud and transferring momentum to the ground near specific stations along the pyroclastic flow path, AUE in this case. Alternatively the extended codas may represent lahars, mixed avalanches, or other flow events that passed near the affected station, with tractions at their bases transferring seismic energy into the ground. Thus, the data suggest that the 0424 AKST and 0847 AKST eruptions (events 3 and 4) were accompanied by pyroclastic flows traveling to the east. Events 1, 9, and 10 showed slightly extended codas for station AUW (fig. 1) to the west, suggesting weak pyroclastic flows traveling to the west (figs. 3*A* and 3*B*). The last two events, numbers 12 and 13, had very long extended codas on station AUW (fig. 3*B*), suggesting sustained pyroclastic flows traveling to the west. The parameters concerning pyroclastic flows are summarized in table 2.

We also checked broadband data and radar data to confirm and to further elucidate these findings. The broadband data did not clip, so instead we see the primary signal from the eruption, followed by relative quiescence, and then an increase in signal level a few minutes later as the pyroclastic flow material applies tractions or transfers momentum near a particular station. The overall principle is the same, but the signals look different on the broadband stations as compared with the short-period stations. The broadband station parameters are also given in table 2. An example of the broadband data is shown in figure 8 for event 8. Here station AU12 (second from the top) shows a second signal pulse between 700 and 900 seconds that does not appear on other stations. This suggests that a pyroclastic or other flow travelled to the north-northwest (see fig. 1 for station locations). Coombs and others (this volume) and Vallance and others (this volume) used similar criteria, as well as spectrograms, to determine which eruptions produced various flow units. Some spectrograms showed higher frequencies for nearby flow events, in contrast to the lower frequencies of the more distant primary explosions. Similar observations were made by Zobin and others (2009) for Colima Volcano, Mexico.

Seismic and Infrasound Origin Times

The event times for the 13 explosive eruptions were assigned to the nearest minute based only on seismic data during the eruption response, mainly as a way to identify and keep track of the separate eruptions. Here we perform retrospective analyses of the origin times using both seismic and infrasound data. The measurements were made for the onset of seismic clipping to the nearest second on station AUH, AUE, or AUW (fig. 1). These are systematically late by about 1 second (the typical time from the onset to clipping), but the signal preceding the explosive eruptions was often contaminated by small earthquakes so the absolute onsets could not be uniformly determined. The acoustic onsets to the nearest second were determined by Petersen and others (2006) for station AUE BDL. Acoustic times for some subevents were determined by the authors. The seismic travel time is a few tenths of a second to station AUH because of the close distance of about 700 m, and assumed

to be 1 second for AUE and AUW. The acoustic travel time is determined to be 10 seconds from detailed analysis of the 2337 AKST event on January 27, which had a very impulsive acoustic onset and also continuous electrical activity which began abruptly at the same time as the acoustic origin time (Thomas and others, this volume). Thus, we determined both seismic and acoustic origin times. These were generally not the same; a comparison (table 3) shows that they differ by 0 to 5 seconds, with the seismic origin time always earlier than the acoustic one. The time difference may be interpreted as a proxy for depth or as the time interval over which the final preeruptive processes occur. The measured time differences do not agree well with the groupings of events as given above (for example, short strong eruptions), although events 1 and 11 both share a seismic versus acoustic time difference of 4 seconds. Of the two events that followed quiescence (events 9 and 10), event 9 had a time difference of 0 seconds, which we interpret to represent an explosive source

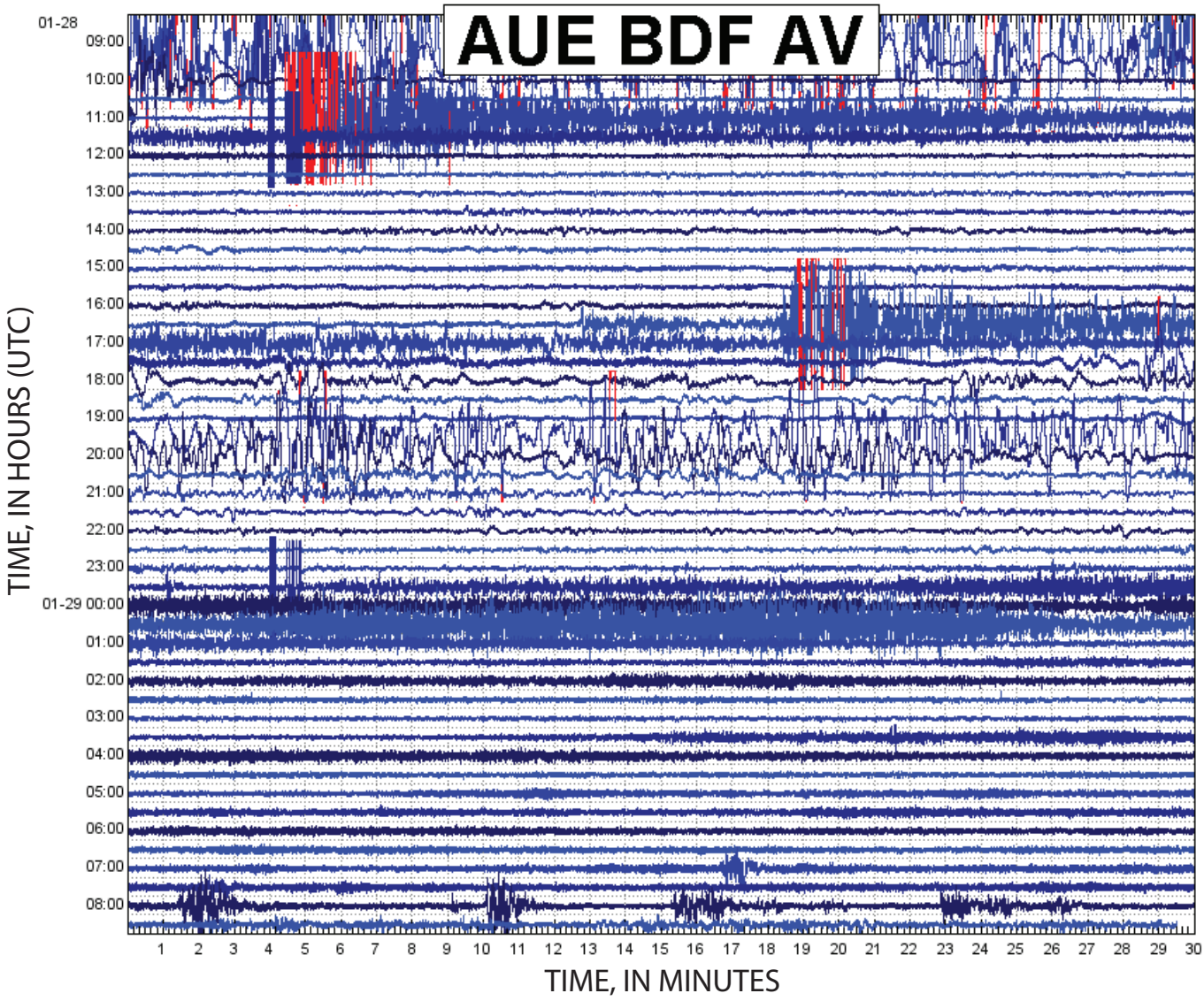

Figure 7. Acoustigram for eruptions at Augustine Volcano on January 28–29, 2006. Twenty-four hours of data are shown for acoustic station AUE BDF (high gain). Each line is 30 minutes. Events 12 (1104 UTC) and 13 (1642 and 1648 UTC) show partially clipped data in red and have codas about 45 minutes long. The event at 2330 UTC is a transitional event that lasts about 2 hours. Starting at 0717 UTC on January 29 are small discrete events occurring every few minutes that were characteristic of the continuous phase of the eruption (Coombs and others, this volume). Strong wind noise occurs from 0900 to 1000 UTC and from 1930 to 2030 UTC. AV is a code for stations maintained by the Alaska Volcano Observatory.

Table 2. Parameters of Augustine Volcano January 11–28, 2006, explosive eruptions showing evidence for pyroclastic flows.

[AKST, Alaska Standard Time; PF, pyroclastic flow; AUW, AU14, and others are seismic stations codes]

Event Number	Date in 2006	Event Onset AKST	Long Coda	Broadband Delayed Pulse	Seismic Station Destroyed	Interpretation
1	January 11	0444	AUW	---		Possible mixed avalanches
2	January 11	0512	---	---		---
3	January 13	0424	AUE	AU14	AUP	PF East
4	January 13	0847	AUE	AU12, AU13		PF East, North, South
5	January 13	1122	---	AU12		PF North
6	January 13	1640	---	AU14		PF East
7	January 13	1858	---	AU12		PF North
8	January 14	0014	---	AU12		PF North
9	January 17	0758	AUE, AUW	AU12, AU15		PF North, East, West, Southwest
10	January 27	2024	AUW	AU15	AUL, AUH	PF West, Southwest, North
11	January 27	2337	---	---		---
12	January 28	0204	AUW	---		PF West
13	January 28	0742	AUW	---		PF West

right at the surface, where the time difference for event 10 could not be determined because the seismic traces were already clipped when the largest phase occurred (table 3). The time differences for the largest group of events, characterized by low D_R and high ash columns (events 2, 3, 4, 5, 6, 7, 8, 12, and 13), spanned the range from 0 to 5 seconds. We note that all the events with a 5 second time difference fell in this group. The large time difference suggests a systematically deeper source or a prolonged initiation process for that group of explosive eruptions.

Discussion

The results, which divide the explosive eruptions into several groups based on common parameters, require a conceptual model of gas storage and release to explain the observations. An example of such a conceptual model is the schematic diagram shown in figure 9. The basic idea is that initially gases are uniformly distributed in the magma at depth. If the magma ascends relatively quickly, the gases remain uniformly distributed at the time of eruption (fig. 9*A*). The resulting eruption would then be expected to have an emergent onset and rather steady gas release throughout. This corresponds to the cases above with low D_R but high ash columns. A second scenario would be slow ascent of magma into a "leaky" system, so that most of the gases escape to the surroundings (fig. 9*B*). This is the scenario corresponding to the eruptions that follow three or more days of quiescence, and the domes that formed represent the accumulation of degassed magma. The third situation is the coalescence of gas into a large irregular pocket or a zone of gas charged magma (fig. 9*C*). This requires slow ascent of magma under sealed conditions so that the gas collects rather than escaping to the surroundings. The resulting eruption would be gas rich (or ash poor) and likely impulsive if the gas pocket ruptures quickly. The short strong eruptions correspond to this case.

This conceptual scheme allows us to use the eruption styles to "map" the pattern of gas distribution or storage underground for the times just before eruptions. Obviously this is a gross simplification; however, the basic elements are straightforward. The conceptual scheme also has testable elements: the deposits resulting from the eruptions may contain textural or other evidence to support the gas distribution hypotheses (Larsen and others, this volume; Coombs and others, this volume; Vallance and others, this volume). A diagram of the pre-eruption gas distribution based on the above scheme is shown in figure 10.

One major data gap is that we do not have high-quality measurements of the volumes of tephra for the various individual eruptions. Augustine is an island, so much of the fall deposits fell in the sea. Only the eruption on January 17

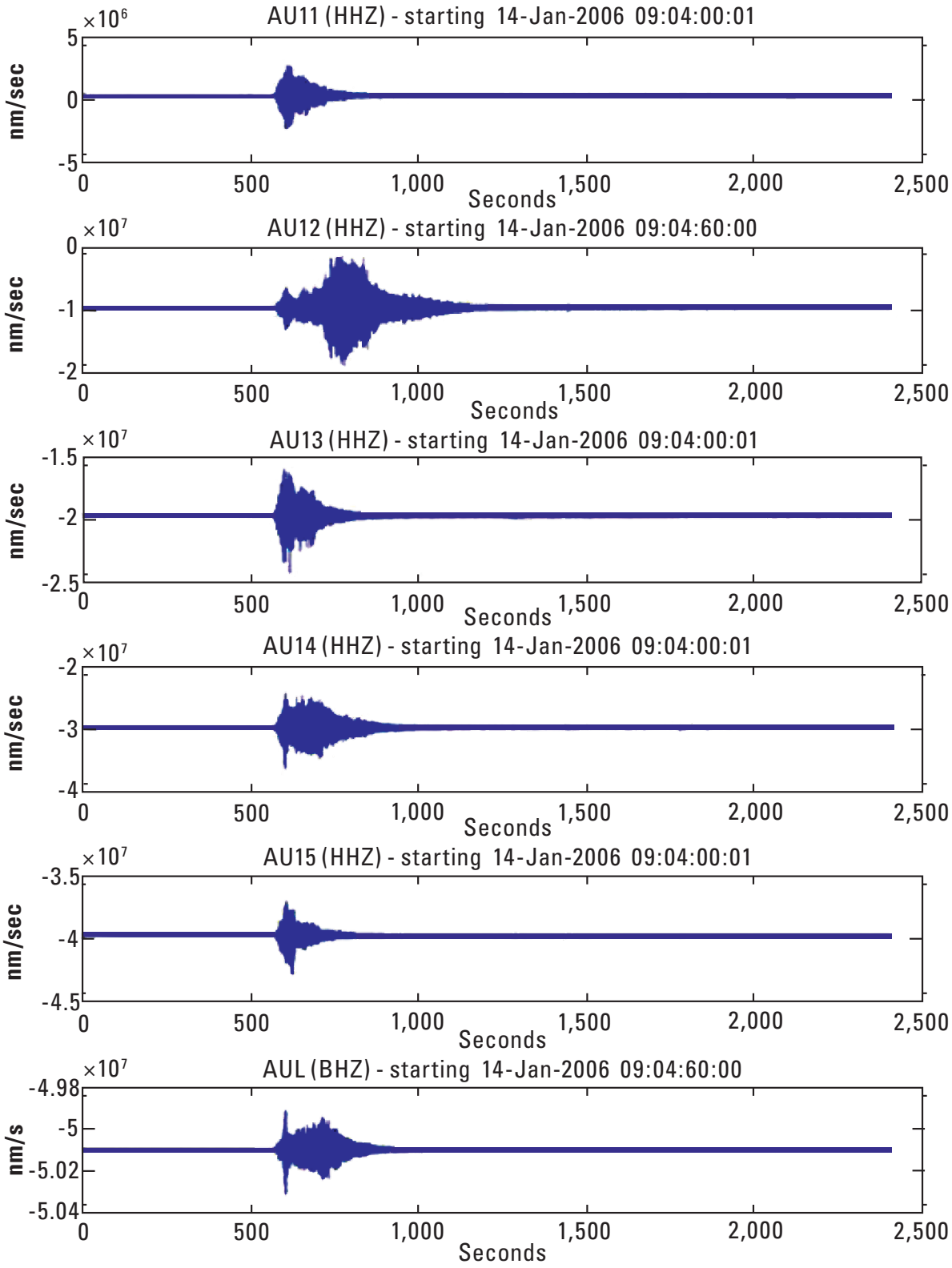

Figure 8. Broadband seismograms from all available stations for Augustine Volcano's January 14, 2006, explosive eruption at 0914 UTC (event 8). Data from the vertical component are shown. Note that the initial part of each trace is similar but that station AU12 (second from the top) shows a strong pulse from 700 to 900 seconds. This is interpreted to represent a pyroclastic flow or other flow event passing near that station only.

Table 3. Timing of seismic and infrasound onsets of Augustine Volcano January 11–28, 2006, explosive eruptions.

[AKST, Alaska Standard Time]

Event Number	Date in 2006	Event Onset AKST	Seismic Onset[1] AKST	Acoustic Onset[2] AKST	Seismic Origin Time[3] AKST	Acoustic Origin Time[4] AKST	Time Difference Seconds	Seismic Station Used
1	January 11	04:44	04:44:40	04:44:55	04:44:40	04:44:45	4	AUH
2	January 11	05:12	05:14:13	05:14:24	05:14:13	05:14:14	2	AUE
3	January 13	04:24	04:24:15	04:24:30	04:24:15	04:24:20	5	AUH
4	January 13	08:47	08:48:14	08:48:25	08:48:14	08:48:15	2	AUE
5	January 13	11:22	11:22:07	11:22:15	11:22:07	11:22:05	1	AUE
6	January 13	16:40	16:40:28	16:40:38	16:40:28	16:40:28	0	AUH
7	January 13	18:58	18:58:02	18:58:17	18:58:02	18:58:07	5	AUH[5]
8	January 14	00:14	00:13:22	00:13:37	00:13:22	00:13:27	5	AUH
9	January 17	07:58	07:58:19	07:58:28	07:58:18	07:58:18	0	AUE
10	January 27	[20:19][6]	20:19:45	---	---	---	---	AUH
		20:24	20:24:49	---	---	---	---	AUH
		[20:27]	20:27:42	---	---	---	---	AUE
		[20:31]	---[7]	20:31:05	---	20:30:55	---	---
11	January 27	23:37	23:37:34	23:37:47	23:37:33	23:37:37	4	AUE
12	January 28	02:04	02:04:15	02:04:26	02:04:14	02:04:16	2	AUE
13	January 28	07:42	07:42:29	07:42:43	07:42:28	07:42:33	5	AUE
		[07:48]	07:48:12	07:48:24	07:48:11	07:48:14	3	AUW

[1] Time of seismic trace clipping continuously.

[2] Acoustic onset time from Petersen and others, 2006.

[3] Seismic origin time assuming v = 3 km/sec (1 sec difference at AUE).

[4] Acoustic origin time assuming v = 320 m/sec (10 sec difference at AUE).

[5] Not clipped but significant pulse.

[6] Brackets [ ] indicate onset times of subevents.

[7] Seismic traces were already clipped so onsets could not be determined.

(event 9) produced a significant deposit on land (West side of Cook Inlet; Wallace and others, this volume) that could be measured sufficiently well to make volume estimates. The volume for this event, about 2 x 10^6 m^3, was then extrapolated from geologic data to make estimates of the total volume of tephra for all the eruptions. However, caution should be used in using extrapolated values because the variance is unknown. Another factor that is poorly known is the vent size and shape. Coombs and others (this volume) estimated the vent dimensions to be 30 by 45 m; assuming these as conduit dimensions yields drawdown depths of about 1.9 km for the eruptions of about 6 x 10^5 m^3 of tephra. Better estimates of these dimensions would help to infer the depths of each batch of magma that formed an eruption and would allow a depth scale to be added to figure 10. More data are needed here, and it is difficult to infer precise mechanisms without the individual volume estimates.

The approach used in this paper may be useful in terms of providing rapid feedback to improve future monitoring efforts at Augustine Volcano and elsewhere. The parameters are easy to measure, so they can be done in a few minutes during crises. They provide additional insight into factors such as likely ash production that are important for aviation safety. An additional benefit of the systematic study of parameters is that they may be combined to provide insight into other related questions. As an example, in figure 11 we plot durations as measured at

AUW (seismic), AUE BDL (infrasound), and on the I53US infrasound array in Fairbanks. The different symbols show which eruptions were accompanied by lightning (Thomas and others, this volume). It is clear that the eruptions that were of long duration both locally (AUE and AUW) and at distance (I53US) produced lightning, whereas the short ones at both did not (lower left of plots). The implication of this is that the longer the eruption, the more tephra is produced; each tephra particle is a potential charge carrier, so the more particles the higher the total charge available for lightning and other electrical phenomena (see also Thomas and others, this volume for additional discussion). From a monitoring perspective, these simple measurements may provide a rapid means of verifying the amount of tephra.

The four eruptions that occurred on January 27–28 were also the four for which we had instrumental data on lightning from the New Mexico Tech LMA stations (Thomas and others, this volume). Otherwise we would not have known the lightning occurred because no lightning was observed due to poor local weather, and further, the signals were not strong enough to show on the Bureau of Land Management (BLM) array in central Alaska. One factor that may have contributed to lightning production was a composition change that occurred approximately January 27 (Larsen and others, this volume; Coombs and others, this volume). The initial explosive eruptions produced mostly low-silica andesite, but for the January 27–28 eruptions the magma composition was dominantly high-silica andesite. The higher silica content may have contributed to greater lightning efficacy, but we cannot address this in detail with the limited data in hand. Another factor was that the January 27 eruption at 2031 AKST produced the largest pyroclastic flow unit, a 10.1×10^6 m^3 unit known as the Rocky Point flow (Coombs and others, this volume) that entered a pond on the north flank of Augustine Volcano (Begét, this volume). We speculate that interaction of the pyroclastic flow with the water in the pond may have created additional charged particles, but we cannot quantify this effect.

The parameters reported here do not permit us to comment on the terminations of the eruptions. Why were there six eruptions on January 13–14 a few hours apart instead of one larger one? Were these separate batches of magma? Did the eruptions stop when the gas-rich part had erupted? Did the vent partially close up or pinch off when the top-most

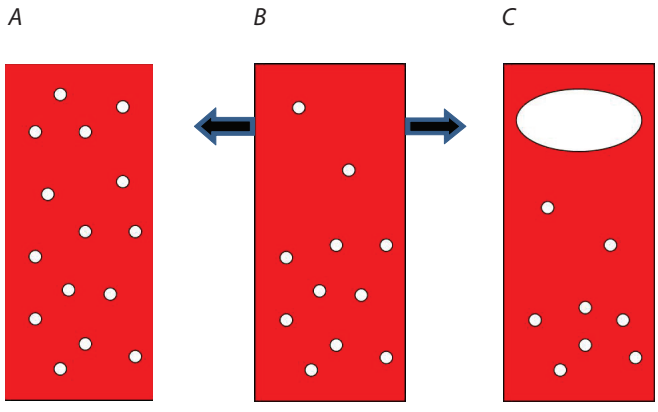

Figure 9. Schematic diagram of gas distribution in magma for three scenarios. *A*, Uniform gas distribution and rapid ascent. *B*, Slow ascent under leaky conditions; upper portion of column is gas poor. *C*, Slow ascent during sealed conditions; gas accumulates in a large bubble or irregular pocket or a gas-rich foam.

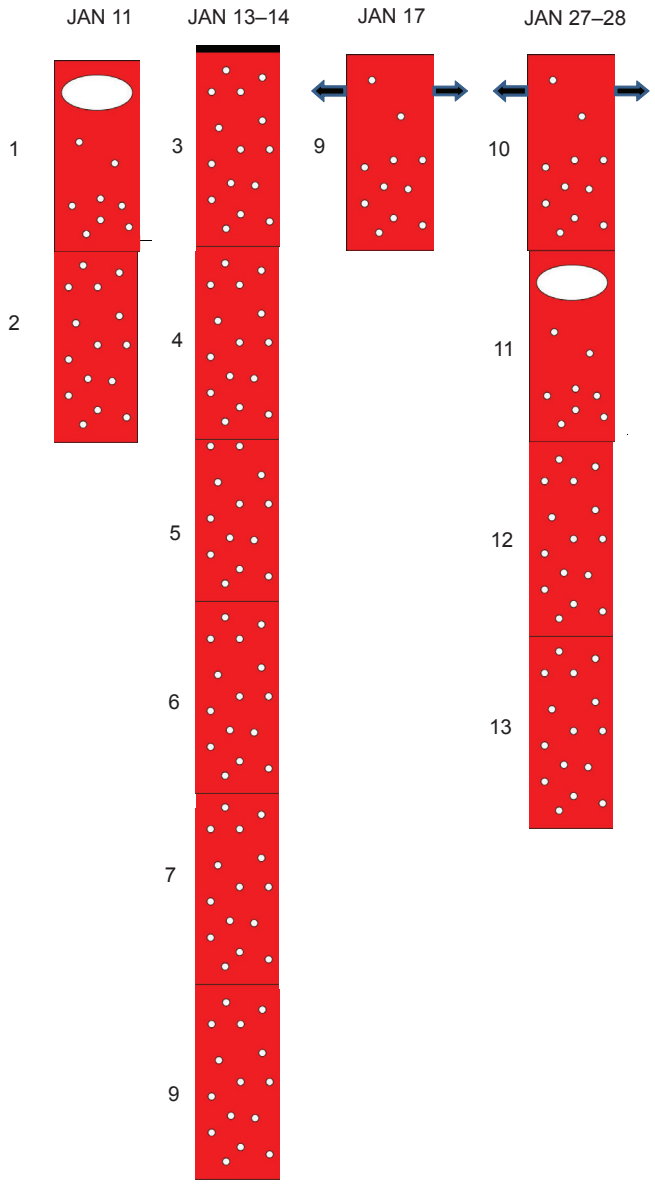

Figure 10. Schematic diagrams of gas distribution in the upper part of the conduit prior to Augustine Volcano's eruptions on January 11, 13–14, 17, and 27–28, 2006. These are "mapped" using the parameters and groupings of this paper to infer underground preeruptive conditions. Numbers to the left correspond the the event index number. The arrows represent gas loss to the surroundings.

material was removed? Some of the data reexamined may help to answer these questions, although they provide only indirect clues. For example the rates of decay of the seismic codas are variable. The coda decayed very abruptly for event 3 (see fig. 2*A*), suggesting possible pinching off of the conduit. The rates of decay were more gradual for most other events, some of which included complications such as small earthquakes in the coda. The codas for events 8, 12, and 13 were very long, suggesting a gradual loss of energy through an open conduit. The rates of decay as seen on broadband data (fig. 4*B*), however, were rather similar.

We briefly compare the Augustine explosive eruptions from 1976, 1986, and 2006. The durations of the largest events were remarkably similar: 11.83 minutes for 1976 (station CKK), 13.6 minutes for 1986, and 11 minutes for 2006 (both at OPT). The 1976 eruption had 13 large tremor events (the terminology used by Reeder and Lahr, 1987) versus 16 events with durations >2 minutes for 1986 (Power, 1988) and 13 large explosive events in 2006 (this paper). An infrasound array in Fairbanks (I53US and its predecessor) recorded 13 events in 1976 (Reeder and Lahr, 1987) and 12 in 2006 (Wilson and others, 2006); the array was not in operation in 1986. The first large explosion in 1976 was noted as being impulsive (Reeder and Lahr, 1987), similar to 2006 (event 1, this paper), whereas 1986 built up more gradually (fig. 22 of Power, 1988). The range of durations of the individual events also appears to be similar for all three eruptions. If one includes smaller events, such as the 35 small tremors in 1976 (Reeder and Lahr, 1987) and the 22+ events with durations between 1 and 2 minutes in 1986 (fig. 22 of Power, 1988)

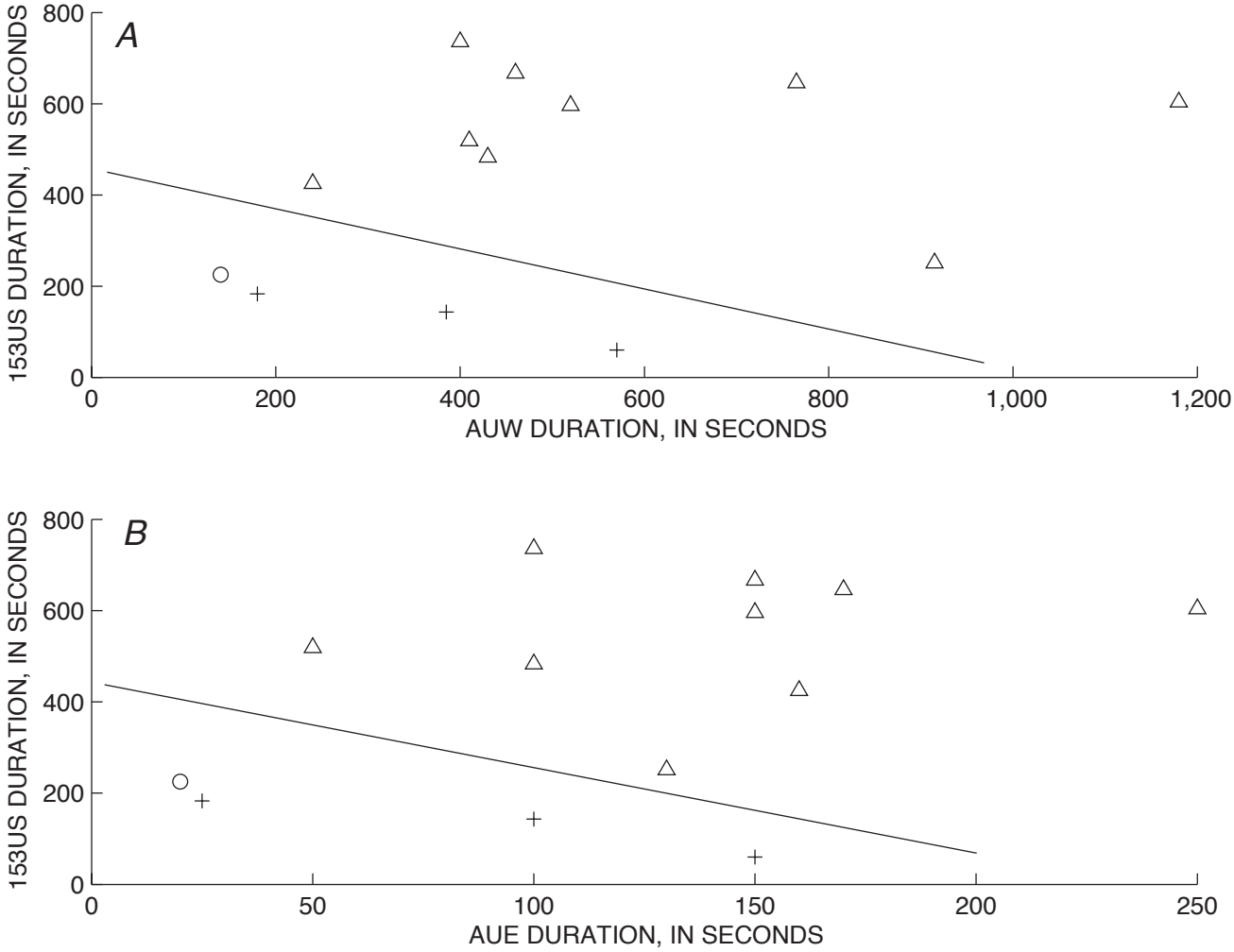

Figure 11. *A*, plot of I53US acoustic array duration (Wilson and others, 2006) versus AUW seismic duration for the 13 large explosive eruptions at Augustine Volcano in 2006. The triangles represent eruptions that were accompanied by lightning, and "+" symbols represent those with no reported lightning. *B*, I53US acoustic array duration versus AUE acoustic duration for the 13 large explosive eruptions. Symbols are as in part *A*. In both *A* and *B* a line is drawn from upper left to lower right to separate the eruptions that had lightning from those that did not. In both cases the eruptions with longer durations produced lightning. The point labeled "o" is event 11 which had only a single weak lightning flash.

then the two earlier eruptions have more events during the explosive phase. The 1976 explosive phase lasted just 4 days, the 1986 explosive phase lasted 14 days, and 2006 explosive phase lasted 18 days, suggesting that the rate of explosions was lowest in 2006. Otherwise the common parameters of the larger events of the three eruptions are quite similar, suggesting that the volcano has characteristic explosive behavior.

The Augustine explosive eruptions were similar to those at Asama (Ohminato and others, 2006), Montserrat (Druitt and other 2002), and Vulcano, Galeras, Ngauruhoe, and Sakurajima (Morrisey and Mastin, 2000) in terms of the strengths of the seismic and acoustic signals. However, there is significant variation in plume heights and volumes of ejecta. For the 2004 eruptions of Asama the infrasound signals ranged from 19 to 205 Pa as measured at a site 8 km away (these would be equivalent to 48 and 513 Pa at the 3.2 km distance of AUE). For Asama the seismic single force intensity was measured and eruption deposits were known for all five eruptions. The air shock intensity showed a positive correlation with the eruptions deposits, whereas the seismic force showed more variability. The differences in the parameters showed a similar spread to those for Augustine.

Vulcanian eruptions at Ngauruhoe, Galeras, and Sakurajima generally had ash plumes up to 4 to 5 km (Morrissey and Mastin, 2000). These most closely resemble the short strong eruptions (events 1 and 11) at Augustine, which had the lowest plume heights and inferred least amounts of ash. The other Augustine events most closely resemble those at Montserrat in terms of ash plume heights (3 to 15 km) and intervals between events (2.5 to 63 hours; Druitt and others, 2002). A full comparative study of these eruptions may be warranted.

Conclusions

Study of the major geophysical parameters of the 13 Augustine Volcano explosive eruptions from January 11–28, 2006, suggests that they fall into four main groups: (1) short strong eruptions (VEI=2), (2) events following quiescent intervals of 3 days or longer, (3) events with small D_R and high ash columns (low VEI=3), and (4) events with long durations and large amounts of tephra leading to high lightning production (high VEI=3). Systematic variations in gas storage and release are used to provide a conceptual basis for the differences in activity. New estimates of event origin times were based on seismic and acoustic data, and seismic evidence for pyroclastic or other flow events is presented. The various parameters are generally easy to measure, hence they could be used to make rapid measurements to aid crisis response. The diverse measurements made at Augustine are potentially useful for comparison with previous eruptions at other volcanoes; however, lack of data on tephra volumes for individual events leaves certain questions beyond reach. The Augustine eruptions are among the larger Vulcanian eruptions known to us and resemble some recent eruptions at Montserratt, 1995–99.

References Cited

Begét, J.E., 2010, Characterizing pyroclastic-flow interactions with snow and water using environmental magnetism at Augustine Volcano, *in* Power, J.A., Coombs, M.L., and Freymueller, J.T., eds., The 2006 eruption of Augustine Volcano, Alaska: U.S. Geological Survey Professional Paper 1769 (this volume).

Coombs, M.L., Bull, K.F., Vallance, J.W., Schneider, D.J., Thoms, E.E., Wessels, R.L., and McGimsey, R.G., 2010, Timing, distribution, and volume of proximal products of the 2006 eruption of Augustine Volcano, *in* Power, J.A., Coombs, M.L., and Freymueller, J.T., eds., The 2006 eruption of Augustine Volcano, Alaska: U.S. Geological Survey Professional Paper 1769 (this volume).

Druitt, T.H., Young, S.R., Baptie, B., Bonadonna, C., Calder, E.S., Clarke, A.B., Cole, P.D., Harford, C.L., Herd, R.A., Luckett, R., Ryan, G., and Voight, B., 2002, Episodes of cyclic Vulcanian explosive activity and fountain collapse at Soufriere Hills Volcano, Montserrat, *in* Druitt, T.H., and Kokelaar, P., eds., The eruption of Soufriere Hills Volcano, Montserratt, from 1995 to 1999: Geological Society London, Memoirs, p. 281–306.

Fehler, M., 1983, Observations of volcanic tremor at Mount St. Helens volcano: Journal of Geophysical Research, v. 88, p. 3476–3484.

Fernandes, J.J., Bellesiles, A.K., and Caplan-Auerbach, J., 2007, Estimates of gas flux from infrasonic signals at Augustine Volcano during the January 2006 eruption—Implications for eruption plume types [abs.]: Geological Society of America Cordilleran Section, 103rd annual mtg., paper no. 32-6.

Johnson, J.B., 2000, Interpretation of infrasound generated by erupting volcanoes and seismo-acoustic energy partitioning during Strombolian explosions: University of Washington, Seattle, Ph.D. dissertation.

Larsen, J.F., Nye, C.J., Coombs, M.L., Tilman, M., Izbekov, P., and Cameron, C., 2010, Petrology and geochemistry of the 2006 eruption of Augustine Volcano, *in* Power, J.A., Coombs, M.L., and Freymueller, J.T., eds., The 2006 eruption of Augustine Volcano, Alaska: U.S. Geological Survey Professional Paper 1769 (this volume).

McNutt, S.R., 1994, Volcanic tremor amplitude correlated with eruption explosivity and its potential use in determining ash hazards to aviation: U.S. Geological Survey Professional Paper 2047, p. 377–385.

McNutt, S.R., Miller, T., and Taber, J.J., 1991, Pavlof Volcano—seismological and geological evidence of increased explosivity during the 1986 eruptions: Bulletin of Volcanology, v. 53, p. 86–98.

Morrisey, M. and Mastin, L., 2000, Vulcanian Eruptions *in* Sigurdsson, H., B. Houghton, S.R. McNutt, H. Rymer, and J. Stix, eds. Encyclopedia of Volcanoes: San Diego, Calif., Academic Press, p. 463–475.

Newhall, C.G., and Self, S., 1982, Volcanic Explosivity Index (VEI)—An estimate of explosive magnitude for historical volcanism: Journal of Geophysical Research, v. 87, p. 1231–1238.

Ohminato, T., Takeo, M., Kumagai, H., Yamashina, T., Oikawa, J., Koyama, E., Tsuji, H., and Urabe, T., 2006, Vulcanian eruptions with dominant single force components observed during the Asama 2004 volcanic activity in Japan: Earth Planets Space, v. 58, p. 583–593.

Olson, J.V., Wilson, C.R., McNutt, S.R., and Tytgat G., 2006, Infrasonic wave observations of the January 2006 Augustine Volcano eruptions: Eos (American Geophysical Union Transactions), v. 87, abs. V51C-1685.

Petersen, T., De Angelis, S., Tytgat, G., and McNutt, S.R., 2006, Local infrasound observations of large ash explosions at Augustine Volcano, Alaska, during January 11–28, 2006: Geophysical Research Letters, v.33, L12303, doi:10.1029/2006GL026491.

Power, J.A., 1988, Seismicity associated with the 1986 eruption of Augustine Volcano Alaska: University of Alaska Fairbanks, M.S. Thesis, 142 p.

Power, J.A., and Lalla, D.J., 2010, Seismic observations of Augustine Volcano, 1970–2007, *in* Power, J.A., Coombs, M.L., and Freymueller, J.T., eds., The 2006 eruption of Augustine Volcano, Alaska: U.S. Geological Survey Professional Paper 1769 (this volume).

Power, J.A., Nye, C.J., Coombs, M.L., Wessels, R.L., Cervelli, P.F., Dehn, J., Wallace K.L., Freymueller, J.T., and Doukas, M.P., 2006, The reawakening of Alaska's Augustine Volcano: Eos (American Geophysical Union Transactions), v. 87, no. 37, p. 373, 377.

Reeder, J.W. and J.C. Lahr, 1987, Seismological aspects of the 1976 eruptions of Augustine Volcano, Alaska: U.S. Geological Survey Bulletin 1768, 32 p.

Schneider, D.J., Scott, C., Wood, J., and Hall T., 2006, NEXRAD weather radar observations of the 2006 Augustine volcanic clouds: Eos (American Geophysical Union Transactions), v. 87, abs. V51C-1686.

Thomas, R.J., Krehbiel, P.R., Rison, W., Hunyady, S.J., Winn, W.P., Hamlin, T., and Harlin, J., 2004, Accuracy of the lightning mapping array: Journal of Geophysical Research, v. 109, no. D14, D14207, doi: 10.1029/2004JD004549

Thomas, R.J., Krehbiel, P.R., Rison, W., Aulich, G., Edens, H., McNutt, S.R., Tytgat, G., and Clark, E., 2007, Electrical activity during the 2006 Mount St. Augustine volcanic eruptions: Science, v. 315, p. 1097.

Thomas, R.J., McNutt, S.R., Krehbiel, P.R., Rison, W., Aulich, G., Edens, H.E., Tytgat, G, and Clark, E., 2010, Lightning and electrical activity during the 2006 eruption of Augustine Volcano, *in* Power, J.A., Coombs, M.L., and Freymueller, J.T., eds., The 2006 eruption of Augustine Volcano, Alaska: U.S. Geological Survey Professional Paper 1769 (this volume).

Vallance, J.W., Bull, K.F., and Coombs, M.L., 2010, Pyroclastic flows, lahars, and mixed avalanches generated during the 2006 eruption of Augustine Volcano, *in* Power, J.A., Coombs, M.L., and Freymueller, J.T., eds., The 2006 eruption of Augustine Volcano, Alaska: U.S. Geological Survey Professional Paper 1769 (this volume).

van Manen, S.M., Dehn, J., West, M.E., Blake, S., and Rothery, D.A., 2010, The 2006 eruption of Augustine Volcano—Combined analyses of thermal satellite data and reduced displacement, *in* Power, J.A., Coombs, M.L., and Freymueller, J.T., eds., The 2006 eruption of Augustine Volcano, Alaska: U.S. Geological Survey Professional Paper 1769 (this volume).

Wallace, K.L., Neal, C.A., and McGimsey, R.G., 2010, Timing, distribution, and character of tephra fall from the 2005 –2006 eruption of Augustine Volcano, *in* Power, J.A., Coombs, M.L., and Freymueller, J.T., eds., The 2006 eruption of Augustine Volcano, Alaska: U.S. Geological Survey Professional Paper 1769 (this volume).

Wilson, C.R., Olson, J.V., Szuberla, C.A.L., McNutt, S.R., Tytgat, G., and Drob, D.P., 2006, Infrasonic array observations at I53US of the 2006 Augustine Volcano eruptions: Inframatics, March 15, 2006, 18 p.

Zobin, V.M., Plascencia, I., Reyes, G., and Navarro, C., 2009, The characteristics of seismic signals produced by lahars and pyroclastic flows—Volcan de Colima, Mexico: Journal of Volcanology and Geothermal Research, v. 179, p. 157–167.

The 2006 Eruption of Augustine Volcano, Alaska
Power, J.A., Coombs, M.L., and Freymueller, J.T., editors
U.S. Geological Survey Professional Paper 1769

Chapter 5

Earthquake Waveform Similarity and Evolution at Augustine Volcano from 1993 to 2006

By Heather R. DeShon[1], Clifford H. Thurber[2], and John A. Power[3]

Abstract

Temporal changes in waveform characteristics and earthquake locations associated with the 2006 Augustine eruption and preeruptive seismicity provide constraints on eruptive processes within the edifice. Volcano-tectonic earthquakes occur within the upper 1 to 2 km at Augustine between and during eruptive cycles, and we use the Alaska Volcano Observatory hypocenter and waveform catalog from 1993 to 2006 to constrain changes in event similarity and location over time. Waveform crosscorrelation with bispectrum verification improves the pick accuracy of the catalog data to yield better locations and allows for identification of families of similar earthquakes. Event waveform similarity is low at Augustine, with ~60 to 70 percent of events failing to form event families of more than 10 events. The remaining earthquakes form event families over multiple time scales. Events prior to the 2006 eruption exhibit a high degree of similarity over multiple years. Earthquakes recorded during the precursory and explosive phases of the 2006 eruption form swarms of similar earthquakes over periods of days or hours. Seismicity rate and event similarity decrease rapidly during the explosive and effusive eruption phases. The largest recorded swarms accompany reports of increased steaming and explosive eruptions at the summit. Relative relocation of some event families indicates upward migration of activity over time, consistent with magma transport by way of an ascending dike. Multiple regions of the edifice generate seismicity simultaneously, however, suggesting the edifice contains a network of fractures and/or dikes.

Introduction

Augustine Volcano is the youngest and historically most active volcano in the Cook Inlet region of Alaska. The edifice is composed primarily of andesitic material and forms a small island with a summit peak at 1.25 km above sea level. Past sector failures of the edifice have excited tsunamis in Cook Inlet. Major eruptions have taken place in 1883, 1935, 1963–64, 1976, 1986, and 2006, and these explosive eruptions created ash-rich plumes that posed significant hazard for overlying aircraft flight paths. The three most recent eruptions have followed similar eruptive sequences: (1) a precursory period of seismic unrest; (2) an explosive phase marked by one or more pyroclastic flow-generating eruptions; and (3) one or more dome-building effusive phases (Power, 1988; Power and Lalla, this volume). Most seismicity recorded at Augustine is volcano-tectonic (VT) in nature, with high-frequency P onsets indicative of shear failure in brittle material, and is confined to the upper 1 to 2 km of the edifice, with limited evidence for activity at 3 to 4 km below mean sea level (b.m.s.l.) (Kienle, 1987; Power, 1988; Power and Lalla, this volume). Low-frequency events associated with fluid processes are less common (Buurman and West, this volume). Magma transport during eruptive cycles at Augustine likely occurs through shallow dike propagation, with new eruptive cycles occurring as a result of an influx of juvenile magma at the base of the system (Cervelli and others, 2006; Roman and others, 2006).

Dike propagation at volcanoes frequently couples with increased rates of seismicity, and seismic monitoring provides useful early warning of major changes within volcanic systems (see McNutt, 2005, for a recent review). Because of the volcanic, seismic, and tsunami hazard posed by Augustine eruptions, the volcano has been seismically monitored since 1970. The Alaska Volcano Observatory (AVO) has maintained digital waveforms recorded by a network of five to eight short-period and broadband seismometers since 1993

[1]Center for Earthquake Research and Information, University of Memphis, 3890 Central Ave., Memphis, TN 38138.

[2]Dept. of Geoscience, University of Wisconsin-Madison, 1215 W. Dayton St., Madison, WI 53706.

[3]Alaska Volcano Observatory, U.S. Geological Survey, 4200 University Drive, Anchorage, AK 99508.

(fig. 1). Volcano seismic networks typically have few stations and marginal geographic coverage, and waveforms recorded at volcanoes are often noisy because of the complex interactions of tectonic and magmatic processes, wind, and poor site conditions. As a result, onset pick accuracy may be highly variable within a phase catalog. Routine catalog locations at Augustine exhibit a high degree of scatter within the shallow edifice that complicates interpretation of magmatic and hydrothermal processes. Scatter may be an artifact of location procedure or imprecise phase onset picks, or it may be a real feature of volcanic activity. Catalog earthquake locations at Augustine are calculated using analyst phase picks and an approximate, one-dimensional (1*D*) velocity model with station corrections developed for Augustine (Power, 1988). More than 3,800 events have been catalogued at Augustine from 1993 through 2006 (Dixon and others, 2008), and ~2,000 of these were related to the 2006 eruptive sequence (fig. 1).

Retrospective analyses of volcano seismic data using waveform crosscorrelation methods can provide insight into the relative similarity of waveforms in time and space, which in turn can reflect the underlying eruptive processes (for example, Got and others, 1994; Rubin and others, 1998; Battaglia and others, 2004; Rowe and others, 2004; DeShon and others, 2007). In this study, waveform crosscorrelation techniques are applied to the seismic event archive for Augustine Volcano extending from 1993 through December 2006. Identification of characteristic families of similar earthquakes provides a clearer picture of how seismicity evolves within the edifice before and during eruptive cycles at Augustine Volcano. We examine temporal changes in waveform characteristics associated with the 2006 Augustine eruption and preeruptive seismicity and identify families of similar earthquakes that occur at multiyear, multimonth, multiday, and multihour timescales. Relative location of selected event families associated with the precursory and explosive phases of the 2006 eruption provides insight into seismic and magmatic processes occurring at Augustine Volcano.

Method

Waveform Crosscorrelation

If two events are closely located in space and share similar source mechanisms, they should generate similar ground motions and be recorded as similar waveforms. Waveform crosscorrelation (CC) of two events recorded at the same station yields: (1) a maximum absolute value of the CC coefficient that varies between 0 and 1, where 1 represents a perfect waveform similarity; and (2) an associated relative time delay or lag

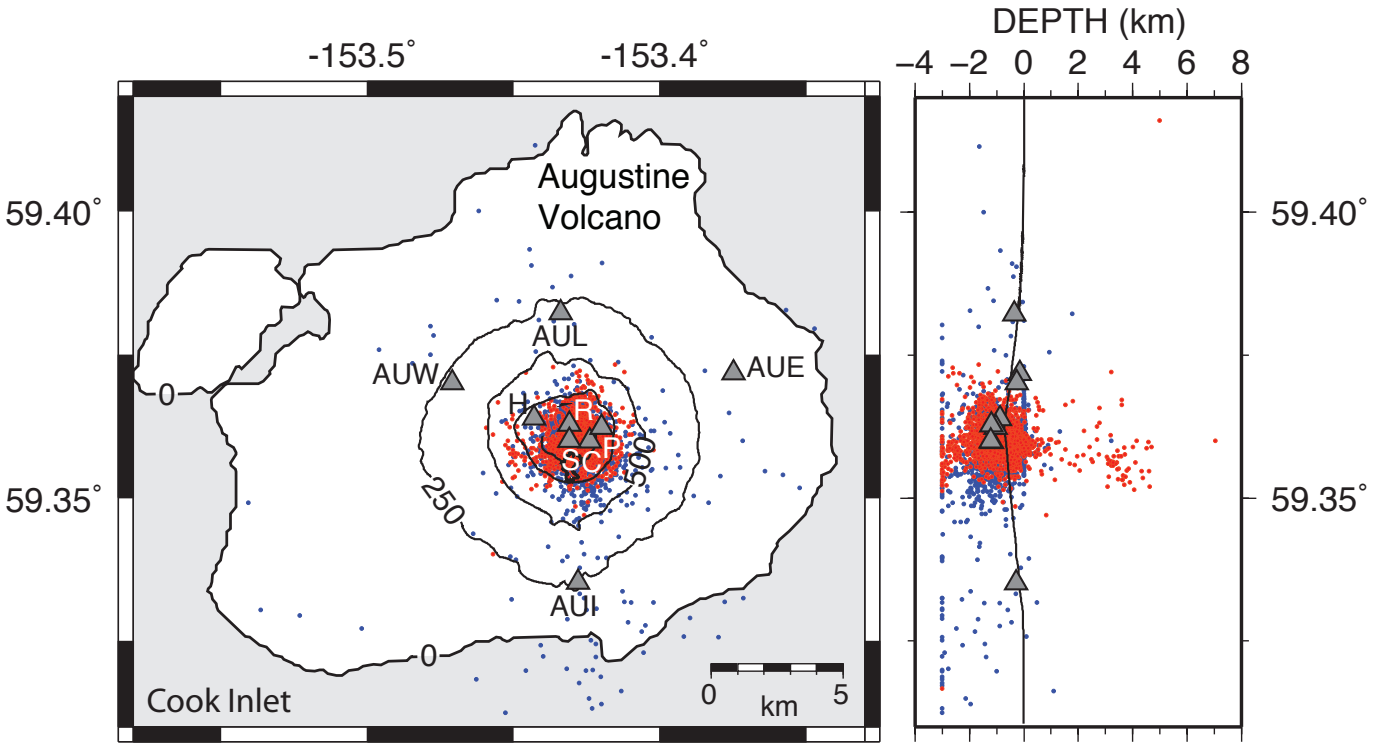

Figure 1. Map view and north-south oriented cross-section of Augustine Volcano. Contour interval is 250 m. Triangles are AVO seismic stations used for waveform crosscorrelation. The "AU" has been left off of the summit stations for drafting clarity. Blue dots are AVO catalog events occurring from 1993 to April 2005. Red dots are AVO catalog events occurring on and after April 2005.

reflecting the time shift necessary to best align the waveforms. High-quality time delay estimates can be identified by finding a threshold value for the CC coefficient that maximizes the number of correlated arrivals while minimizing the number of false-positive correlations (for example, Schaff and others, 2002). Correlation lag estimates can be used to correct inconsistent picks and revise absolute arrival times (for example, Dodge and others, 1995; Dodge, 1996; Shearer, 1998; Aster and Rowe, 2000; Rowe and others, 2002a). CC coefficients contain valuable information on event similarity and can be used to identify families of similar waveforms (Rowe and others, 2002a).

CC coefficients may be low if the underlying signals are not time-delayed similar waveforms, or if high levels of noise contaminate the underlying time-delayed signals. In the presence of correlated Gaussian noise, traditional CC methods may provide low coefficients for similar events, or high correlations with the estimated correlation lag driven by the correlated noise, rather than the signal of interest (Du and others, 2004). Correlated or partially correlated noise may result at individual stations because of a combination of constant predominant noise sources such as wind and site response effects. Bispectrum crosscorrelation (BCC), or CC in the third-order spectral domain, suppresses correlated Gaussian noise or low-skewness noise sources (Nikias and Raghuveer, 1987; Nikias and Pan, 1988; Yung and Ikelle, 1997) and can effectively identify the global CC time shift in cases where traditional methods fail because of correlated noise contamination. BCC produces time delay estimates consistent with traditional second-order spectral domain methods when noise is not correlated (Du and others, 2004).

The bispectrum crosscorrelation package for seismology (BCSEIS) verifies traditional CC time delay estimates by additionally computing a BCC lag prediction for filtered and unfiltered waveforms (Du and others, 2004). The use of BCSEIS with Augustine data closely follows the approach outlined for data from Redoubt Volcano, Alaska (DeShon and others, 2007). For Augustine data, the BCSEIS verification threshold was set to twice the sampling interval, and waveforms were filtered using a three pole, two pass, Butterworth bandpass filter with a low frequency corner at 1 Hz and a high frequency corner at 20 Hz. CC was performed using a window extending from 0.3 seconds before to 0.7 seconds following the P-wave arrival (fig. 2). This window was large enough to allow CC of the P-wave coda to identify similar families of earthquakes and incorporate large mispicks. The bulk of seismicity is small magnitude, near-summit events with high frequency P onsets and no discernable S-wave arrivals as recorded on the vertical component, short period summit stations. At the summit stations, the CC window may contain P and S wave information. We were primarily interested in identifying families of similar earthquakes, however, and crosscorrelation of P or P and S energy does not significantly bias our results.

Event Clustering and Pick Adjustments

We identified families of similar earthquakes using the verified CC coefficients and a dendrogram-based, hierarchical pair-group algorithm (Rowe, 2000; Rowe and others, 2002a). CC coefficients are used to fuse event pairs with high

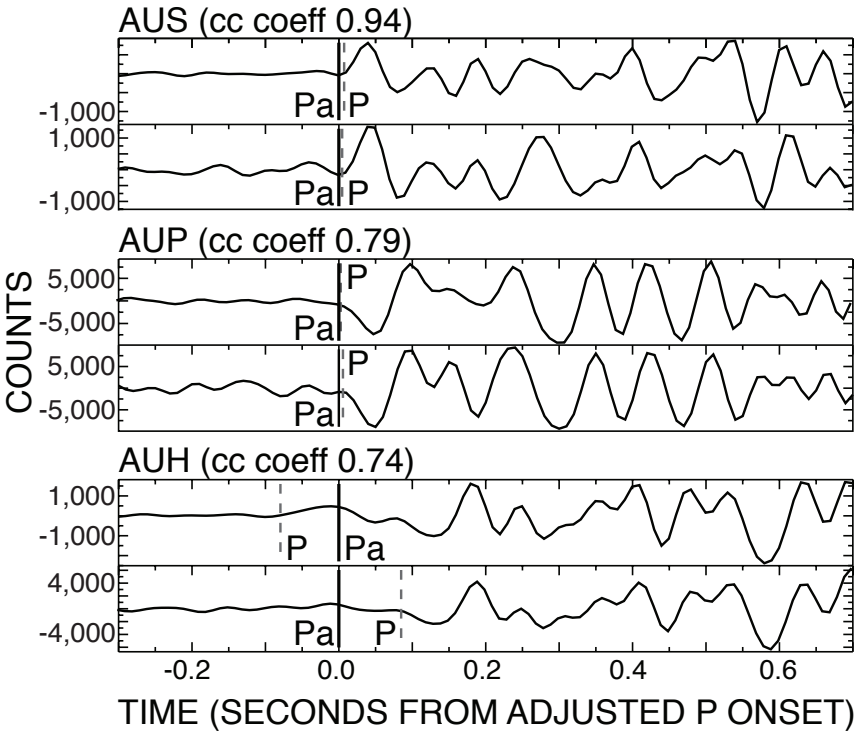

Figure 2. An example of bispectrum crosscorrelation package for seismology (BCSEIS) analysis for two Augustine earthquakes. The waveforms are aligned on the adjusted P onset (Pa) based on crosscorrelation (CC) and event clustering results. The original catalog P onset (P) is also marked. The associated CC coefficient for each event pair is shown next to the station name. Event pairs at each station with CC values ≥0.79 are automatically accepted for use with clustering techniques. Event pairs with CC values ≥0.30 are accepted if at least one other station reports a CC value ≥0.88 for the same data. For this event pair, CC coefficients and predicted lag estimates at AUS, AUP, and AUH would be accepted.

waveform similarity into clusters, and clustering is considered complete when a user-defined CC coefficient cutoff threshold is reached (see Rowe and others, 2002a, for further details). For the Augustine data, this threshold was set to 0.80. The set of time delays associated with each intracluster event pair, weighted by the associated standard deviation calculated during waveform CC, are inverted to solve for a set of phase onset corrections. Inversion is calculated using an iterative, conjugate gradient approach that minimizes the L1-norm misfit (Aster and Rowe, 2000; Rowe and others, 2002a).

We used the above process to solve for clusters or multiplets of highly similar waveforms at all stations within the Augustine network. Event pairs with BCC-verified CC values ≥0.79 were used during event clustering. Additionally, for a given event pair, if at least one station has a verified CC coefficient ≥0.88, then other stations need only have a verified CC coefficient ≥0.30 to also be included in the clustering analysis. Augustine events primarily separate into small clusters with fewer than six events, and approximately one-third of events do not get included in any cluster. This suggests that discrete, dissimilar earthquakes and/or noisy waveforms dominate the Augustine catalog. Visual analysis of clusters containing six or more events suggested that some could be combined to form larger clusters with similar, but not identical, waveforms. We combined like clusters and grew clusters by incorporating events that may have one or more verified and reported lag adjustments to other cluster members; these new events were confirmed as new cluster members by visual comparison. Clusters were then compared across the network to identify event families, or sets of events that generated similar waveforms at all stations (fig. 3). We interpret those families with ≥10 member events in this report.

Results

The seismic record at Augustine Volcano recorded from 1993 to 2005 is dominated by small-magnitude shallow edifice events occurring at rates as high as 54 events/month (fig. 4). Approximately 60 to 70 percent of recorded events are not associated with event families containing more than 10 earthquakes, based on waveform similarity measured by crosscorrelation. Waveform dissimilarity is the dominant feature of catalog seismicity. Waveform similarity, when present, increases with small accelerations in seismicity rate (fig. 4). The resulting families of similar earthquakes contain multiplets of temporally related events over short time scales (days and hours). The similarity of some of the sets of multiplets over longer periods of time (years and months) suggests that intrafamily clusters share source location and process and that some regions of the edifice may be reactivated.

Before the seismicity rate increase in April 2005, event families contain 10 to 20 events (fig. 4*A*), with similar waveforms separated in time by months to years. Figure 5 illustrates a typical event family extending from late 1998 to late 2000 (family S in fig. 4*A*). The family consists of 4 events in 1998, 5 events in 1999, and 10 events in 2000. Waveforms exhibit similarity in P onset, suggesting a similar location, source, and/or path, especially at summit stations AUP and AUH. Waveform similarity in the P coda at summit station AUR is not as high as at the other recording summit stations, which may be indicative of changes in path characteristics over time. As the seismicity rate increases during the early precursory stage in April 2005, event families occur over months and weeks rather than years (fig. 4*B*).

Family LM is an interesting example of both a long-term (year) and mid-term (month) time scale for waveform similarity. The family extends from 1997 through 1998 and reappears from 2004 through 2005 (figs. 4*A*, 4*B,* 6). The set of waveforms was originally identified as two separate clusters because of the opposite sign of the P onset at AUS (fig. 6); however, the seismometer at station AUS was replaced on September 19, 2003, at which point the orientation of the vertical channel was reversed. Waveforms in this family have a highly similar P onset on the summit stations but more variable P coda characteristics. Coda similarity is highest within the temporally related swarms that make up the family (fig. 6). The overall similarity of the waveforms suggests that the same region of the edifice was active throughout much of 1998 during a brief increase in seismicity rate and again during the precursory stages of the 2006 eruption (fig. 4*A*).

During November and December 2005, seismicity rate increases significantly, and the time scale of event similarity switches from years and months to weeks and days (fig. 4*C*). The average size of the families does not change significantly and consists of 10–20 events. Swarms of similar earthquakes occur over periods of hours and days followed by periods of quiescence. The same area of the edifice may reactivate days to weeks later, as illustrated by the time separation between events in families AI and AC (figs. 4*C*, 7). We also identified small swarms of highly similar events that appear to grade into one another over a period of days. This behavior is illustrated in figure 8 using families C, BC, and B, which occur during a period of increased seismicity from December 9 to 11, 2005 (fig. 4*C*). Individually, each family of ~15 events contains highly similar waveforms that occur over a period of hours. The P onset at each of the summit stations suggests a highly similar source process or location, but the P coda remains distinct between families (fig. 8). Over this same time period, events occur in other regions of the edifice, generating P onsets with opposite sign (fig. 9).

The shortest duration family consists of a swarm of ~70 similar earthquakes on January 11, 2006, from ~2000 to 2200 AKST (Alaska Standard Time) (family AD, fig. 4*C*). These events were recorded between the first two stages of explosive activity on January 11 and 13, 2006. Though these events are highly similar, the waveforms evolve over time, likely reflecting small changes in source process, source location, changes in path characteristics, or some combination of factors (fig. 10). Following this swarm, ~30 events with a similar high-frequency content but different onset and coda characteristics were recorded at the summit stations (family AH, figs. 4*C*,

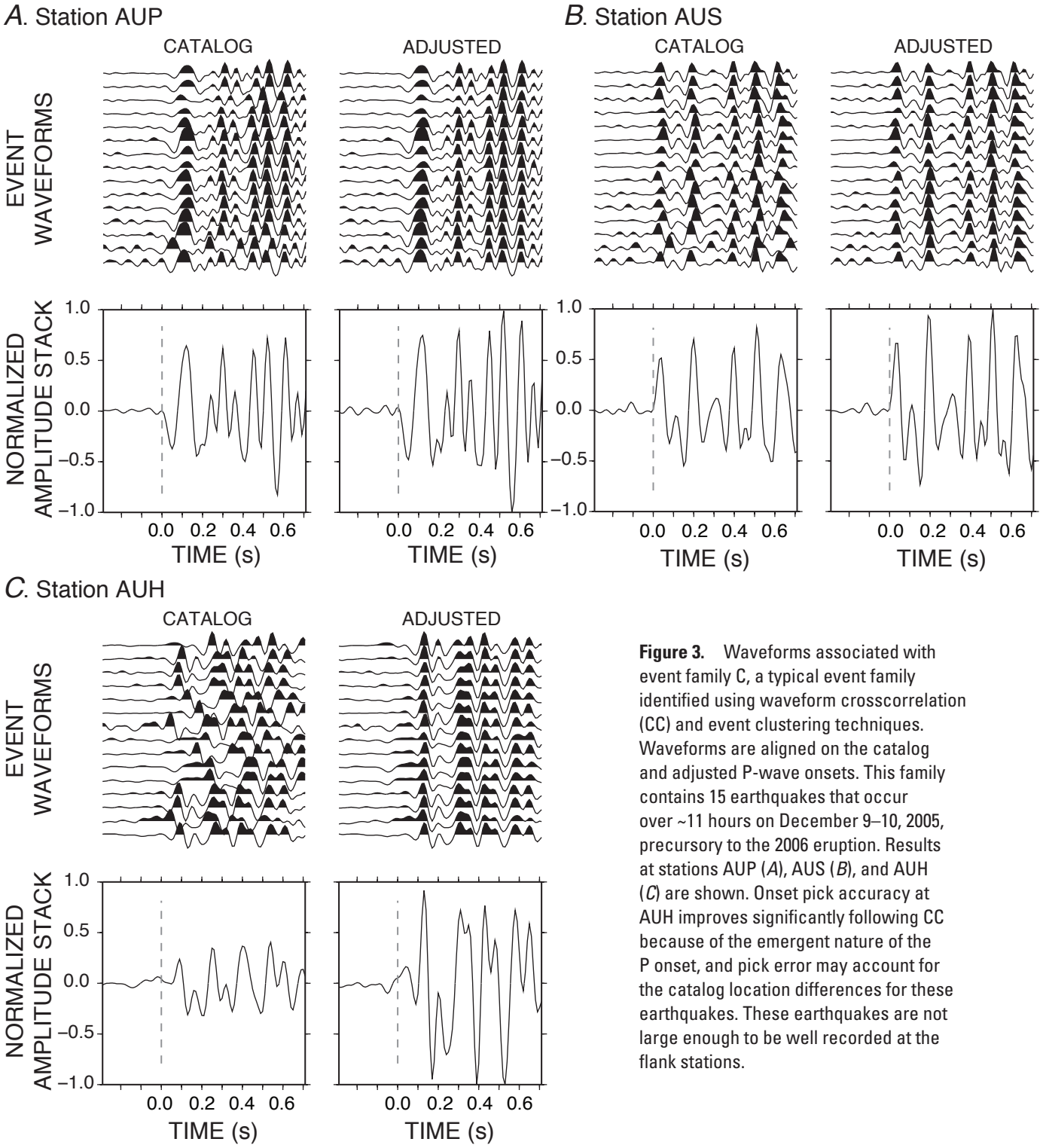

Figure 3. Waveforms associated with event family C, a typical event family identified using waveform crosscorrelation (CC) and event clustering techniques. Waveforms are aligned on the catalog and adjusted P-wave onsets. This family contains 15 earthquakes that occur over ~11 hours on December 9–10, 2005, precursory to the 2006 eruption. Results at stations AUP (*A*), AUS (*B*), and AUH (*C*) are shown. Onset pick accuracy at AUH improves significantly following CC because of the emergent nature of the P onset, and pick error may account for the catalog location differences for these earthquakes. These earthquakes are not large enough to be well recorded at the flank stations.

11). These events were not well recorded on the flank stations, however, so the catalog location quality is poor.

Events within each family exhibit waveform similarity that should correspond to spatial similarity, but catalog locations for events within individual families generally have a high degree of scatter. For example, family AD waveforms are linked by an average CC coefficient of 0.92 at station AUP, but the catalog depths for these events range from –3.0 to 0.0 km b.m.s.l. Events with identical source process and location should also exhibit identical differences in absolute arrival time between any two stations. This differential arrival time is independent of origin time but is sensitive to changes in path velocity over the time between earthquakes. For swarm activity over small time scales, we can assume the velocity

along the path from earthquake to station does not change significantly, and we can use differential arrival times to prove colocation. We present an example of this process using family AD. We calculated the difference in absolute arrival time between summit station AUP and (1) summit station AUH; (2) flank station AUL; and (3) flank station AUW (fig. 12). These four stations exhibit high signal-to-noise ratio for events in family AD (fig. 10). We removed the median value of the differential times to find a time residual; residuals should be zero for colocated earthquakes. For family AD, the time residuals for each station-pair have a zero mean and scatter is small (fig. 12). The increased scatter in time residuals for AUP-AUL reflects the relatively poorer recording of these earthquakes at station AUL (fig. 10).

The mean differential arrival times for sets of station-pairs for each family contain information on relative locations between families. If families are separated in space, then the differential time median at any given station-pair should differ. In figure 13, we show the relationship between median differential times for station-pairs AUP-AUH, AUP-AUW, and AUP-AUL. Because of the assumption that path velocity does not vary over time, we show only event families with relatively short durations that occur during the 2006 Augustine eruption. Family AD, which occurred during the explosive phase, clearly separates from families A, B, BC, and C that occurred during the early precursory phase in November and December 2005 (fig. 13). The spatial similarity between the December 2005 events is consistent with the high degree

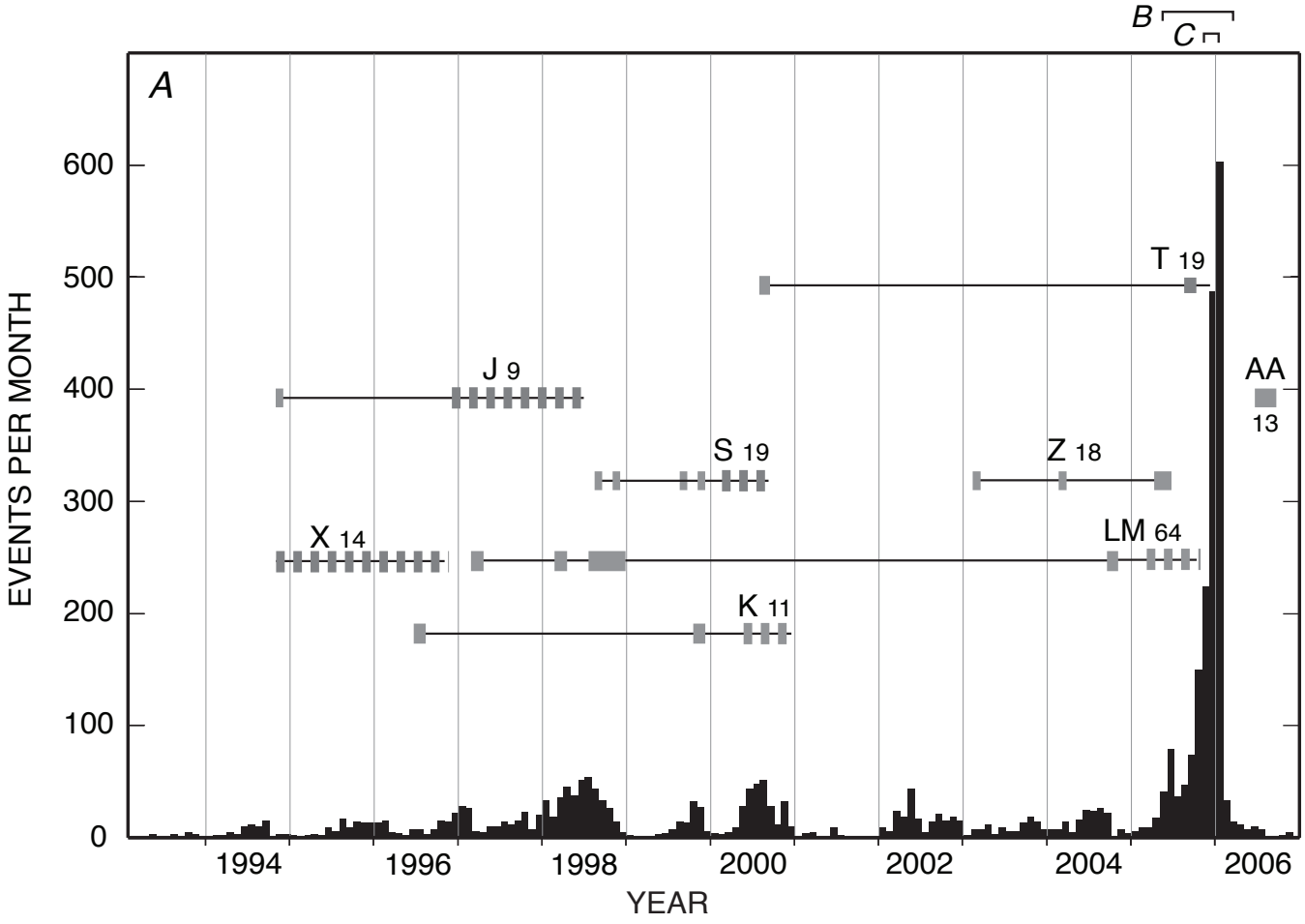

Figure 4. Seismicity rate and event families identified using the Augustine Alaska Volcano Observatory (AVO) catalog. On each panel, the histogram indicates seismicity rate over time and horizontal black lines indicate the extent in time of waveform families. Family names are indicated by letters and are followed by the number of member events. Solid squares represent time periods over which multiplets of earthquakes occur within each family. *A*, Histogram of the number of catalog earthquakes per month from 1993 to 2006. Event families with a time range on the month to year scale are shown. Bars indicate the time periods shown in panels *B* and *C*. *B*, Histogram of the number of catalog earthquakes per day during the 2006 eruption and precursory period. Seismicity rate decreases significantly following explosive eruptions in January 2006. Bar indicates the time period shown in panel *C*. *C*, Histogram of number of catalog earthquakes per day in November and December 2005, and in January 2006. Arrows mark periods of explosive, plume-forming eruptions. Black: first motion down at AUP. Gray: first motion up at AUP.

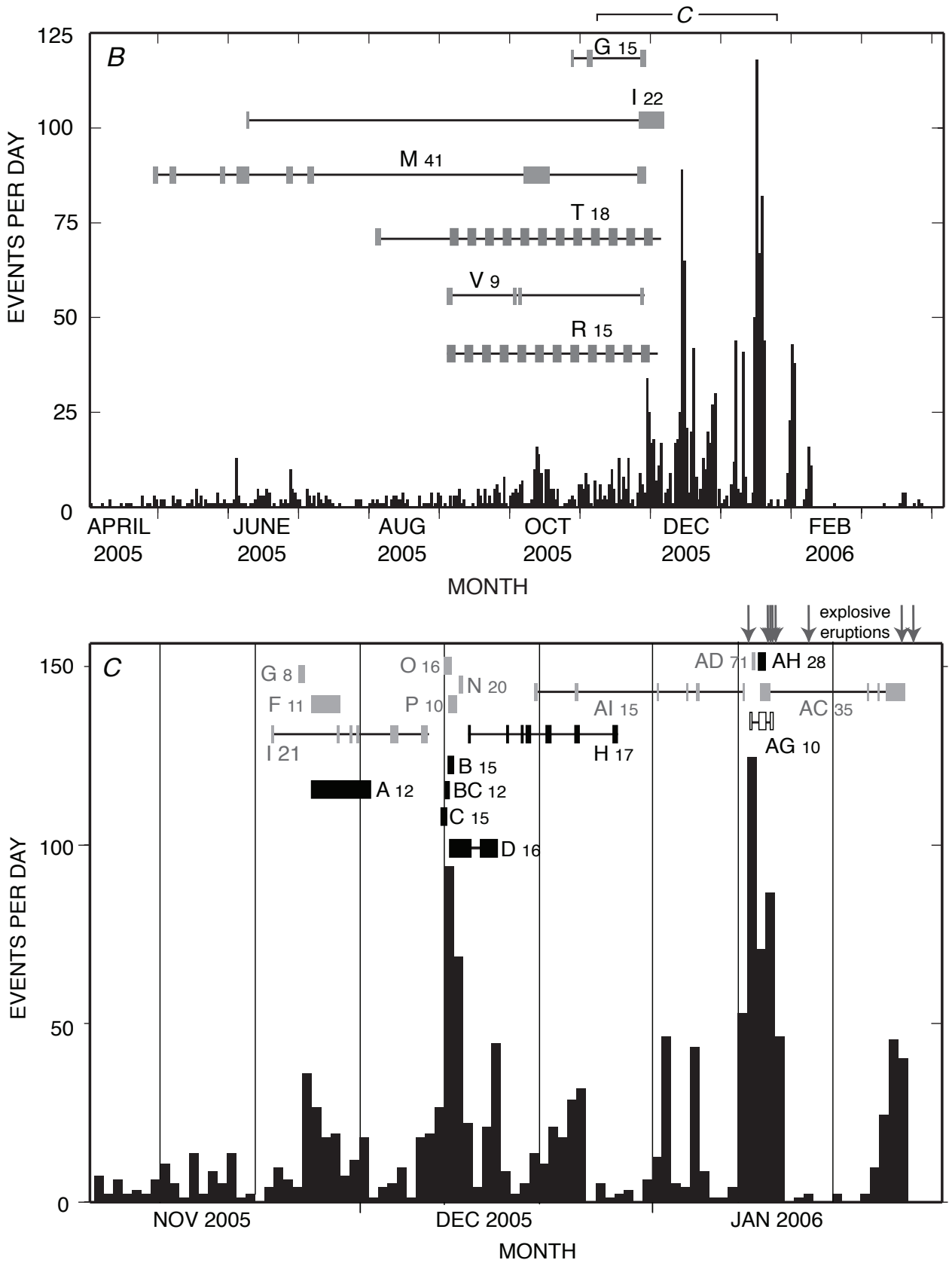

Figure 4.—Continued.

of intracluster waveform similarity between these clusters (fig. 8). On the basis of network geometry, the lower values for AUP-AUW and AUP-AUL for family AD likely indicate a shallower depth for these events relative to the other families. Shallow events should generate higher differential arrival times between summit and flank stations than events within the edifice near sea level because the sea level, events are actually closer to the flank stations than to the summit stations. Clusters O and N occur over the same period of time as families B, BC, and C but have opposite first motion polarity at AUP (fig. 9), and they appear separated in this diagram. This relationship suggests that multiple regions of the edifice can be simultaneously active.

We can further take advantage of the differential arrival-time medians for each cluster by inverting these data to solve for relative locations between families when families are well recorded on more than three stations. This location methodology is a variant of the method of hyperbolas (Milne, 1886) and the related equal-differential-time method (Zhou, 1994). To test this method, we relocated families A, B, and AD and used all station-pair combinations of summit stations AUP, AUS, and AUH and flank stations AUL and AUW. We solved for an initial cluster location by computing the misfit between the set of observed and calculated station-pair differential times. We solved for the location that minimizes the station-pair residuals, applying weighting to stabilize the inversion.

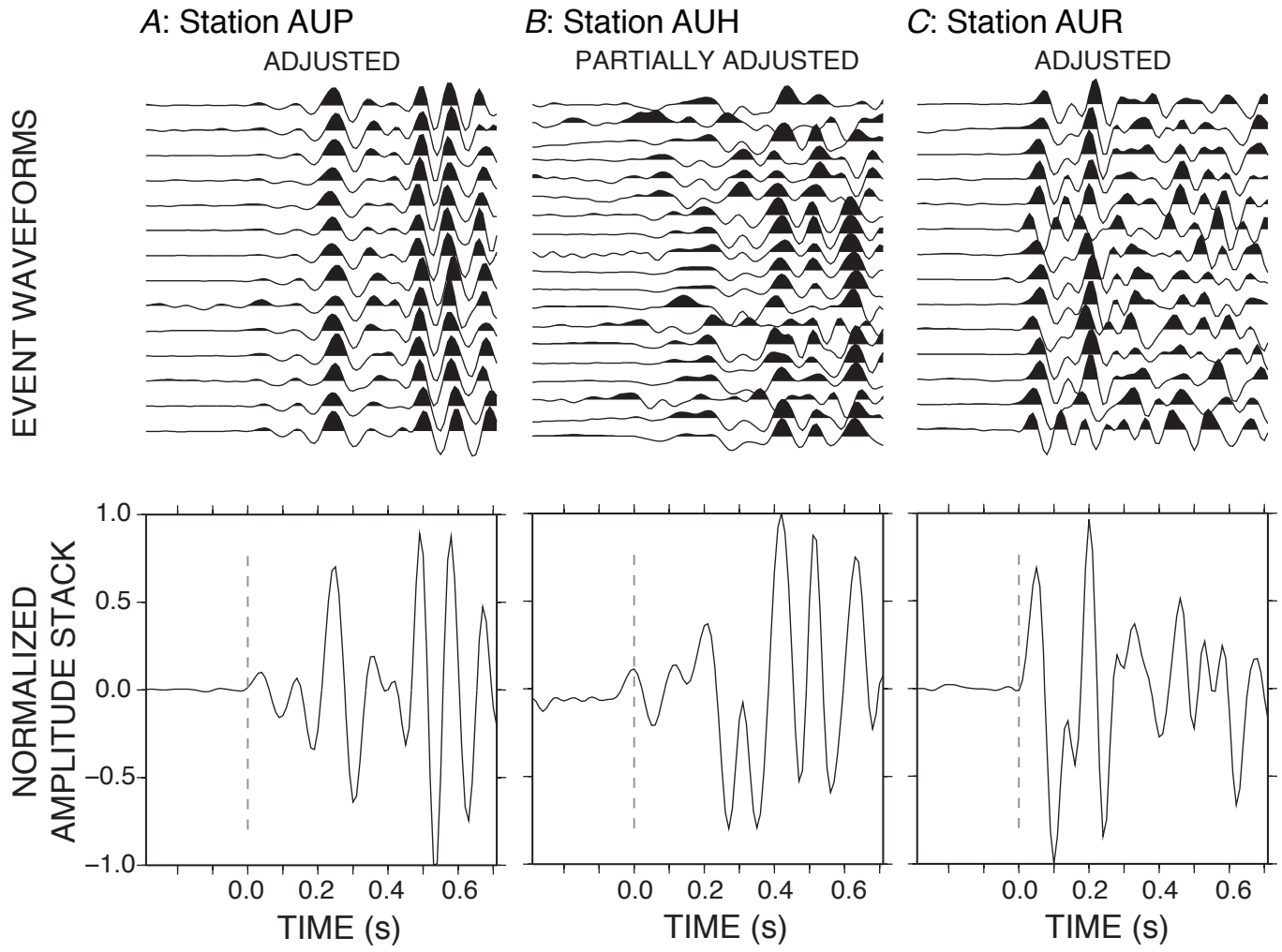

Figure 5. Waveforms and normalized amplitude stacks for event family S, which occur from June 22, 1998, through September 23, 2000 (see fig. 4*A* for full time extent), at stations AUP (*A*), AUH (*B*), and AUR (C). Waveforms are shown aligned on adjusted P onset and filtered between 1 and 20 HZ (upper panel) and as an normalized amplitude stack (lower panel). At all summit stations, such as the examples at AUP and AUR, the waveforms exhibit similarity in P onset, suggesting a similar location, source and path, but they are not identical. Because of the emergent nature of P onset at AUH, pick quality in the initial catalog was poor. The number of verified time delays between all possible event pairs was not sufficient for the inversion process to correctly adjust P onsets at this station.

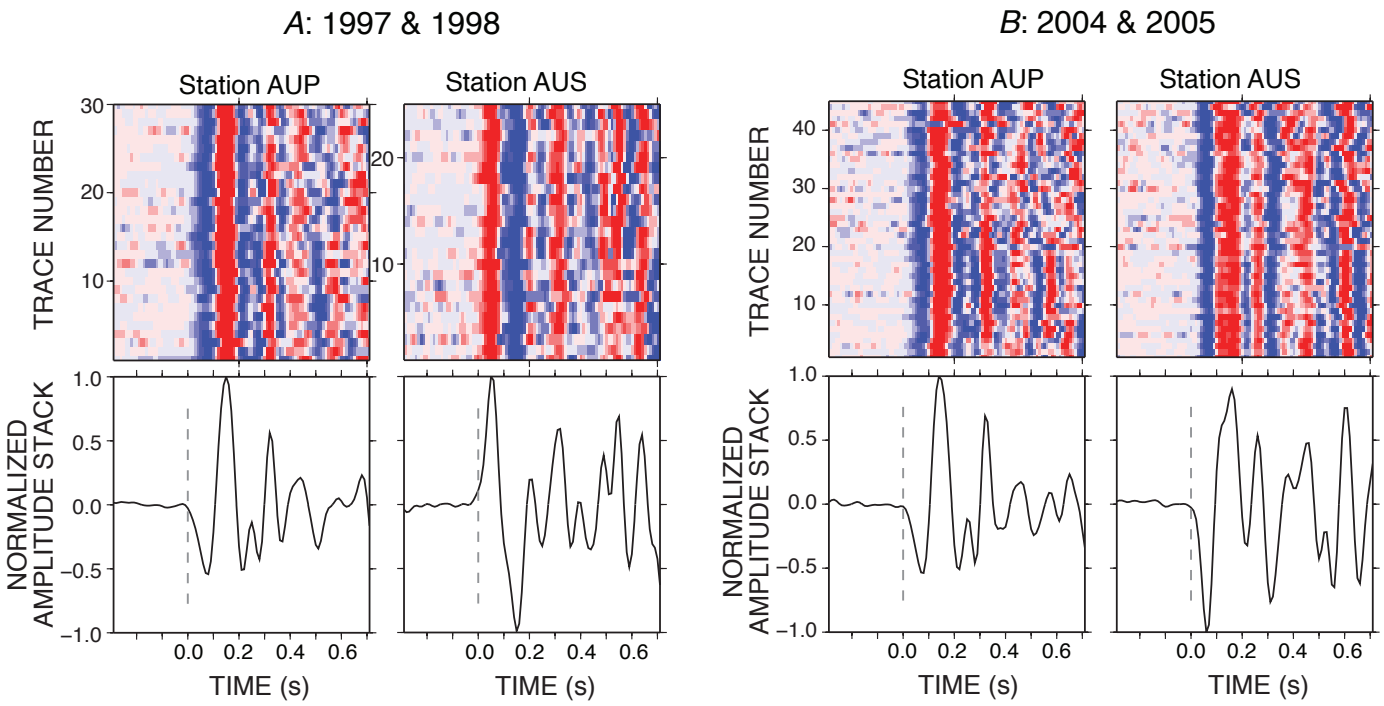

Figure 6. Waveforms for family LM recorded at summit stations AUP and AUS. A, Events from 1997 through 1998. B, Events from 2004 through 2005. Though the waveforms at AUS have different first motion P onsets, this reflects a change in vertical component orientation and not a change of source. Upper panels: Waveforms are visualized as wigglegrams (Rowe and others, 2002b), where red indicates positive and blue indicates negative normalized amplitude. Color intensity scales with normalized amplitude. Waveforms are aligned on the adjusted P onset and sorted by time (trace 1 being the earliest occurring event). Lower panels: Stack of amplitude normalized waveforms. The dashed line indicates P onset. Wigglegrams are used throughout this study to visualize families with more than 20 member events.

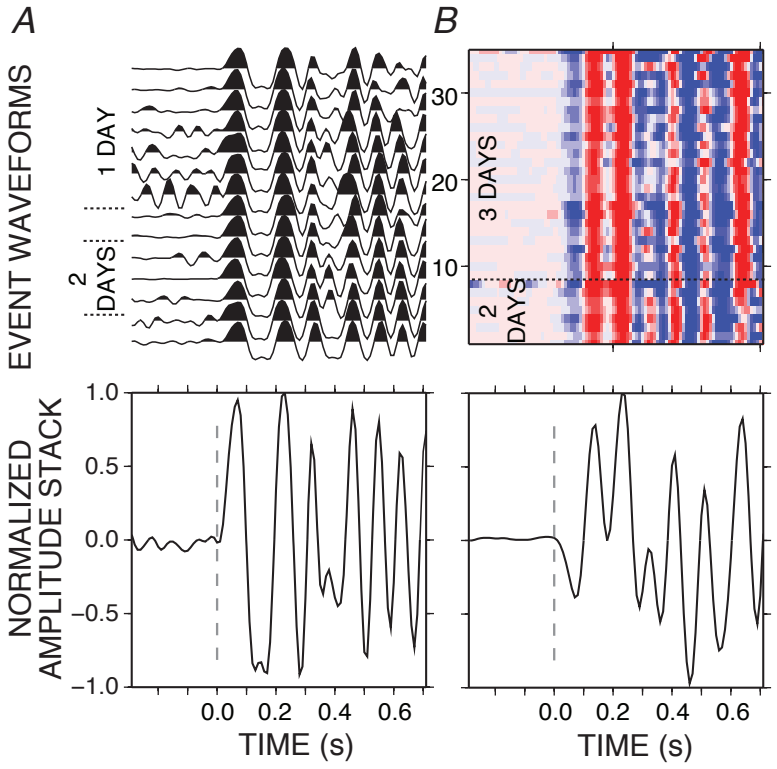

Figure 7. Waveforms and stacks for family AI at summit station AUP (*A*) and family AC at summit station AUH (*B*). Events making up these two families recur over multiple weeks (see fig. 4*B* for full time extent). Each family consists of subsets of single or multiplets of earthquakes that occur over much shorter time scales (one to three days), as noted by small dashed lines on the upper panel. Upper panels: Waveforms are aligned on the adjusted P onset and sorted by time. Family AC contains more than 30 events and is shown as a wigglegram. Lower panels: Stack of amplitude normalized waveforms. The dashed line indicates P onset.

Summit-to-summit times were assigned weight 1.0, and summit-to-flank and flank-to-flank stations were set to 0.02. We assumed a constant velocity half space of 3.5 km/s for P waves, which is slightly faster than the average edifice velocities in the 1D AVO velocity model for Augustine. Edifice velocities are poorly constrained at Augustine, however, and there is some evidence that edifice velocities may be as high as 4.4 km/s (Power, 1988). Families A and B are separated by ~100 m, but more significantly are located 400 m to the south, 200 m to the east, and 800 m deeper than family AD, which is associated with explosive eruptions.

Sumiejski and others (2009) extended this approach of using station-pair differential times to derive family locations for the 2006 Augustine eruption. They used the CC coefficients derived in this study for nine families (A, AC, AD, AH, B, BC, C, LM, and O) using all 36 Augustine station-pairs and incorporated a linear-gradient velocity model obtained from preliminary forward modeling of the data. They also calculated quality weights for each of the station-pair time differences and solved for location using both a grid search and a modified Geiger's method of iterative, reweighed least squares (see Sumiejski and others, 2009, for further information). The results indicated that family LM occurs at ~300 m b.m.s.l. Precursory activity A, B, BC, and C located at ~500 m above m.s.l. (a.m.s.l.), as does family AC that is associated in time with the explosive phase. Families AD and AH, also associated with the explosive phase, located near the Augustine summit at ~1,200 m a.m.s.l.

Deep events (below ~3 km b.m.s.l.) are fairly rare at Augustine. Fifty-four catalog events occur between 2.5 and 6 km b.m.s.l. at Augustine, and all but five of these occur in 2006. Power and Lalla (this volume) showed that all but 18 of these events are mislocated shallow earthquakes. Deep events at Augustine are not expected to be well recorded at summit stations (Lalla and Kienle, 1980), and most summit stations

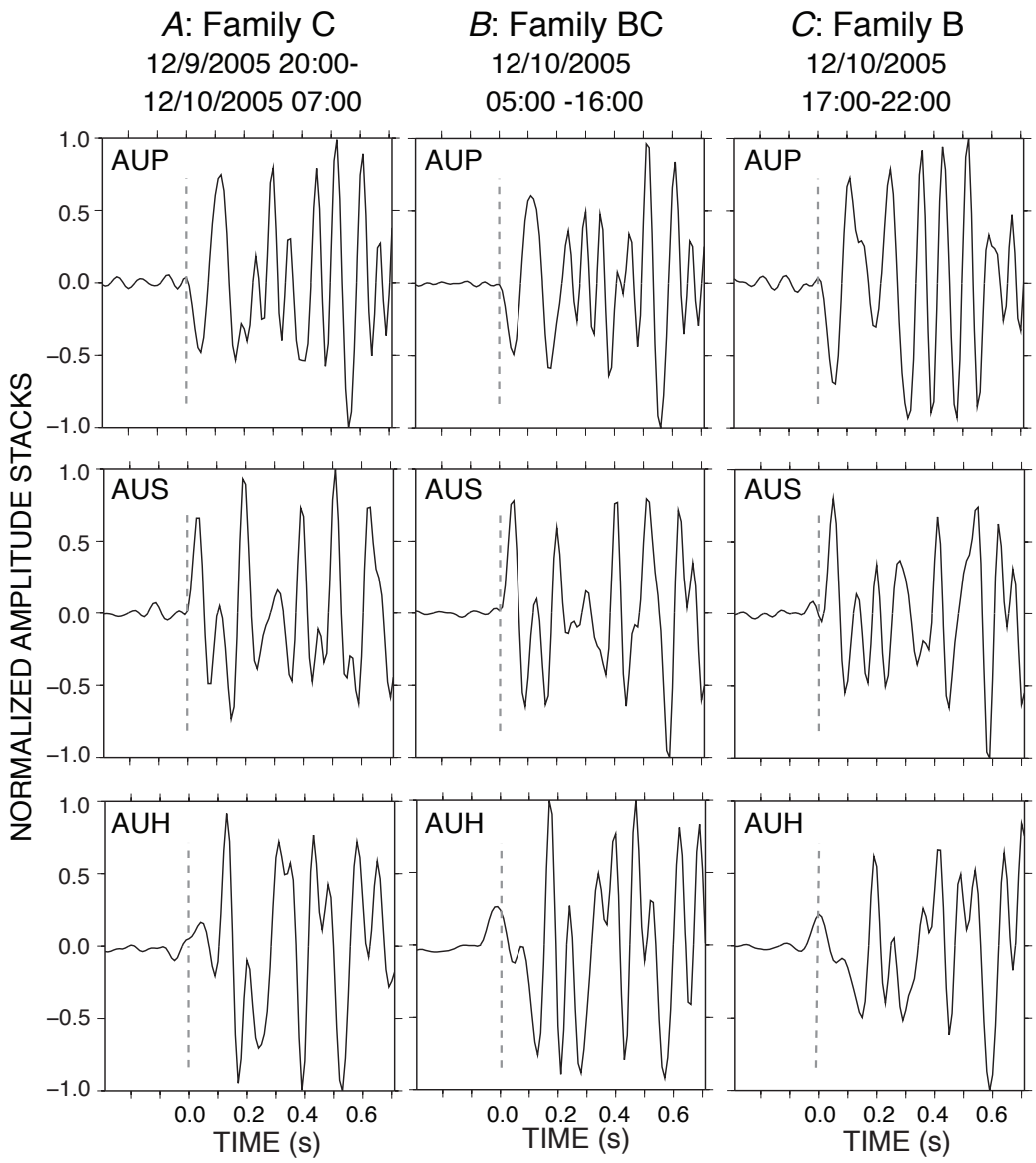

Figure 8. Normalized amplitude waveform stacks at stations AUP, AUS, and AUH aligned on adjusted P onset for event families C (*A*), BC (*B*), and B (*C*). These families occur consecutively in time during December 9–10, 2005, and the exact time extent of each is shown as date and hours AST. The event families are very similar in P onset and frequency content. Difference in P coda may be due to spatial migration or small changes in source mechanism. The mean centroid for each family is at ~ –0.68 km b.m.s.l.; the individual catalog hypocenter depth ranges are from –3 to 0 km b.m.s.l. The dashed line indicates P onset.

went offline following the explosive eruptions in January 2006. Of the remaining deep events, eleven of these events have fairly similar P onsets (fig. 14) and form event family AA (fig. 4*A*). The events occur throughout a 3-month period following the cessation of explosive activity. No deep seismicity was recorded during or following the 1986 Augustine eruption, although some activity was located at these depths before the 1976 eruption (Power and Lalla, this volume). Changes in network geometry between the 1976 and 1986 eruptions could account for this feature of the seismicity. Kienle (1987) interpreted seismicity occurrence at 3 to 4 km b.m.s.l. to be indicative of magma transport within or out of a storage body associated with the 1976 eruption. If a storage system is present at these depths and provided source material for the 2006 eruption, deep seismicity appears primarily linked to posteruptive processes.

Discussion

Seismic unrest prior to the 2006 eruption began as a steady increase in microearthquakes beneath the volcano, ranging from 1 to 2 events located in the AVO catalog per day in May of 2005 to 15 per day in mid-December. Over this period, continuous GPS (cGPS) sites located on the volcano flanks began to move away from one another in a radial manner, indicating inflation of the edifice. On November 17, 2005, the east-west baseline abruptly offset and motion at each station accelerated (Cervelli and others, 2006). On January 11, 2006, the eruption entered the explosive phase and generated the first of 13 explosive eruptions that continued throughout the month. During January 12–13, 2006, explosive eruptions ceased but seismicity rate reached a peak of 130 events/day (fig. 4*C*). At this time, a cGPS site located on the summit moved ~10 cm northeast. Six explosive eruptions commencing on January 13 and ending January 14, 2006, destroyed all summit seismic and cGPS stations. A large pyroclastic flow related to the January 28, 2006, explosive eruption buried the northernmost cGPS station and seismic stations AUL and AUH (fig. 1). Over February and March 2006, quieter magma effusion led to numerous pyroclastic flows, formation of a new lava dome, and magma flows on the north and northeast flanks. Seismicity rate returned to pre-2005 levels by late February 2006.

Cervelli and others (2006) modeled the Augustine cGPS data using an ascending dike source. They showed that the precursory-stage radial pattern recorded by the cGPS is consistent with an initial source with a top no higher than sea level. Mattia and others (2008) modeled the initial source as a vertical ellipsoid at ~300 m b.m.s.l. Summit cGPS data were well fit by a dike beginning to ascend on November 17 and reaching near the surface by mid-December 2005, likely coincident with increased edifice activity on December 9–11, 2005 (fig. 4*C*). The ascending dike likely did not breach the summit until the explosive eruption of January 13, 2006. The initial explosive eruption of January 11 contained no juvenile material, whereas the January 13 magmas were dominated by juvenile material (Wallace and others, this volume; Cervelli and others, 2006). This observation is consistent with the continuing motion recorded by the summit cGPS station through January 13, 2006.

The above model of the 2006 eruption is broadly consistent with a model for the 1986 eruption based on melt inclusion data (Roman and others, 2006). Roman and others (2006) found that the 1986 erupted magmas contained

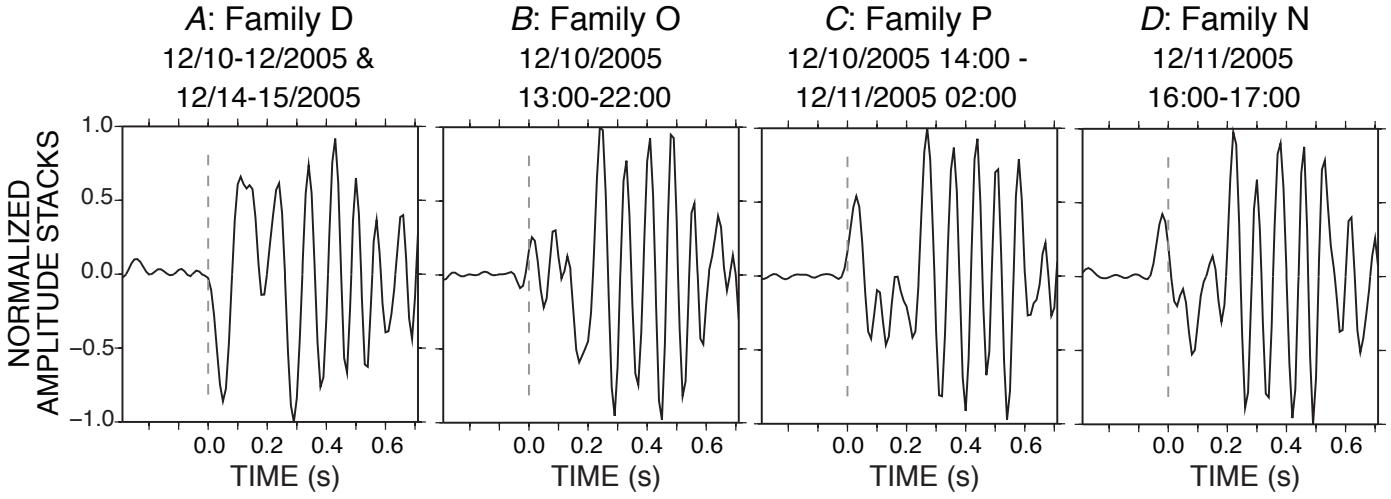

Figure 9. Normalized amplitude waveform stacks at station AUP for event families D (*A*), O (*B*), P (*C*), and N (*D*). These families occur from December 10 to 15, 2005, and hence overlap in time those shown in figure 8. Families O, P, and N have opposite first motion at AUP than either family D or families C, BC, and B (fig. 8). Similarly, the mean centroid of family D is –0.67 km b.m.s.l., much like that for the families shown in figure 8. Families O, P, and N have mean centroids of –0.62 km, –0.63 km, and –0.92 km b.m.s.l., respectively. This suggests that multiple regions of the edifice are generating volcano-tectonic earthquakes over the same temporal period. The time extent of each family is shown as date and hours AKST. The dashed line indicates P onset.

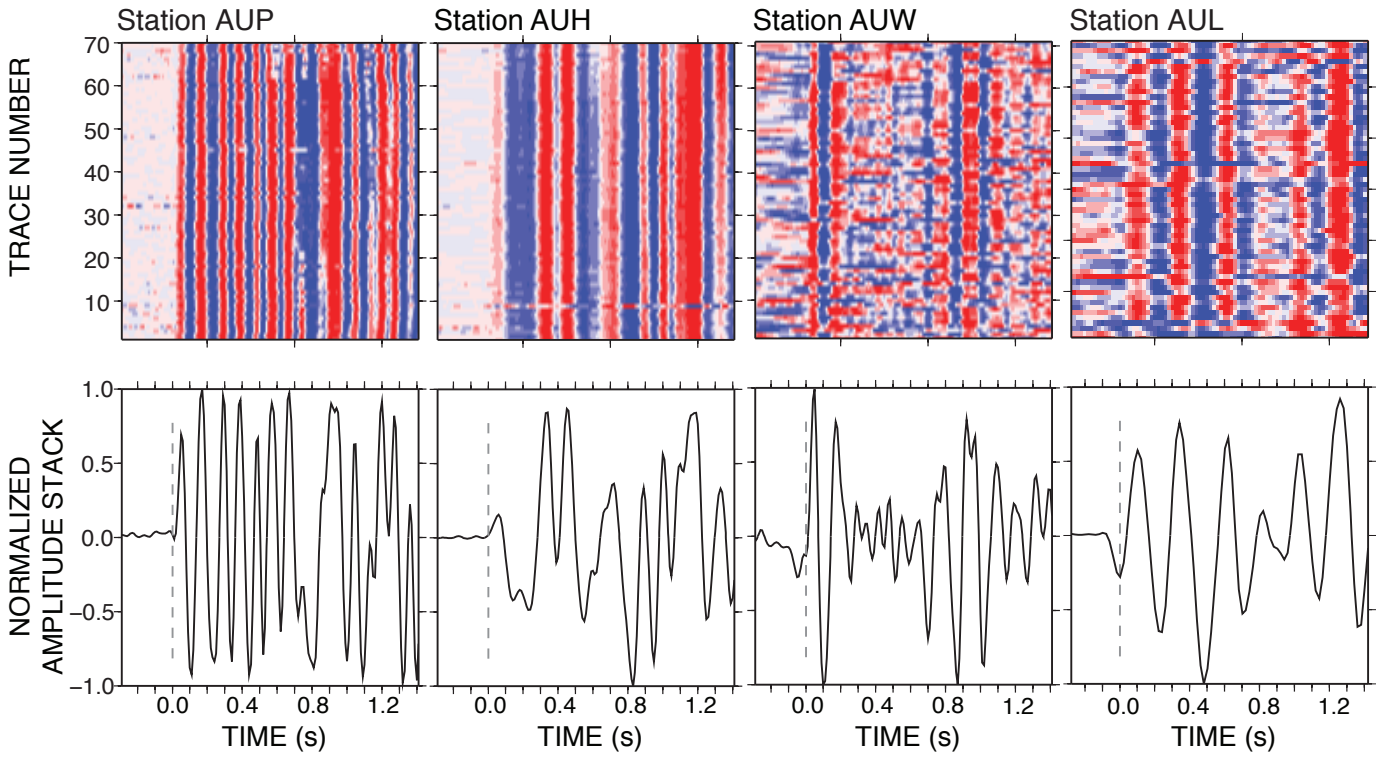

Figure 10. Wigglegrams and normalized amplitude waveform stacks for a swarm of ~70 earthquakes on January 11, 2006, which extended from ~2000 to 2200 AKST (family AD on fig. 4*C*). Waveforms are aligned on the adjusted P onset at summit stations AUP and AUH and at flank stations AUW and AUL. Though these events are highly similar, the waveform does evolve over time, likely reflecting small changes in source process or path. The dashed line indicates P onset.

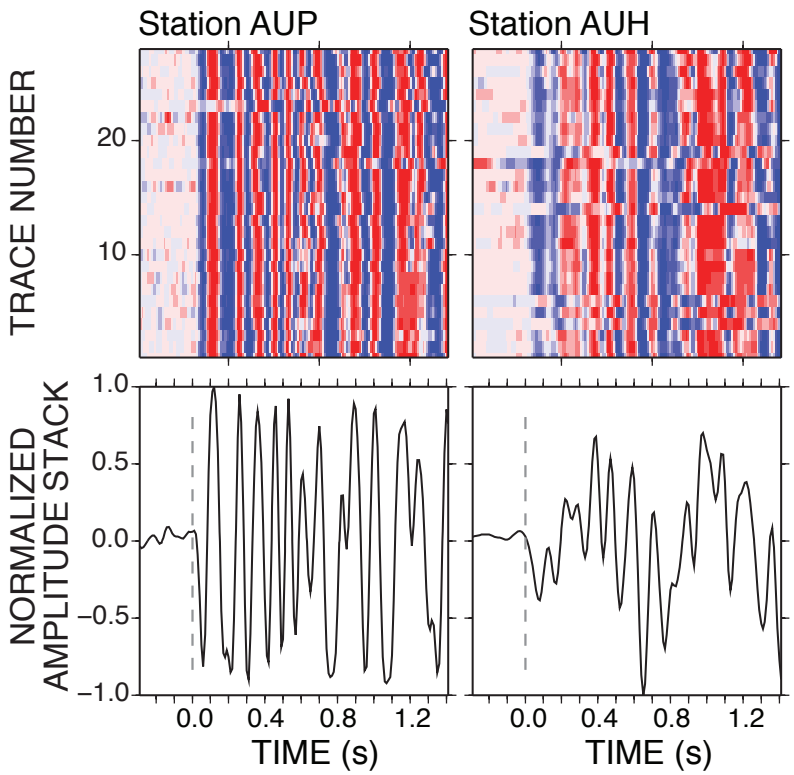

Figure 11. Wigglegrams and normalized amplitude waveform stacks for 28 similar earthquakes that occurred over a 13-hour period during the initial explosive stage (family AH on fig. 4*C*). Waveforms are aligned on the adjusted P onset at summit stations AUP and AUH. These events start to occur a few hours after the large swarm shown in figure 10 and contain the same overall frequency content of the larger swarm. However, first motion polarity is opposite. The dashed line indicates P onset.

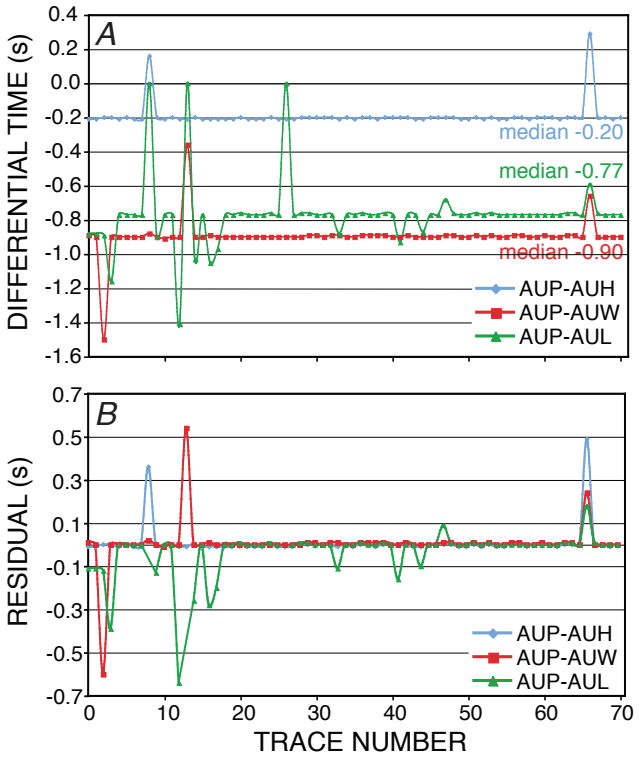

Figure 12. Collocated events should generate identical arrival-time differences at any two stations, as shown here for event family AD. *A*, Differential arrival times for 72 events in family AD indicate a very high degree of waveform similarity at stations AUP, AUH, AUW, and AUL. Differential times are calculated using the adjusted P-wave onset based on waveform crosscorrelation. The median value is noted. *B*, The residual time is calculated by removing the median for each station pair. The mean of the residuals for each station pair is 0.0 s, a strong indication that individual member events are collocated.

evidence for mixing between dacitic and more mafic source magma. Magma remained compositionally heterogeneous over the length of that eruption. They concluded that the 1986 eruption resulted from an injection of hot, mafic magma stored between 3 and 4 km b.m.s.l. This material mixed with more dacitic residual magma left in the edifice following the 1976 eruption. The source depth of 3 to 4 km is significantly deeper than the source constrained by cGPS modeling of the 2006 eruption, however. Both models suggest that magma storage and transport in the Augustine edifice takes place through a series of dikes, some of which are interconnected and some of which are not.

Volcano-tectonic (VT) seismicity caused by fluid and volatile transport is a commonly recorded feature of volcanoes before and during volcanic eruptions (for example, McNutt, 2005). Hill (1977) proposed that earthquake swarms result from the migration of fluids through a series of en echelon extension fractures linked to each other by small crack-tip shear fractures. Fracture mesh formation occurs within a constant stress field within a volume of rock, most favorably in materials with a high degree of heterogeneity and in the presence of low effective stress (Sibson, 1996), conditions likely to exist in a volcanic edifice. VT activity along the mesh

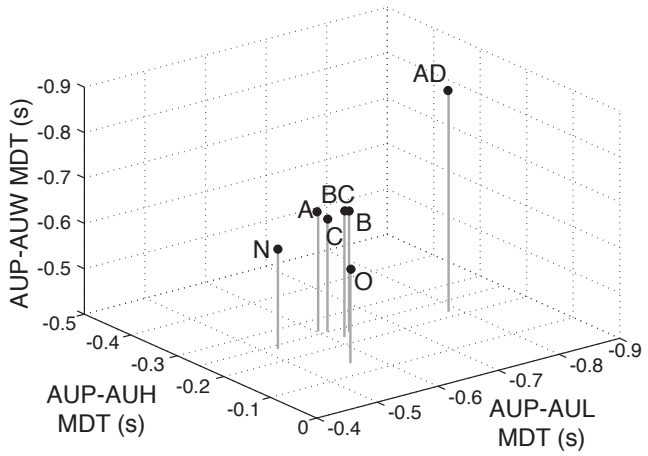

Figure 13. The median differential times (MDT) for a set of station-pairs for each family contain information on the relative location of event families in space. Here, the MDTs for station pairs AUP-AUH, AUP-AUL, and AUP-AUW are plotted for a number of well-recorded clusters occurring the 2006 eruption (see fig. 4*C* for family time ranges). On the basis of geometric arguments, family AD occurs higher in the edifice than the other families. Families C, BC, B, O, and N occur over the same period in early December but are not collocated on this diagram, indicating that multiple regions of the edifice can be simultaneously active.

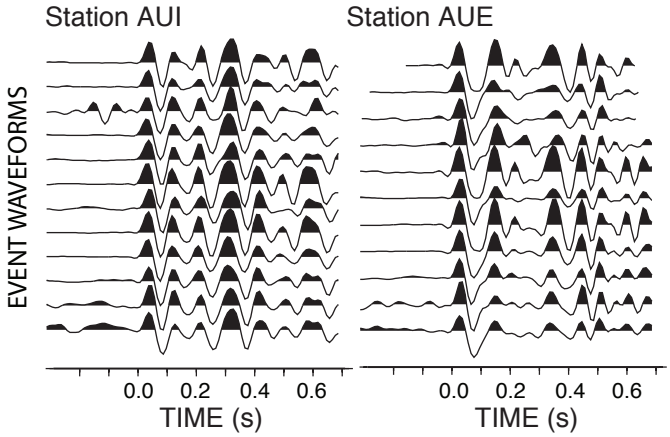

Figure 14. Waveforms for family AA, here shown at stations AUI and AUE, consist of deep earthquakes (~3 km b.m.s.l.) that occur from May through July 2006. All deep earthquakes in the AVO catalog occur in mid to late 2006. Only the flank stations recorded these earthquakes because of the timing.

of shear fractures could appear to be spatially and temporally variable (for example, Roman and Cashman, 2006), with small swarms of activity localizing on individual shears over shorter time scales. Magma transport through dike emplacement, as modeled for the 2006 Augustine eruption, can also generate VT swarms. Ukawa and Tsukahara (1996) suggested that VT swarm activity forms because of extension of wallrock ahead of a propagating dike tip. This model implies a spatial and temporal migration of seismicity in the direction of dike propagation. Roman (2005) showed that inflation of a dike would compress the surrounding wallrock and lead to generation of seismicity in a temporally and spatially random manner. Modeling suggests that seismicity caused by dike-tip propagation and by wallrock compression could be active at the same time (Roman and Cashman, 2006). Roman and Cashman (2006) compare seismicity and fault plane solutions at a number of volcanoes to each of the above models and conclude that at most compressive arc settings, the Roman (2005) and to a lesser extent the Hill (1977) model best explain recorded VT activity. Fracture mesh orientation would be controlled by the regional stress regime, while wallrock failure would reflect local perturbations to this regime. Well-constrained focal mechanism solutions can be used to distinguish between these two processes (Roman and Cashman, 2006).

Our observation that some waveforms repeat over multiple years suggests that in some regions of the edifice the VT source mechanism is nondestructive. Of the three models presented, this seems most consistent with the idea of shear failure along a fracture mesh. Volcanic edifices are fluid-rich and volatile-rich environments, and transport of materials within the edifice must constantly occur. Reported rates of fumoralic activity are fairly constant at Augustine. If transport does occur through a series of interconnected extension and shear fractures, periods of increased transport rate may lead to the periods of increased activity we identify as swarms making up individual event families. The mesh must evolve because of precipitation and mineralization within the fractures (Sibson, 1996). Seismicity not included in event families may be localized to shear fractures that form or reactivate variably in both space and time.

This interpretation does not preclude VT activity due to dike inflation or deflation within the edifice. If dikes are the primary magma transport and storage mechanism at Augustine, then wallrock adjustments due to volumetric changes in the existing dike complex may generate VT seismicity by locally perturbing the local stress field. Inflation may induce short-term compression in the surrounding wallrock and induce swarms of temporally and spatially related seismicity (Roman, 2005). Dike ascent during the precursory stage of the 2006 Augustine eruption is accompanied by increased seismicity rates (Cervelli and others, 2006; Mattia and others, 2008). If the ascending dike interacted with a preexisting dike network, as is posited for the 1986 Augustine eruption, then multiple dikes could have inflated or deflated over the course of the 2006 eruption. This may explain both the cloud-like pattern of dissimilar earthquakes that dominate the entire Augustine catalog and the swarms of highly similar waveforms generated during the 2006 eruption.

The largest identified swarms occurred as the ascending source dike reached near-surface elevations on December 9–11, 2005, and between explosive eruptions through January 2006 (fig. 4*C*). Locations of families identified during this period suggest that some seismicity generated over December 9–11, 2005, occurred ~700 to 800 m below the activity in January 2006 (this study; Sumiejski and others, 2009). We suggest that event families A, B, BC, and C are directly related to this ascending dike. All share similar waveform characteristics, such as frequency content and P onset sign (fig. 8), and the clusters are located very close to each other in space (fig. 13). However, we cannot distinguish if these swarms form because of failure along a propagating dike tip or within the surrounding wallrock during dike ascension. Cervelli and others (2006) and Mattia and others (2008) suggest that the ascending dike breaches the surface during the January 13, 2006, eruption. It is therefore likely that this dike causes the seismicity associated with the January 11 swarm (family AD). Seismicity occurring throughout the remainder of January is both related to summit activity (family AH) and to wallrock adjustments to changing pressures within the dike source at ~500 m a.m.s.l (family AC) (Sumiejski and others, 2009). Longer term magma storage may take place nearer ~300 m b.m.s.l. on the basis of modeling of cGPS data (for example, Mattia and others, 2008) recorded during the early precursory stage and the location of multiyear family LM (for example, Sumiejski and others, 2009).

Conclusions

Waveform similarity at Augustine volcano derived using waveform crosscorrelation techniques occurs over a number of time scales. Approximately 60 to 70 percent of volcano-tectonic events in the AVO catalog are not associated with event clusters containing more than 10 earthquakes. These events may be forming along shear fractures that form in conjunction with extension fractures and facilitate fluid movement within the volcanic edifice. Alternately, these events may reflect long-term wallrock failure caused by local stress perturbations associated with a series of interconnected storage dikes. Events forming families before the 2006 eruption exhibit a high degree of similarity over multiple years but generally consist of subsets of small temporally related swarms. These events would be consistent with either reactivation of shear fractures that form the fracture mesh systems or failure in wallrock near long-lived inflating or deflating dikes. Focal mechanisms would help distinguish between these two models.

Earthquakes recorded during the precursory phases of the 2006 eruption occur as swarms of similar earthquakes over periods of days or hours. The largest identified precursory swarms accompany reports of increased steaming and explosive eruptions at the summit, which are consistent with discrete dikes/sills opening to accommodate magma transport

to the surface. Some event families appear directly associated with an ascending dike through late November and December 2006, but we cannot say whether these events occur along a propagating dike tip or within the surrounding wallrock without focal-mechanism data. Other event families clearly occur at the same time as dike ascension but occur throughout the volcanic edifice, suggesting that local stress perturbations activate a network of fractures or preexisting dikes. Combined with the generally low degree of event similarity at Augustine, the seismic results agree well with the hypothesis that magma transport and storage during eruptions involves numerous dikes located throughout the edifice (Roman and Cashman, 2006; Cervelli and others, this volume; Larsen and others, this volume; Power and Lalla, this volume).

Seismicity rate and event similarity decrease rapidly over the course of the 2006 eruption. The only family identified during the late eruptive and effusive phases contains relatively deep earthquakes between 3 and 5 km b.m.s.l. If the source dike for the 2006 eruption ascends from 0 km b.m.s.l. or deeper, these events may reflect posteruptive magma transport at the base of the Augustine magmatic system.

Acknowledgments

We thank James Dixon and the Alaska Volcano Observatory for access to waveform and pick data. Waveforms, shot locations and times, and parametric data from the active source experiment were obtained from the IRIS DMC. Stephanie Prejean provided helpful discussions. We thank Jeffery Freymueller, Charlotte Rowe, and Maurizio Battaglia for insightful reviews. Waveforms, picks, and crosscorrelation data reported in this study may be obtained by request through Heather DeShon. The material is based on research supported by NSF grant EAR-0409291 to Clifford Thurber.

References Cited

Aster, R.C., and Rowe, C.A., 2000, Automatic phase pick refinement and similar event association in large seismic datasets, *in* Thurber, C.H., and Rabinowitz, N., eds, Advances in seismic event location: Kluwer, Amsterdam, p. 231–263.

Battaglia, J., Thurber, C.H., Got, J.L., Rowe, C.H., and White, R.A, 2004, Precise relocation of earthquakes following the 15 June 1991 eruption of Mount Pinatubo, Philippines: Journal of Geophysical Research, v. 109, B07302, doi:10.1029/2003JB002959.

Buurman, H., and West, M.E., 2010, Seismic precursors to volcanic explosions during the 2006 eruption of Augustine Volcano, *in* Power, J.A., Coombs, M.L., and Freymueller, J.T., eds., The 2006 eruption of Augustine Volcano, Alaska: U.S. Geological Survey Professional Paper 1769 (this volume).

Cervelli, P.F., Fournier, T., Freymueller, J., and Power, J.A., 2006, Ground deformation associated with the precursory unrest and early phases of the January 2006 eruption of Augustine Volcano, Alaska: Geophysical Research Letters, v. 33, L18304, 10.1029/2006GL027219.

Cervelli, P.F., Fournier, T.J., Freymueller, J.T., Power, J.A., Lisowski, M., and Pauk, B.A., 2010, Geodetic constraints on magma movement and withdrawal during the 2006 eruption of Augustine Volcano, *in* Power, J.A., Coombs, M.L., and Freymueller, J.T., eds., The 2006 eruption of Augustine Volcano, Alaska: U.S. Geological Survey Professional Paper 1769 (this volume).

DeShon, H.R., Thurber, C.H., and Rowe, C., 2007, High-precision earthquake location and three-dimensional P wave velocity determination at Redoubt Volcano, Alaska: Journal of Geophysical Research, v. 112, B07312, doi:10.1029/2006JB004751.

Dixon, J.P., Stihler, S.D., Power, J.A., and Searcy, C., 2008, Catalog of earthquake hypocenters at Alaskan volcanoes; January 1 through December 31, 2006: U.S. Geological Survey Data Series 326, 78 p.

Dodge, D.A., 1996, Xadjust; a Matlab-based cross correlation analysis package: Seismological Research Letters, v. 67, p. 36.

Dodge, D.A., Beroza, G.C., and Ellsworth, W.L., 1995, Foreshock sequence of the 1992 Landers, California, earthquake and its implications for earthquake nucleation: Journal of Geophysical Research, v. 100, p. 9865–9880.

Du, W., Thurber, C.H., and Eberhart-Phillips, D., 2004, Earthquake relocation using cross correlation time delay estimates verified with the bispectrum method: Bulletin of the Seismological Society of America, v. 94, p. 856–866.

Got, J.L, Frechet, J., and Klein, F.W., 1994, Deep fault plane geometry inferred from multiplet relative relocation beneath the south flank of Kilauea: Journal of Geophysical Research, v. 99, p. 15375–15386.

Hill, D.P., 1977, A model for earthquake swarms: Journal of Geophysical Research, v. 82, p. 1347–1352.

Kienle, J., 1987, Mt. St. Augustine works, but how? [abs.]: Hawaii Symposium on How Volcanoes Work, Abstract Volume, p. 139.

Lalla, D.J., and Kienle, J., 1980, Problems in volcanic seismology on Augustine Volcano, Alaska [abs.]: Eos (Transactions American Geophysical Union), v. 61, p. 68.

Larsen, J.F., Nye, C.J., Coombs, M.L., Tilman, M., Izbekov, P., and Cameron, C., 2010, Petrology and geochemistry of the 2006 eruption of Augustine Volcano, *in* Power, J.A.,

Coombs, M.L., and Freymueller, J.T., eds., The 2006 eruption of Augustine Volcano, Alaska: U.S. Geological Survey Professional Paper 1769 (this volume).

Mattia, M., Palano, M., Aloisi, M., Bruno, V., and Bock, Y., 2008, High rate GPS data on active volcanoes; an application to the 2005-2006 Mt. Augustine (Alaska, USA) eruption: Terra Nova, v. 20, no. 2, p. 134–140.

McNutt, S.R., 2005, Volcanic seismology: Annual Reviews of Earth and Planetary Science, v. 33, p. 461–491.

Milne, J., 1886, Earthquakes and other earth movements: New York, D. Appleton and Company, 363 p.

Nikias, C.L., and Pan, R., 1988, Modeling of the 4th-order cumulants and phase estimation: Circuits Systems Signal Processing, v. 7, p. 291–325.

Nikias, C.L., and Raghuveer, M.R., 1987, Bispectrum estimation—a digital signal-processing framework: Proceedings of the IEEE, v. 75, p. 869–891.

Power, J.A., 1988, Seismicity associated with the 1986 eruption of Augustine Volcano, Alaska: Fairbanks, University of Alaska, M.S. thesis, 142 p.

Power, J.A., and Lalla, D.J., 2010, Seismic observations of Augustine Volcano, 1970–2007, *in* Power, J.A., Coombs, M.L., and Freymueller, J.T., eds., The 2006 eruption of Augustine Volcano, Alaska: U.S. Geological Survey Professional Paper 1769 (this volume).

Roman, D.C., 2005, Numerical models of volcanotectonic earthquake triggering on non-ideally oriented faults: Geophysical Research Letters, v. 32, L02304, doi:10.1029/2004GL021549.

Roman, D.C., and Cashman, K.V., 2006, The origin of volcano-tectonic earthquake swarms: Geology, v. 34, p. 457–460.

Roman, D.C., Cashman, K.V., Gardner, C.A., Wallace, P.J., and Donovan, J.J., 2006, Storage and interaction of compositionally heterogeneous magmas from the 1986 eruption of Augustine Volcano, Alaska: Bulletin of Volcanology, v. 68, p. 240–254, doi:10.1007/s00445-005-003-z.

Rowe, C.A., 2000, Correlation-based phase pick corrections and similar earthquake family identification in large seismic waveform catalogs: Socorro, New Mexico Institution of Mining & Technology, Ph.D. Thesis, 187 p.

Rowe, C.A., Aster, R.C., Borchers, B., and Young, C.J., 2002a, An automatic, adaptive algorithm for refining phase picks in large seismic datasets: Bulletin of the Seismological Society of America, v. 92, p. 1660–1674.

Rowe, C.A., Aster, R.C., Phillips, W.S., Borchers, B., Jones, R.H., and Fehler, M.C., 2002b, Using automated, high-precision repicking to improve delineation of microseismic structures at the Soultz geothermal reservoir: Pure and Applied Geophysics, v. 159, p. 563–596.

Rowe, C.A., Thurber, C.H., and White, R.A., 2004, Dome growth behavior at Soufriere Hills Volcano, Montserrat, revealed by relocation of volcanic event swarms, 1995-1996: Journal of Volcanology and Geothermal Research, v. 134, p. 199–221.

Rubin, A.M., Gillard, D., and Got, J.L., 1998, A reinterpretation of seismicity associated with the January 1983 dike intrusion at Kilauea Volcano, Hawaii: Journal of Geophysical Research, v. 103, p. 10003–10015.

Schaff, D.P., Bokelmann, G.H.R., Beroza, G.C., Waldhauser, F., and Ellsworth, W.L., 2002, High-resolution image of Calaveras Fault seismicity: Journal of Geophysical Research, v. 107, p. 2186, doi:10.1029/2001JB000633.

Shearer, P.M., 1998, Evidence from a cluster of small earthquakes for a fault at 18 km depth beneath Oak Ridge, southern California: Bulletin of the Seismological Society of America, v. 88, p. 1327–1336.

Sibson, R.H., 1996, Structural permeability of fluid-driven fault-fracture meshes: Journal of Structural Geology, v. 18, p. 1031–1042.

Sumiejski, L., Thurber, C., and DeShon, H.R., 2009, Relocation of eruption-related earthquake clusters at Augustine Volcano, Alaska, using station-pair differential times: Geophysical Journal International, v. 176, p. 1017–1022.

Ukawa, M., and Tsukahara, H., 1996, Earthquake swarms and dike intrusions off the east coast of Izu Peninsula, central Japan: Tectonophysics, v. 253, p. 285–303, doi:10.1016/0040-1951(95)00077-1.

Wallace, K.L., Neal, C.A., and McGimsey, R.G., 2010, Timing, distribution, and character of tephra fall from the 2005–2006 eruption of Augustine Volcano, *in* Power, J.A., Coombs, M.L., and Freymueller, J.T., eds., The 2006 eruption of Augustine Volcano, Alaska: U.S. Geological Survey Professional Paper 1769 (this volume).

Yung, S.K., and Ikelle, L.T., 1997, An example of seismic time picking by third-order bicoherence: Geophysics, v. 62, p. 1947–1952.

Zhou, H., 1994, Rapid three-dimensional hypocentral determination using a master station method, Journal of Geophysical Research: v. 99, p. 15439–15455.

The 2006 Eruption of Augustine Volcano, Alaska
Power, J.A., Coombs, M.L., and Freymueller, J.T., editors
U.S. Geological Survey Professional Paper 1769

Chapter 6

Distal Volcano-Tectonic Seismicity Near Augustine Volcano

Michael A. Fisher[1], Natalia A. Ruppert[2], Randall A. White[1], Ray W. Sliter[1], and Florence L. Wong[1]

Abstract

Clustered earthquakes located 25 km northeast of Augustine Volcano occurred more frequently beginning about 8 months before the volcano's explosive eruption in 2006. This increase in distal seismicity was contemporaneous with an increase in seismicity directly below the volcano's vent. Furthermore, the distal seismicity intensified penecontemporaneously with signals in geodetic data that appear to reveal a transition from magmatic inflation of the volcano to dike injection. Focal mechanisms for five events within the distal cluster show strike-slip-fault movement. Directly above the earthquake cluster, shallow (<5 km deep) folds and faults mapped using multichannel seismic-reflection data strike northeast, parallel to the regional structural grain. About 10 km northeast of Augustine Volcano, however, the Augustine-Seldovia arch, an important trans-basin feature, strikes west and intersects the northeast-striking structural zone. We propose that the fault causing the distal earthquake cluster strikes northwest, subparallel to the arch, and is a right-lateral strike-slip fault. Future earthquake monitoring might show whether increasing activity in the remote cluster can aid in making eruption forecasts.

Introduction

Augustine Volcano most recently erupted explosively during 2006, and intense shallow seismicity directly below the volcano's vent of the volcano preceded and accompanied this eruption (Cervelli and others, 2006, and this volume; Power and others, 2006). Contemporaneously with this volcanic and earthquake activity, seismicity occurred in a cluster located 25 km northeast of the volcano (figs. 1, 2). This distal seismicity ceased about 9 months after the eruption ended. On a worldwide basis, similar distal seismicity has occurred before many explosive eruptions (for example, White and Rowe, 2006). Thus, a future increase in distal seismicity near Augustine Volcano might help predict an eruption.

Regional Setting and Basin Structure

Augustine Volcano is part of the active magmatic arc associated with plate convergence at the Alaska-Aleutian subduction zone. The volcano lies within the southwestern part of the Cook Inlet forearc basin (fig. 1) and rests on a thick section of sedimentary and volcanic rocks that indicate protracted near-trench tectonics, including Late Triassic rocks that signal a transition from reef building far from volcanic sources to proximal magmatic-arc sedimentation (Wang and others, 1988), and thick Early Jurassic volcaniclastic rocks that record a vigorous volcanic arc near the Cook Inlet basin (Detterman and Hartsock, 1966; Fisher and Magoon, 1978). The Jurassic and Cretaceous batholiths exposed extensively along the northwest side of the Cook Inlet basin indicate active subduction during that period.

These plutonic rocks likely form the basement complex beneath the Cook Inlet basin, especially near Augustine Volcano. The basement complex might also include early Mesozoic oceanic crust, following from a tectonic analogy we draw between the Cook Inlet basin and the Great Valley of California, both of which are Mesozoic forearc basins. The Great Valley appears to be floored by oceanic crust, the distribution and structure of which is much debated (see summary cross sections in Constenius and others, 2000). The point is that the basement under Cook Inlet might have a complex structure.

We determined the upper-crustal structure near Augustine Volcano from a grid of multichannel seismic-reflection (MCS) lines collected by Western Geophysical, Inc., in 1975 (fig. 1). The data were obtained with an Aquapulse source, an array of six sleeve exploders in which propane and oxygen

[1] U.S. Geological Survey, 345 Middlefield Rd., Menlo Park, CA 92028.

[2]Geophysical Institute, University of Alaska Fairbanks, 903 Koyukuk Dr., Fairbanks, AK 99775.

were detonated to produce an acoustic pulse with reduced bubble oscillation. The survey ship employed two streamers—one 2,380 m long with 72 recording channels, and the other 184 m long with 12 channels designed to achieve a high spatial resolution.

MCS data reveal that the Iniskin structural zone strikes northeast through lower Cook Inlet (fig. 1). The structural zone is made up of reverse faults and faulted anticlines (fig. 3). The vertical component of offset along some faults amounts to 500 m. The total along-strike length of this zone is unknown but is at least 70 km. The MCS section in figure 3*C* shows the Iniskin structural zone extending southwestward to within about 10 km of Augustine Volcano (fig. 1). However, this zone's total southwestward extent remains unknown because the zone is not evident in Mesozoic rocks exposed on the northern part of the Alaska Peninsula, southwest of Augustine Volcano.

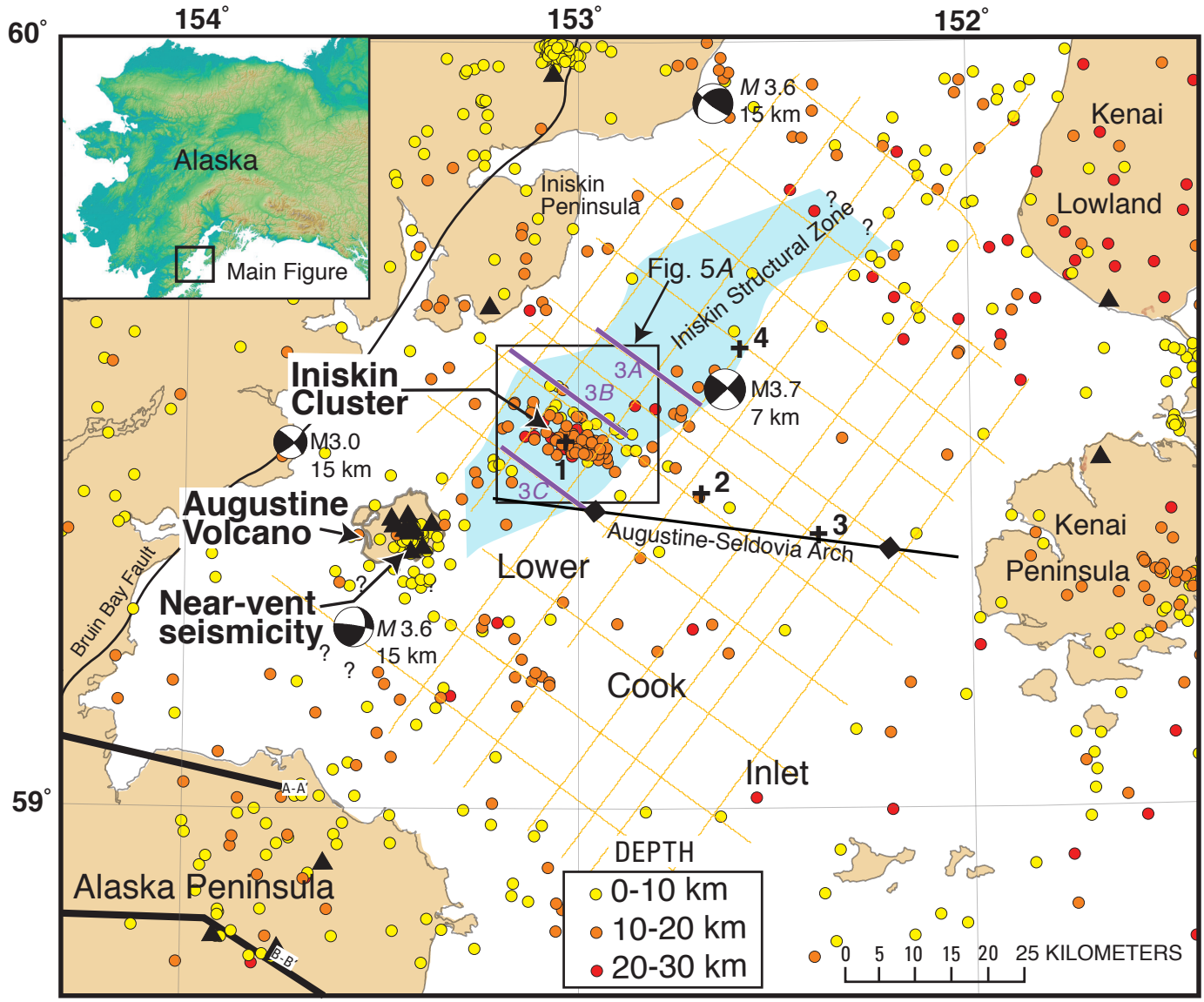

Figure 1. Map of Lower Cook Inlet, Alaska, showing the location of Augustine Volcano, the Iniskin earthquake cluster, and the Iniskin structural zone (blue area). Seismic events (colored dots) have not been relocated. Black rectangle on index map denotes area of relocated events in figure 5. Orange lines, show track lines of 1975 Western Geophysical, Inc., seismic-reflection survey; purple lines, multichannel seismic reflection sections shown in figure 3; Black lines labeled A-A' and B-B' indicate geologic cross sections by Detterman and Reed (1980) and Riehle and others (1993), respectively. Numbered black crosses show oil wells near Augustine Volcano: 1, Hawk #1; 2, Ibis #1; 3, South Arch #1; 4, COST #1. Earthquake epicenters are from the Alaska Earthquake Information Center (AEIC) catalog (1971-2006); earthquake focal mechanisms are lower-hemispheric projections. Black triangles show seismograph stations.

Geologic cross sections (A–A', B–B', fig. 1) from there show little-deformed, mainly flat lying rocks (Detterman and Reed, 1980; Riehle and others, 1993).

Folds and faults within the Cook Inlet basin strike consistently northeast (fig. 4). Northwest-striking structures are not evident in offshore areas, nor do such structures deform the major faults, such as the Bruin Bay Fault, that bound the basin on the northwest and southeast. The Iniskin structural zone strikes northeast, conforming to the regional structural grain.

The prime exception to the consistent northeastward strike is the westward strike of the Augustine-Seldovia arch, which extends across the basin to near Augustine Volcano (figs. 1 and 4). This arch is a fundamental feature of the Cook Inlet basin because it forms the south flank of the thick (7 km) accumulation of Cenozoic rocks north of the arch (for example Kirschner and Lyon, 1973). South of the arch, Cenozoic rocks are thin (<1 km thick) or absent (Fisher and Magoon, 1978). Evidently, the arch forms a trans-basin hinge that enabled rapid Cenozoic deepening of the northern part of the basin.

Seismicity

The regional seismicity of lower Cook Inlet, recorded in by the Alaska Earthquake Information Center (AEIC) catalog (1971–2006), is diffuse and reveals few patterns in map view (fig. 1), except in two areas of heightened activity. The first area encompasses abundant shallow earthquakes directly below the volcano's vent. This seismicity was recorded by seismographs located on the volcano and on nearby parts of

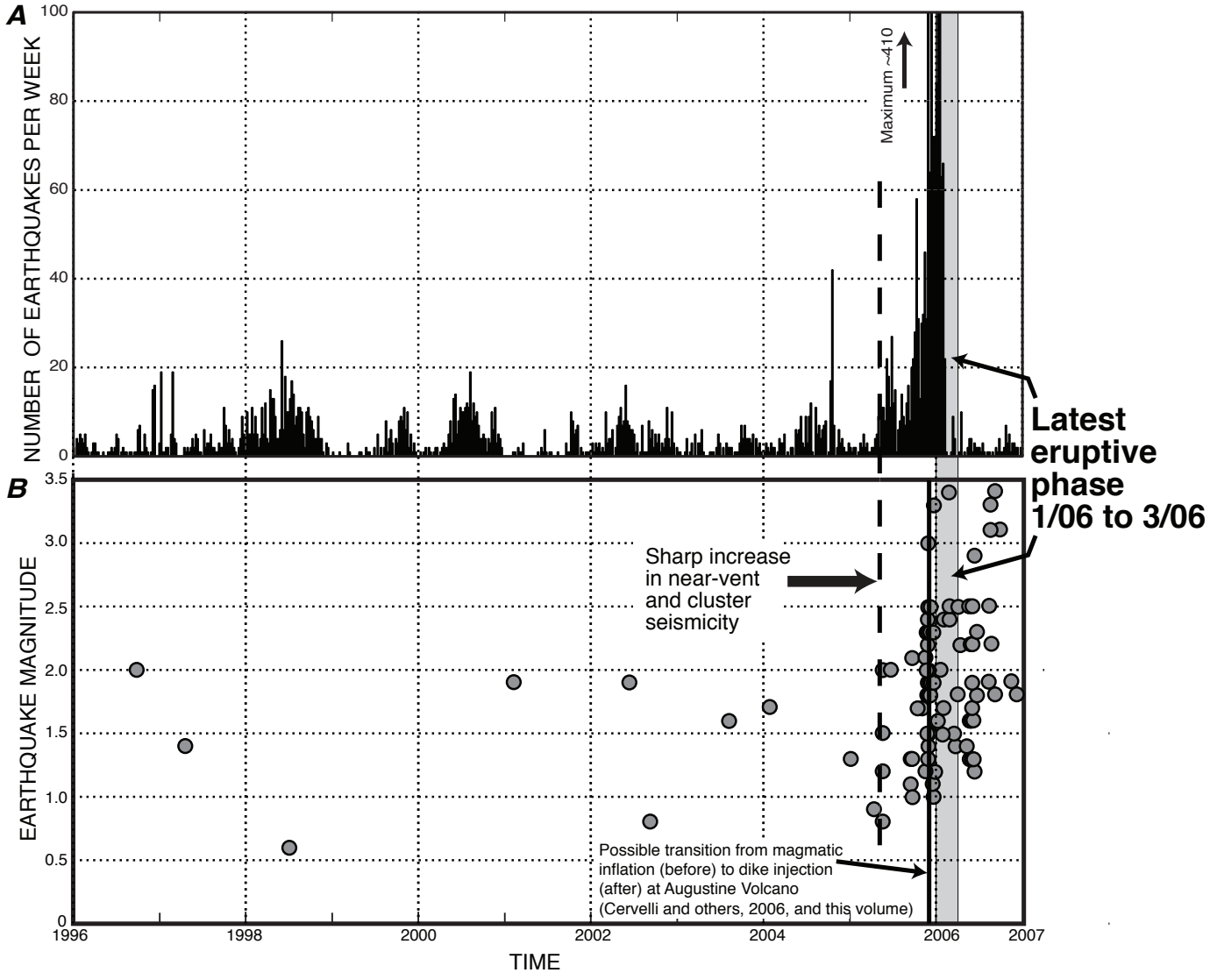

Figure 2. Earthquake activity over time at Augustine Volcano. *A*, near vent seismicity, *B*, seismicity within the Iniskin cluster. Cluster activity began about 8 months before the 2006 eruption and ended about 9 months afterward. Vertical dashed line denotes the abrupt increase in activity in late 2005.

the Alaska mainland. In general, near-vent earthquakes have very small magnitudes (M<=1.2). This activity has been attributed to volcanic processes because it is concentrated near sea level, directly below the volcanic vent. After 1996, near-vent seismicity oscillated between infrequent and moderately frequent until late 2005, when the frequency intensified to more than 100 events per week (fig. 2*A*).

The second area of heightened activity, which we call the Iniskin cluster, is located 25 km northeast of the volcano (fig. 1). Events making up this cluster were recorded by the Alaska regional seismic network; the nearest seismic stations are located on Augustine Volcano (fig. 1). Before we relocated the cluster events, their average horizontal and vertical location uncertainties were 3.6 and 4.1 km, respectively, at the 67 percent confidence level. In the worst case of the smallest events recorded by only a few stations, such uncertainties were as large as 10 km. Before being relocated, the group of epicenters was elongated northwest-southeast ward (fig. 1), but as we describe below, the relocated epicenters fill a compact area with a poorly expressed elongation.

Since 1996, near-vent earthquakes have numbered nearly 3,000 (Dixon and others, 2007), but only about 100 events have occurred within the Iniskin cluster. Cluster earthquakes were infrequent until mid-2005, when they became more frequent (fig. 2*B*). This increase in frequency occurred contemporaneously with the rapid rise in near-vent seismicity (compare figs. 2*A* and 2*B*), and both increases preceded by about 8 months the latest explosive eruption of Augustine Volcano. The level of earthquake activity within the Iniskin cluster remained relatively high throughout most of 2006, slowing only toward the end of the year. No events occurred in October and November, and only one in December.

An abrupt offset in geodetic data recorded during November 2006 indicates a change in the style of deformation at Augustine Volcano (Cervelli and others, 2006, and this volume). Before this offset, geodetic data most likely reveal magmatic inflation of the volcano, whereas afterward such data point to the onset of dike intrusion. The timing of this change in style of deformation coincides with a sharp increase in seismicity within the Iniskin cluster (fig. 2*B*).

To evaluate the detailed distribution of earthquakes within the Iniskin cluster, we relocated events, using the double-difference algorithm hypoDD (Waldhauser and

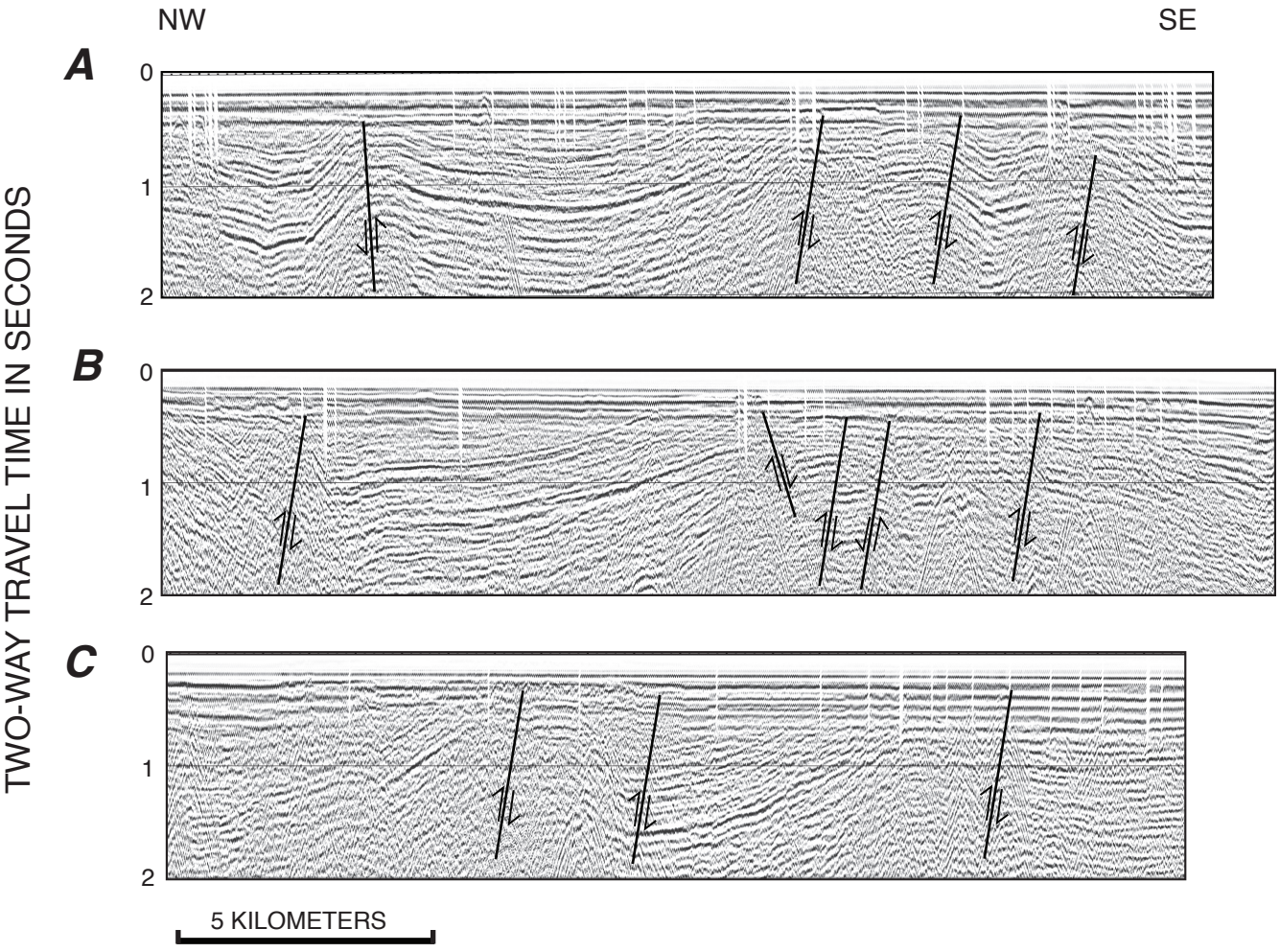

Figure 3. Multichannel seismic-reflection sections in lower Cook Inlet (fig. 1), collected with short survey streamer across the folds and faults of the Iniskin structural zone northeast of Augustine Volcano.

Ellsworth, 2000). Altogether, we relocated 108 events within 20 km of the center of the Iniskin cluster, using the catalog p- and s-wave arrivals and the standard plane-layer velocity model utilized by the AEIC for locating events in the study area (fig. 1). Because the number of events was small, we were able to use the singular-value decomposition approach, which is useful for working with small earthquake groupings because it provides information on the resolvability of hypocentral parameters and adequately represents location errors (Waldhauser, 2001). We allowed a maximum separation of 20 km between linked events and a maximum station distance of 300 km. The average offset between linked events was 4.6 km, and each event pair averaged 11 links.

The relocated events collapsed into a dense cluster less than 5 km across and from 11 to 16 km deep (figs. 5*B*–5*E*). The mean absolute location errors were 0.9 km horizontally and 1.2 km vertically, and the relative location accuracy between events was 32 m horizontally and 47 m vertically.

We calculated focal mechanisms for five events with magnitudes ranging from 3.1 to 3.4, using p-wave first motions and the program FPFIT (fig. 6) (Reasenberg and Oppenheimer, 1985). For all five events, the number of available first-motion picks ranged from 11 to 20; only one event had fewer than 15 picks. Regional stations in Cook Inlet provide good azimuthal coverage of the focal sphere. All mechanisms consistently indicate strike-slip faulting (fig. 5*A*). Although some uncertainity may remain in the focal-plane strike and dip estimates, the overall strike-slip sense of motion inferred from the five focal mechanisms is well constrained. By analyzing p-wave first motions for the events for which focal-mechanism data are available, we noted that earthquakes within the Iniskin cluster are spatially diverse but occupy a small volume and reflect a consistent mode of faulting.

Discussion

Strike of the Seismogenic Fault

Focal mechanisms for five earthquakes within the Iniskin cluster (fig. 5*A*) and for an M 3.7 event, 7 km deep and located northwest of the cluster along the Iniskin structural zone (fig. 1), all indicate that cluster seismicity results from strike-slip faulting. The main unresolved question is which nodal plane reveals the seismogenic fault.

One answer to this question is obtained from correlating nodal planes to the northeastward strike of the Iniskin structural zone (fig. 1). The northeast-striking nodal planes from all focal mechanisms closely parallel the strike of this zone, which, in turn parallels the regional structural grain of the basin (fig. 4). If this correlation is correct, then the cluster seismicity results from left-lateral oblique faulting. An important consideration in this analysis is that MCS data (for example fig. 3*C*), show the Iniskin structural zone extending southwestward from the Iniskin cluster, and so choosing the northeast-striking nodal plane relates the seismicity to a through going structure that connects the cluster with the volcano.

Alternatively, the northwest-striking nodal planes might be associated with one or more faults subparallel to the Augustine-Seldovia arch. About 10 km northeast of Augustine Volcano, this west-striking arch intersects the northeast-striking Iniskin structural zone (figs. 1, 4). As mentioned above in the section entitled "Regional Setting and Basin Structure," this arch is the primary transverse structure within the southern part of the Cook Inlet basin. Although raw earthquake

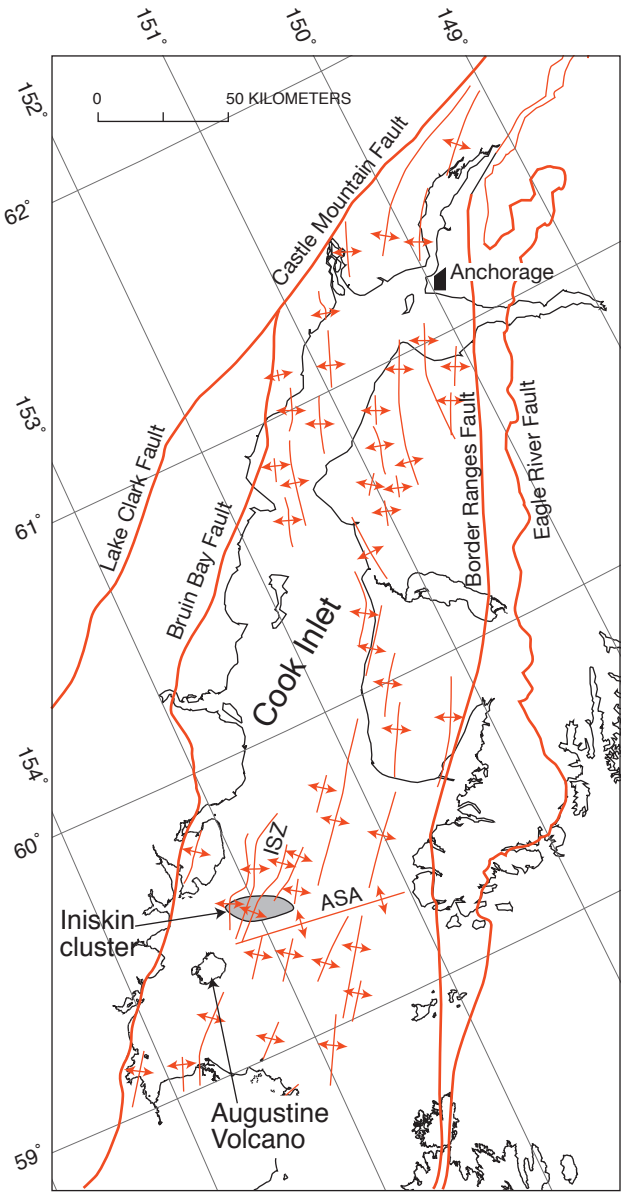

Figure 4. Map of geologic structures and major basin-bounding faults in the Cook Inlet basin. All features share a regional northeastward strike (Kirschner and Lyon, 1973; Magoon and others, 1976; Fisher and Magoon, 1978; Wilson and others, 1999; Haeussler and others, 2000). ISZ, Iniskin Structural Zone; ASA, Augustine-Seldovia Arch.

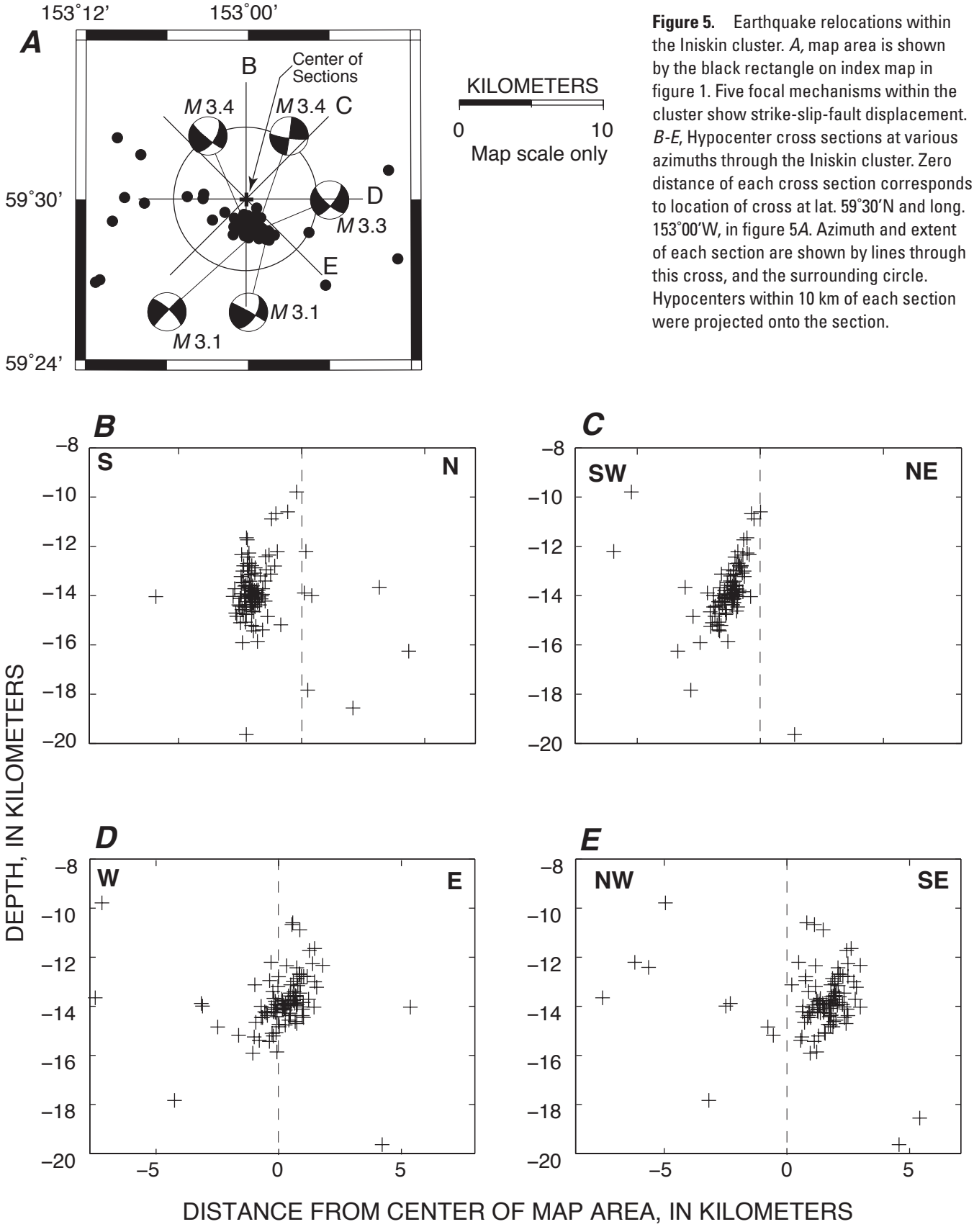

Figure 5. Earthquake relocations within the Iniskin cluster. *A,* map area is shown by the black rectangle on index map in figure 1. Five focal mechanisms within the cluster show strike-slip-fault displacement. *B-E*, Hypocenter cross sections at various azimuths through the Iniskin cluster. Zero distance of each cross section corresponds to location of cross at lat. 59˚30'N and long. 153˚00'W, in figure 5*A*. Azimuth and extent of each section are shown by lines through this cross, and the surrounding circle. Hypocenters within 10 km of each section were projected onto the section.

epicenters of events within the Iniskin cluster portray the cluster with a strong northwest-southeastward elongation (fig. 1), which seemingly fits this alternative answer, the relocated events form a dense central group with scattered outlying epicenters (fig. 5*A*). Overall, the relocated events show only a weak geographic elongation.

Of the four hypocenter cross sections in figure 5, the northwest-southeast cross section (fig. 5*C*) seems to be most nearly perpendicular to the earthquake cluster, indicating a northwest-striking right-lateral strike-slip fault sub parallel to the Augustine-Seldovia arch and perpendicular to the regional structural grain. Furthermore, regional stress determined from studies of earthquake activity at volcanoes near Augustine, notably Mounts Spurr, Iliamna, and Redoubt, indicate a northwestward direction of maximum principal stress (Jolly and others, 1994; Roman and others, 2004; Sanchez and others, 2004), suggesting that right-lateral strike-slip faults would strike northwest, at an angle of about 30˚ to the maximum stress direction. This northwestward direction of maximum principal stress agrees with the observations by Ruppert (2008), who used earthquake focal mechanisms from southern Alaska to calculate best-fitting stress tensors. Near Augustine Volcano, west- or northwest-striking strike-slip faults should predominate.

The ambiguity concerning the nodal plane partly arises because MCS data reveal the structure only of shallow (<7 km) crustal levels, because of limited seismic-source strength, whereas the relocated hypocenters in the Iniskin cluster range from 11 km to 16 km in depth. In comparison, near Augustine Volcano, the top of basement is about 10 km deep (see Fisher and Magoon, 1978, fig. 10). Thus, the seismicity appears to have originated within the basement complex below the Cook Inlet basin.

The northwest-striking nodal plane, then, may reveal a basement fault that could have originated as long ago as the early Mesozoic, the likely age of the basement complex. To produce the cluster seismicity, this fault would have been reactivated under the current stress regime as a right-lateral strike-slip fault.

Clearly, Augustine Volcano is situated at a complex structural crossroads. In our opinion, the Iniskin cluster most likely occurred along a northwest-striking right-lateral strike-slip fault associated with the trans basin Augustine-Seldovia arch. The fault might be a reactivated basement structure. The most troublesome aspect of this interpretation is that MCS data do not reveal a right-lateral transverse offset in the Iniskin structural zone directly above the Iniskin cluster.

Connection Between Seismicity and Volcanism

The close temporal association between abrupt increases in near-vent and cluster seismicity (figs. 2) and the fact that both increases preceded an explosive eruptive phase at Augustine Volcano by about 8 months suggest that magma flux and the seismogenic strike-slip fault are closely linked within the crustal stress field, as has been reported for other volcanoes. In fact, numerous studies of volcanic regions detail the close

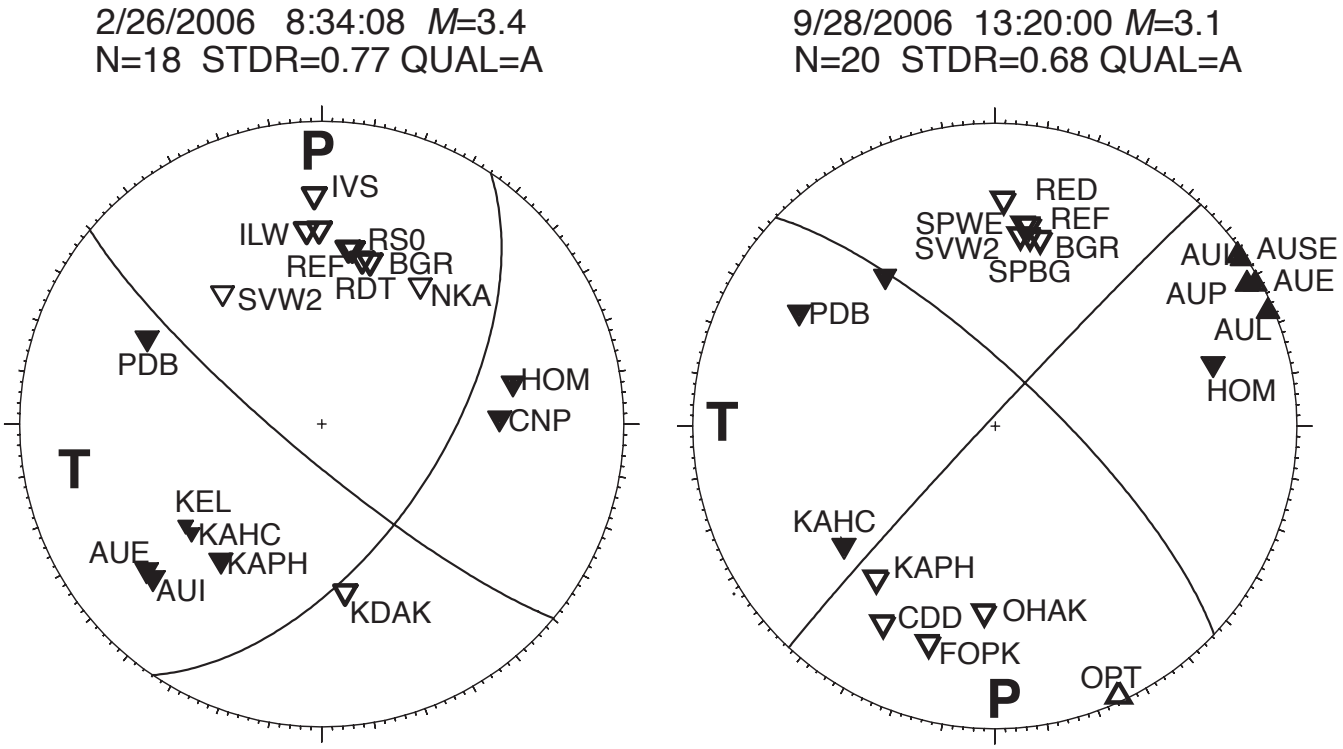

Figure 6. Two examples of p-wave first-motion focal mechanisms for events in the Iniskin cluster, both showing strike-slip motion.

coupling between earthquakes and volcanism and show that magmatic activity can trigger seismicity, and vice versa (Nostro and others, 1998; Hill and others, 2002; Toda and others, 2002; Feuillet and others, 2004; Diez and others, 2005; Manga and Brodsky, 2006; Parsons and others, 2006). Commonly, this triggering requires only subtle changes in Coulomb stress because the volcanic and earthquake systems are poised near critical points. White and Rowe (2006) compiled 25 examples from around the world in which distal earthquake clusters, such as the one we report on here, occurred from 2 to 30 km away from volcanoes just before they erupted. For example, Plinian eruptions of El Chichón (1982; Jimenez and others, 1999) and Mount Pinatubo (1991; Harlow and others, 1996) were preceded by distal earthquake swarms that began 2-26 months before cataclysmic eruptions. The ongoing eruption of South Soufriere Hills Volcano that began in 1995 was preceded by distal seismicity that occurred during the preceding 2 years (Aspinall and others, 1998). Thus, the distal volcano-tectonic seismicity we describe at Augustine Volcano conforms with observations worldwide.

Near Augustine Volcano, the coincident near-vent and distal seismicity appears to have occurred only once because no previous eruption of the volcano is known to have stimulated seismicity in the area of the Iniskin cluster. No candidate events are evident in the AEIC catalog. One possible reason for the dearth of earlier events is poor detection by the dispersed regional seismic network in Alaska before the 1990s. Another possible reason is that before 2005, shear stress within the asperity causing the Iniskin cluster had not attained near-critical values, and so volcanism before the 2006 eruption was an insufficient trigger. If so, then stress in the asperity causing the Iniskin cluster may need to rebuild after the 2006 seismicity. This conclusion bears critically on the use of distal seismicity, like the Iniskin cluster, to predict future eruptions at Augustine Volcano.

Conclusion

Clustered earthquakes located 25 km northeast of Augustine Volcano became more numerous over the 8 months just before the volcano's 2006 explosive phase, and this seismicity abated within the 9 months after the eruption ceased. Focal mechanisms from events within the cluster reveal strike-slip faulting. We conclude that the earthquake cluster occurred along a northwest-striking right-lateral strike-slip fault because the cluster occurred near the trans-basin Augustine-Seldovia arch. The fault may be a reactivated basement structure. This interpreted fault strikes perpendicularly to a shallow structural zone, interpreted from MCS data, which includes reverse faults and anticlines. These structures, however, reveal no transverse offset. The clustered earthquakes near Augustine Volcano are similar to many examples of preeruption seismicity reported at volcanoes around the world. Recurrence of earthquake activity in or near the Iniskin cluster might be useful in predicting an imminent eruption of Augustine Volcano.

Acknowledgments

We thank the Geophysical Institute, University of Alaska Fairbanks and the Office of the Alaska State Seismologist for their support of part of this research. Reviews of the manuscript by Judith E. Fierstein and Thomas E. Moore of the U.S. Geological Survey, as well as two anonymous reviewers greatly improved this report.

References Cited

Aspinall, W.P., Miller, A.D., Lynch, L.L., Latchman, J.L., Stewart, R.C., White, R.A., and Power, J.A., 1998, Soufriere Hills eruption, Montserrat, 1995–1997; volcanic earthquake locations and fault plane solutions: Geophysical Research Letters, v. 25, p. 3397–3400.

Cervelli, P.F., Fournier, T.J., Freymueller, J.T., and Power, J.A., 2006, Ground deformation associated with the precursory unrest and early phases of the January 2006 eruption of Augustine Volcano, Alaska: Geophysical Research Letters, v. 33, doi:10.1029/2006GL027219, p. 5.

Cervelli, P.F., Fournier, T.J., Freymueller, J.T., Power, J.A., Lisowski, M., and Pauk, B.A., 2010, Geodetic constraints on magma movement and withdrawal during the 2006 eruption of Augustine Volcano, *in* Power, J.A., Coombs, M.L., and Freymueller, J.T., eds., The 2006 eruption of Augustine Volcano, Alaska: U.S. Geological Survey Professional Paper 1769 (this volume).

Constenius, K., Johnson, R.A., Dickinson, W.R., and Williams, T.A., 2000, Tectonic evolution of the Jurassic-Cretaceous Great Valley forearc, California; Implications for the Franciscan thrust-wedge hypothesis: Geological Society of America Bulletin, v. 112, p. 1703–1723.

DeShon, H.R., Thurber, C.H., and Rowe, C., 2007, High-precision earthquake location and three-dimensional P wave velocity determination at Redoubt Volcano, Alaska: Journal Geophysical Research, v. 112, doi:10.1029/2006JB004751, 24 p.

Detterman, R.L., and Reed, B.L., 1980, Stratigraphy, structure, and economic geology of the Iliamna Quadrangle, Alaska: U.S. Geological Survey Bulletin 1368-B, p. B1-B86, 81 sheet, scale 1:250,000.

Detterman, R.L., and Hartsock, J.K., 1966, Geology of the Iniskin-Tuxedni region, Alaska: U.S. Geological. Survey Professional Paper 512, p. 1–78.

Diez, M., La Femina, P.C., Connor, C.B., Strauch, W., and Tenorio, V., 2005, Evidence for static stress changes triggering the 1999 eruption of Cerro Negro Volcano, Nicaragua and regional aftershock sequences: Geophysical Research Letters, v. 32, doi:10.1029/2004GL021788, p. 4.

Dixon, J.P., Stihler, S.D., and Power, J.A., 2007, Catalog of earthquake hypocenters at Alaskan volcanoes: January 1 through December 31, 2006: U.S. Geological Survey Data Series 326, 79 p. Also available online at [http://pubs.usgs.gov/ds/367].

Feuillet, N., Nostro, C., Chiarabba, C., and Cocco, M., 2004, Coupling between earthquake swarms and volcanic unrest at the Alban Hills Volcano (central Italy) modeled through elastic stress transfer: Journal of Geophysical Research, v. 109, doi:10.1029/2003JB002419, p. 16.

Fisher, M.A., and Magoon, L.B., 1978, Geologic framework of lower Cook Inlet, Alaska: American Association of Petroleum Geologists Bulletin, v. 62, p. 373–402.

Haeussler, P.J., Bruhn, R.L., and Pratt, T.L., 2000, Potential seismic hazards and tectonics of the upper Cook Inlet basin, Alaska, based on analysis of Pliocene and younger deformation: Geological Society of America Bulletin, v. 112, p. 1414–1429.

Harlow, D.H., Power, J.A., Laguerta, E.P., Ambubuyog, G., White, R.A., and Hoblitt, R.P., 1996, Percursory seismicity and forecasting of the June 15, 1991, eruption of Mount Pinatubo, *in* Newhall, C.G., and Punongbayan, R.S., eds., Fire and mud; eruptions and lahars of Mount Pinatubo: Seattle, University of Washington Press, p. 285–306.

Hill, D.P., Pollitz, F., and Newhall, C., 2002, Earthquake-volcano interactions: Physics Today, v. 55, no. 11, p. 41–47.

Jimenez, Z., Espindola, V.H., and Espindola, J.M., 1999, Evolution of the seismic activity from the 1982 eruption of El Chinchon volcano, Chiapas, Mexico: Bulletin of Volcanology v. 61, p. 411–422.

Jolly, A.D., Page, R.A., and Power, J.A., 1994, Seismicity and stress in the vicinity of Mount Spurr volcano, south central Alaska: Journal of Geophysical Research v. 99, p. 15,305–15,318.

Kirschner, C.E., and Lyon, C.A., 1973, Stratigraphic and tectonic development of Cook Inlet petroleum province, *in* Pitcher, M.G., ed., Arctic Geology, American Association of Petroleum Geologists Memoir 19, p. 396–407.

Magoon, L.B., Adkison, W.L., and Egbert, R.M., 1976, Map showing geology, wildcat wells, Tertiary plant fossil locations, K-Ar dates, and petroleum operations, Cook Inlet area, Alaska: U.S. Geological Survey Miscelaneous Investigations I-1019, 3 sheets, scale 1:250, 000.

Manga, M., and Brodsky, E., 2006, Seismic triggering of eruptions in the far field; volcanoes and geysers: Annual Reviews of Earth Planetary Science, v. 34, p. 263–291.

Nostro, C., Stein, R.S., Cocco, M., Belardinelli, M.E., and Marzocchi, W., 1998, Two-way coupling between Vesuvius eruptions and southern Apennine earthquakes, Italy, by elastic stress transfer: Journal of Geophysical Research, v. 103, p. 24,487–424,504.

Parsons, T., Thompson, G.A., and Cogbill, A.H., 2006, Earthquake and volcano clustering via stress transfer at Yucca Mountain, Nevada: Geology, v. 34, p. 785–788.

Power, J.A., Nye, C.J., Coombs, M.L., Wessels, R.L., Cervelli, P.F., Dehn, J., Wallace, K.L., Freymueller, J.T., and Doukas, M.P., 2006, The reawakening of Alaska's Augustine volcano: Eos (American Geophysical Union Transactions), v. 87, no.37, p. 373, 377.

Reasenberg, P., and Oppenheimer D.H., 1985, FPFIT, FPPLOT, and FPPAGE; Fortran computer programs for calculating and displaying earthquake fault-plane solutions: U.S. Geological Survey Open File Report. 85-739, 37 p.

Riehle, J.R., Detterman, R.L., Yount, M.E., and Miller, J.W., 1993, Geologic map of the Mount Katmai Quadrangle and adjacent parts of the Naknek and Afognak Quadrangles, Alaska: U.S. Geological Survey Miscellaneous Investigations Series Map 2204, p. 1 sheet, scale 1:250,000.

Roman, D.C., Power, J.A., Moran, S.C., Cashman, K.V., Doukas, M.P., Neal, C.A., and Gerlach, T.M., 2004, Evidence for dike emplacement beneath Iliamna Volcano, Alaska in 1996: Journal of Volcanology and Geothermal Research, v. 130, p. 265–284.

Ruppert, N.A., 2008, Stress map for Alaska from earthquake focal mechanisms, *in* Freymueller, J.T., Haeussler, P.J., Wesson, R.L., and Ekstrom, G., eds., Active tectonics and seismic potential of Alaska: American Geophysical Union Monograph 179, p. 351–369.

Sanchez, J.J., Wyss, M., and McNutt, S.R., 2004, Temporal-spatial variations of stress at Redoubt volcano, Alaska, inferred from inversion of fault plane solutions: Journal of Volcanology and Geothermal Research, v. 130, p. 1–30.

Toda, S., Stein, R.S., and Sagiya, T., 2002, Evidence from the A.D. 2000 Izu Islands earthquake swarm that stressing rate governs seismicity: Nature, v. 419, p. 58–61.

Waldhauser, F., 2001, HypoDD – A program to compute double-difference hypocenter locations, U.S. Geological Survey Open-File Report 01-113, 25 p.

Waldhauser, F., and Ellsworth, W.L., 2000, A double-difference location algorithm: Method and application to the northern Hayward fault, California: Bulletin of the Seismological Society of America, v. 90, p. 1353–1368.

Wang, J., Newton, C.R., and Dunne, L., 1988, Late Triassic transition from biogenic to arc sedimentation on the Peninsular terrene—Puale Bay, Alaska Peninsula: Geological Society of America Bulletin, v. 100, p. 1466–1478.

White, R., and Rowe, C., 2006, Volcano-tectonic earthquake sequences near active volcanoes and their use in eruption forecasting [abs.]: Seismological Research Letters, v. 77, no. 2, p. 240.

Wilson, F.H., Detterman, R.L., and DuBois, G.D., 1999, Digital data for the geologic framework of the Alaska Peninsula, southwest Alaska, and the Alaska Peninsula terrane: U.S. Geological Survey Open-File Report 99-317 [http://wrgis.wr.usgs.gov/open-file/of99-317/].

The 2006 Eruption of Augustine Volcano, Alaska
Power, J.A., Coombs, M.L., and Freymueller, J.T., editors
U.S. Geological Survey Professional Paper 1769

Chapter 7

A Two-Step Procedure for Calculating Earthquake Hypocenters at Augustine Volcano

By Douglas J. Lalla[1] and John A. Power[2]

Abstract

This chapter describes a two-step technique for determining earthquake hypocenters at Augustine Volcano. The algorithm, which was originally developed in the mid-1970s, was designed both to overcome limitations in the standard earthquake-location programs available at the time and to take advantage of the detailed seismic-velocity information obtained at Augustine Volcano. Hypocenters are calculated on the basis of a two-dimensional (2D) ray-tracing procedure that accounts for in plane lateral discontinuities within the seismic velocity structure. This algorithm calculates the minimum P- and S-wave travel time between theoretical grid points embedded in the velocity structure to each station in the seismic network. Station corrections that account for the differences between the model and actual velocity structure are derived from a time-term analysis of the 1975 active-source seismic experiment. Each relocated hypocenter is assigned to the grid point with the lowest rms residual between observed and calculated arrival times. Statistical techniques are used to assess the effect of random errors in P-wave-arrival determination on hypocentral location. These tests suggest that the 2D ray-tracing procedure presented here is able to resolve earthquake hypocenter depths to within 0.25 km between the volcano's summit and sea level and within 0.5 km from sea level to depths of 2 km below sea level.

Introduction

Augustine Volcano is a 1,200-m-high stratovolcano on a small (8 by 11 km) island southeast of Anchorage, Alaska (fig. 1). The volcano consists of a complex of summit lava domes and flows surrounded by an apron of pyroclastic, lahar, avalanche, and ash deposits. The volcano is frequently active, with major eruptions recorded in 1883, 1935, 1963–64, 1976, 1986, and 2006 and minor eruptive events reported in 1812, 1885, 1908, 1944, and 1971. Because of its frequent eruptive activity and associated hazards and proximity to communities in south-central Alaska, Augustine Volcano has been continuously seismically monitored since 1970 (see Power and Lalla, this volume).

Earthquake activity at Augustine is dominated by volcano-tectonic earthquakes that occur within 1 km of sea level with local magnitudes (M_L) generally smaller than 1.2 (see Power and Lalla, this volume). During inter-eruptive periods, the Alaska Volcano Observatory (AVO) typically locates 100 to 200 small earthquakes each year at Augustine (Dixon and others, 2008). These small earthquakes generally have well-defined to emergent P-wave arrivals and poorly formed to emergent S-wave arrivals. Most earthquakes have P- and S-wave arrivals that are best defined at stations higher on the volcanic edifice, located on the central lava domes and flows, and degrade quickly at stations located closer to the coast on the apron of unconsolidated sedimentary deposits. Additionally, stations close to the island's shoreline are subject to large microseismic noise caused by ocean surf. A representative volcano-tectonic waveform is shown in figure 2. By the time of the 1976, 1986, and 2006 eruptions the volcano was monitored by networks of five, four, and eight permanent short-period seismometers, respectively (fig. 3).

Augustine Volcano was the target of an extensive active-source seismic experiment in 1975 that involved the detonation of 10 chemical explosions which were recorded at 14 temporary seismic stations, as well as at the five permanent stations operating on the island at the time. Data from this experiment were combined with the results from an earlier seismic refraction survey along the north shore of Augustine Island (Kienle and others, 1979) and with seismic-velocity

[1]5106 Wesleyan Drive, Anchorage, AK 99508.

[2]Alaska Volcano Observatory, U.S. Geological Survey, 4210 University Drive, Anchorage, AK 99508.

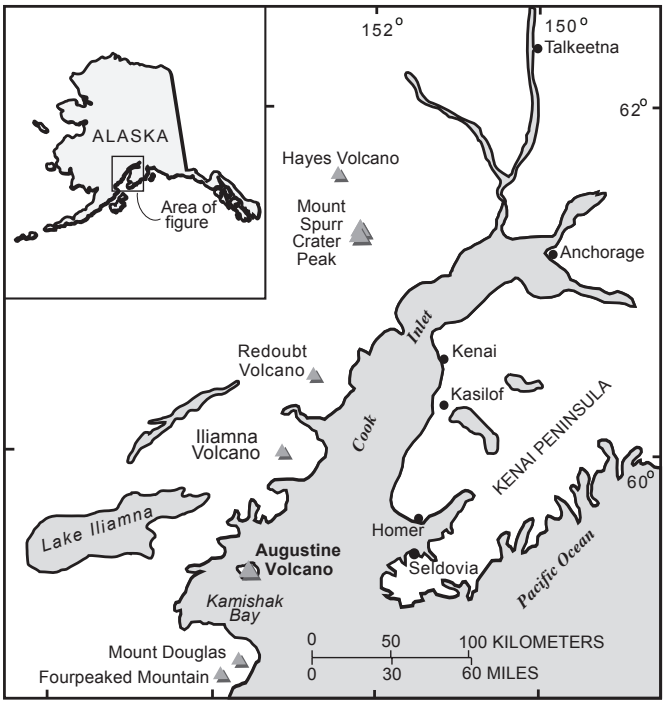

Figure 1. Map showing the Cook Inlet region of Alaska, location of Augustine Volcano, other nearby volcanoes and communities.

data from exploratory oil wells drilled in southern Cook Inlet to determine a three-dimensional (3D) seismic-velocity model of the volcano (fig. 4; Kienle and others, 1979).

Accurate calculation of earthquake hypocenters at Augustine Volcano is unusually difficult because of the high relative topography, the resulting large differences in the elevations of seismic stations, and the heterogeneity of Augustine's seismic-velocity structure. Early computerized earthquake-location algorithms such as HYPO71 (Lee and Lahr, 1971), HYPOINVERSE (Klein, 1978), and HYPOELLIPSE (Lahr, 1989), accounted for station elevations and horizontal changes in seismic-velocity structure through station corrections. Each of these algorithms assumed that the hypocenter was below the elevation of the lowest station. At such stratovolcanoes, as Augustine, this approach presented a serious limitation because topography dictates that many seismic stations are located near sea level and many earthquakes occur in the upper portions of the cone. To overcome this problem, more recent earthquake-location algorithms such as HYPOCENTER (Lienert and others, 1986) and HYPOELLIPSE (Lahr and others, 1994) allow a flat-layered seismic velocity model wherein the highest station can match the highest local topography and stations at lower elevation are embedded within the model. In these algorithms, raypaths and traveltimes are computed for the relative locations of source and receiver.

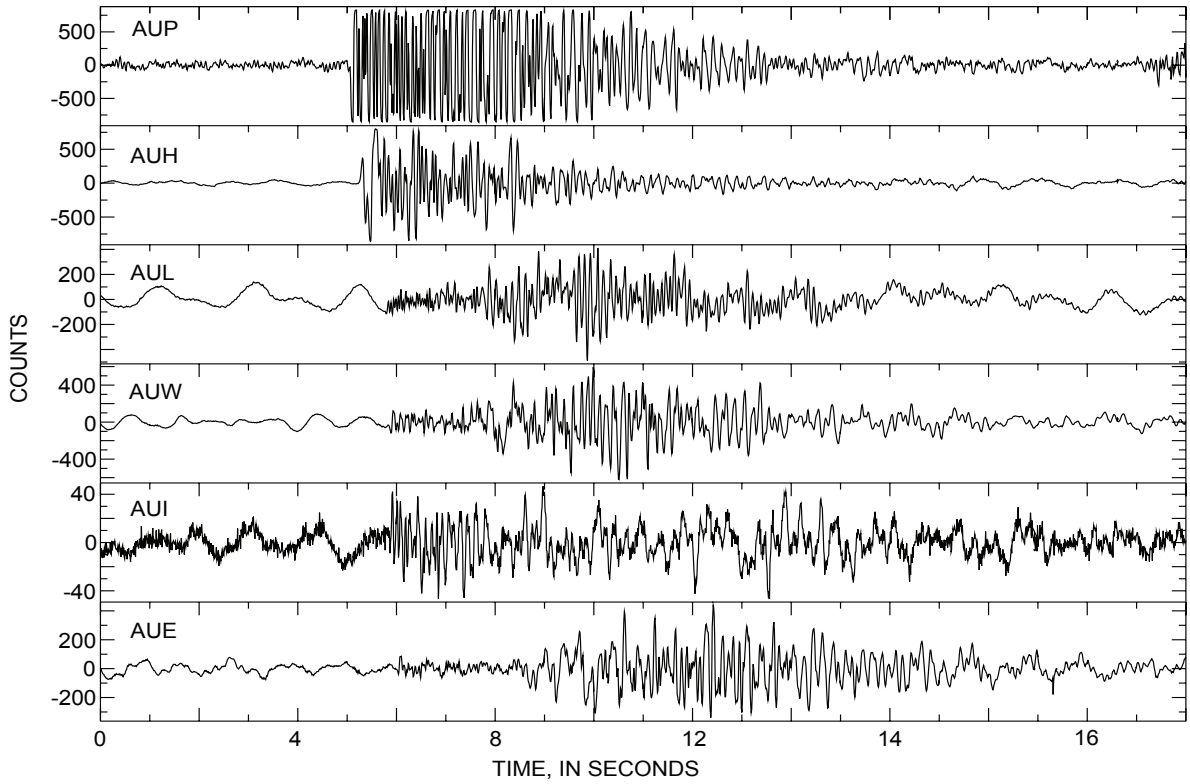

Figure 2. Volcano-Tectonic (VT) earthquake waveforms recorded at Augustine Volcano on January 3, 2006. Hypocenter was at a depth of 0.66 km a.m.s.l. and the local magnitude (M_L) was 0.6. See figure 3 for station locations.

To more accurately locate earthquakes at Augustine, we have developed a two-step procedure to calculate earthquake hypocenters for shocks that occur within a maximum radial distance of 3 km from the volcano's summit and between 1 km above mean sea level (a.m.s.l.) and 8 km below mean sea level (b.m.s.l). This procedure first uses a standard earthquake-location algorithm, such as HYPO71 or HYPOELLIPSE, to determine whether the shocks are occurring beneath the volcano's summit. Earthquakes that meet this criterion are then relocated by using a computer algorithm that calculates hypocenters within the 3D seismic-velocity model of Augustine Volcano shown in figure 4.

This algorithm, which was originally developed in the mid-1970s, was designed both to overcome limitations in the standard earthquake-location programs available at the time and to take advantage of the detailed seismic-velocity information at Augustine Volcano. The algorithm is based on a two-dimensional (2D) ray-tracing procedure that accounts for lateral discontinuities within the seismic-velocity structure. The algorithm calculates the minimum P- and S-wave traveltimes between theoretical grid points embedded in the velocity structure to each station in the seismic network. The grid is a 3 km by 3 km square centered on the summit of the volcano that extends from 1 km a.m.s.l. to 8 km b.m.s.l.; the spacing between grid points is 0.25 km in all three directions. The spatial extent of the grid is shown in figure 5. Station corrections derived from a time-term analysis (Scheidegger and Wilmore, 1957) of the 1975 active-source seismic experiment are applied to calculated traveltimes in order to account for discrepancies between the seismic-velocity model and the measured P-wave traveltime to each station. Each earthquake hypocenter is assigned to the grid point with the lowest residual between observed and calculated arrival times.

In this chapter, we describe details of the two-step hypocenter-relocation procedure and the algorithm that performs the 2D ray tracing and earthquake location within the Volcano's seismic-velocity structure. We also describe calculation of the travel time-terms and station corrections, using data from the 1975 active source seismic experiment. We then evaluate the precision and accuracy with which earthquakes can be located at Augustine with this technique by modeling the known sources of error. Finally, we compare the results of this algorithm with hypocenters calculated with the most recent version of HYPOELLIPSE (Lahr, 1999), using several station configurations.

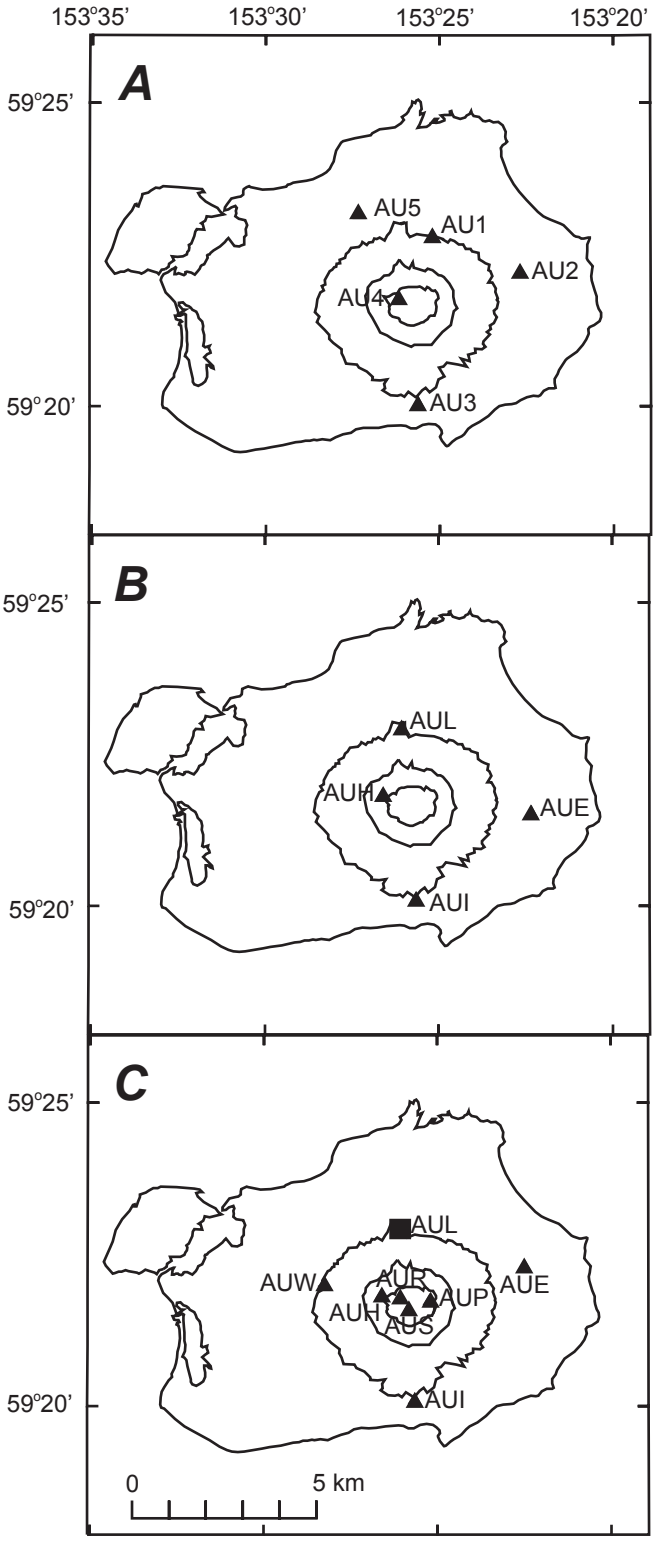

Figure 3. Map of Augustine Island, showing locations of short-period seismic stations on Augustine Volcano in *A*, 1975, *B*, 1985, and *C*, 2005. Triangles, short-period seismometers; squares broadband seismometers. Sea-level, 1,000-ft, 2,000-ft, and 3,000-ft contours are shown in map view.

Seismic-Velocity Model

In August 1975, Kienle and others (1979) conducted an active-source seismic experiment that involved the detonation of 10 chemical explosions on Augustine Island. These explosions were recorded by 14 temporary seismometers, as well as at four stations that were operating on the island as part of the permanent seismic network. The locations of shot points and

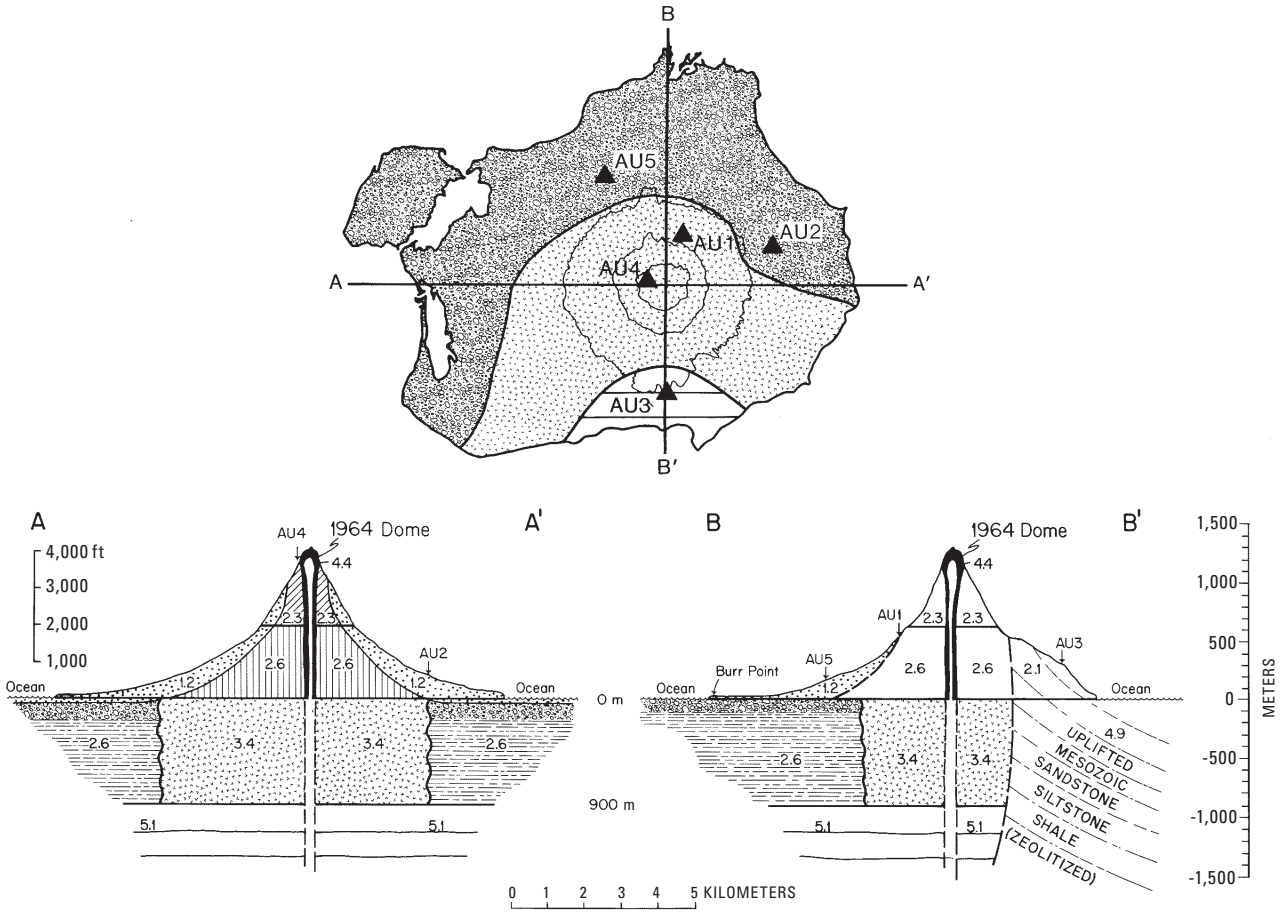

Figure 4. Map view and west-east and north-south cross sections illustrating generalized three-dimensional velocity model of Augustine Island (after Kienle and others, 1979). Map view of island shows velocity boundaries at sea-level (see fig. 3 for explanation of contour lines). Numbers represent seismic velocities in kilometers per second. Triangles note locations of seismic stations that operated in 1975.

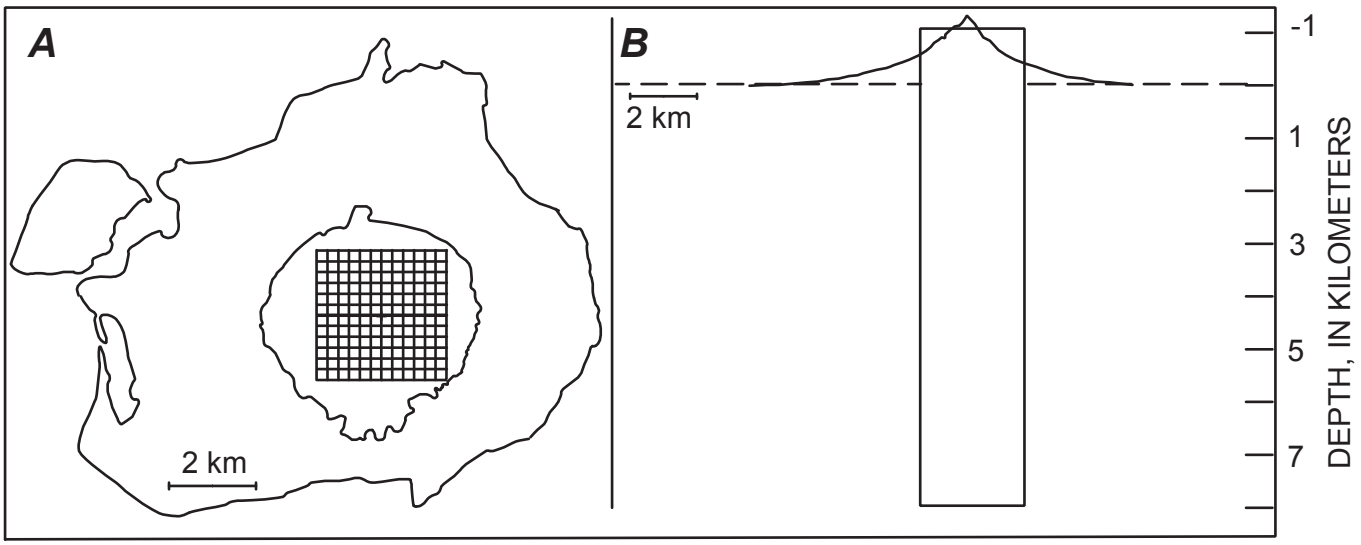

Figure 5. Map view and cross section of Augustine Volcano, showing *A*, the horizontal and *B*, vertical extent of the three-dimensional location grid in relation to volcano. Sea-level and 1,000-ft contour lines are shown in map view.

receivers are shown in figure 6. This combined network measured a total of 66 seismic rays that traversed all parts of the Island and the volcanic cone. These data provided the means to produce the 3D seismic-velocity structure shown in figure 4. An earlier 2D seismic-velocity model of Augustine Volcano was constructed by Pearson (1977), using the 1975 explosion data. A second, smaller active-source seismic experiment constructed in August 1995 measured similar seismic velocities on the volcanic cone (Clippard, 1998).

The major elements of the 3D seismic-velocity model are the cylindrical volcanic cone that comprises the central complex of lava domes and flows and has a P-wave velocity of 2.6 km/s between sea level and 600-m elevation. The seismic velocity decreases outward and upward to 2.3 km/s from 600-m elevation to the summit. The unconsolidated pyroclastic, avalanche, and lahar deposits that surround this central core have a P-wave velocity of 1.2 km/s. The layer between sea level and 0.90-km depth is laterally heterogeneous, increasing in seismic velocity from north to south across the island. The northern part of the island is underlain by a 2.6-km/s velocity layer that was interpreted as non-zeolitized sedimentary deposits. Beneath the central part of the volcano is a layer with a P-wave velocity of 3.4 km/s, perhaps consisting of interlaced volcanic dikes and sills. Near the south shore of the island, the zeolitized sedimentary deposits have been uplifted to near sea level, and in this area the seismic-velocity is 4.85 km/s. The southern part of the volcanic edifice to 600-m elevation is composed of uplifted sedimentary deposits with a P-wave velocity of 2.1 km/s. The stratum of the volcano beneath 0.90 km b.m.s.l. is modeled as a half-space with a P-wave velocity of 5.1 km/s. This layer is believed to represent zeolitized Lower Cretaceous sedimentary deposits (Detterman, 1973). The extent of each of these units is shown in figure 4. A detailed description of this model was presented by Kienle and others (1979).

Earthquake-Location Technique and Methodology

In the first step in calculating an earthquake hypocenter, we determine an initial location for each shock, using a standard algorithm, such as HYPO71 or HYPOELLIPSE with a flat-layered one-dimensional model, similar to the standard processing used to produce the AVO earthquake catalog (Dixon and others, 2008). We then remove earthquakes with hypocenters outside the location grid (fig. 5).

In the second step, we relocate the selected earthquakes, using the 2D ray-tracing procedure implemented by three computer programs written in the FORTRAN4 computer language. The programs are called TRAVEL, NORMAL and FASTM2; copies of them are contained on the DVD-ROM disc included with this volume (see appendix).

The program TRAVEL calculates traveltimes from all points in the three by 3 km by 3 km by 9 km grid to five seismic stations located on Augustine Island. To calculate the minimum traveltime between each grid point and each station, both the critical and refracted wave paths are considered. The minimum travel time from each grid point to each station is stored in a lookup table.

The program TRAVEL was originally coded to calculate traveltimes for the five stations in the 1976 Augustine seismic network. For this discussion, we refer to station names from the 1975 network (fig. 3*A*). To run with later network configurations, TRAVEL was modified with appropriate station coordinates and elevations. The reference elevation for this technique is sea level, with negative depths reflecting height above sea level.

The seismic-velocity model (fig. 4) is approximated as follows:

1. For stations AU5 and AU2, the contact between the 3.4 and the 2.6-km/s velocity zone (stippled area, fig. 4) is approximated by a circular arc with a radius of 2.2 km and a center at the volcano's summit (taken to be 59°21.65'N., 153°25.650' W.). Only within this layer, situated between sea level and 0.9-km depth, is a lateral velocity discontinuity allowed.

2. The volcanic cone is modeled as two bounded plane layers. From sea level to 600-m elevation the P-wave velocity is 2.6 km/s, and above 600-m elevation it is 2.3 km/s.

3. The seismic velocity model for rays traveling to station AU3 is considered to be a simple set of plane layers 2.1 km/s-velocity overlying a 3.4-km/s-velocity layer from sea level to 0.9-km depth.

4. Below 0.9 km b.m.s.l., a half space with a constant velocity of 5.1 km/s is assumed.

5. The central high-seismic-velocity conduit is assumed to affect only station AU4 and is modeled by applying a station correction that is proportional to the depth of the grid point below the station in the region between the summit and sea level. For grid points below sea level, the station correction is fixed at a maximum value of -0.1 s.

For homogenous plane-layered waves, we use the standard expressions to calculate traveltimes derived by many workers, such as Lee and Stewart (1981). For waves that meet a lateral discontinuity, the traveltime path is formulated for the specific ray path and seismic-velocity structure at Augustine.

The program NORMAL applies station corrections to the traveltime table and the calculated traveltimes are then normalized relative to station AU1 or its equivalent and stored in a second lookup table. To decrease the required computational time, this second lookup table is stored in binary rather than ASCII format.

The program FASTM2 performs a direct search of the traveltime lookup table and matches the normalized calculated

traveltimes with normalized observed arrival times. Each earthquake hypocenter is then assigned to the grid point with the lowest value between the calculated and observed arrival times. The coordinates of this point are determined by a point to point search over all the grid points. Origin times are determined simultaneously in this process. This procedure considers both P- and S-wave arrival times, although the program is typically run without S-wave phases, which are difficult to determine at the vertical short-period stations on Augustine Island (fig. 2). The S-wave traveltime table is computed by assuming a constant V_p/V_S ratio of 1.78.

Station Corrections and Time-Term Analysis

To account for discrepancies between the actual and modeled traveltimes to individual seismic stations, we have applied traveltime corrections for the individual seismic stations that we use on Augustine Island. Station corrections are calculated by using a time-term analysis (Scheidegger and Wilmore, 1957) with observed traveltimes from the 1975 active-source seismic experiment (Kienle and others, 1979); the time terms are the observed traveltimes between the 5.1-km/s -velocity refractor (fig. 4) at the base of the 3D seismic-velocity model and each seismic station.

The time-term analysis for calculating station corrections relies on the following assumptions (Scheidegger and Wilmore, 1957): 1, the refractor velocity is uniform, 2, the refractor boundary is uniform and has negligible dip, and 3, the seismic-velocity structure of the overburden beneath any station is a function of only the depth normal to the refractor within the cone defined by the critically refracted waves. Under these assumptions, the traveltime between any two points s_i and s_j can be expressed by the following equation:

$$T_{ij} = d_i + d_j + \frac{L_{ij}}{V_r}\ , \qquad (1)$$

where T_{ij} is the traveltime between points s_i and s_j; d_i, d_j are the timeterms for points s_i and s_j, respectively; L_{ij} is the horizontal distance between points s_i and s_j, and V_r is the seismic-velocity of the refracting layer. The time-term is the summation of the total traveltime reduction needed for any number of plane layers above the refractor.

The part of the Augustine seismic-refraction dataset applicable to the time-term analysis consists of 31 critically refracted raypaths (fig. 6) and 15 unknown variables, which 14 are shot point or station time-terms and one is refractor slowness ($1/V_r$). One equation can be written for each shot point/receiver-site pair. Station 8 and shot point 4 occupied the same site in the 1975 active-source seismic experiment (Kienle and others, 1979). This station-shot point position overlap allows the system of equations to be solved uniquely for the unknown variables; without it, the system of equations could be solved only for relative time-terms.

The QR decomposition method of Lawson and Hanson, (1974) was used to solve this problem in a least-squares sense. We chose this method over formulating normal equations for two reasons: 1, solving the normal equations requires n^2 precision, whereas the QR decomposition method requires only n precision, so round-off errors are minimized; and 2, the QR decomposition method solves for a variable only if that column does not cause the condition number of the matrix to fall below the value allowed by consideration of the precision of the data, thus preventing problems associated with the precision of ill-conditioned matrices.

The standard deviation of each variable is estimated from the diagonal terms of the unscaled variance- covariance matrix and the residual solution vector. We assume that errors are additive and uncorrelated and have a consistent variance and that the mean is zero. The results of the time-term analysis are plotted in figure 6 and listed in table 1. The inversion yields a seismic velocity of the underlying refractor of 5.0±0.2 km/s, in agreement with the seismic velocity of 5.1±0.2 km/s calculated from the generalized model of Kienle and others (1979).

The station correction that we apply in the program NORMAL is the difference between the modeled traveltime from the 5.1 km/s -velocity refractor and the traveltime to the station calculated by time-term analysis. The station corrections thus account for discrepancies between the seismic-velocity model and the actual velocity structure beneath each station; we also increase the traveltime to account for the elevation of each station. Station corrections for all the stations used with the 2D earthquake-location algorithm are listed in table 2.

Implementation with 1976, 1986, and 2006 Seismic Networks

The Augustine seismic network has changed somewhat since this hypocenter-relocation procedure was originally formulated to locate earthquakes with the five-station network on the volcano in 1975 (see Power and Lalla, this volume). Some stations have been moved and renamed, and a number of stations were added to the network (fig. 3); stations AU4–AUH, AU3–AUI, AU2–AUE, and AU5–AUL have operated consistently since the early 1970s. This hypocenter- relocation procedure was used to determine earthquake hypocenters before the 1976 (Lalla and Kienle, 1978) and 1986 (Power, 1988) eruptions. During these periods, the Augustine seismic network consisted of five and four stations, respectively. This procedure has also been used to locate earthquakes before the 2006 eruptions of Augustine Volcano (see Power and Lalla, this volume).

Although many of the permanent stations on the island were located at shot-points or receiver sites used in the 1975 active-source seismic experiment (compare figs. 3 and 6), none of the 1975 shot-points and receiver sites was located at the exact position of stations AUI, AUL, or AU1; however, measurements were available for sites with equivalent positions with respect to major features of the seismic-velocity model (fig. 3). The time terms established for stations AU3, AU5, and R5 were used for stations AUI, AUL, and AU1, respectively (fig. 6). Additional travel time to compensate for changes in station elevation were added to each of these station corrections as needed.

For stations AU4 and AUH, a proportional correction was used to account for the effects of the 4.4-km/s-velocity central core of the volcano that extends from the summit to sea level (fig. 4). This correction makes a –0.025-s adjustment to each grid point for every 0.25 km the point is below the top of the model. A total correction of –0.1 s was applied to all grid points at sea level and below.

To relocate earthquakes in 2006, we observed that a four-station network provided hypocenters with the lowest average rms values. The four stations used were AUE, AUH, AUI and AUL (fig. 3*C*). We attempted to include stations AUP and AUW, using time-terms and station corrections from receivers

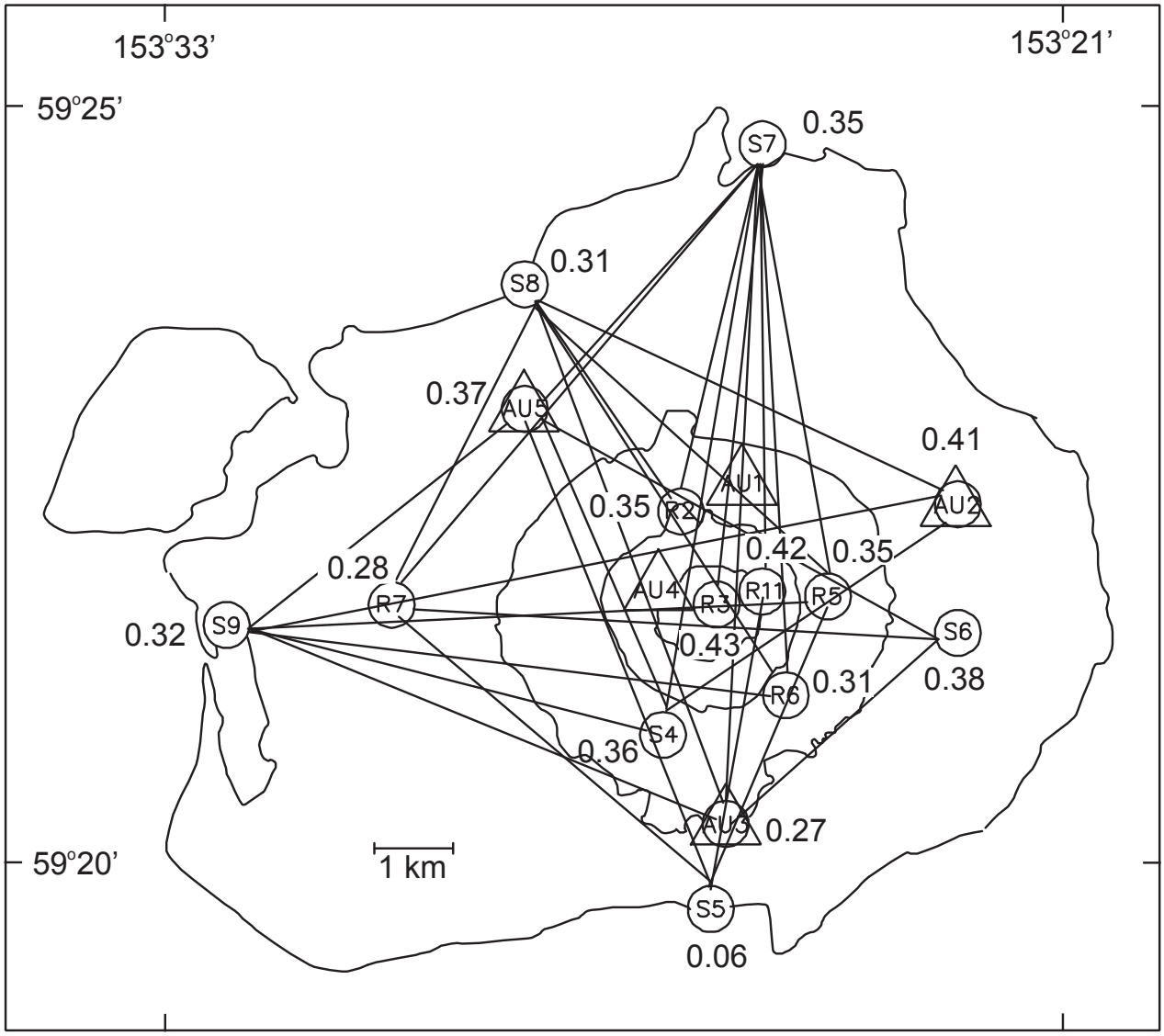

Figure 6. Map of Augustine Island showing locations of shot-points (S) and receiver sites (R) and time terms (numbers) from the 1975 active-source seismic experiment. Straight lines note ray paths used in calculation of time terms and stations corrections. Note that shot point 4 and receiver site 8 were collocated. Permanent short-period stations operating in 1975 are noted by triangles. Contour interval is 1,000 ft. Calculated time-terms are listed in table 1, and station corrections in table 2.

Table 1. Time-terms calculated for shot points and seismic stations.

Station	Time-term (s)	Standard deviation	Station elevation (km)
Shot point 4	0.36	0.04	0.00
Shot point 5	0.06	0.04	0.00
Shot point 6	0.38	0.04	0.17
Shot point 7	0.35	0.04	0.00
Shot point 8	0.31	0.04	0.00
Shot point 9	0.32	0.04	0.00
Station AU2	0.41	0.03	0.20
Station AU3	0.27	0.04	0.29
Station AU5	0.37	0.03	0.15
Station 2	0.35	0.04	0.68
Station 3	0.43	0.05	1.21
Station 5	0.35	0.03	0.50
Station 6	0.31	0.04	0.50
Station 7	0.28	0.04	0.15
Station 11	0.42	0.04	1.03

Table 2. Time-terms and station corrections.

Station	Time term	Model value	Station correction
AU1[1]	0.34	0.49	0.15
AU2	0.40	0.46	-0.06
AU3	0.28	0.21	-0.07
AU5	0.37	0.20	0.17
AUE[2]	0.27	0.31	-0.04
AUI[3]	0.38	0.43	-0.05
AUL	0.28	0.34	-0.06
AUE[4]	0.27	0.31	-0.06

[1] Time term from station S5 assumed, correction adjusted for elevation.

[2] Time term from station AU2 assumed, correction adjusted for elevation.

[3] Time term from station AU3 assumed, correction adjusted for elevation.

[4] Time term from station AU2 assumed, correction adjusted for elevation.

R7 and R11 (fig. 6), but this inclusion produced much greater average errors than in the four-station solutions. We also attempted to include station AUP, using the same proportional correction as for station AUH, but this inclusion also produced greater errors in test runs of the program. These results suggest that the parameterization of the seismic-velocity model by Kinele and others (1979) may not be accurate for stations at these locations. We did not attempt to expand the programs to include the other stations located on Augustine Island in 2005 and 2006 (fig. 3*C*).

Analysis of Error, Precision, and Accuracy

Our ability to determine earthquake hypocenters depends on our knowledge of the seismic-velocity structure of the Earth, the number and distribution of recording stations, and accurate measurement of the arrival times of seismic waves. A review of standard methods of determining earthquake hypocenters was presented by Lee and Stewart (1981). Earthquake-hypocenter determinations contain both systematic and random errors. Systematic errors result from errors in the velocity model, misidentification of phases, or timing errors and affect the accuracy of the hypocenter determination. The effects of systematic errors can be evaluated through controlled experiments, such as locating manmade explosions. Random errors result from errors in determining phase arrivals and affect the precision with which hypocenters can be calculated. The effects of random errors are generally estimated through the use of standard statistical techniques.

To estimate the effect of phase misidentification on the accuracy of earthquake locations at Augustine Volcano with the 2D ray-tracing procedure, we determined the precision with which we can measure P-wave arrivals. We then used a Monte Carlo simulation (Beck and Arnold, 1977) to evaluate our calculated hypocenters. The method consists of generating a population of synthetic arrival times for a given grid point within the location space calculated by the program TRAVEL. The initial arrivals for the "seed" event are taken from the traveltime lookup table, and a set of synthetic arrival times is generated by adding errors with a Gaussian distribution, a zero mean, and a standard deviation that corresponds to the precision with which we can determine P-wave arrivals for local earthquakes at the Augustine seismic stations. This method depends on the characteristics of the earthquakes, the individual stations in the seismic network, and the recording media used at the time of the earthquake.

To calculate the precision in measuring P-wave arrivals at each station, we measured the P-wave arrival times for groups of earthquakes located at Augustine a second time. The sum of the average difference between the two sets of P-wave arrivals and the associated standard deviation was taken to be an estimate of the precision of P-wave arrival determination at that station. Seismic data at Augustine were recorded on photographic film from 1970 to 1989 and digitally by various computerized acquisition systems after 1989 (see Power and Lalla, this volume). The average precision of P-wave-arrival determination was 0.034 s (Lalla and Kienle, 1980) at stations that operated in 1975 (fig. 3*A*), 0.06 s (Power, 1988) at the stations that operated in 1985 and 1986 (fig. 3*B*) and 0.02 s at the stations that operated in 2005, as determined by picking a set of 25 earthquakes that occurred in December of 2005 a second time. We believe that the improvement in precision in the 2005 data set reflects the higher-quality digitally recorded data and associated computerized analysis techniques.

To evaluate our ability to locate earthquakes at Augustine Volcano with the 2D ray-tracing procedure, we ran the Monte Carlo simulation with the stations used with this technique in the 1975, 1985 and 2005 networks (fig. 3) and allowed the average precision of P-wave-arrival determination to follow a Gaussian distribution centered at 0.02, 0.05, and 0.10 s, with seed events at 0.25-km intervals for grid points directly beneath the volcano's summit to a depth of 7.75 km b.m.s.l.

These simulations allowed us to estimate the standard horizontal and vertical location errors that are typically referred to as ERZ and ERH. We define ERZ as

$$\mathrm{ERZ} = \sqrt{\sum_{1}^{n} \frac{(Z_i - \overline{Z})^2}{n-1}}\ , \qquad (2)$$

where Z_i is the hypocentral depth, $\overline{Z}$ is the average hypocentral depth, and n is the number of hypocenters. ERH is calculated in the same way as ERZ, except that the horizontal rather than the vertical position is used. For each grid point, the estimated shift in ERZ and ERH represents the mean value of 100 test events, the results of which are summarized in figures 7 and 8. We also used this technique to estimate the expected shift in hypocentral depth for the networks operating in 1975, 1985–86 and 2005–6 (fig. 9).

We used these simulations to evaluate the shift in hypocenter position as a result of the changing array configuration in 1975. During 1975 five stations were operating on the island, four of which had temporary failures. For this evaluation, we ran these tests without phase readings from one of the stations in the 1975 network to simulate periods when the four stations were operational. Again, we ran these tests with a sample population of 100 test events for each grid point. The results of these simulations, showing the expected shifts in vertical and horizontal errors and in depth are summarized in figure 10.

These tests suggest that the 2D ray-tracing procedure presented here is able to resolve earthquake hypocenter depths to within 0.25 km for shocks located above sea level and within 0.5 km for shocks located between sea level and 2 km b.m.s.l. when the average network P-wave-arrival determination is 0.05 s. This result is similar to the precision estimates calculated for the 1975 (Lalla and Kienle) and 1985–86

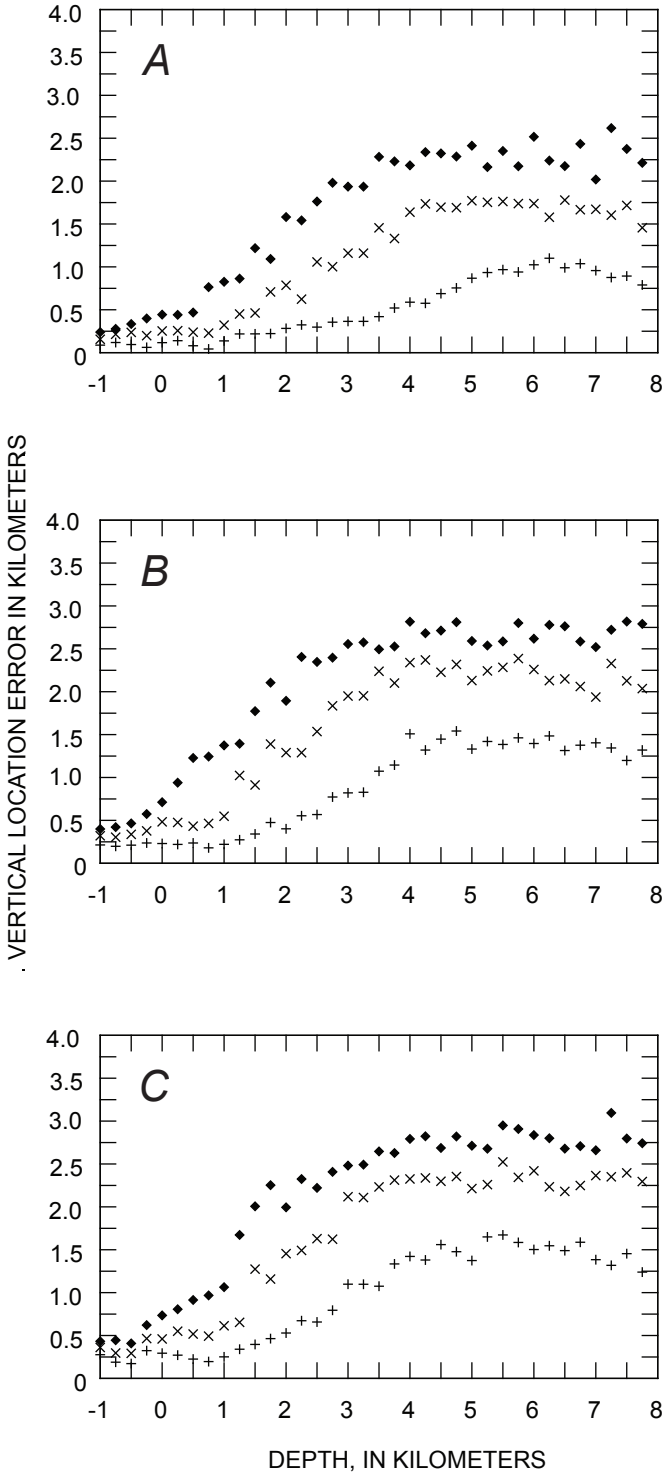

Figure 7. Simulated values of vertical location error (ERZ) based on three error levels of P-wave arrival determination for seismic networks used for the 2D ray tracing procedure in *A*, 1975, *B*, 1985–1986, and *C,* 2005–2006. The pluses, crosses, and diamonds, correspond to the 0.02-, 0.05- and 0.10-second P-wave reading errors, respectively. Each data point represents the mean ERZ for 100 simulated events.

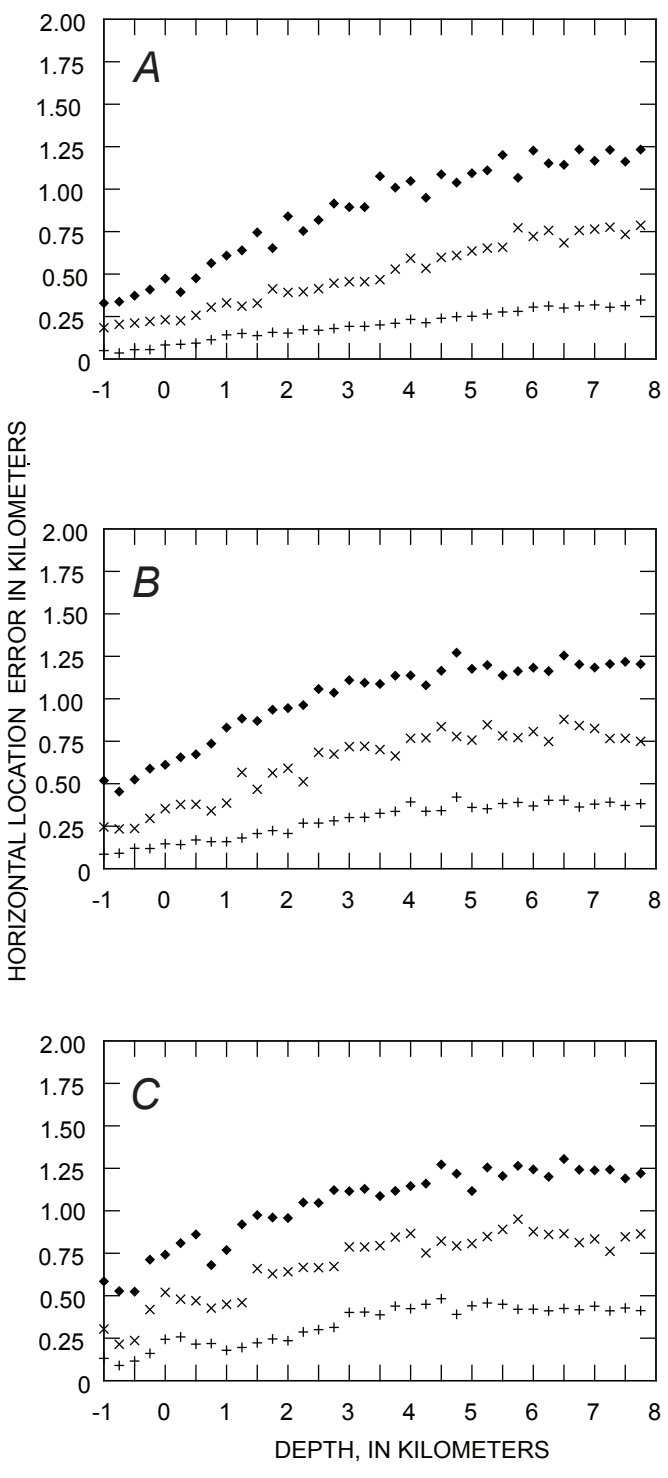

Figure 8. Simulated values of horizontal location error (ERH) based on three error levels of P-wave-arrival determination for seismic networks used for the 2D ray-tracing procedure in *A,* 1975, *B,* 1985–1986, and *C,* 2005–2006. The pluses, crosses, and diamonds, correspond to the 0.02-, 0.05-, and 0.10-second P-wave reading errors, respectively. Each data point represents the mean ERH for 100 simulated events.

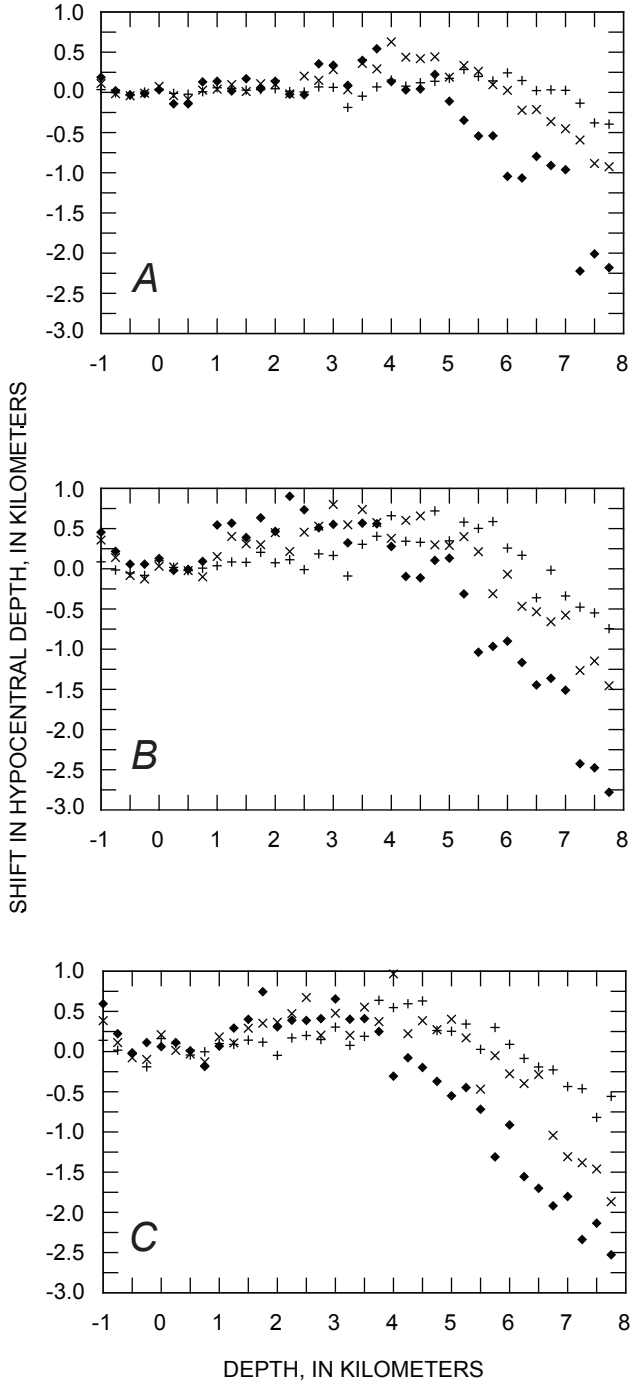

Figure 9. Simulated shifts in hypocentral depth based on three error levels of P-wave-arrival determination for seismic networks used for the 2D ray-tracing procedure in *A,* 1975, *B,* 1985–1986, and *C,* 2005–2006. The pluses, crosses, and diamonds correspond to the 0.02-, 0.05- and 0.10-second P-wave reading errors respectively. Every point represents the mean value of the shift in depth of 100 synthetic earthquake hypocenters.

(Power, 1988) networks, using the same statistical approach. These simulations also suggest that after 1993, when digital data allows us to determine P-wave-arrivals to within 0.02 s, that hypocentral depths can be determined to less than 0.25 km above sea level and less than 0.5 km above 2 km b.m.s.l. using a four-station network (figs. 7, 9, 10). The simulations for various four-station networks in 1975 plotted in figure 10 also indicate that a station high on the volcanic cone, such as station AU4 (fig. 3*A*) is critical for determining hypocentral depth. Changes in horizontal position for the same set of tests fig. 8) indicate an even smaller shift in calculated epicenter position as a result of our ability to determine P-wave arrivals. However, our ability to accurately determine earthquake depths rapidly diminishes below 3 km b.m.s.l.

The use of S-wave-phases was not considered in these simulations. We note that these uncertainties apply only for reading errors with a Gaussian shape.

Comparison with the Program HYPOELLIPSE

To further evaluate the accuracy of earthquake locations calculated with the 2D ray-tracing procedure, we located a subset of 30 well-recorded earthquakes that occurred between May 20 and December 10, 2005, with this technique and the program HYPOELLIPSE (Lahr, 1999), using two separate station configurations. For HYPOELLIPSE, we used a one-dimensional seismic-velocity model consisting of six horizontal layers with boundaries at depths of –1.2, –0.7, 0.0, 1.0, 9.0, and 44.0 km. The top of the model at 1.2 km a.m.s.l. corresponds approximately to the summit of the volcano. The respective P-wave velocities for each layer are 2.3, 2.6, 3.4, 5.1, 6.3, and 8.0 km/s. These layer boundaries and velocities, which were determined by using the results of the 1975 active-source seismic experiment (Kienle and others, 1979), were observed to minimize residuals in several test runs of HYPOELLIPSE. The station configurations used for HYPOELLIPSE were the entire permanent network in 2005 and a four-station network with only stations AUE, AUH, AUI, and AUL (fig. 3*C*), the same four stations used with the 2D ray-tracing procedure.

The average hypocentral depth and standard deviation for the 30 earthquakes sampled for each earthquake-location technique are listed in table 3, and calculated depths are compared in figure 11. These results suggest that hypocenters calculated with the 2D ray tracing procedure presented here yield earthquake depths by using P-wave-arrivals from four stations that are comparable to those calculated with HYPOELLIPSE by using the eight available stations of the 2005 network. The 2D relocations of our sample have a slightly higher standard deviation, indicating a greater scatter in depth. The run of HYPOELLIPSE with only four stations returns a deeper average depth and a higher standard deviation, suggesting that these hypocenters are not so reliable. These results indicate that the 2D relocations are preferable for periods when only

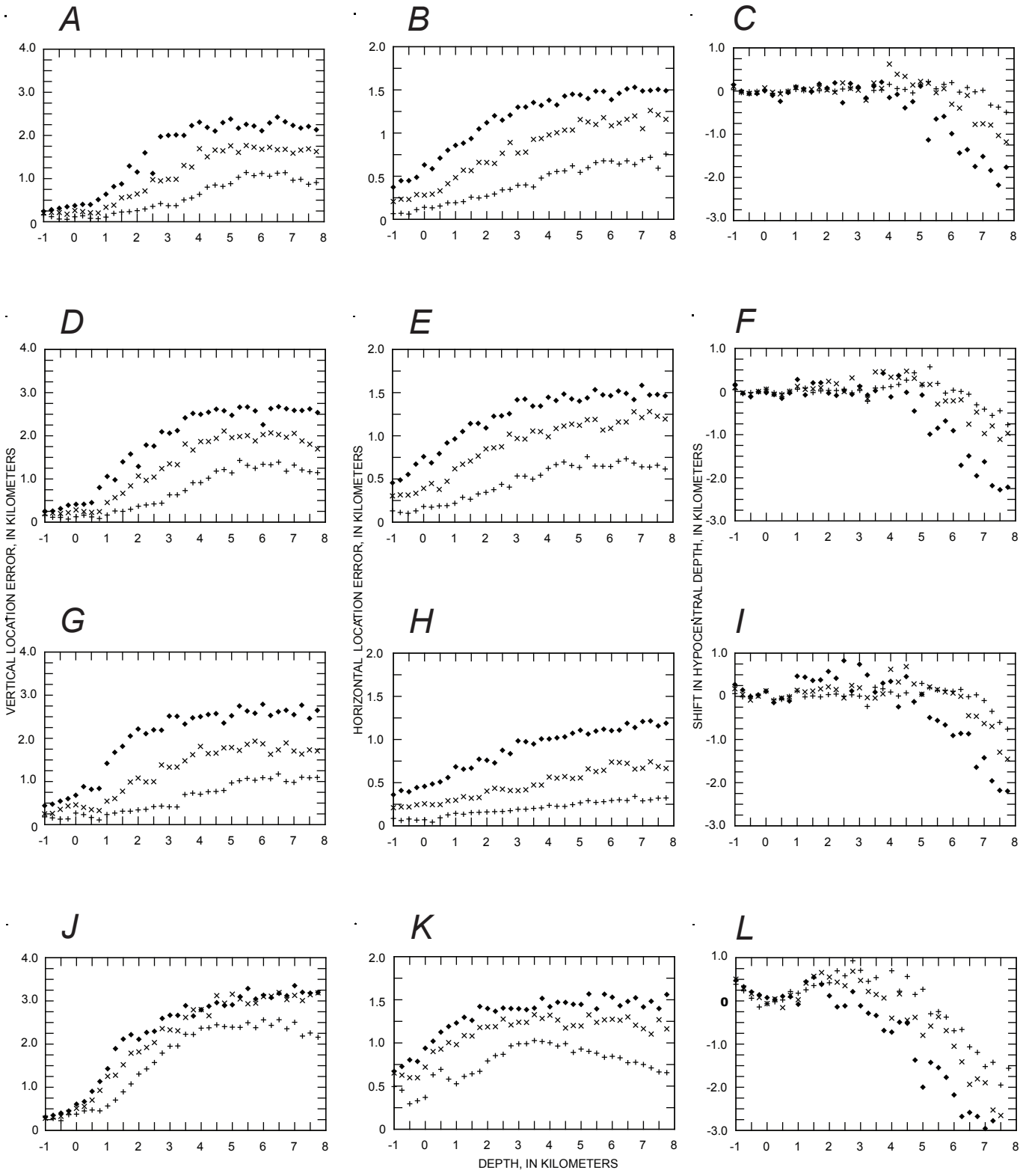

Figure 10. Simulated values of vertical location error (ERZ), horizontal location error (ERH), and shifts in hypocentral depth based on three error levels of P-wave arrival determination for various four station network configurations used to locate earthquakes on Augustine Island in 1975. The pluses, crosses, and diamonds correspond to the 0.02-, 0.05- and 0.10-second P-wave reading errors, respectively. Each data point represents the mean values for 100 synthetic earthquake hypocenters. *A–C*, correspond to hypocenters calculated without station AU2; *D–F,* to hypocenters calculated without station AU3; *G–I*, to hypocenters calculated without station AU4; and *J–L,* to hypocenters calculated without station AU5. See figure 3*A* for station locations.

four stations are operating on the volcano (fig. 11; table 3). The hypocenters calculated from HYPOELLIPSE might be improved further if station corrections were applied as described by Lahr and others (1994), which was not done for this comparison.

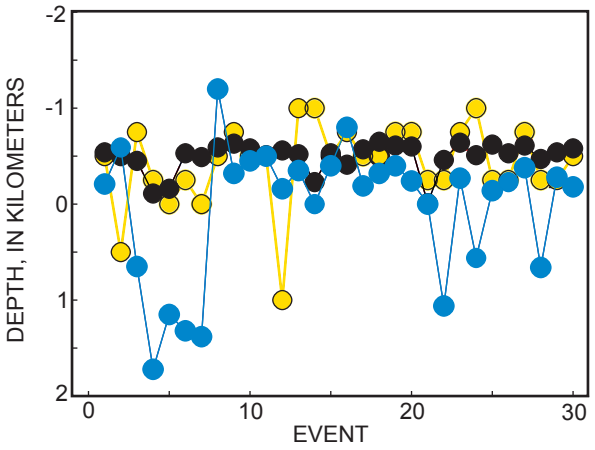

Figure 11. Comparison of earthquake hypocentral depths calculated with the 2D ray-tracing procedure and the program hypoellipse for a set of 30 earthquakes that occurred on Augustine Island in December of 2005. Black dots represent hypocentral depths calculated with the program hypoellipse, using the complete network in 2005; yellow dots represent hypocentral depths calculated with the 2D ray-tracing procedure; blue dots represent hypocentral depths calculated with the program hypoellipse, using only the same four stations used with the 2D ray-tracing procedure.

Summary and Conclusions

The two-step earthquake hypocenter-relocation procedure described here is able to resolve hypocentral depths to within 0.25 km for shocks that occur above sea level and to within 0.5 km for shocks above 2.0 km b.m.s.l. by using the seismic data collected at Augustine Volcano from 1972 to 2007. Hypocenters calculated with this procedure compare favorably with the results from the program HYPOELLIPSE, using the entire eight-station network present on Augustine Island in 2005. These results suggest that the two-step hypocenter-relocation procedure reliably calculates hypocenters at Augustine Volcano during periods when as few as four stations were operating on the island. Augustine Volcano was monitored by four- to five-station networks from 1972 to 1988 (see Power and Lalla, this volume). A study of comparative earthquake hypocenters at Augustine is presented by Power and Lalla (this volume).

Several limitations are inherent in the 2D ray-tracing procedure presented here: 1, it allows for variation of seismic velocity in only two directions, and raypaths are strictly confined to the vertical plane that intersects the station and event location; 2, it takes into account only a simple box discontinuity located between sea level and 0.9 km b.m.s.l. and all other layers are considered to be homogenous and flat laying; 3, locations are not allowed to fall outside the average radius of the volcanic cone at the elevation of consideration; and 4, it can only be used to locate within 2.2 km of the volcano's summit (lat 59°21.65' N., long 153°25.69' W.). Earthquake hypocentral depths at Augustine calculated by using this technique with the seismic-velocity model of Kienle and others (1979) were found to be sensitive to a station located high on the volcanic edifice (fig. 10). Thus, the design of future networks should include several stations high on the Augustine cone, such as AUH, AUP, AUS, and AU4 (fig. 3). Ideally, these stations would have horizontal components, so that reliable S-wave readings could also be included in the hypocenter determination.

If this technique is to be used for future earthquake studies at Augustine, we recommend its expansion to include all available stations in the Augustine seismic network be evaluated. Should additional stations be added to the network, consideration should be given to placing these instruments at shot-points or receiver-sites used in the 1975 active source seismic experiment (fig. 6). Before this technique is used further, we recommend that the relative advantages of other hypocenter-relocation techniques, such as those described by Rowe and others (2004) and Deshon and others (this volume), should be carefully considered.

Table 3. Hypocentral-depth comparisons.

Location technique	Average depth (km)	Standard deviation
Two-Dimensional ray-tracing procedure	–0.425	0.426
Hypoellipse (all stations)	–0.491	0.159
Hypoellipse (four stations)	0.0733	0.679

Acknowledgments

We thank Jurgen Kienle and Chris Pearson for useful discussions and insight into the Augustine seismic velocity structure. Diana Roman and Matt Haney provided helpful reviews of the manuscript.

References Cited

Beck J.V., and Arnold, K.J., 1979, Parameter estimation in science and engineering: New York, John Wiley and Sons, 499 p.

Clippard, J., 1998, Advances in seismic tomography with application to tunnel detection and volcano imaging: University of Alaska Fairbanks, Ph.D. dissertation, 298 p.

DeShon, H.R., Thurber, C.H., and Power, J.A., 2010, Earthquake waveform similarity and evolution at Augustine Volcano from 1993 to 2006, *in* Power, J.A., Coombs, M.L., and Freymueller, J.T., eds., The 2006 eruption of Augustine Volcano, Alaska: U.S. Geological Survey Professional Paper 1769 (this volume).

Detterman, R.L., 1973, Geologic map of the Iliamna B-2 quadrangle, Augustine Island, Alaska: U.S. Geological Survey Map GQ-1068.

Dixon, J.P., Stihler, S.D., Power, J.A., Tytgat, G., Estes, S., and McNutt, S.R., 2006, Catalog of earthquake hypocenters at Alaskan volcanoes: January 1 through December 31, 2005: U.S. Geological Survey Open-file Report 2006-1264, 78 p. [http://pubs.usgs.gov/of/2006/1264/].

Dixon, J.P., Stihler, S.D., Power, J.A., and Searcey, C., 2008, Catalog of earthquake hypocenters at Alaskan Volcanoes—January 1 through December 31, 2006: U.S. Geological Survey Data Series 326, 78 p.

Kienle, J., Lalla, D.J., Pearson, C.F., and Barrett, S.A., 1979, Search for shallow magma accumulations at Augustine volcano: Geophysical Institute, University of Alaska Fairbanks, final report to U.S. Department of Energy, 157 p.

Klein, F.W., 1978, Hypocenter location program HYPOINVERSE; part 1, Users guide to versions 1, 2, 3, and 4; part 2, Source listings and notes: U.S. Geological Survey Open-File Report 78-694, 114 p.

Lalla, D.J., and Kienle, J., 1978, Evolution of seismicity at Augustine Volcano, 1970 to 1976 eruption [abs.]: Geological Society of America, Abstracts with Programs, v. 10, p. 113.

Lalla, D.J., and Kienle, J., 1980, Problems in volcanic seismology on Augustine Volcano, Alaska [abs.]: Eos (American Geophysical Union Transactions), v. 61, p. 68.

Lawson, C.L., and Hansen, R.J., 1974, Solving least squares problems: Englewood Cliffs, N.J., Prentice-Hall, 340 p.

Lee, W.H.K., and Stewart, S.W., 1981, Principal and applications of microearthquake networks: New York, Academic Press, 340 p.

Lienert, B.R., Berg, E., Frazer, N. L., 1986, Hypocenter: an earthquake location method using centered, scaled, and adaptively damped least squares: Seismological Society of America Bulletin, v. 76, p. 771–783.

Pearson, C.F., 1977, Seismic refraction study of Augustine Volcano: Fairbanks, University of Alaska Fairbanks, M.S. thesis, 131 p.

Power, J.A., 1988, Seismicity associated with the 1986 eruption of Augustine Volcano, Alaska: Fairbanks, University of Alaska Fairbanks, M.S. thesis, 142 p.

Power, J.A., and Lalla, D.J., 2010, Seismic observations of Augustine Volcano, 1970–2007, *in* Power, J.A., Coombs, M.L., and Freymueller, J.T., eds., The 2006 eruption of Augustine Volcano, Alaska: U.S. Geological Survey Professional Paper 1769 (this volume).

Rowe, C.A., Thurber, C.H., and White, R.A., 2004, Dome growth behavior at Soufriere Hills Volcano, Montserrat, revealed by relocation of volcanic event swarms, 1995–1996: Journal of Volcanology and Geothermal Research, v. 134, p. 199–221.

Scheidegger, A.E., and Wilmore, P.L., 1957, The use of least squares method for the interpretation of data from seismic surveys: Geophysics, v. 22, p. 9–22.

Appendix 1. FORTRAN programs TRAVEL, NORMAL, and FAST configured for the 1975, 1985–86 and 2005–06 seismic networks at Augustine Volcano

This appendix contains the FORTRAN programs TRAVEL, NORMAL, and FAST configured for the 1975, 1985–86 and 2005–06 seismic networks at Augustine Volcano. These programs are contained on the DVD-ROM disc included with this volume.